MODELING OF CARBON DIOXIDE SEQUESTRATION IN A DEEP SALINE AQUIFER

A THESIS SUBMITTED TO
THE GRADUATE SCHOOL OF NATURAL AND APPLIED SCIENCES
OF
MIDDLE EAST TECHNICAL UNIVERSITY

BY

BAŞAR BAŞBUĞ

IN PARTIAL FULFILLMENT OF THE REQUIREMENTS
FOR
THE DEGREE OF MASTER OF SCIENCE
IN
PETROLEUM AND NATURAL GAS ENGINEERING

JULY 2005

Approval of the Graduate School of Natural and Applied Sciences

Prof. Dr. Canan ÖZGEN
Director

I certify that this thesis satisfies all the requirements as a thesis for the degree of Master of Science.

Prof. Dr. Birol DEMİRAL
Head of Department

This is to certify that we have read this thesis and that in our opinion it is fully adequate, in scope and quality, as a thesis for the degree of Master of Science.

Prof. Dr. Fevzi GUMRAH
Supervisor

Examining Committee Members

Prof. Dr. Ender OKANDAN	(METU, PETE)	
Prof. Dr. Fevzi GÜMRAH	(METU, PETE)	
Prof. Dr. Nurkan KARAHANOĞLU	(METU, GEOE)	
Assoc. Prof. Dr. Serhat AKIN	(METU, PETE)	
Mrs. Ilhan TOPKAYA, Msc.	(TPAO)	

I hereby declare that all information in this document has been obtained and presented in accordance with academic rules and ethical conduct. I also declare that, as required by these rules and conduct, I have fully cited and referenced all material and results that are not original to this work.

Başar BAŞBUĞ

ABSTRACT

MODELING OF CARBON DIOXIDE SEQUESTRATION

IN A DEEP SALINE AQUIFER

BAŞBUĞ, Başar

M.S., Department of Petroleum and Natural Gas Engineering

Supervisor : Prof. Dr. Fevzi Gümrah

July 2005, 245 pages

CO_2 is one of the hazardous greenhouse gases causing significant changes in the environment. The sequestering CO_2 in a suitable geological medium can be a feasible method to avoid the negative effects of CO_2 emissions in the atmosphere. CO_2 sequestration is the capture of, separation, and long-term storage of CO_2 in underground geological environments.

A case study was simulated regarding the CO_2 sequestration in a deep saline aquifer. The compositional numerical model (GEM) of the CMG software was used to study the ability of the selected aquifer to accept and retain the large quantities of injected CO_2 at supercritical state for long periods of time (200 years). A field-scale model with two injectors and six water producers and a single-well aquifer model cases were studied.

In a single-well aquifer model, the effects of parameters such as vertical to horizontal permeability ratio, aquifer pressure, injection rate, and salinity on the sequestration process were examined and the sensitivity analyses were performed after simulating the field-scale model.

The supercritical CO_2, one-state fluid which exhibits both gas and liquid-like properties, and gaseous CO_2 were sequestered in the forms of free CO_2 bubble, dissolved CO_2 in brine and precipitated CO_2 with calcite mineral in a deep saline aquifer. The isothermal condition was assumed during injection and sequestration processes. The change in porosity and permeability values that might have occurred due to mineralization and CO_2 adsorption on rock were not considered in this study.

Vertical to horizontal permeability ratio and initial pressure conditions were the most dominating parameters affecting the CO_2 saturation in each layer of the aquifer whereas CO_2 injection rate influenced CO_2 saturation in middle and bottom layers since CO_2 was injected through bottom layer.

Keywords: Supercritical CO_2, Sequestration, Deep Saline Aquifer, CMG / GEM simulator,

ÖZ

DERİN TUZLU SU AKİFERLERİNDE KARBON DİOKSİT

TECRİDİNİN MODELLENMESİ

BAŞBUĞ, Başar

Yüksek Lisans, Petrol ve Doğal Gaz Mühendisliği Bölümü

Tez Yöneticisi: Prof. Dr. Fevzi Gümrah

Temmuz 2005, 245 sayfa

Karbon dioksit (CO_2) çevreye zararlı etkileri olan sera gazlarından biridir. Atmosfere yayılan CO_2'in zararlı etkilerinden korunmak için uygulanabilecek çözümlerden biri, CO_2'in uygun yeraltı jeolojik ortamlarında tecrididir. CO_2 tecridi, CO_2'in tutulması, taşınması ve depolanması aşamalarından oluşmaktadır.

Bu çalışmada, CO_2'in derin tuzlu su akiferinde depolanmasına yönelik saha uygulaması yapılmıştır. CMG yazılımının bileşik bir modülü olan GEM simulatörü süperkritik özellikte basılan CO_2'in seçilen akiferde 200 yıllık zaman diliminde tecridi için kullanılmıştır. Bu çalışmada, iki enjeksiyon kuyusu ve altı su üretim kuyusu bulunan saha ve tek kuyu olmak üzere iki durum incelenmiştir.

Tek kuyu çalışmasında, dikey-yatay geçirgenlik oranının, akiferin basıncının, enjeksiyon debisinin ve akiferin tuzluluğunun tecrid işlemi üstüne olan etkileri incelenmiş ve hassasiyet çalışmaları yapılmıştır.

Gaz ve sıvı faz özelliklerini birarada gösterebilen süperkritik özellikte basılan CO_2, derin tuzlu su akiferlerinde serbest gaz kabarcığı, suyun içerisinde çözünmüş ve kalsit mineraliyle çökelmiş hallerde tecrid edilmiştir. CO_2'in basılması ve tecridi aşamalarında, sıcaklığın değişmediği varsayılmıştır, mineralleşmeden kaynaklanan gözeneklilik ve geçirgenlik değerlerinde oluşabilecek değişikler ve CO_2'in kayaç tarafından emilmesi ihmal edilmiştir.

Bu çalışmanın sonucunda, dikey yatay geçirgenlik oranının ve başlangıç basınç koşullarının, CO_2 doymuşluğunu akiferin her katmanında etkileyen en önemli parametreler oldukları görülmüştür. Buna karşın, CO_2'in basılma debisinin akiferin orta ve alt tabakalarında CO_2 doymuşluğunu etkilediği gözlenmiştir.

Anahtar Kelimeler: Süperkritik CO_2, Tecrid, Derin Tuzlu Su Akiferi, CMG / GEM simulatörü,

To My Family

ACKNOWLEDGEMENTS

I would like to express my deepest gratitude to my supervisor Prof. Dr. Fevzi GÜMRAH for his guidance, encouraging support and trust throughout this study.

I would like to express my gratitude to my family and my friends for their generous attitude and support.

I would like to express my gratitude to Bora ÖZ for his support throughout this study.

I would also like to thank Computer Modeling Group (CMG) for providing the software.

TABLE OF CONTENTS

LIST OF TABLES

LIST OF FIGURES

NOMENCLATURE

Symbol	Description
$E_{a\beta}$	Activation Energy
K	Rock matrix thermal conductivity
K_{eq}	Chemical-Equilibrium Constants
k_β	Rate constants
k	Permeability
$k_r^{'}$	Relative permeability at endpoint concentration
M	Mobility Ratio
P	Pressure
Q_β	Source Term
q	Flow rate
T	Temperature
S	Liquid Saturation
U_α	Internal energy
X_α	Mass fraction of CO_2 in the phase α

Greek

β	Energy, mass, CO_2
ϕ	Porosity
α	Phase
ρ_α	Density of phase
μ	Viscosity
$\hat{A}_\beta$	Reactive surface area
$\nabla . j_\beta$	Flux

Abbreviations

CMG	Computer Modeling Group
DEA	Diethanolamine
DOE	Department of Energy
EGR	Enhanced Gas Recovery
EOR	Enhanced Oil Recovery
EOS	Equation of State
GHGs	Greenhouse Gases
GWP	Global Warming Potential
HFCs	Hydroflourocarbons
IGCC	Integrated gasification combined cycle
IPCC	Intergovernmental Panel on Climate Change
MDEA	Methyldiethanolamine
MEA	Monoethanolamine
NGCC	Natural gas fired combined cycle
NMVOC	Non-methane volatile organic compound
PF	Pulverized coal fired
PFCs	Perflourocarbons
TDS	Total Dissolved Solids

CHAPTER 1

INTRODUCTION

Carbon Dioxide sequestration is the capture of, separation, and long-term storage of CO_2 in underground reservoirs for environmental purposes. CO_2 is one of the hazardous greenhouse gases causing significant changes in global temperature and sea-levels [1], which could have negative consequences for people in many parts of the world. Scenarios for stabilizing atmospheric CO_2 at reasonable levels will eventually require substantial cuts in overall emissions over the next few decades [1, 2]. If usage of fossil fuels is to continue at current levels while avoding undesirable climate change, technical means need to be found to reduce the carbon dioxide emitted to the atmosphere in the production and consumption of fossil fuels [3].

CO_2 sequestration can be regarded as one possible solution for reducing the CO_2 emissions in a form where they will not reach the atmosphere. Disposal environments for CO_2 sequestration can be divided into four different categories. Oceans, terrestrial basins, biological environment and geologic formations are the candidates for disposal of CO_2. Among these alternatives, geologic formations can be regarded as the best possible environment to sequester CO_2 because of the fact that storage of CO_2 in geologic formations is self-containing and volumetrically efficient.

In geologic formations, CO_2 can be sequestered in porous or non-porous media. Depleted oil and gas reservoirs, aquifers and coal beds can be categorized in the porous medium whereas salt caverns and lined-rock caverns can be regarded as non-porous medium.

In geologic formations, the potential storage capacity in depleted natural gas fields is estimated between 600 and 1500 G-tones CO_2 and in depleted oil fields between 200 and 400 G-tones CO_2. If a structural trap is required the storage capacity in aquifers is about 200 G-tones of the CO_2 whereas storage potential might be up to several tens of thousands if a structural trap is not required [4].

Gunter et al. [5] provided a critical look at capacities, retention times, rates of uptake and costs for CO_2 disposal in different classes of CO_2 sinks at three scales, global, national (Canada) and provincial (Alberta). Among the geological formations, deep saline aquifers seem to be the most promising avenues for CO_2 disposal [6,7] as they are widely distributed, underlie most point sources of CO_2 emission and are not limited by the reservoir size.

Tanaka et al. [8] discussed different structures for CO_2 sequestration in Japan. These consist of (1) oil and gas reservoirs with neighboring aquifers (potential sequesterable amount = 2 billion tones of CO_2), (2) aquifers in anticlinal structures (1.5 billion tones of CO_2), (3) aquifers in monoclinal structures on land (16 billion tones of CO_2), and (4) aquifers in monoclinal structures offshore (72 billion tones of CO_2). Oil and gas reservoirs with neighboring aquifers in category 1 are still active and will be producing for some time in the future. Even depleted, these reservoirs can be used for underground gas storage. Consequently, aquifers in categories (3) and (4) are the most attractive candidates for CO_2 sequestration. Aquifers in category (3) are being developed as water-dissolved gas fields and some data on the structure, extent, porosity and permeability, etc. are available. Koide et al. [9,10] provided additional discussions on the merit of disposing CO_2 in deep saline aquifers around the world in general and in Japan in particular.

Krom et al. [11] discussed the potential, the feasibility and the operational and economical implications of disposing CO_2 in deep saline aquifers in Denmark. Disposal structures and capacities, contact areas between the gas phase and the aqueous phase, chemical reactions, disposal management, risks, costs and data requirements are aspects that need to be addressed in the design and operation of CO_2 disposal process.

Baklid et al., Kongsjordan et al, and Chatwick et al. [12,13,14] described the Sleipner Vest CO_2 storage project in the North Sea. The rich gas of the Sleipner Vest field contains sizable amounts of CO_2 (9%). CO_2 is removed using an activated amine and reinjected into an aquifer in the Utsira formation.

Emberley et al. [15] discussed the CO_2 storage process in the CO_2-EOR injection project in Weyburn, Saskatchewan, Canada.

Van der Meer [16] reviewed significant milestones and successes achieved in underground CO_2-storage technology over the past few years. All underground options including aquifer storage, EOR processes, CO_2 storage in depleted gas and oil fields, and Enhanced Coal Bed Methane is reviewed. He noted that Sleipner project has proven to be a successful storage project.

In this study, engineering design aspects of CO_2 sequestration in a deep saline aquifer were examined numerically. A case study was simulated using the code **gem-ghg_200319d.exe** of the CMG (Computer Modeling Group) software programs [17]. Effects of aquifer parameters such as vertical to horizontal permeability ratio, aquifer pressure, injection rate, and salinity on the sequestration process were examined and the sensitivity analyses were performed after simulating the field case.

CHAPTER 2

SOURCES OF GREENHOUSE GASES AND ITS EFFECT ON CLIMATE CHANGE

2.1. World Approach

Global climate change is one of the most prominent environmental and energy policy issues of our age. Although scientific and economic uncertainties remain, there is little doubt that human beings are altering the Earth's climate [18-21]. Through the burning of fossil fuels, certain industrial processes, and various land use practices, we are contributing greatly to the accumulation of so-called greenhouse gases (GHGs) in the atmosphere, which trap heat and block outward radiation. Intergovernmental Panel on Climate Change [22] (IPCC) reported at 2001 that the observed global warming over the past 50 years is the result of the increase of greenhouse gas concentrations. CO_2, CH_4, N_2O, hydrofluorocarbons (HFCs), perfluorocarbons (PFCs) and SF_6 are the most important greenhouse gases affecting the global warming. Among these GHGs, the most prevalent of them is CO_2. For instance, CO_2 accounted for 82% of total U.S. GHG emissions from 1991 to 2000 [21]. About 96% of these carbon emissions resulted from using fossil fuels for energy [23].

Table 2.1 indicates six greenhouse gases and their emissions in the U.S. in 1990 and 1998 [24, 25].

Table 2.1 Six greenhouse gases and their emissions in the U.S. between 1990 and 1998 [24, 25]

Greenhouse Gas (GHG) compound	Global warming potential (GWP)	% of U.S. GHG emissions (1990)	% of U.S. GHG emissions (1998)
Carbon dioxide, CO_2	1	~85	~81
Nitrous oxide, N_2O	310	~2.5	~7
Methane, CH_4	21	~12	~10
Hydro fluorocarbons, HFC	140-11700	<1	<1
Perfluorucarbons, PFC	7400	<1	<1
Sulphur hexafluoride, SF_6	23900	<1	<1

Global atmospheric concentration, rate of concentration change and atmospheric lifetime of these greenhouse gases are illustrated in Table 2.2 [22].

Table 2.2 Global atmospheric concentration (ppm unless otherwise specified), rate of concentration change (ppm/year) and atmospheric lifetime (years) of selected greenhouse gases [22]

Atmospheric Variable	CO_2	CH_4	N_2O	SF_6[a]	CF_4[a]
Pre-industrial era atmospheric concentration	278	0.7	0.27	0	40
Atmospheric concentration (1998)	365	1.745	0.314	4.2	80
Rate of concentration change[b]	1.5[c]	0.007[c]	0.0008	0.24	1
Atmospheric Lifetime	50-200[d]	12[e]	114[e]	3200	>50000

[a] Concentrations in parts per trillion (ppt) and rate of concentration change in ppt/year.
[b] Rate is calculated over the period 1990 to 1999.
[c] Rate has fluctuated between 0.9 and 2.8 ppm/year for CO_2 and between 0 and 0.013 ppm/year for CH_4 over the period 1990 to 1999.
[d] No single lifetime can be defined for CO_2 because of the different rates of uptake by different removal processes.
[e] This lifetime has been defined as an 'adjustment time' that takes into account the indirect effect of the gas on its own residence time.

There is some evidence from climate modelling that increased atmospheric concentrations of CO_2 may be the chief contributor to 'global warming,' currently estimated to be 0.3-0.6 °C during the last 150 years [26] and global temperature increase of almost 2°C above 1990 levels by 2100 [27]. According to IPCC reports, in the mid-1990s annual CO_2 emissions to the atmosphere amounted to 7.4 billion tones of carbon (GtC), mostly from fossil fuel combustion. It was estimated that 2.2 GtC were taken up by the oceans and 1.7 GtC by photosynthesis and plant growth, with 3.5 GtC entering the atmosphere as free carbon dioxide [28] and it was foreseen that annual global emissions of carbon dioxide rise from this 7.4 to 26 GtC in the year 2100. Atmospheric carbon dioxide concentrations would have doubled from pre-industrial revolution levels by 2050, and the rate of increase would grow thereafter [29].

Stationary sources including fossil-fired power stations, petroleum developments, steel and non-ferrous metal plants can be given as sources of greenhouse gases. Among these sources, fossil fuel combustion is the major contributor to CO_2 emissions releasing to the atmosphere. Fossil fuels, which today provide about 75% of the world's energy, are likely to remain a major component of the world's energy supply for at least the next century because of their inherent advantages, such as availability, competitive cost, ease of transport and storage and large resources [30, 31].

Table 2.3 summarizes CO_2 emissions from the burning of the three principal fossils fuels in different world regions in 1990 and 1998 [32]. As will be seen, emissions of carbon from the burning of fossil fuels increased by over 21% between 1990 and 1998. Although emissions fell throughout Europe, they almost doubled in the Middle East and Far East/Oceania regions, and increased significantly in the Americas. Emissions from the use of natural gas have been increasing most rapidly. Several projections suggest that emissions will continue to rise, for example by 2.2% globally between 2000 and 2020 and 3.3% for developing countries in the same period [33].

Table 2.3 Global Carbon Dioxide Emissions (Mtc) by fuel in 1990 and 1998 [32]

Region	Natural Gas		Oil		Coal	
	1990	**1998**	**1990**	**1998**	**1990**	**1998**
North America	339	384	732	771	414	574
Central/South America	22	57	141	180	11	19
Western Europe	116	206	572	550	335	241
Eastern/Central Europe	209	323	415	193	488	284
Middle East	53	102	83	159	1	7
Far East/Oceania	43	144	431	706	503	985
Total	812	1264	2432	2658	1807	2202

For these reasons, climate change discussions have tended to focus on the reduction of CO_2 emissions being responsible for about 64% of the enhanced 'greenhouse effect' [34]. There are three obvious ways of reducing emissions of carbon dioxide [35].

1. Reducing overall demand for energy, e.g. by increasing energy prices or improving energy efficiency.
2. Switching from fossil fuels to zero-carbon sources such as nuclear power and renewables.
3. Sequestering the emissions, either directly by capturing the emissions before they reach the atmosphere and storing them (perhaps in some suitable geologic formation) or by removing carbon dioxide from the atmosphere, e.g. by increased levels of a forestation.

Among these three alternatives, third option can be regarded as the most promising one.

2.2. Situation in Turkey

Turkey ranks among the fastest growing energy markets in the world and is the fastest among member countries of the International Energy Agency. Oil accounted for 38 percent of Turkey's energy use in 2000, followed by coal at 25 % and natural gas at 17 % (Figure 2.1). However, gas use is increasing rapidly. Energy-related carbon emissions have been growing much faster than the economy at annual rate of 6 % per year since 1990. Industry accounts for half of total carbon dioxide emissions, with the residential and transportation sectors contributing roughly one-fifth each (Figure 2.1) [36].

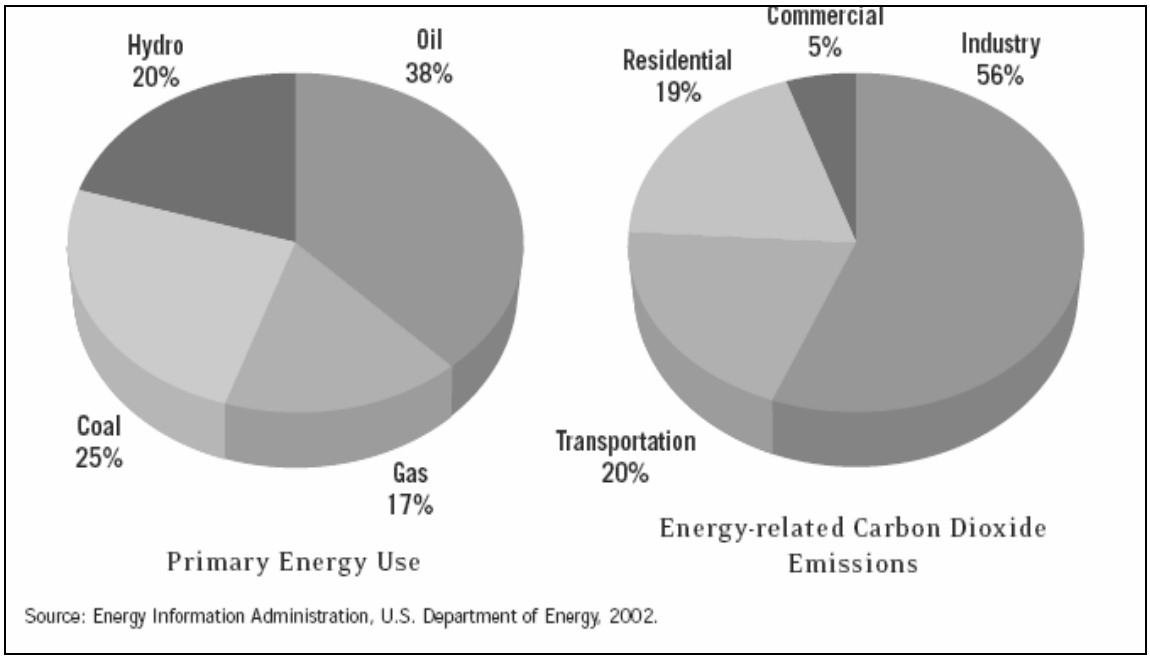

Figure 2.1 Energy and Emissions in Turkey, 1998 [36]

According to United Nations Framework Convention held on Rio de Janerio in June 1992, European Union and 174 countries ratified to the convention in order to stabilize greenhouse gases concentrations in the atmosphere at a level that would prevent dangerous anthropogenic interference with climate system. Although Turkey has accepted the objectives of the Convention, it has not already ratified to the convention and Kyoto Protocol, accepted in the third Conference Parties (COP3). But Turkey is responsible for the stabilization of greenhouse gases at 1990 level and provides technical and financial support to the developing countries since Turkey is a member of OECD where it is placed in Annex 1 countries [37].

Sources of greenhouse gas emissions were expressed in Table 2.4 [38] calculated according to IPCC methodology [39].

According to the greenhouse gas emissions calculated by using IPCC guideline [39], direct greenhouse gas emissions as CO_2 equivalents were estimated as 68.25 million tonnes in 1970, as 200.7 million tonnes in 1990 and as 271.2 million tonnes in 1997. In 2010 direct greenhouse gas emissions will be estimated to reach 567 million tonnes (Table 2.5) [37].

IPCC guideline [39] define carbon dioxide (CO_2), methane (CH_4) and nitrous oxide (N_2O) as direct greenhouse gases and nitrogen oxides (NO_x), carbon monoxides (CO), non-methane volatile organic compound (NMVOC), hydro-fluoro carbons (HFCs), per-fluoro-carbons (PFCs), sulphur hexafluoride (SF_6) and sulphur dioxide (SO_2) as indirect greenhouse gases.

Table 2.4 Emission Sources of Greenhouse Gases, Data Sources and Greenhouse Gases in Turkey [38]

Sources	Data Types	Data Sources	Greenhouse Gases
ENERGY (FUEL CONSUMPTION AND FUGITIVE SOURCES)			
Fuel Consumption	Amount of fuel consumption by sectors (energy, manufacturing industry, transportaion, other)	Ministry of Energy and Natural Sources (1970-2010)	CO_2, CH_4, N_2O, NOx, CO, SO_2, NMVOC,
Coal Mining	Amount of coal production from underground and surface mining	SIS, Mine Statistics Division (1970-1997)	CH_4
Fugitive emissions from coal and oil	Amount of transported crude oil	General Directorate of Petroleum Works	CH_4
INDUSTRIAL PROCESSES			
Industrial processes	Amount of production	Turkish Cement Manufacturer's Association (1970-1997), SIS, Industrial Production Statistics (1987-1997), General Directorate of Turkish Cellulose and Paper Industry (Kocaeli) (1970-1997)	CO_2, CH_4, N_2O, NOx, NMVOC, CO, SO_2
AGRICULTURAL FACILITIES			
Enteric fermentation and manure management	Number of livestock by provinces, average temperatures by provinces	SIS, Agricultural Statistics Division, General Directorate of State Meteorological Works (1970-1997)	CH_4
Rice Cultivation	Cultivated rice lands by provinces, average monthly temperature by provinces	SIS, Agricultural Statistics Division, General Directorate of State Meteorological Works (1970-1997)	CH_4
Burning of agricultural residues	Amounts of wheat, barley, maize, oat and rye	SIS, Agricultural Statistics Division (1970-1997)	CH_4, N_2O, NOx, CO
Agricultural soil	Total use of synthetic fertilizer, total stock of livestock, amount of dry legumes and soybeans, amount of dry production of other crops, area of cultivated organic soils	No data available	N_2O
LAND USE AND FORESTY			
Forest lands	Stock changes in forest and woody biomass	Ministry of Forest (1970-1997)	CO_2
Land use change	Conversion of forests and graslands, Abandonment of managed lands	No data available	CO_2, CH_4, CO, N_2O, NO_X
WASTES			
Solid Wastes	Amount of solid wastes stored in landfills, Amount of organic matter under biochemical decomposition	SIS, Environmental Statistics Division	CH_4
Wastewater	Amount of domestic and industrial wastewater and sludge, annual BOD	No data available	CH_4

Table 2.5 Direct and indirect greenhouse gas emissions by sources between 1970 and 2010 in Turkey (Gg) [37]

	Years										
Greenhouse gases	**1970**	**1975**	**1980**	**1985**	**1990**	**1992**	**1995**	**1997**	**2000**	**2005**	**2010**
Direct greenhouse gases [1]	68,250	94,998	110,216	133,056	200,723	214,972	241,717	270,520	333,956	428,376	567,637
Carbon dioxide (CO_2)[2]	44,775	69,840	81,889	108,923	177,973	188,485	211,299	241,151	303,079	397,351	535,966
Methane (CH_4) [3]	22,954	24,495	27,574	23,265	21,621	22,565	24,390	24,886	26,221	26,167	26277
Original values	*(1093)*	*(1166.4)*	*(1313)*	*(1107.8)*	*(1029.4)*	*(1074.4)*	*(1161.4)*	*(1185)*	*(1248.6)*	*(1215.7)*	*(1220.9)*
Nitrous oxide (N_2O) [4]	521	663	753	868	1,131	3,925	6,116	4,483	4,656	4,858	5,394
Original values	*(1.68)*	*(2.14)*	*(2.43)*	*(2.80)*	*(3.64)*	*(12.66)*	*(19.73)*	*(14.47)*	*(15.02)*	*(15.67)*	*(17.40)*
Indirect greenhouse gases											
Nitrogen oxide (NO_x) [5]	219	335	380	493	680	703	814	837	1,154	1,513	2,073
Carbon monoxide (CO) [5]	2,008	2,665	2,936	3,115	3,773	3,853	4,022	4,198	8,454	9,616	11,497
Non methane volatile organic carbon (NMVOC) [5]	241	332	360	380	524	543	599	632	1,415	1,638	1,991
Sulphur dioxide (SO_2) [6]	61	127	210	501	808	864	987	1208	1126	1166	1166
Direct and indirect greenhouse gas emissions generated from fuel consumption											
Direct greenhouse gases [1]	43,976	68,087	79,023	105,083	146,736	156,086	172,934	195,513	258,314	352,733	491,995
CO_2	41,581	65,208	75,687	101,267	142,727	151,943	169,182	191,650	253,578	347,850	486,465
CH_4	1,946	2,315	2,691	3,066	3,143	3,238	2,849	2893	3,592	3,538	3,648
N_2O	450	564	645	750	866	905	903	970	1,144	1,345	1,882
Indirect greenhouse gases											
NO_x	214	327	372	484	659	679	786	842	1,125	1,484	2,044
CO	1,772	2,329	2,564	2,718	3,258	3,359	3,536	3687	7,943	9,105	10,986
NMVOC	240	331	359	378	479	496	548	575	1,359	1,582	1,935
SO_2	59	123	205	494	740	790	908	1112	1030	1070	1070
CH_4 emissions generated from transportation of crude oil											
CH_4	0.063	0.042	0.021	0.063	0.168	0.378	0.336	0.315	0.315	0.315	0.315
CH_4 emissions generated from coal mining											
CH_4	210.63	259.98	303.45	600.39	436.8	969.78	823.83	1344.5	1344.5	1344.5	1344.5
Direct and indirect greenhouse gas emissions generated from industrial processes											
Direct greenhouse gases [1]	3,194	4,632	6,202	7,656	35,425	39,480	47,252	52,929	52,929	52,929	52,929
CO_2	3,194	4,632	6,202	7,656	35,246	36,542	42,117	49,501	49,501	49,501	49,501
CH_4	.	.	.	.	50	49	47	49	49	49	49
N_2O	.	.	.	.	128	2,889	5,088	3,379	3,379	3,379	3,379
Indirect greenhouse gases											
NO_x	0.09	0.26	1.26	0.37	11.25	13.67	18.50	19.21	19.21	19.21	19.21
CO	0.34	0.97	0.96	1.38	59.87	57.62	62.63	65.52	65.52	65.52	65.52
NMVOC	0.23	0.64	0.64	0.91	44.36	47.40	50.66	56.58	56.58	56.58	56.58
SO_2	2.34	4.47	5.09	6.98	68.25	74.15	78.92	95.50	95.50	95.50	95.50

Table 2.6 Direct and indirect greenhouse gas emissions by sources between 1970 and 2010 in Turkey (Gg) (continuation) [37]

Greenhouse gases	Years										
	1970	1975	1980	1985	1990	1992	1995	1997	2000	2005	2010
Direct and indirect greenhouse gas emissions generated from the burning of agricultural residues											
Direct greenhouse gases [1]	306.92	433.73	478.52	513.44	591.05	567.63	550.25	578.50	578.50	578.50	578.50
CH_4	235.62	334.53	370.02	395.64	454.65	437.43	423.15	445.20	445.20	445.20	445.20
N_2O	71.30	99.20	108.50	117.80	136.40	130.20	127.10	133.30	133.30	133.30	133.30
Indirect greenhouse gases											
NO_x	5.33	7.55	8.34	8.97	10.30	9.93	9.58	10.09	10.09	10.09	10.09
CO	235.83	334.80	370.47	396.00	455.08	437.91	423.50	445.66	445.66	445.66	445.66
CH_4 emissions generated from livestock (enteric fermentation and manure management)											
CH_4	19,820.6	20,953.4	23,641	18,542.8	17,052.2	17,433.4	16,469	15,372.4	15,372.4	15,372.4	15,372.4
CH_4 emissions generated from rice cultivation											
CH_4	741.3	631.5	568.5	660	480.9	434.1	541.2	577.5	577.5	577.5	577.5
CH_4 emissions generated from landfills											
CH_4	-	-	-	-	-	-	3232.3	4840	4840	4840	4840
Absorbed CO_2 emissions											
CO_2 [7]	.	39200	40400	41300	43800	44500	45500	49700	.	.	.

[1] Direct greenhouse gases, CH_4 and N_2O emission values were given as CO_2 equivalents, for 100 years peiod conversion coefficients are given as 21 for CH_4 and as 310 for N_2O.

[2] Only cement industry was included between 1970 and 1985. Emissions from all manufacturing industries were included fro between 1990 and 2010.

[3] For between 1990 and 2010 emission values cover only chemical industry among all manufacturing industries.

[4] Emissions generated from nitric acid production in chemical industry were included fro between 1990 and 2010.

[5] Only paper industry was included for between 1970 and 1985. Emissions generated from all manufacturing industries were included for between 1990 and 2010.

[6] Only cement and paper industries were included for between 1970 and 1985. Emissions generated from all manufacturing industries were included for between 1990 and 2010. For between 1970 and 2010 emissions generated from thermal power plants were covered.

[7] Absorbed CO_2 emissions were calculated by Ministry of Forest for between 1970 and 1997.

Table 2.7 Direct greenhouse gas emissions by sectors between 1990 and 2010 in Turkey (%) [37]

Greenhouse gases	Years						
	1990	1992	1995	1997	2000	2005	2010
Total direct greenhouse gases (Gg) [1]	200,720	214,972	241,717	271,176	333,320	427,739	567,000
CO_2 (%)	88.67	87.68	87.42	88.93	90.93	92.90	94.53
CH_4 (%)	10.77	10.50	10.05	9.42	7.68	5.97	4.52
N_2O (%)	0.56	1.83	2.53	1.65	1.40	1.14	0.95
Emission fractions generated from fuel consumption							
Direct greenhouse gases (Gg) [1]	146,735	156,086	172,933	195,591	258,314	352,733	491,995
CO_2 (%)	97.3	97.3	97.8	98.0	98.2	98.6	98.9
CH_4 (%)	2.1	2.1	1.6	1.5	1.4	1.0	0.7
N_2O (%)	0.6	0.6	0.5	0.5	0.4	0.4	0.4
Emission fractions generated from industrial processes							
Direct greenhouse gases (Gg) [1]	35,424	39,481	47,251	52,929	52,929	52,929	52,929
CO_2 (%)	99.5	92.6	89.1	93.5	93.5	93.5	93.5
CH_4 (%)	0.1	0.1	0.1	0.1	0.1	0.1	0.1
N_2O (%)	0.4	7.3	10.8	6.4	6.4	6.4	6.4
Emission fractions generated from the burning of agricultural residues							
Direct greenhouse gases (Gg) [1]	591.05	567.63	550.25	578.5	578.5	578.5	578.5
CH_4 (%)	76.92	77.06	76.90	76.96	76.96	76.96	76.96
N_2O (%)	23.08	22.94	23.10	23.04	23.04	23.04	23.04

From Table 2.7, it was observed that CO_2 is the main contributor of the greenhouse effect. In 2000, 90.93 % of total greenhouse gas emissions were CO_2, 7.68 % of these CH_4 and 1.40 % of these were N_2O. In the estimation of 2005 and 2010, the ratio of CO_2 emissions among the total direct greenhouse gas emissions has a tendency to increase 94.53 % in 2010 [37].

Most of CO_2 emissions are generated from fuel consumption and industrial processes. While in the year of 1990 the ratio pf CO_2 emissions among direct greenhouse gas emissions was estimated as 97.3 %, in 1997 this ratio was estimated as 98 %. It was assumed that product per production was constant in manufacturing industry since 1997, the ratio of CO_2 emissions among direct greenhouse gas emissions will be estimated to reach 98.9 % in 2010 (Table 2.7) [37].

CO_2 emissions generated from fuel consumption by sectors for years between 1990 and 2010 were also shown in detail in Table 2.8. In 1997, 37 % of CO_2 emissions was generated from energy and transformation sector, 26 % from industrial sector, 18 % from transportation sector and 19 % from other sectors (residential, agriculture, commercial and forest). The estimation for the year of 2010 shows that the ratio of energy and transformation sector will be increased to 46 % and the ratio of industrial sectors will be 27 %, transportation sector will be 16 % and other sectors will be 11 % [37].

Table 2.8 Distribution of greenhouse gas emissions by sources between 1990 and 2010 in Turkey (%) [37]

Emissions	Years						
	1990	1992	1995	1997	2000	2005	2010
CO_2 Emission Fractions							
Fuel Consumption (%)	80	81	80	79	84	88	91
Energy and Transformation Sectors (%)	36	37	36	37	39	43	46
Industry (%)	26	26	25	26	21	24	27
Transportation (%)	19	17	20	18	21	18	16
Other (%)	19	20	19	19	19	15	11
Industrial Processes (%)	20	19	20	21	16	12	9
CH_4 Emission Fractions							
Fuel Consumption (%)	14.54	14.35	11.68	11.32	14.04	13.86	14.23
Coal Mining (%)	2.02	4.30	3.38	5.26	3.26	3.27	3.25
Transportation of Crude Oil (%)	0.001	0.002	0.001	0.001	0.001	0.001	0.001
Refined Oil (%)	0.01	0.01	0.01	0.01	0.01	0.01	0.01
Industrial Processes (%)	0.23	0.22	0.19	0.19	3.26	0.19	0.19
Rice Cultivation (%)	2.22	1.92	2.22	2.26	2.26	2.26	2.25
Livestock (enteric fermentation and manure management) (%)	78.87	77.26	67.53	60.26	60.08	60.21	59.95
Burning of Agricultural Residues (%)	2.10	1.94	1.73	1.74	1.74	1.74	1.74
Landfills (%)	-	-	13.25	18.95	18.43	18.47	18.39
N_2O Emission Fractions							
Fuel Consumption (%)	77	23	15	22	25	28	35
Industrial Processes (%)	11	74	83	75	73	70	63
Burning of Agricultural Residues (%)	12	3	2	3	3	3	2
NO_x Emission Fractions							
Fuel Consumption (%)	96.83	96.64	96.55	96.64	97.46	98.06	98.59
Industrial Processes (%)	1.65	1.94	2.27	2.20	1.66	1.27	0.93
Burning of Agricultural Residues (%)	1.51	1.41	1.18	1.16	0.87	0.67	0.49
CO Emission Fractions							
Fuel Consumption (%)	86.35	87.18	87.91	87.82	93.95	94.69	95.55
Industrial Processes (%)	1.59	1.46	1.56	1.56	0.78	0.68	0.57
Burning of Agricultural Residues (%)	12.06	11.36	10.53	10.61	5.27	4.63	3.88
NMVOC Emission Fractions							
Fuel Consumption (%)	91.53	91.27	91.54	91.05	96.00	96.50	97.20
Industrial Processes (%)	8.47	8.73	8.46	8.95	4.00	3.50	2.80
SO_2 Emission Fractions							
Fuel Consumption (%)	92	91	92	92	91	92	92
Industrial Processes (%)	8	9	8	8	9	8	8

CHAPTER 3

CAPTURING, TRANSPORTATION AND SEQUESTRATION OF CO_2

CO_2 sequestration process consists of capturing of CO_2 from stationary emission sources and storing it safely in suitable environment to reduce the emissions of CO_2 into the atmosphere. CO_2 capture involves the separation of CO_2 from the hydrocarbon gases, the dehydration and initial compression of CO_2 so that CO_2 is suitable for transportation by pipeline. Chemical absorption, cryogenic, physical adsorption and membrane are the main technologies to separate CO_2 from other flue gases.

3.1 Technologies for capturing of CO_2

3.1.1 Separating CO_2

3.1.1.1 Chemical Absorption

In chemical absorption, CO_2 reacts with chemical solvents to form weakly bonded intermediate compounds, which are then broken down by the application of heat, regenerating the original solvents for reuse and producing a CO_2 stream. Alkanolamines such as monoethanolamine (MEA), diethanolamine (DEA) and methydiethanolamine (MDEA) are the commonly used solvents for chemical absorption process. MEA can reduce the CO_2 concentration to as low as 100 ppm at low pressure (1.4 MPa or 200 psi). DEA is a suitable solvent when the CO_2 concentration is high and the total pressure is high. MDEA has high selectivity for H_2S in the presence of CO_2 and is ideally suited for bulk removal of CO_2 from high CO_2 content natural gas streams. Especially, MDEA

absorbs CO_2 at high-pressure conditions, requires a modest heat input for regeneration and promotes less corrosion [40].

3.1.1.2 Cryogenic technology

Cryogenic technologies are high pressure but low temperature physical approach in which CO_2 is separated directly by condensing or by using a solvent such as a C_4 hydrocarbon. Cryogenic methods generally require the pressure of feed gas to be raised substantially. They offer an advantage of producing CO_2 at high pressure and partially reduce the compression cost when geologic disposal requires CO_2 to be at high pressure [40].

3.1.1.3 Physical Absorption

In physical absorption, CO_2 is physically absorbed in a solvent according to Henry's law and then regenerated using either or both heat or pressure reduction in which little or no energy is required. Typical solvents are Selexol (dimethylether of polyethylene glycol) and Rectisol (cold methanol). In general, physical absorption is considered when the partial pressure of CO_2 in the feed gases is greater than 0.35 MPa (50 psi), heavy hydrocarbon concentration is low and bulk removal of CO_2 is desired. This process was used in a gas treating facility to produce CO_2 for enhance oil recovery (that requires 98% CO_2 stream) use and food grade (that requires highly pure CO_2 stream) use from a raw natural gas containing 65% CO_2 by volume [41].

3.1.1.4 Membrane

Gas separation and gas absorption are the two types of membrane operations. Gas separation membranes work on the difference in physical and chemical interaction between gas components with the membrane material. This causes some gas components to permeate faster through the membrane than the other ones. CO_2, H_2, He and water vapor are generally more mobile gases. Therefore, as feed gases passes over the membrane at some set pressure, the permeate gases on the lower pressure side of the membrane have higher concentration of CO_2 than in the feed gases.

Gas absorption membranes are used as contacting media between the feed gases flow and absorption fluid flow. The absorption fluid selectively removes certain gas components from the feed gases on other side of the membrane. The membranes simply provide a contacting area without mixing feed gas and liquid flow. The gas absorption membranes have no selectivity to gas components like gas separation membranes. The absorption fluid could be amine solutions [40].

3.1.2 Dehydrating CO_2

The separation processes generally cannot produce pure CO_2. Other gases such as water vapor could be present in the CO_2 stream. CO_2 must be dried in order to make it suitable for transportation. Dehydration has the dual purpose of preventing both corrosion and formation of hydrates. CO_2 hydrates can form in the presence of free water (when water content exceeds its saturation level) at pipeline operating pressures and temperatures up to about 11°C [40]. These solids can create numerous operating problems such as plugging equipment and flow lines and fouling heat exchangers.

3.2 Transporting CO_2

3.2.1 Compressing CO_2

In order to transport CO_2 in a pipeline, it must be compressed to pressures above 8 MPa (1200 psi) [40] to ensure that a single-phase flow is achieved while keeping the density high. Compressing CO_2 requires energy, which might be supplied by a CO_2 emission source. Figure 3.1 indicates the isothermal work requirement to compress the CO_2 at 35°C from an initial pressure of 0.101 MPa [42]. For instance, Ennis-King and Paterson [42] stated in their study that compressing 1 kg of CO_2 from 0.101 MPa (14.7 psia) to 12 MPa (1740 psia) requires 0.275 MJ. Assuming CO_2 emission rate at a coal-fired power plant is 0.8 kg/kWh ($2.2 * 10^{-7}$ kg/J), the CO_2 produced through power generation for compression is about 0.0605 kg. In other words, CO_2 production through compressor's power consumptions in this case is about 6.05 % of the CO_2 being compressed.

This number is lower if the energy comes from less CO_2 production types of power plants such as natural gas-fired. Higher intake pressure also saves compression energy over lower intake pressure.

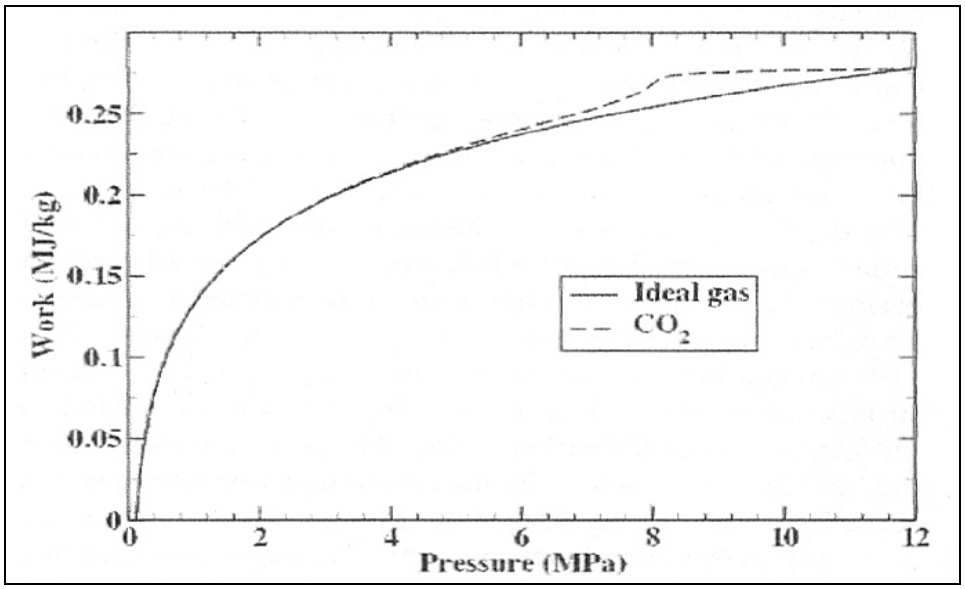

Figure 3.1 Isothermal work to compress CO_2 at 35° C [42]

3.2.2 Pipeline transportation of CO_2

Pipeline transportation of CO_2 is more appropriate solution since transporting CO_2 by truck or rail or combination of these two was ruled out as they are more expensive than pipeline, [43]**.** For pipeline transport, the most widely used operating condition is to maintain the CO_2 at pressure higher than its critical pressure (7.4 MPa) since at above the critical pressure, CO_2 exists as a dense single phase over a wide range of temperatures. CO_2 pipeline is usually operated at pressure between 8 and 17 MPa [40]. Operating the system with CO_2 in a single phase avoids problems associated with two-phase flow in the subsequent pipeline and injection stages. Two-phase flow induces

pressure surges and is more expensive because of the need for larger pipelines or the construction and operation of additional compression stations. The pipeline diameter is determined by several factors including entrance pressure at the beginning of the pipeline, required pressure at the end of the pipeline, maximum and minimum operating pressures, elevation, ambient temperature, pipeline length, CO_2 flow rate and whether boosting compressors are installed along the pipeline. Table 3.1 shows the operating pipeline capacities for CO_2 [44].

Table 3.1 Operating pipeline capacities for CO_2 [44]

Diameter	Flow Range	
mm	m^3/s	MMcf/d
168 (6 in)	8-10	23-31
219 (8 in)	16-21	48-64
273 (10 in)	28-38	84-115
324 (12 in)	43-55	130-168
356 (14 in)	56-77	170-235
406 (16 in)	75-108	230-330
507 (20 in)	131-180	400-550

3.3 Sequestration of CO_2

One possible solution avoiding the negative effects of CO_2 emissions in the atmosphere is to store or sequester CO_2 in a suitable environment. Sequestration is the removal of CO_2, either directly from anthropogenic sources, or from the atmosphere, and disposing of it either permanently or for geologically significant time periods. After the transportation, CO_2 must be injected into a suitable environment and monitored to complete the sequestration process.

CHAPTER 4

CO_2 SEQUESTRATION IN UNDERGROUND GEOLOGICAL MEDIA

4.1 Introduction

Carbon Dioxide is one of the hazardous greenhouse gases causing significant changes in the environment. Disposal environments for CO_2 sequestration can be divided into four different categories.

i. oceans,
ii. terrestrial basins,
iii. biological environment and
iv. geologic formations

Table 4.1 [35] shows the potential global capacities and carbon dioxide residence times for different carbon sinks**.** Figure 4.1 [48] indicates large potential worldwide storage capacity. Among these alternatives, underground geologic formations can be regarded as the best possible environment to sequester CO_2 because of the fact that storage of CO_2 in geologic formations is self-containing and volumetrically efficient. Utilization in Enhanced Oil Recovery (EOR) operations, disposal in depleted oil and gas reservoirs, replacement of methane in coal beds, injection in deep saline aquifers, and storage in salt caverns is the various alternatives to sequester CO_2 in geological media. To examine the potential of a sedimentary basin for CO_2 sequestration, tectonic setting and geology of the basin, the basin geothermal regime, the hydrodynamic regime of formation waters, the hydrocarbon potential and basin maturity economic aspects relating to access and infrastructure and socio-political conditions should be considered carefully.

Table 4.1 Potential global capacities and carbon dioxide residence times for different carbon sinks [35]

Sink	Capacity (GtC)	Retention (years)
Oceans	1000-10000[a], 50-350[b]	Up to 1000
Forestry	60-90	50
Agriculture	45-120	50-100
Enhanced oil recovery	20-65	Tens
Coal beds	80-260	>100000
Depleted oil and gas reservoirs	130-500	>100000
Deep aquifers	30-650[c]	>100000

[a] Estimated physical capacity, from [45].
[b] Assumes limitations through environmental considerations [46].
[c] Hendricks puts the total geologic capacity at up to 14000 GtC if structural traps are not required for secure storage [47].

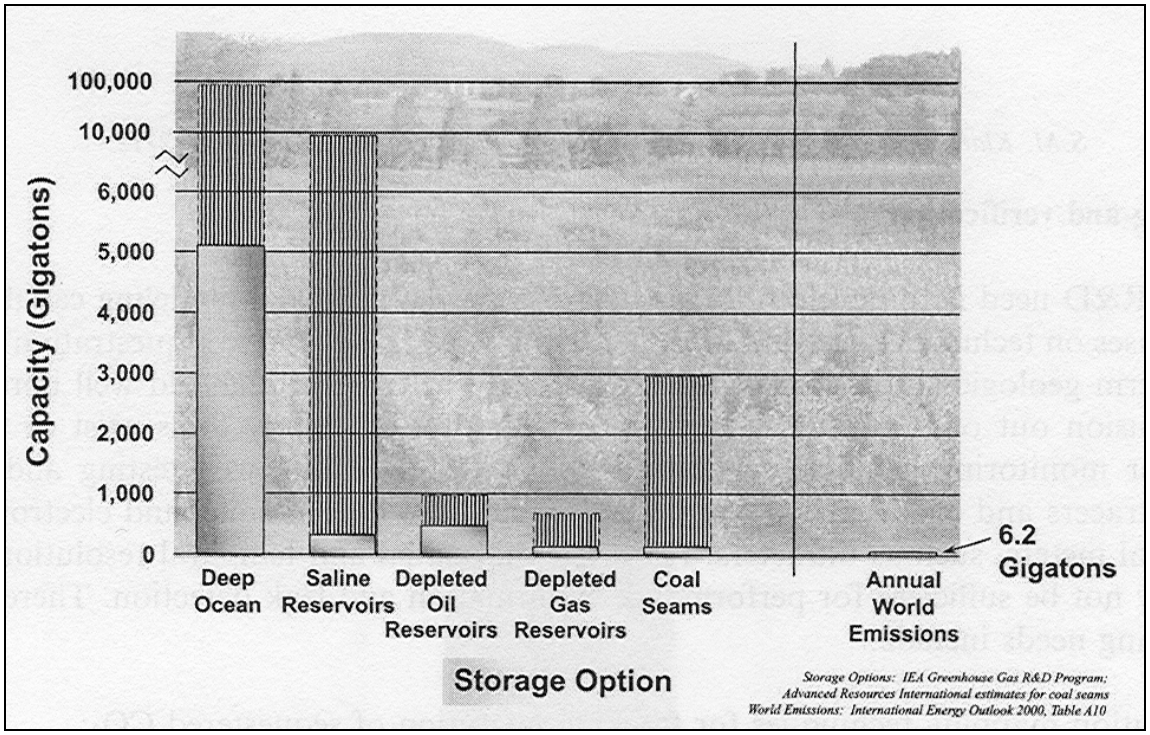

Figure 4.1 Large potential worldwide storage capacity [48]

Depleted oil and gas reservoirs may be two candidates for CO_2 sequestration. The trapping mechanism that retained hydrocarbons in the first place should ensure that CO_2 does not reach the surface. The proven trap, known reservoir properties and existing infrastructure make storage of CO_2 in depleted hydrocarbon reservoirs a simpler and cheaper option than other forms of CO_2 sequestration. As in the case of ocean disposal, EOR and Enhanced Gas Recovery (EGR) operations, most oil and gas reservoirs are not located near primary sources of CO_2 production; so new pipelines will be needed to connect the CO_2 sources with suitable sequestration sites [49].

Storage in salt caverns could provide a very long-term solution to CO_2 sequestration in geological media. The technology has been already developed and applied for underground storage of petroleum, natural gas and compressed air or for salt mining for public and industrial use. Currently, single salt caverns are up to $5*10^5$ m^3 in volume and can store fluids at pressures up to 80% of the fracturing threshold. Although salt and rock caverns theoretically have a large storage capacity, the associated costs are too high, and the environmental problems relating to rock and brine disposal are significant [49].

Injecting CO_2 into coal beds that are too deep or uneconomic for coal mining presents a twofold advantage [50]. First, CO_2 is sequestered by adsorption on the coal matrix. Second, methane is produced, which, although it is also a greenhouse gas, it can be used instead of coal as much cleaner fuel, implicitly reducing CO_2 emissions. Thus, depending on geological conditions, CO_2 sequestration in coal beds has potential for the mid to long term.

Carbon dioxide is a good solvent for organic compounds [51] because it reduces oil viscosity and the interfacial tension (capillary pressure). Based on this property, it was or is currently used worldwide in more than 70 tertiary EOR operations to increase oil mobility and to displace up to 40% of the residual oil left in active reservoir after primary production and water flooding [52].

Among these underground disposal alternatives, in the longer term, deep aquifers seem to be more preferable alternative for disposing the large quantities of waste gases. Their global distribution and their large disposal volume are appealing for disposal of waste fluids and gases, particularly from point emission sources [53, 54]. CO_2 is an ideal candidate for aquifer disposal because of its high density and high solubility in water at the relatively high pressures, which may be disposed in aquifers.

4.2 CO_2 Sequestration into Deep Saline Aquifers

Aquifers can be divided into two categories-freshwater aquifers (with less than about 1000 to 3000 mg/l of dissolved solids) and brackish or saline aquifers. Freshwater aquifers are mainly at shallow depths, where pressures are too low for economic storage of CO_2 as a high-density fluid. Deep aquifers contain fossil, high salinity connate water that is not fit for industrial and agricultural use or for human consumption. Such aquifers are already used for injection of hazardous and non-hazardous liquid waste. The high pressures encountered in deep aquifers indicate that they can withstand CO_2 injection. So, the most suitable aquifers for disposal of CO_2 are the deep saline aquifers in terms of volume, duration, economics and minimum or null environmental impact. Also, in these deep saline aquifers, for the temperature and pressure range of interest the supercritical state of CO_2 which is characterized by a gas type of behavior with a liquid type of density is the most desirable phase for the injection purposes.

In deep saline aquifers, CO_2 can be stored as free CO_2 in rock pore space previously occupied by phreatic water and displaced by the injected CO_2 (Structural Trapping). It can be chemically bonded with components in the rock (Mineral Trapping) or stored in water as a result of its solubility in water (Solubility Trapping). It is important to be able to predict the quantitative influence of these storage systems in a preliminary stage of developing an underground CO_2 storage project.

Structural and solubility trapping can be combined under the name of hydrodynamic trapping. As Bachu [55] stated, geological time-scale trapping of CO_2 in deep regional aquifers, caused by very low flow velocity, was named 'hydrodynamic' trapping because it depends on the hydrodynamic regime of formation waters. Some of the injected CO_2 (up to 29%) will dissolve in the water and the rest will form a plume that will over-ride at the top of the aquifer**.** While the dissolved CO_2 will travel with the velocity of formation waters (1 to 10 cm/year), the CO_2 plume will be driven both by the natural hydrodynamic flow and by its buoyancy with respect to water. Thus, the closer the density of CO_2 is to that of water, the lesser buoyancy effects that drive the flow of CO_2 in aquifers will be. CO_2 is hydrodynamically sequestered in deep saline aquifers for geological periods of time. This is because of the slow spreading from the injection well and hydrodynamic dispersion in the aquifer once outside the well radius of influence and of extremely long residence time due to the very low velocity of formation waters (less than 10 cm/year) [55, 56].

The numerical simulations carried out by Bachu and Law (1996) have shown that, depending on aquifer temperature; a significant amount of CO_2 dissolves into aquifer water (17-25 wt %) and travels within the hydrodynamic system in the aqueous phase. The rest of injected CO_2 remains in an immiscible supercritical phase, with the tendency of gravity segregation and override at the top of the aquifer because of lower density and higher mobility of the supercritical CO_2 phase than the aqueous phase. The CO_2 override increases with aquifer thickness. However, the supercritical CO_2 density increases and the mobility ratio decreases with depth, such that associated gravity segregation, overriding, and fingering effects become less important, even negligible. Because of different mobility, the advancing CO_2 front provides a large contact zone between the aquifer fluid and injected CO_2. Due to the generally low aquifer permeability, the CO_2 in either phase propagates less than 5 km away from the injection well after a period of 30 years [56].

Super-critical CO_2, with a density of approximately 0.6 times the density of typical brines, would be expected to rise to the top a formation because of buoyancy. Also, since CO_2 at prevailing underground pressures and temperatures often has lower viscosity than water, fingering would occur, that is, channeling and accelerated flow of the CO_2 phase relative to the native fluid. The CO_2 would tend to travel along the upper surface of the formation, moving rapidly in a geometry resembling fingers of flow out from the injection well and leaving behind pockets of the brine phase. Only a fraction of the native fluid in the aquifer would be displaced, and only a fraction of the aquifer volume would be filled by CO_2. The CO_2 would be expected to fill any trap it might encounter, since the CO_2 is lighter than the formation water. Eventually, the CO_2 would continue on and reach the edge of the formation and escape earlier than the time calculated for the native fluid. It has been estimated that possibly only 2-4 percent of the total volume of an aquifer would be filled CO_2 because of these unfavorable properties [57].

Carbon dioxide could also be permanently sequestered in deep aquifers by mineral immobilization, although extremely large periods of time are needed for sequestration through geochemical reactions.

The geochemical computer codes SOLMINEQ.88 [58] and PATHUBC.80 [59] were previously used to model water-rock reactions driven by the formation of carbonic acid when CO_2 is injected into deep aquifers; and it was found that mineral trapping depends on the mineralogy of the aquifer.

4.2.1 Criteria for CO_2 Sequestration into Deep Saline Aquifers

Meer [57] proposed that the storage system could be subdivided into four: the surface transport system, the injection system, the storage reservoir and the integrity of the total storage system. The density of the goods to be transported dictates the efficiency of any transport and/or storage system. For the temperature and pressure range of interest the supercritical state is the most desirable. For practical purposes a delivery pressure of 10

to 12 MPa at the injection location has to be assumed. CO_2 has to be delivered as pure as possible, the water content must be below 500 ppm by weight. Pure CO_2 as such is not corrosive. The presence of contaminants such as water (H_2O) and Sulphur Dioxide (SO_2) will enhance the corrosiveness of the fluid mixture. Water condensing from the CO_2 in the pipeline will cause serious problems and could lead to 'slugs' of the liquid being delivered at the CO_2 storage location. In general the CO_2 production site will be an average distance of 100 km from the storage location. For a CO_2 flow rate of 15000 ton/day (CO_2 emission of a 750 MW coal-fired power station) it was calculated that a line with a 600mm (24 inch) internal diameter would be needed. The pressure drop for this system was calculated to be less than 1 MPa. Using stainless steel for the transport and injection system is unpractical, for reasons of incremental cost.

According to Meer [57], for well injection rates of 1,500,000 Nm^3 the minimum diameter of the tubing is 5.5 inches. The aquifer should, by definition, possess intergranular pore space within the rock. Its constituent rock must be permeable to a fluid. The top of the aquifer must be located at a depth of at least 800 m.

CO_2 is disposed at supercritical conditions in order to avoid the separation of CO_2 into gas and liquid phases during injection process. A minimum depth of 2625 ft (800 m) is required to sustain the supercritical conditions of CO_2 with realistic subsurface conditions, i.e. a geothermal gradient of 30 °C/km and a pressure gradient of 10.5 MPa/km [60].

The sizes of the reservoir, the injection rate, the porosity and the density of CO_2 are the parameters, which determine the CO_2 storage capacity of the reservoir. But, CO_2 storage capacity depends strongly on the injection rate. At high flow rates the displacement is dominated by viscous forces and CO_2 flows rapidly through the most permeable paths, and the storage capacity reaches a constant lower limit. At lower rates gravity forces dominate the flood. The displacement front becomes stabilized, and after drainage of water increases the storage capacity further. The storage capacity is also sensitive to

permeability. Well perforations and gridding of the reservoir had less influence on the storage capacity of CO_2. Simulated storage capacities for CO_2 injection into an aquifer vary in the range 13-68 % pore volume, depending on the prevailing displacement mechanisms [61].

The permissible injection flow rate depends on the rock permeability in the aquifer. If the permeability is low, the injection rate must be kept low to avoid excessive pressure. A pressure that is too high can cause either fracture of the cap rock and loss of containment or leakage around the injection well, or other wells nearby, within the cone of influence. Multiple injection wells will undoubtedly be required. The CO_2 emitted from one moderately sized power plant is too much to be injected into underground storage sites through a single well [62].

4.3 Physical Properties of CO_2

At normal atmospheric conditions, CO_2 is a thermodynamically very stable gas heavier than air. The phase diagram of pure CO_2 shows a critical temperature of 31°C and a critical pressure of 7.38 MPa. Below this temperature and/or pressure the CO_2 is either in a liquid or vapor phase, as can be seen in Figure 4.2, [63]. At temperatures and pressures above the critical values the pure CO_2 is in supercritical state. At these pressure and temperature conditions, CO_2 behaves still like a gas by filling all the available volume, but has a 'liquid' density that increases, depending on pressure and temperature, from 200 to 900 kg/m^3 Figure 4.3 [64, 65], thus approaching water density. CO_2 is soluble in water; its solubility increases with pressure and decreases with temperature and water salinity. The supercritical CO_2 is immiscible in water [64, 66]. At low temperatures and elevated pressures, CO_2 forms a solid hydrate heavier than water. Another important property of CO_2 is its affinity to coal, which is almost twice as high as methane, a gas abundantly found in coal beds. Depending on reservoir temperature and original pressure, CO_2 can be stored as a compressed gas, liquid or in supercritical phase.

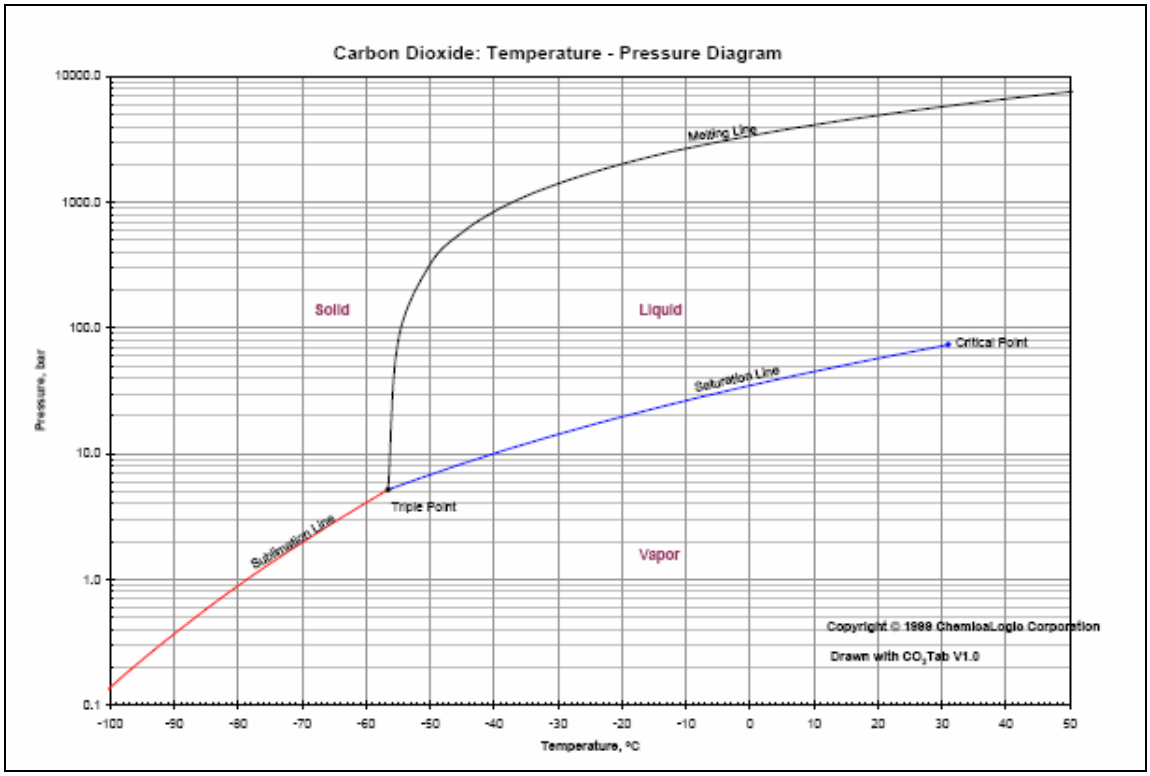

Figure 4.2 Phase Diagram of CO_2 [63]

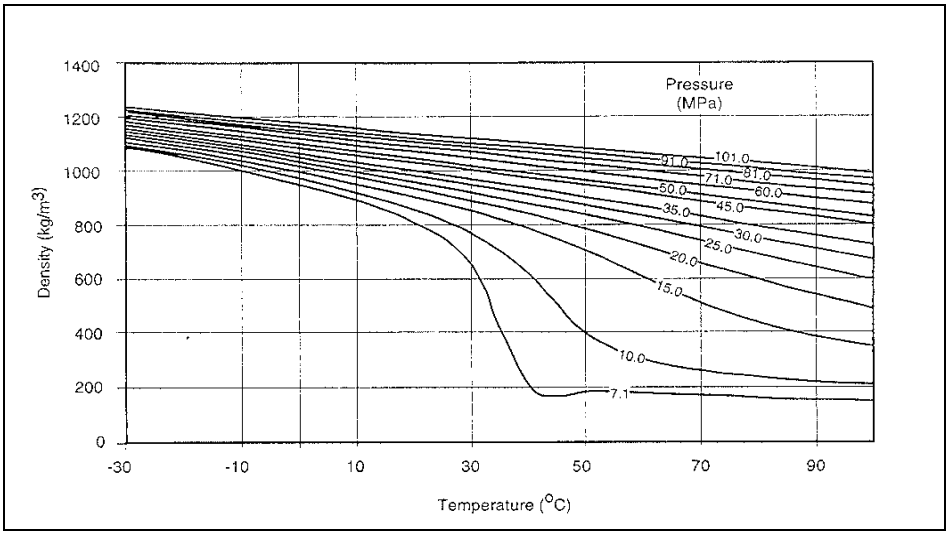

Figure 4.3 Variation of liquid CO_2 density as a function of temperature and pressure [64, 65]

4.4 CO_2-Water Rock Interactions

4.4.1 CO_2-Water System

Formation water properties are controlled by pressure and temperature, which vary in sedimentary basins from atmospheric conditions to more than 100 MPa and 300°C, respectively, and, on the type and amount of dissolved solids and gases such as CO_2 and CH_4. The salinity or total dissolved solids (TDS), of formation waters vary over a wide range, reaching in excess of 350000 mgL^{-1} [67]. The effect of dissolved gas on water density and viscosity can be negligible because the amount of dissolved gases is usually small whereas salinity and temperature are the major parameters that affect water density and viscosity. For a given driving force, the flow rate and injectivity depend also on viscosity.

The chemical character of any water depends on the original water composition and rock mineralogy, and is the product of time-dependent processes, such as rock-water interactions and transport processes, i.e. diffusion, dispersion, mixing, and convection.

Waters from basins worldwide have been subdivided into three major types. Waters with TDS lower than 10000 mgL^{-1} usually contain major anions other than Cl^-, e.g. Na-HCO_3 or Na-SO_4 waters. The second, most prevalent water type is characterized by NaCl, but is not saturated by halite. Hyper-saline brines, with salinity greater than 300000 mgL^{-1}, contain mostly Cl^-, and Na^+, with a varying proportion of Mg^{+2}, K^+, and Ca^{+2} [67].

Seven published, widely-used in modeling studies of basin evolution, hydrocarbon migration and accumulation of mineral deposits and geothermal reservoirs, expressions for the density of brine or NaCl solutions are presented in Table 4.2 by giving the applicability range of various algorithms for calculating brine density [68]. All algorithms describe an increase in water density with increasing salinity. Over a range of 0-30 wt% NaCl, water density increases more than 200 kgm^{-3}, or approximately 20% of fresh water density at laboratory conditions (STP).

Table 4.2 Applicability range of various algorithms for calculating brine density at various temperature, pressure and salinity conditions [68]

Study	Fluid	P (MPa)	T (°C)	S (mg L^{-1})‡
Rowe & Chou (1970)	NaCl solution	≤35	20–150	≤330 000
Phillips *et al*. (1981)	NaCl solution	≤50	10–350	≤260 000
Gill (1982)	seawater	≤100	≤40	≤42 000
Kemp *et al*. (1989)	electrolyte solution	≤100	≤174	≤600 000
McCain (1991)	brine	0.69–69	≤127	≤450 000
Batzle & Wang (1992)	NaCl solution	5–100	20–350	≤320 000*
Palliser & McKibbin (1998b)	NaCl solution	0.1–300	0–374.15	≤1 000 000†

*Estimate of maximum salinity determined from published graphs; †Equilibrates with solid NaCl; ‡As determined at 25 °C and 1 atm.

In the subsurface, elevated temperatures reduce brine density, whereas higher pressure increases density [68].

Water or brine viscosity is strongly dependent on temperature (decreases with increasing temperature), less dependent on salinity, and almost negligibly dependent on pressures (increases with increasing salinity or pressure) [68].

For the formation water density**,** the McCain [69] and Batzle & Wang [70] algorithms seem to be the most versatile. For viscosity, the Kestin [71] algorithm seems to be the most versatile for basin conditions. These algorithms are explained in detail in the subjected papers.

If carbon dioxide is dissolved into either brine water (i.e. TDS is greater than 100,000 mg/l) or brackish water (i.e. TDS lies between 1000 and 10,000 mg/l) with no formation minerals present, no new minerals are precipitated. The water becomes more acidic and

the amount of dissolved carbon dioxide is only a function of pressure and of fluid composition. A salting out effect occurs as the water becomes more concentrated.

CO_2 was numerically dissolved stepwise into the brackish formation water of ionic strength 0.063 at 25°C. A CO_2 pressure of 15 MPa was reached after 4 moles CO_2 had been added to each 1000 grams of water whereas the total CO_2 added to reach a CO_2 pressure of 15 MPa is approximately 2 moles per 1000 grams of water for the brine formation water (ionic strength 4.0), just half of the amount added to the brackish formation water. This salting out effect is due to increasing importance of hydration with salt content. As the ionic strength of the formation water increases to that of brine, the activity coefficient of H_2CO_3 increases from 1 to 2. Obviously to maximize CO_2 solubility, dilute formation waters are favored [72].

4.4.2 CO_2-Rock System

As previously stated, stored CO_2 may also react with the solid porous medium. The amount of CO_2 consumed in this manner depends on the mineralogy.

Carbonate aquifers were found to be limited in the quantity of CO_2, which can be trapped by mineral reaction. The reactions between CO_2, water and aquifer solids in the carbonate aquifers can be described in two steps: dissolution of calcite and adsorption of dissolved calcium on clays. The dissolving CO_2 is neutralized to form bicarbonate ion due to the buffering action of carbonate dissolution, whereas the effect of ion exchange is to minimize the amount of dissolved calcium. In both cases the amount of reaction is small [73].

Siliciclastic aquifers were predicted to have the best potential for trapping CO_2 when they contain an assemblage of basic aluminosilicate minerals such as feldspars, zeolites, chlorites and smectites, which consume acid. When reacted with CO_2, they break down to form kaolinite and CO_2 is neutralized. Neutralization of CO_2 results in substantial

trapping and immobilization of CO_2, such that there is no possibility of the CO_2 reaching the surface [73].

Both the water-rock experiments and modeling [74] indicate that geochemical-trapping reactions of CO_2 are slow on the order of tens to hundreds of years.

If carbon dioxide is dissolved in a fluid in equilibrium with a carbonate formation (the formation mineralogy is comprised of calcite and/or dolomite), the total amount of CO_2 dissolved into the fluid is greater than the amount of CO_2 dissolved in the brine. In fact, the formation carbonate minerals dissolve into the fluid and partially neutralize the acid created by the addition of the carbon dioxide. The dominant reaction for calcite can be written as:

$$CO_2 + H_2O + \text{Calcite} = Ca^{++}\ (\text{ion}) + 2HCO_3^-\ (\text{ion}) \qquad (4.1)$$

Depending upon the specific formation water chemistry, reaction of a carbonate formation can result in an increase of dissolved carbon dioxide by 1 to 4%. If clays are present with a high cation exchange capacity, they will buffer the calcium and magnesium in the formation water, allowing more calcite and dolomite to dissolve. This effect is most pronounced for low ionic strength formation waters where CO_2 capture can be increased to 2 to 8% [72].

Siliciclastic aquifers containing basic silicate minerals (i.e. anorthitic feldspar, chlorite, albitic feldspar and potassium feldspar) can absorb more CO_2 [74] than other aquifers through a complex set of water-rock reactions. These reactions can be summarized in a general sense by the reaction of feldspar and clay silicate minerals with CO_2.

$$\text{Feldspar} + \text{Clays} + CO_2 \rightarrow \text{Kaolinite} + \text{Calcite} + \text{Dolomite} + \text{Quartz} \qquad (4.2)$$

The maximum amount of CO_2 can be trapped in a siliciclastic aquifer containing brackish formation water. The amount of CO_2 trapped is dependent upon the amount of and type of basic minerals (feldspar and clays) present in the formation. Magnesium- and calcium-rich siliciclastic aquifers are favored for neutralization and trapping of the injected CO_2 through the precipitation of calcite (calcium carbonate), dolomite (calcium magnesium carbonate) or magnesite (magnesium carbonate). The amount of CO_2 captured can be increased through formation aqueous complexes and precipitation by more than a factor of two over solubility in brackish formation water. The exact amount depends upon the amount of available calcium and/or magnesium in the formation minerals and the pressure of CO_2. Sodium-rich siliciclastic aquifers will absorb CO_2, neutralizing it to form bicarbonate ions and thus converting the brackish chloride formation water to bicarbonate brine. The increase in CO_2 solubility due to formation of bicarbonate is only partially balanced by the salting out effect due to the increased ionic strength. Sodium-rich formation mineralogy may be favored, as a disposal site when the precipitation of carbonates minerals must be avoided. Potassium-rich siliciclastic aquifers equilibrate more rapidly than their sodium counterparts and only limited amounts of bicarbonate ion are formed. Thus, CO_2 capture is not enhanced significantly for potassium-rich siliciclastic aquifers.

In the near well region of a CO_2 injection well, permeability and porosity should increase in both carbonate and siliciclastic aquifers. Resolution of the permeability changes in a siliciclastic reservoir can only be addressed by physical simulation using core plugs under the actual conditions of aquifer disposal; where CO_2-charged water would be flowed through an aquifer core at different rates and the permeability changes monitored as a function of time [75].

In detail, Gunter [50, 72, 73, and 74] provides a comprehensive description of the mineral trapping of CO_2 through chemical reactions between aqueous and mineral species.

Reactions of the following types occur when CO_2 dissolves in water (aqueous phase):

$$CO_2\,(aq) + H_2O = HCO_3^- + H^+ \quad \text{(bicarbonate)} \tag{4.3}$$

$$HCO_3^- = CO_3^{--} + H^+ \quad \text{(carbonate)} \tag{4.4}$$

Where CO_2 (aq) is used to denote the CO_2 that is soluble in the aqueous phase. The above two reactions could be combined to yield the following:

$$CO_2\,(aq) + H_2O = CO_3^{--} + 2H^+ \tag{4.5}$$

Under favorable conditions, the carbonate ion CO_3^{--} will react with the different metal ions present in the formation water to precipitate carbonate minerals. Overall reactions for the most common carbonate minerals are:

$$CO_3^{--} + Ca^{++} = CaCO_3 \text{ (Calcite)} \tag{4.6}$$

$$2CO_3^{--} + Ca^{++} + Mg^{++} = CaMg\,(CO_3)_2 \text{ (dolomite)} \tag{4.7}$$

$$CO_3^{--} + Fe^{++} = FeCO_3 \text{ (siderite)} \tag{4.8}$$

$$CO_3^{--} + Mg^{++} = MgCO_3 \text{ (magnesite)} \tag{4.9}$$

Reservoirs that favor CO_2 precipitation in the form of carbonates minerals contain minerals that consume H^+ and produce metal ions (Ca^{++}, Mg^{++}, Fe^{++}). Consumption of H^+ will favor the formation of additional CO_3^{--} according to the chemical reaction (Eq. 4.5). The additional metal ions will combine with CO_3^{--} to precipitate carbonates according to the chemical reactions (Eq. 4.6). If the reservoir contains only carbonate minerals, there is neither consumption of H^+ nor release of additional metal cations, and therefore mineral trapping is small. Mineral traps for CO_2 are most effective in

reservoirs that have large protons sinks such as feldspar and clay minerals. Typical reactions for a sandstone reservoir containing of Quartz, K-Feldspar and Illite (clay mineral) are:

$$\text{Quartz} + 2H_2O = H_4SiO_4 \tag{4.10}$$

$$\text{K-Feldspar} + 4H^+ + 4H_2O = K^+ + Al^{+++} + 3H_4SiO_4 \tag{4.11}$$

$$\text{Illite} + 8H^+ + 2H_2O = 0.6K^+ + 0.25\ Mg^{++} + 2.3Al^{+++} + 3.5H_4SiO_4 \tag{4.12}$$

The ions H^+ and $CO_3^{- -}$ from the dissociation of CO_2 (aq) will react with the different minerals resulting in an overall reaction of the form [56, 72]:

$$\text{Feldspar} + \text{Clays} + CO_2 = \text{Kaolinite} + \text{Carbonate Minerals} + \text{Quartz} \tag{4.13}$$

The above reaction is similar to the weathering reactions of silicates [76] followed by the deposition of carbonate minerals. Gunter [50, 72, 73, 74] concluded from their modeling and experimental work that siliciclastic (e.g. sandstone) aquifers appear to be better hosts for mineral trapping than carbonate aquifers as far as CO_2 disposal is concerned.

4.5 Flow Dynamics during CO_2 Sequestration into Aquifers

Mathematical background behind the flow dynamics during CO_2 sequestration into aquifers can be defined by following equations proposed by Weir [77].

The conservation equations for heat, mass, and CO_2 flow in porous media can be described as follows;

$$\frac{\partial \rho_\beta}{\partial t} + \nabla . j_\beta = Q_\beta \qquad \beta = (\text{Energy, Mass, } CO_2) \tag{4.14}$$

Where the density terms (ρ) and fluxes (j) are given by

$$\begin{aligned}
\rho_{CO_2} &= \phi X_l \rho_l S + \phi X_v \rho_v (1-S) \\
\rho_M &= \phi \rho_l S + \phi \rho_v (1-S) \\
\rho_E &= (1-\phi)\rho_m U_m + \phi \rho_l U_l S + \phi \rho_v U_v (1-S) \\
j_{CO_2} &= \rho_l X_l q_l + \rho_v X_v q_v \\
j_m &= \rho_l q_l + \rho_v q_v \\
j_e &= \rho_l h_l q_l + \rho_v h_v q_v - K \nabla T
\end{aligned} \tag{4.15}$$

ϕ is the porosity, K the rock matrix thermal conductivity, Q_β is a source term, X_α is the mass fraction of CO_2 in the phase α=(liquid, vapor), ρ_α is the density of phase α, S is the liquid saturation, U_α is the internal energy of phase α, T is the temperature and P the pressure. The subscript m refers to the rock matrix.

The volume fluxes q_l and q_v are obtained from Darcy's equation;

$$q_\alpha = -k \frac{k_\alpha}{\mu_\alpha} (\nabla P - \rho_\alpha g)(\alpha = (liquid, vapor)) \tag{4.16}$$

The displacement process is affected by fluid properties at reservoir conditions, specific conditions of the rock matrix and depositional environment of the geological formation. In order to explain the dispersive character and the fluid flow mechanism of CO_2 in an aquifer system, these individual mechanisms affecting the displacement process should be well defined. The relative ability of the two fluids to flow in the porous medium is one of the most significant parameters in a displacement process.

When one fluid displaces another, the mobility ratio, M, of the displacement is defined as the mobility of the displacing fluid divided by the mobility of the displaced fluid. When CO_2 displaces water with a sharp interface, the mobility ratio can be defined as:

$$\frac{k'_{rCO_2} / \mu_{CO_2}}{k'_{rw} / \mu_w} = M \tag{4.17}$$

Where, k'_r = relative permeability at endpoint concentration and μ =viscosity

If $M \geq 1$ it means that, under an imposed pressure differential, the CO_2 is capable of traveling at a velocity equal to, or greater than, that of water.

In general, the dispersion or spreading out of CO_2 in an aquifer can be described at three different scales. The small-scale processes are active in the larger scale process but will play only a minor role.

- Displacement effects at microscopic scale
  - Molecular Diffusion
  - Microscopic Convective Dispersion
  - Longitudinal and Transverse Dispersion
- Displacement effects at macroscopic scale
  - Mixing of CO_2 and water by Dispersion
  - Longitudinal and Transverse Dispersion
- Displacement effects at megascopic scale
  - Displacement Regimes and Vertical Displacement
  - Viscous Fingering
  - Gravity Segregation

A CO_2/water displacement process at a shallow depth (500-1000 meters) will in the first place be dominated by a gravity segregation effect. Because of the large difference in the densities of CO_2 and water, CO_2 will force its way upwards in the reservoir. The second dominating effect results from the difference in mobility between CO_2 and water.

The concept of water displacement by CO_2 in aquifer can be illustrated with the help of Figure 4.4 [78]. Four distinct displacement types can be identified during the active injection of CO_2 storage. The part of the displacement profile labeled ‘A’ is typified by a shock front that results of CO_2 dissolving in water and being absorbed as a result of

geochemical reactions. Part 'B' of the displacement front is the result of the two-phase flow mixing. This dispersal of CO_2 occurs in the pore space of the reservoir rock and is largely affected by the non-uniform shape and sizes of reservoir sand or rock grains and the heterogeneity or the depositional environment of the aquifer. Part 'C' is typified by maximum CO_2 saturation in the presence of irreducible water. The part 'D' area is typed by a very high CO_2 saturation resulting from the absorption of water in the dry injected CO_2.

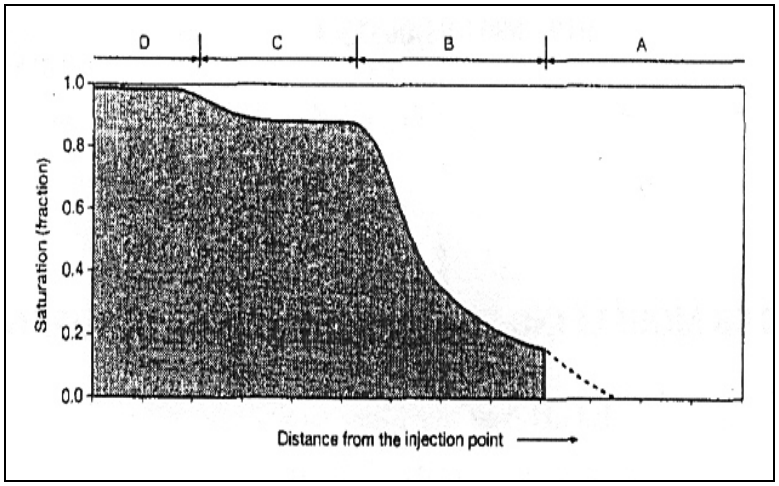

Figure 4.4 Displacement Concept [78]

4.5.1 Flow Instabilities

Carbon dioxide injection into saline aquifers can be classified as immiscible displacement of an aqueous phase by a less dense and less viscous gas phase. Because of the lower viscosity and density of CO_2 compared to water, the injection of CO_2 will have a tendency to produce hydrodynamic instabilities, leading to viscous fingering and gravity override, which results in enhanced dissolution and possibly poor sweep efficiency [79].

The displacement of one fluid by another in a homogeneous porous media is mechanically simple when the mobility ratio of the two fluids is less than or equal to one and when gravity does not influence the displacement by segregating the two fluids. For these conditions, the displaced fluid is moving efficiently ahead of the displacing fluid and the latter only penetrates the displacing fluid by dispersion. For mobility ratios greater than one, the displacement has a very different character. The displacing fluid front becomes unstable, and numerous fingers of displacing fluid develop and penetrate the displaced fluid in an irregular fashion. In the case of a CO_2 storage process these fingers will result in poor sweep efficiency and early breakthroughs of the CO_2 at possible spill points of a storage reservoir. Viscous fingering will dominate the displacement front at shallow reservoirs.

As stated before, for the injection process of CO_2 into aquifers, the minimum aquifer depths of approximately 800 m would be required to sustain a supercritical pressure regime. Figure 4.5 constructed by Pruess [79] shows the calculated CO_2 viscosity profile and the corresponding viscosity ratio (μ_{H_2O}/μ_{CO_2}) up to a depth of 2000m. For this calculation a temperature gradient of 3°C /100 m and surface temperature of 10°C was assumed. Below 800 m the viscosity contrast between CO_2 and water is moderate with a viscosity ratio ranging from 22 at 800 m, to 10 at 2000 m.

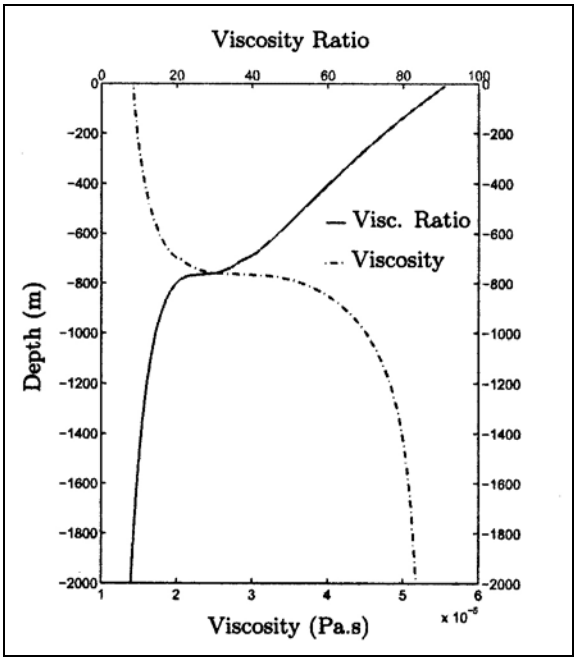

Figure 4.5 CO_2 Viscosity and viscosity ratio (μ_{H_2O}/μ_{CO_2}) [79]

4.6 Technical and Economical Feasibility of CO_2 Sequestration

CO_2 sequestration in underground geological formations involves separating of CO_2, dehydrating and compressing CO_2, transporting it by pipeline to injection site, re-compressing if applicable, injecting it into geological reservoirs and monitoring its movement and behavior after sequestration. Each of these processes should be carefully examined while evaluating the economic feasibility of the CO_2 sequestration project. For instance, in Australia, the costs of sequestration could vary from below US$5 to over US$20 per tone of CO_2, which largely depends on the amount of CO_2, distance and reservoir properties [40, 80] where as in Canada, disposal costs are approximately equal to $52 per tone of CO_2 ($2.67 per mscf of CO_2) [56].

Among the sources of CO_2 emissions, fossil-fired power plants and petroleum extraction activities are the main contributors of CO_2 emissions.

4.6.1 Capturing CO_2 from Power Plants, Petroleum and Extraction Process

Fossil-fired power plants emit CO_2 together with other gases such as nitrous oxides (NO_x), oxides Sulphur (SO_x), nitrogen (N_2), oxygen (O_2) and water vapor in the flue gas stream. The CO_2 concentration in the flue gas depends on whether the fuel is gas or coal, on particular power station technology and the age of the plant. For example, three fossil-fired power generation technologies such as pulverized coal fired (PF), natural gas fired combined cycle (NGCC) and Integrated gasification combined cycle (IGCC) generally release flue gas at different rates per Megawatt hour of electricity produced and have different CO_2 concentrations in the flue gas. Figure 4.6 [80] shows these three power station technologies in terms of gas flow rates.

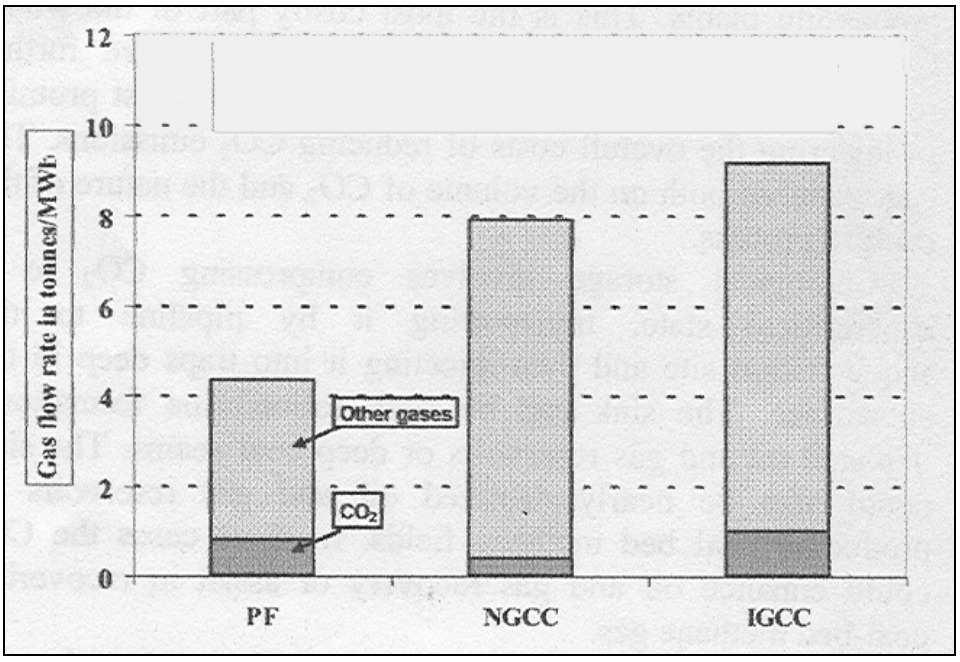

Figure 4.6 Flue gas flow rates for different types of power plants [80]

There are two options for capturing CO_2 from power plants. The first option is to separate CO_2 from flue gas and to store only CO_2. This would lead to higher capture cost but lower subsequent storage costs. The second option is to capture CO_2 together with other gases and then store the mixture. This can significantly reduce the unit capture cost. However, it requires higher transport and injection cost by comparison with storing only CO_2. This option would be economically attractive over the other option if the reduction in capture cost could outweigh the increase in storage costs. Another advantage is that storing CO_2 together with other gases such as SO_x and NO_x would result in the emission of fewer greenhouse gases [80].

The cost of capturing CO_2 from power stations is a function of the cost of the capture plant itself and the cost of electricity needed to operate the plant. Figure 4.7 shows the published capture costs of CO_2 [80].

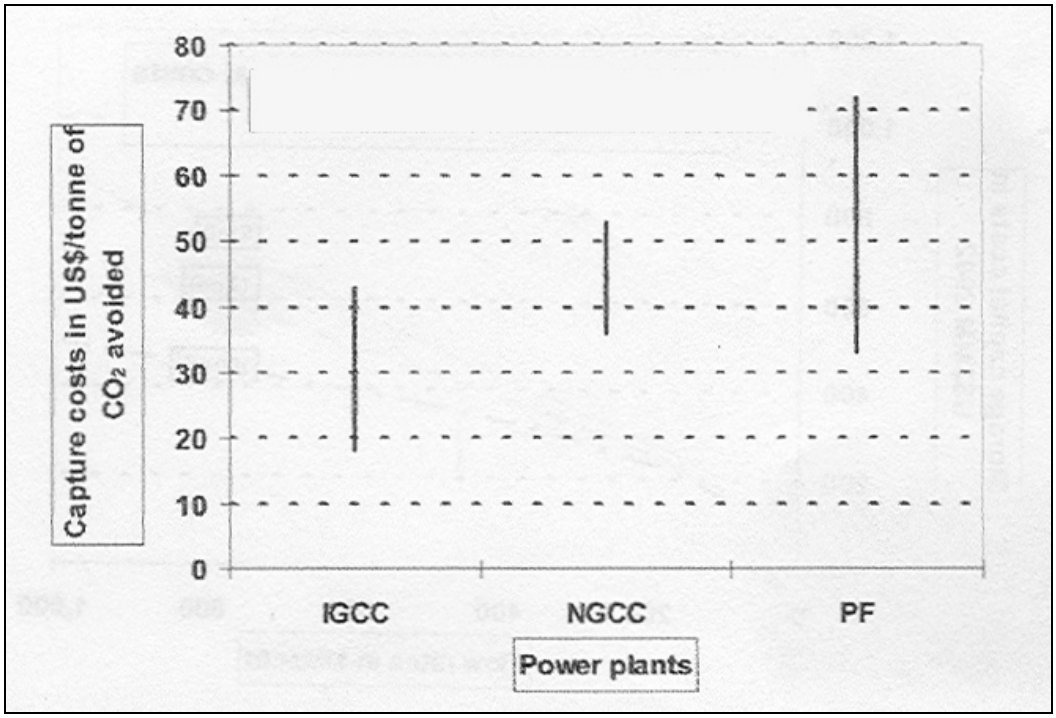

Figure 4.7 Published Capture Costs [80]

In addition to power stations, oil and gas extraction activities emit substantial amounts of CO_2 although not in such large quantities as are emitted by the power industry. The exhaust gas stream from a petroleum extraction process plant is often rich in acid gases such as CO_2 and H_2S. However, the acid-gas rich exhaust gas streams from a petroleum extraction process plant usually also contain water. Therefore the stream would require dehydration to avoid the need for expensive steels for subsequent transport and injection. Compression would also be required before the gas is transported and injected.

4.6.2 The Cost of Compression and Pipeline Transport

The cost of compression and pipeline transport is essentially a function of the rate of CO_2 throughput and the distance from source to sink. For an offshore pipeline, the cost also depends on water depth. A large rate of throughput or longer distance would result in higher-pressure losses. Therefore, it is required a bigger pipeline or more intermediate compressor stations. Installing intermediate pressure boosting stations is easier (and less expensive) for onshore situations. Intermediate compression offshore is more expensive because it requires additional platforms to house the additional compressors. In order to illustrate the relationships, Figure 4.8 indicates sequestration capital costs in terms of CO_2 flow rate for different distances in Australian conditions [40].

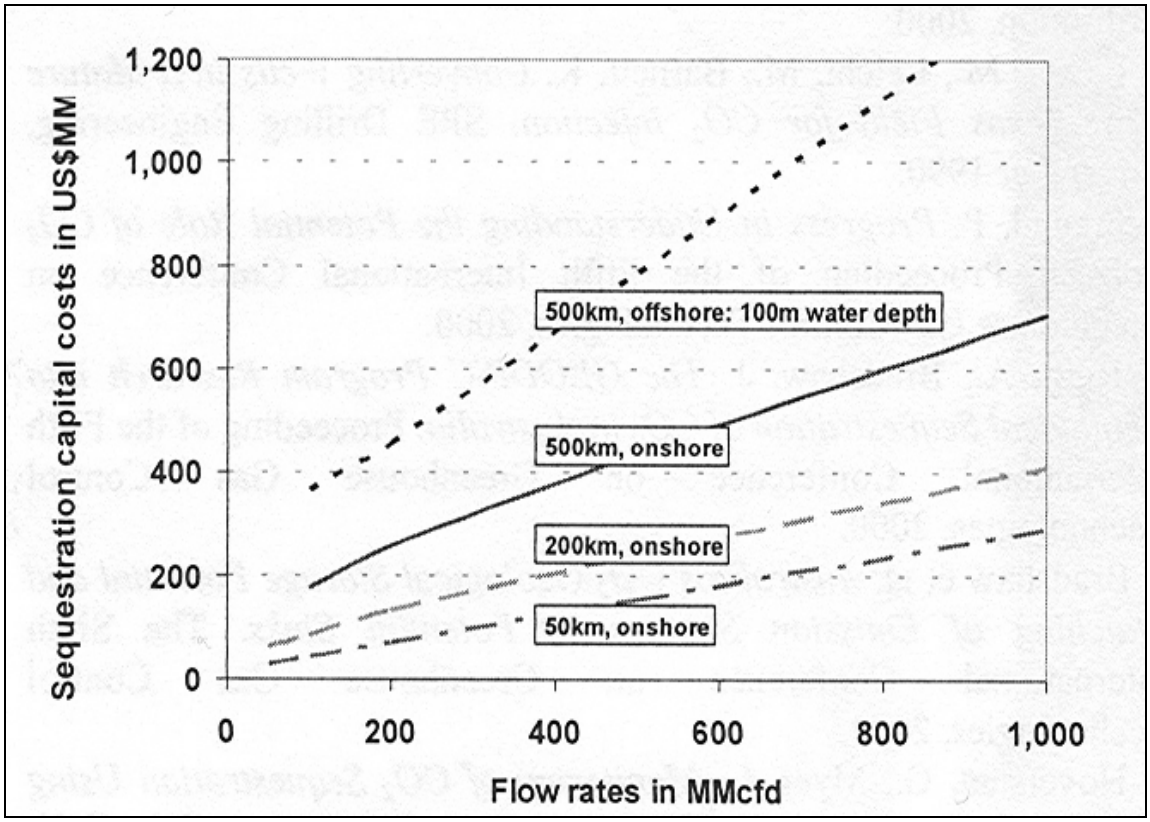

Figure 4.8 Sequestration capital costs against CO_2 flow rates and distances [40]

4.6.3 The Cost of Recompression and Injection

The capital expenditure includes well costs, recompression costs (if needed) and platform costs (as appropriate). The cost is highly dependent on the rate of throughput, the reservoir depth, the water depth (if offshore) and reservoir properties. Poor reservoir permeability (high injectivity), high reservoir pressure, a deep reservoir, or a high rate of throughput would require a large number of wells and therefore would be expensive. To investigate the relationships, Figure 4.9 shows sequestration capital costs against flow rates for reservoir permeabilities of 5, 10 and 100 millidarcies (assuming 500 km distance, onshore location) [40].

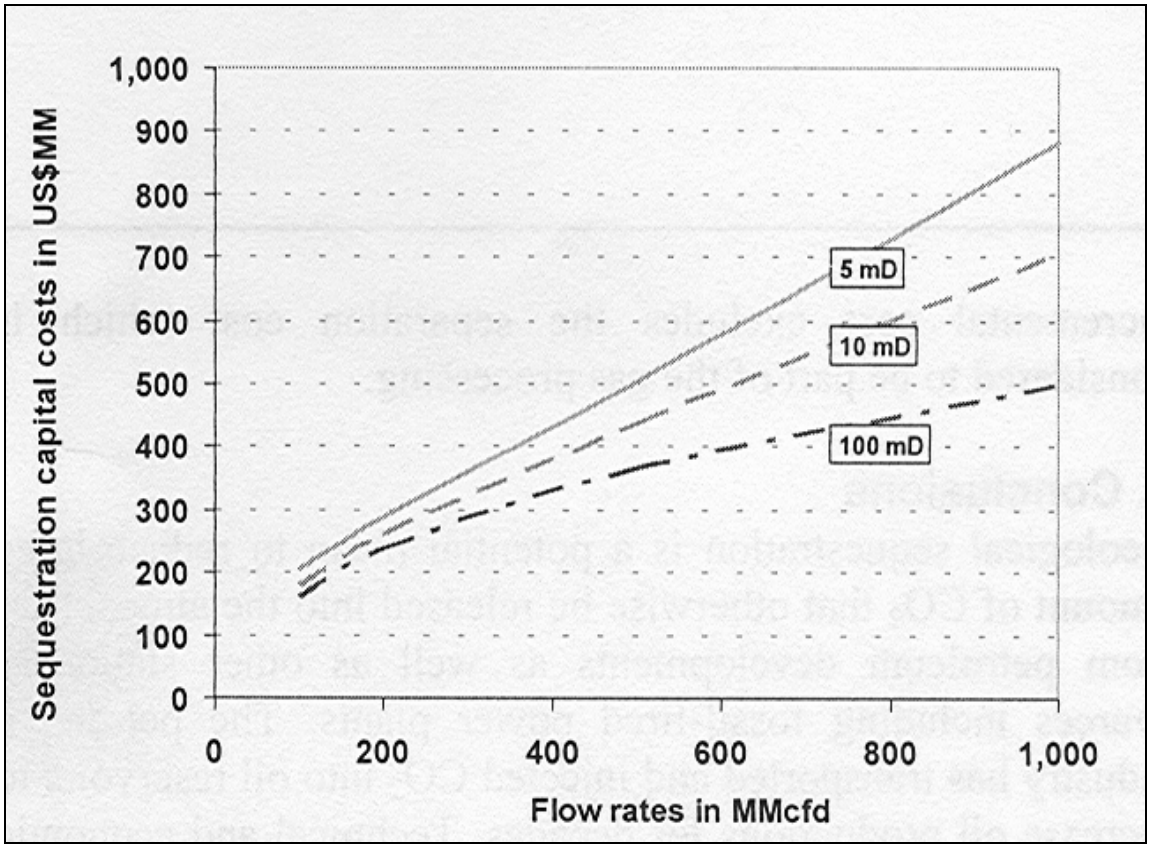

Figure 4.9 Sequestration capital costs against reservoir permeability [40]

In order to examine sequestration costs per tone of CO_2, Nguyen and Allinson's [80] studies of over 50 source and sink combinations in Australian show that sequestration unit cost (cost per tone of CO_2 sequestered) can vary from below US$5 per tone of CO_2 to over US$20 per tone of CO_2. The cost highly depends on throughput volume (the higher the volume the lower the unit cost), distance form source to sink and whether it is an offshore or onshore injection site. Figure 4.10 shows the effects of flow rate, distance and sink location on sequestration cost of CO_2 [40].

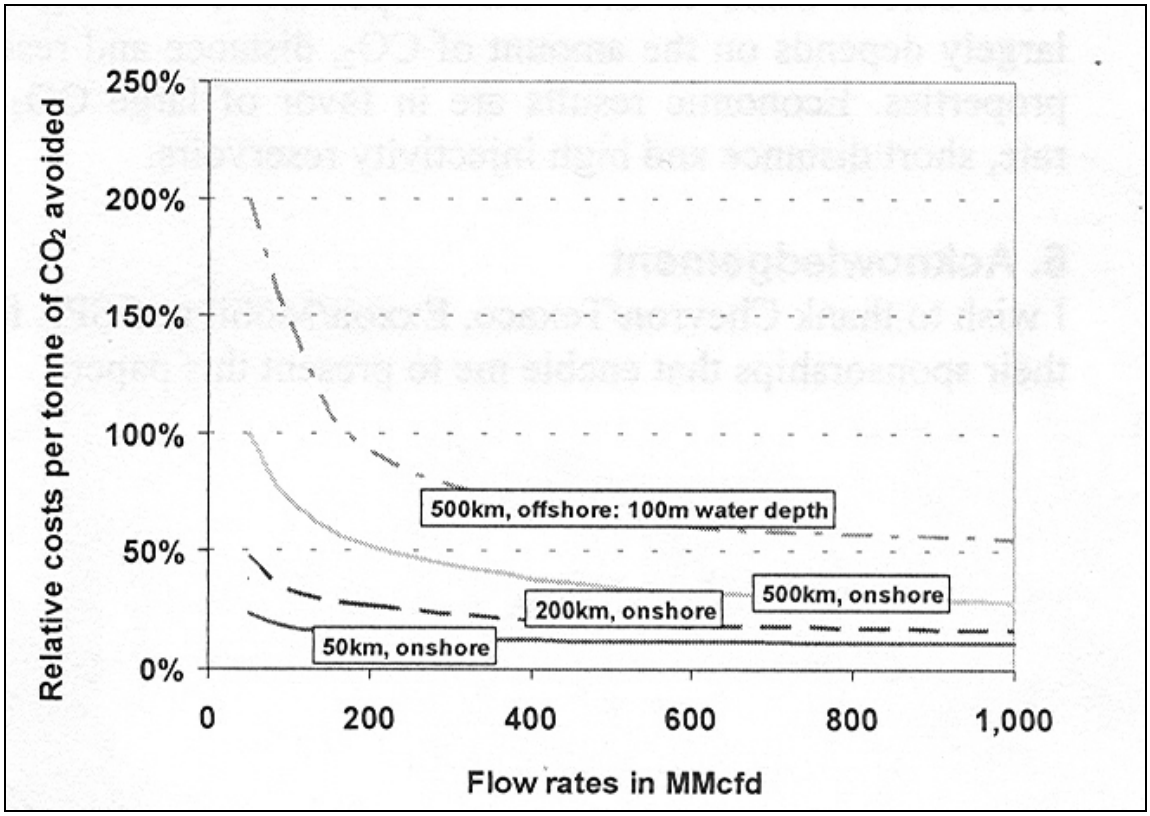

Figure 4.10 Indicative sequestration unit costs against flow rates and distances [40]

4.6.4 The Effect of Impurities on Sequestration Costs

Storing CO_2 with other gases called impurities will require more compression, or a larger pipeline, or more wells, or a combination of these. This will increase the capital cost by comparison with transporting and injecting only CO_2. Figure 4.11 indicates the cost per tone of CO_2 avoided when storing CO_2 with impurities against the cost of pure CO_2 storage [40].

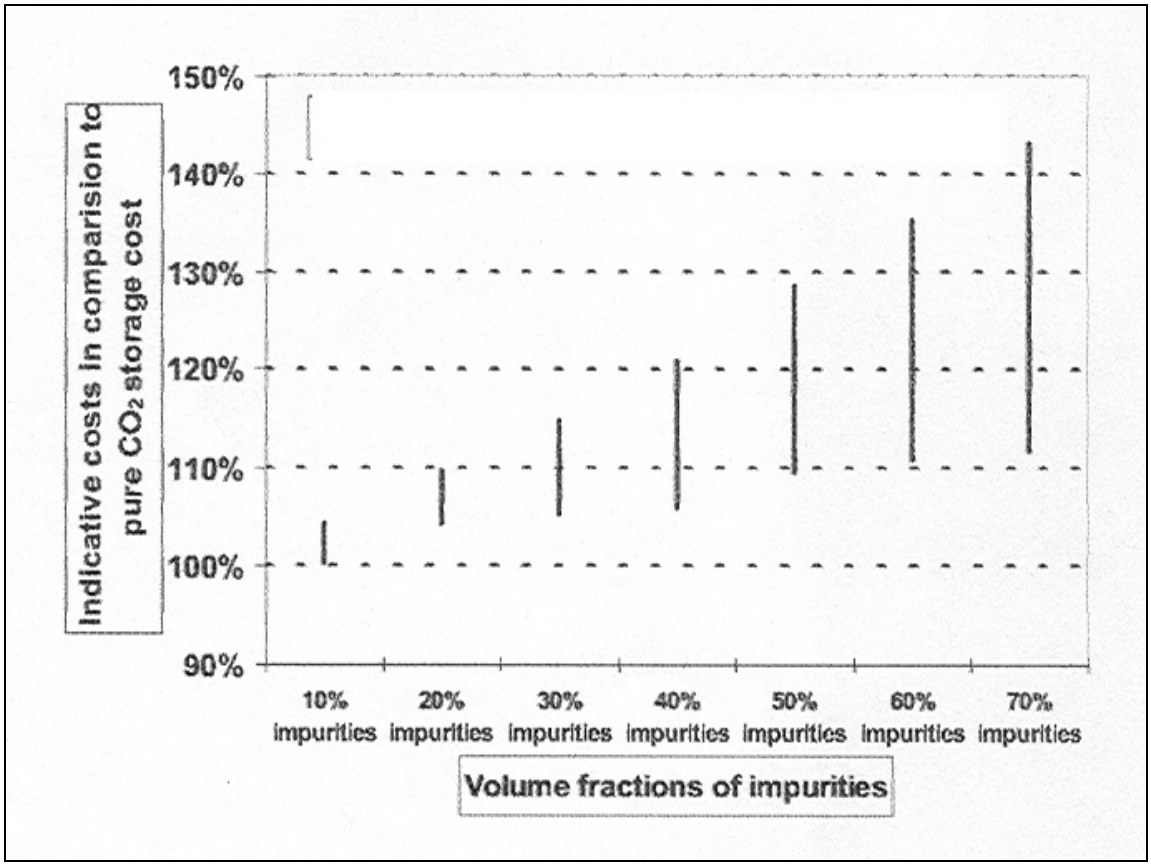

Figure 4.11 Indicative costs against impurities [40]

After analyzing the technical and economical view of CO_2 sequestration, it is needed to confirm practical considerations, such as economics, safety, stability, permanence and public acceptance. Monitoring and verification, health, safety and environmental risk assessment, knowledge base and technology for CO_2 storage reservoirs are the three major research trusts of the geologic sequestration activity.

4.6.5 Monitoring and Verification

A critical research and development project requires developing a comprehensive monitoring and modeling capability that not only focuses on technical issues but also can help ensure that geologic sequestration of CO_2 is safe. Many tools exist or are being developed for monitoring geologic sequestration of CO_2, including well testing and pressure monitoring; tracers and chemical sampling; surface and bore hole seismic; and electromagnetic/geo-mechanical meters, such as tilt meters. However, the spatial and temporal resolution of these methods may not be sufficient for performance confirmation and leak detection [48]. Further, monitoring needs to include high resolution mapping techniques for tracking migration of sequestered CO_2, deformation and micro-seismicity monitoring and remote sensing for CO_2 leaks and land surface deformation. For instance, Figure 4.12 indicates monitoring and verification mechanism applied by Department of Energy (DOE) carbon sequestration program [81].

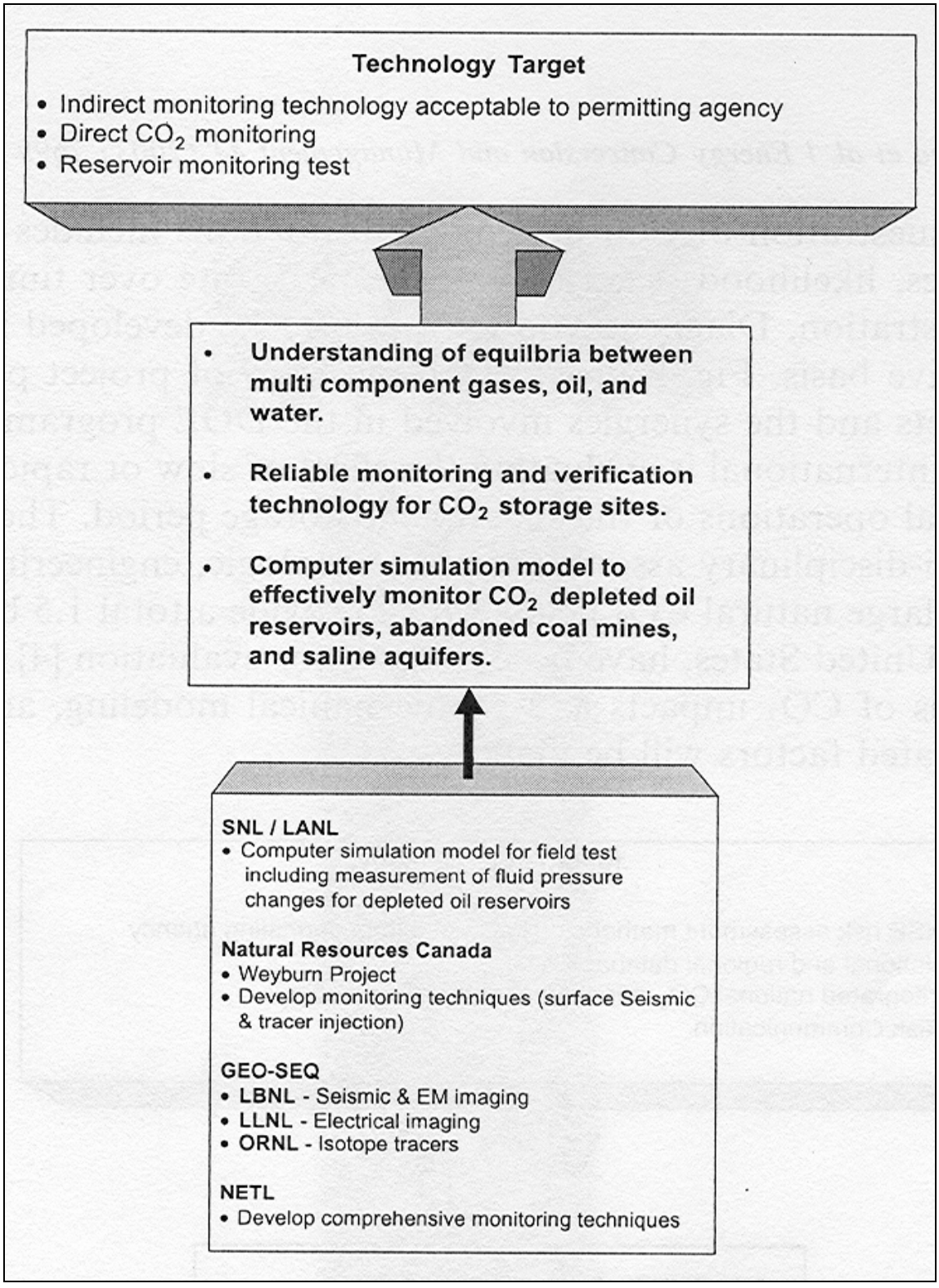

Figure 4.12 Monitoring and Verification (DOE) [81]

4.6.6 Health and Risk Assessment

Health, safety and environmental risk assessment is a process for identifying adverse health, safety and environmental consequences and their associated probabilities. The assessment of the risks associated with sequestration of CO_2 in geologic formations includes identifying potential subsurface leakage modes, likelihood of an actual leak and leak rate over time and long term implications for safe sequestration. For example, in Figure 4.13, approach, technology targets and synergies of Department of Energy (DOE) carbon sequestration program is identified [81].

To examine the knowledge base and technology for CO_2 storage reservoirs, the approach of DOE is illustrated in Figure 4.14 [81].

An integrated collaboration project applied by BP on CO_2 sequestration can be a good example for understanding the importance of monitoring and verification, health, safety and environmental risk assessment and knowledge base, technology for CO_2 storage reservoirs. In Figure 4.15 BP carbon capture project is shown [48].

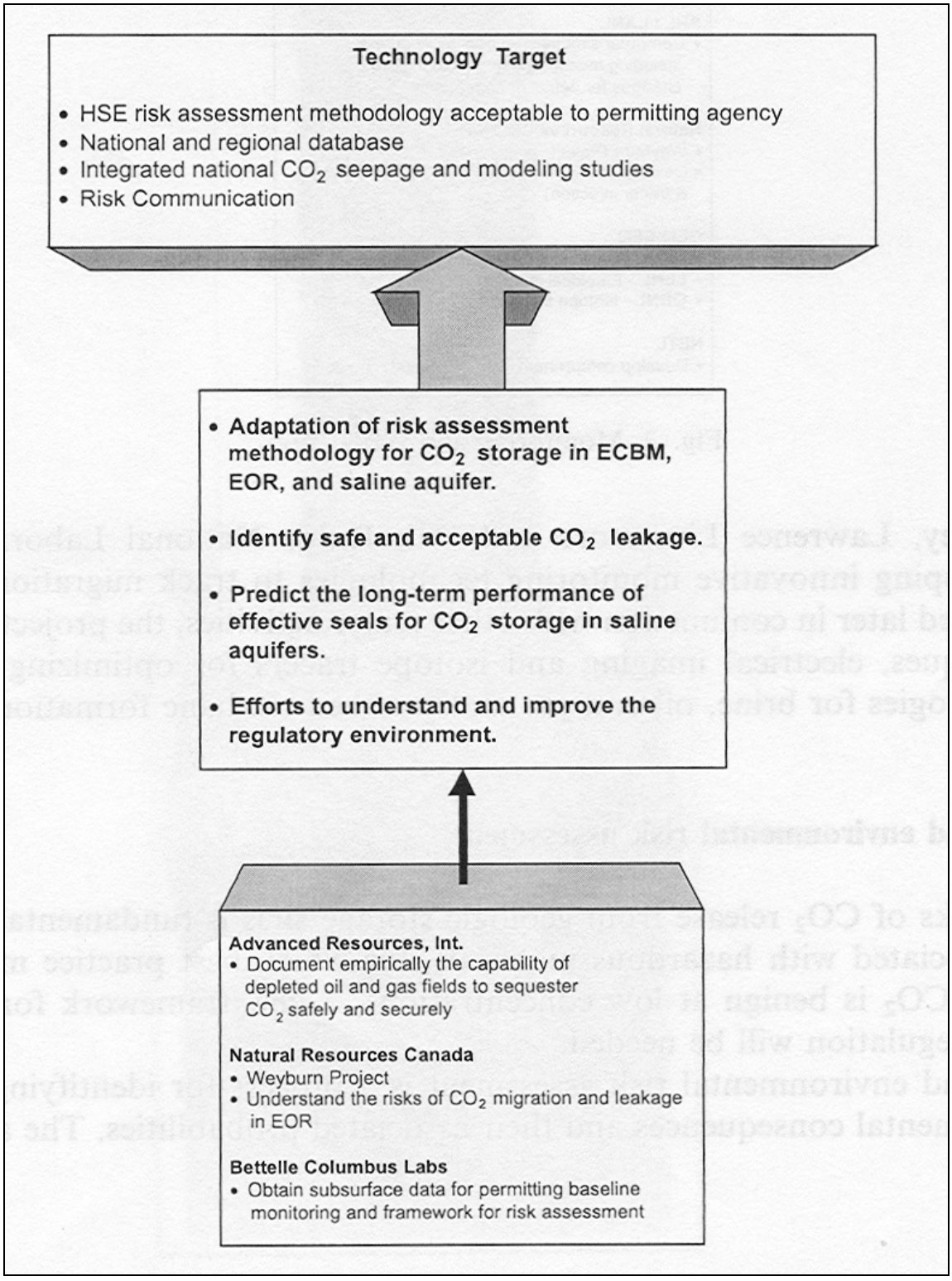

Figure 4.13 Health, safety and environmental risk assessment (DOE) [65]

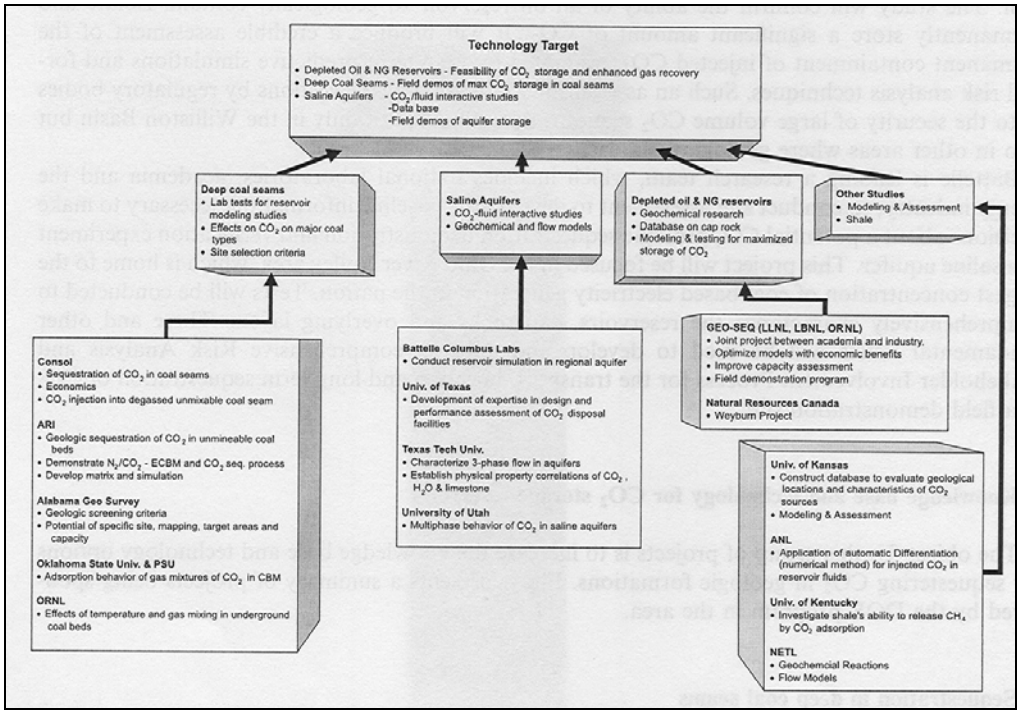

Figure 4.14 Knowledge base and technology for CO_2 storage reservoirs [81]

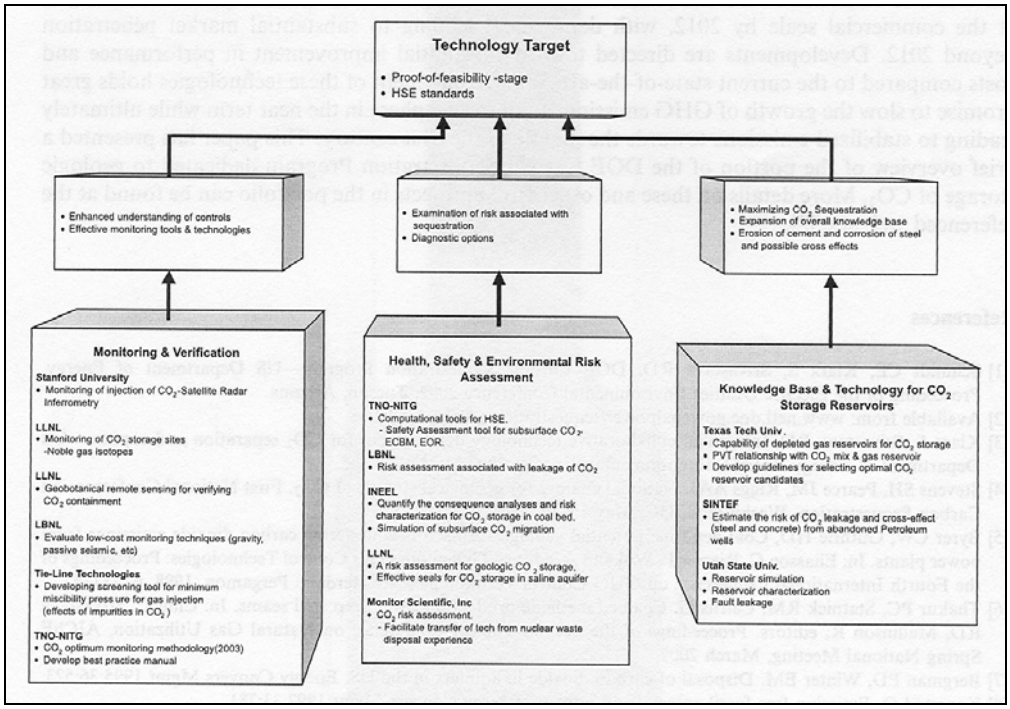

Figure 4.15 BP Carbon capture project (CCP) [48]

4.7 Modeling Studies of CO_2 Sequestration into Aquifers

The mathematical models suitable for modeling the displacement process consist of a set of differential equations for each grid cell, which describe the conservation of mass, and superficial velocity for each of the phases (water, oil, gas). A numerical solution technique can be developed to solve these equations using a finite difference presentation of these differential equations. The relationship between surface and the reservoir conditions are laid down in a set of PVT functions. These PVT functions contain the formation volume factors for three phases (water, oil, gas) and a relation of the gas-oil ratio, all as function of pressure. In addition to these three- phase simulators, compositional reservoir simulators, which are more complex forms of simulators, can simultaneously solve a set of mass and energy conservation equations and associated constraint equations for each of a number of grid cells representing a reservoir. A mass balance equation is written for each of the components Nc included in the process description, and an overall energy balance equation represents thermal effects. The constraint equations express the requirements that the saturation's must sum to unity and so must the mole fraction of components in each phase. The mass and energy balance equations are written in finite-difference form in order to use the most numerical efficient and stable formulation. These models describe mass transport by Darcy flow too, incorporating gravity, viscous and capillary forces. The density and viscosity of each of the phases are a function of that phase's composition, pressure and temperature. The transport of a phase in the simulator is controlled by the mobility in relation to other phases present. The phase's mobility is largely dependent on the phase's relative permeability [78].

4.7.1 Developed and Available Models for CO_2 Sequestration

There are several studies attempted to simulate CO_2 storage activities on a field scale. Three of the main studies are reported by Gunter [74], scientists at Statoil (Norway) and van der Meer [78]. All used different approaches to take account of the solubility of CO_2 in water. None had a direct solution for accounting for geochemical effects. All used

commercially available oil industry reservoir simulators. Gunter [74] used a four-phase, multi-component thermal Steam and Additive Reservoir Simulator (STARS) developed by the Computer Modeling Group in Calgary. In this model CO_2 was allowed to dissolve in water by user-defined K values. Statoil [78] used 3-dimensional, 3-phase and isothermal simulator (ECLIPSE of Intera) to predict the effects of a CO_2 storage operation. In normal use, this type of simulator is unable to simulate any absorption in the water phase. Statoil [78] ignored the water phase. They used the oil phase to simulate brine in an aquifer and the gas phase to simulate CO_2. This approach enabled them to use the Gas Solution Ratio (R_s) function to explain the CO_2 solubility in water. Van der Meer [78] used the same type of simulator (SIMBEST II, SSI). He used the gas-water option to simulate CO_2 storage. The gas and water phases are immiscible.

Comparing three main studies performed to simulate CO_2 storage activities results in the following observations [78]:

a. All three simulators are based on the Darcy flow equation and consequently phase movement is controlled by relative permeability. The use of relative permeability will guarantee a distributed phase interface (part "B" in Figure 4.4).

b. None of the simulators is able to simulate small-scale effects to reservoir scale. The main reason for this is the use of relatively large grid cells with average reservoir properties, which represent corresponding large sections of the reservoir.

c. The simulators were used for test problems of CO_2 injection in aquifers. At initial conditions the aquifers contained water only. In all three cases CO_2 injection was controlled either by well injection or a maximum injection rate. All injected fluids volumes were maintained in the reservoir. The only difference concerning the volumes of CO_2 in the reservoir is the tracking

method. Both Gunter [74] and Meer [78] subdivided the CO_2 in the reservoir into free CO_2 and CO_2 in solution in the water. Van der Meer was unable to make this distinction. But the total volumes of CO_2 in the reservoir were the same.

4.7.2 Aquifer properties and injection conditions for CO_2 sequestration

Several studies are reported [11, 57, 61, 72, 82, 83, 84] for CO_2 sequestration in saline aquifers. Table 4.3 shows the aquifer properties and injection conditions used in these modeling studies.

Table 4.3 Aquifer Properties used in modeling studies

Aquifer Properties	Krom (1993) [11]	Meer (1993) [57]	Gunter (1993) [72]		Holt (1995) [62]	Bachu (1996) [56]		Lindeberg (1997) [82]	Pruess (2001) [83]	Doughty (2003) [84]	
Formation	Carbonate	Carbonate	Carbonate	Sandstone	Sandstone	Sandstone	Carbonate	Sandstone	Sandstone	Sandstone	Sandstone
Depth (m)	1500	1800	2000	1400	2600	1480	1860	1200	2700	NA*	NA
Porosity (%)	30	30-36	10	10	23	6-12	6-12	30	12	30	25
Permeability (md)	NA	50-600	2	2	340	6	47	2000	100	200	80
Thickness (m)	100	50	100	100	185	13	60	160	100	100	12
k_v/k_h	NA	0.1	NA	NA	0.02	0.3	0.3	0.1	0.1	NA	0.4
Reservoir Pressure (MPa)	NA	NA	NA	NA	20	12.4	16	NA	10	18.8	15
Reservoir Temperature (°C)	35	NA	NA	NA	62	50	60	30	40	78	64
Salinity (g/L)	NA	NA	NA	NA	NA	40,000	190,000	NA	50,000	100,000	100,000
Well bore radius (m)	NA	0.1397	NA	NA	NA	NA	NA	NA	NA	NA	NA
CO_2 injection pressure (MPa)	20	10-12	15	15	NA	20	30	NA	26	NA	NA
CO_2 injection rate (t/d/well)	1000	2,500	NA	NA	3,900	2,000	11,800	16,438	30,000	1,863	250
CO_2 injection rate $*10^6$ (sm^3/d/well)	0.5347	1.337	NA	NA	2.0856	1.0695	6.31	8.79	16.043	0.9962	0.1337
CO_2 injection time (years)	30	20	NA	NA	25	30	30	25	30	20	0.05
Area (km^2)	200	1500	NA	NA	NA	900	900	5.5	1	1	0.20

* NA, not available

CHAPTER 5

STATEMENT OF THE PROBLEM

Carbon Dioxide is one of the hazardous greenhouse gases causing significant changes in the environment. The negative effects of CO_2 emissions in the atmosphere can be solved by sequestering CO_2 in a suitable environment. CO_2 sequestration into deep saline aquifers is one of the possible solutions.

Engineering design aspects of CO_2 sequestration into a deep saline aquifer will be investigated numerically. A case study will be simulated using the code **gem-ghg_200319d.exe** [17] one of the CMG software programs.

In this study, some of the aquifer properties of field-A [85] will be used. A field-scale aquifer and a single-well aquifer cases will be studied. Sensitivity analyses will be performed by analyzing the effects of parameters such as vertical to horizontal permeability ratio, initial reservoir pressure conditions, injection rate and salinity on the sequestration process.

CHAPTER 6

METHOD OF SOLUTION

In this study, a fully coupled geochemical compositional Equation-of-State (EOS) (GEM/CMG) simulator which can simulate all the important mechanisms of a miscible gas injection process, i.e. vaporization and swelling of oil, condensation of gas, viscosity and interfacial tension reduction, and the formation of a miscible solvent bank through multiple contacts was used to model CO_2 sequestration into deep saline aquifers [17].

6.1 GEM/CMG Compositional Simulator

This simulator models the following phenomena [86]:

1. Convective and dispersive flow in porous media
2. Phase equilibrium between oil, gas and aqueous phase
3. Chemical equilibrium for reactions between the aqueous components
4. Mineral dissolution and precipitation kinetics

GEM can be run in explicit, fully implicit and adaptive implicit modes. In many cases, only a small number of grid blocks need to be solved fully implicitly; most blocks can be solved explicitly. The adaptive implicit option selects a block's implicitness dynamically during the computation and is useful for coning problems where high flow rates occur near the wellbore, or in stratified reservoirs with very thin layers. Several options are provided for selecting implicit treatment [87].

GEM utilizes either the Peng-Robinson or the Soave- Redlich-Kwong equation of state to predict the phase equilibrium compositions and densities of the oil and gas phases, and supports various schemes for computing related properties such as oil and gas viscosities [87].

The quasi-Newton successive substitution method, QNSS, as developed at CMG, is used to solve the nonlinear equations associated with the flash calculations. A robust stability test based on a Gibbs energy analysis is used to detect single phase situations. GEM can align the flash equations with the reservoir flow equations to obtain an efficient solution of the equations at each time step [87].

CMG's WINPROP equation of state software can be used to prepare EOS data for GEM [87].

GEM uses CMG's Grid Module for interpreting the Reservoir definition keywords used to describe a complex reservoir. Grids can be of Variable Thickness - Variable Depth type, or be of Corner Point type, either with or without user-controlled Faulting. Other types of grids, such as Cartesian and Cylindrical, are supported as well as locally Refined Grids of both Cartesian and Hybrid type. Note that Hybrid refined grids are of a locally cylindrical or elliptical nature that may prove useful for near-well computations [87].

Regional definitions for rock-fluid types, initialization parameters, EOS parameter types, sector reporting, aquifers, are available. Initial reservoir conditions can be established with given gas-oil and oil-water contact depths. Given proper data (such as from WINPROP), fluid composition can be initialized such that it varies with depth. A linear reservoir temperature gradient may also be specified [87].

Aquifers are modeled by either adding boundary cells which contain only water or by the use of the analytical aquifer model proposed by Carter and Tracy [87].

Dual porosity modeling can be done with GEM. Each cell is assigned separate matrix and fracture pore spaces. Shape factors describing flow between porosities are implemented based on the work of Gilman and Kazemi [87]. Additional transfer enhancements are available to account for fluid placement in the fractures. The GEM user can also specify a dual permeability model which allows fluid flow between adjacent matrix blocks. This option is useful when matrix-matrix mass transfer processes are important, such as in situations dominated by gas-oil gravity drainage processes.

GEM uses AIMSOL, which is a state-of-the-art linear solution routine based on incomplete Gaussian Elimination as a preconditioning step to GMRES iteration. AIMSOL has been developed especially for adaptive implicit Jacobian matrices [87].

For almost all applications, the default control values selected by GEM will enable AIMSOL to perform efficiently. Thus, GEM users do not require detailed knowledge of the matrix solution methods [87].

GEM uses run-time dimensioning as well to make the most efficient use of computer resources [86].

Various types of Simulation Results Files can be written while GEM is running, including files for CMG's RESULTS. RESULTS is CMG's visualization software that can be used to examine 2-D and 3-D reservoir displays, as well as XY plots of important dynamic data [87].

GEM uses the data set that you create initially and then creates three other files. Each GEM run may create an output restart file (RST), an output Simulation Results File (SRF), and an output file [87]:

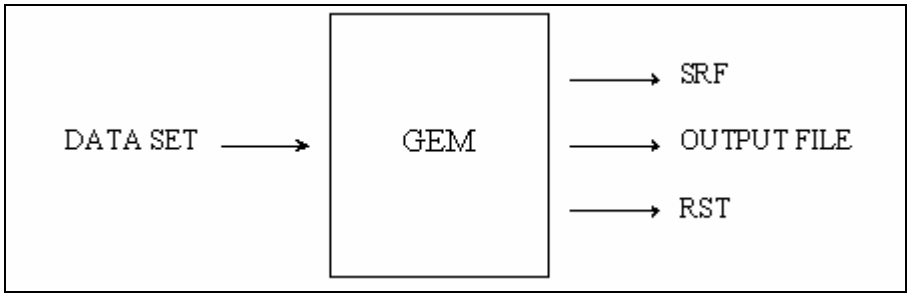

Figure 6.1 Sample Input and Output Data Configuration for GEM Simulator [87]

If a restart run is desired, then several existing files are needed and another three are generated. This is illustrated in the diagram:

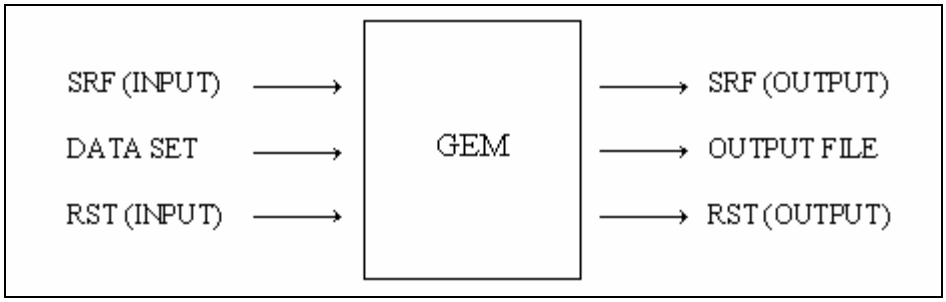

Figure 6.2 Sample Input and Output Data Configuration for Restart Run for GEM Simulator [87]

In the simulator, all equations are solved simultaneously for numerical robustness and stability [86]. In our study, it was applied to the simulation of typical field-scale CO_2 sequestration processes, showing the migration of CO_2 (g) and CO_2 (aq), the dissociation of CO_2 (aq) into HCO_3^- and its subsequent conversion into minerals. Convection of high-density plumes of CO_2-rich brine in conjunction with CO_2 mineralization around the plumes was also illustrated.

CHAPTER 7

AQUIFER DESCRIPTION

7.1 Aquifer Identification and Characterization

The aquifer properties of field-A [85] were used while developing the numerical model. The aquifer was studied in a field scale and a single well case. Figure 7.1 [88] was used in order to determine the storage pressures at a reference depth. Top of Mt. Simon structural contour map of field-A is given in Figure 7.2 [85].

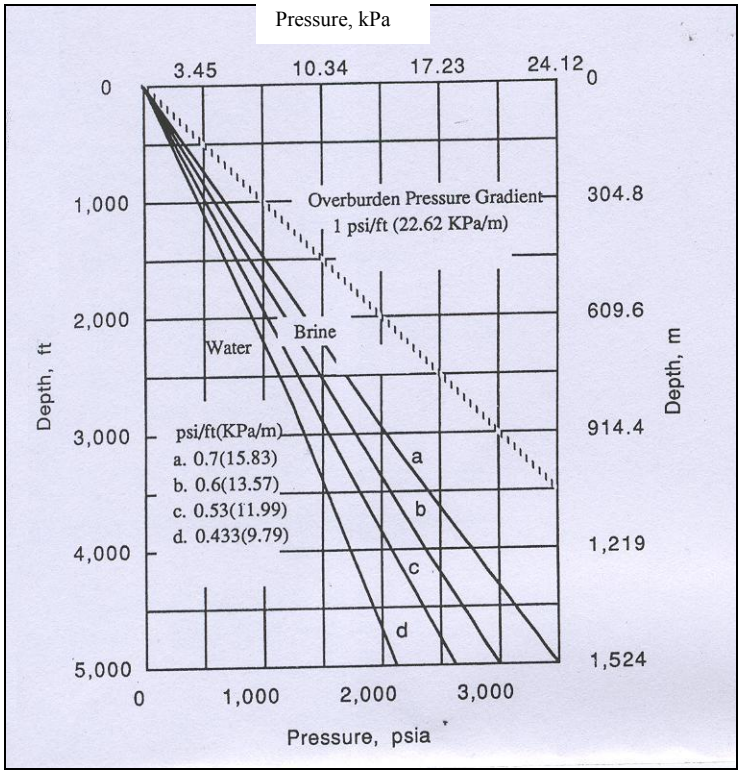

Figure 7.1 Pressure gradient for the brine [88]

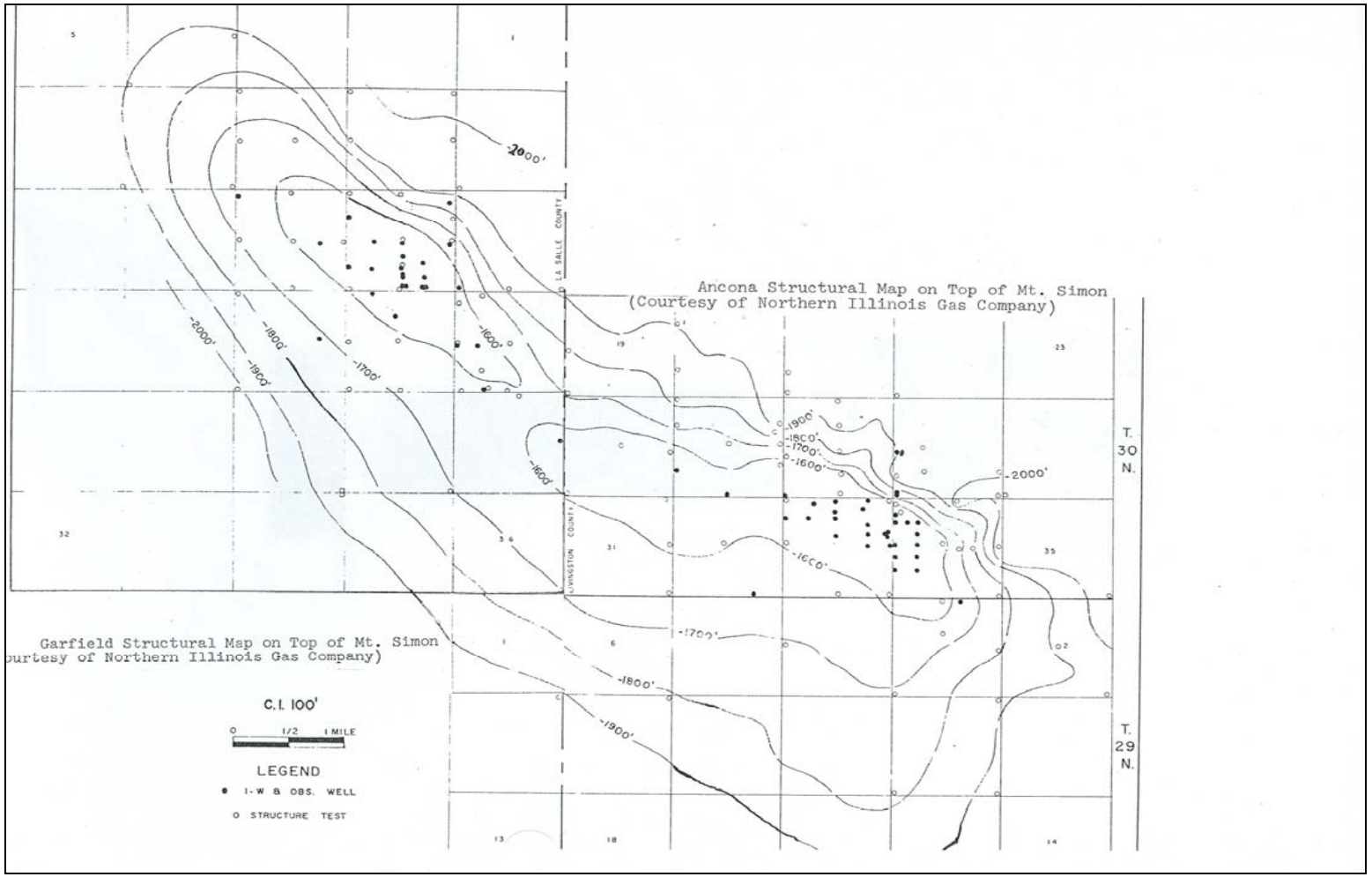

Figure 7.2 Top of Mt. Simon Structural Contour Map of Field-A [85]

7.1.1 Field-Scale Aquifer Model

The ranges for three layered aquifer parameters are summarized in Table 7.1.

Table 7.1 Aquifer Properties

Number of grids (X*Y*Z)	35*31*3
Horizontal permeability (md)*	
Layer-1	22-114
Layer-2	9-45
Layer-3	30-152
Vertical / horizontal permeability ratio	0.1
Depth of reservoir top (m)	850- 900
Total formation thickness (m)	182
Layer-1	41
Layer-2	30
Layer-3	111
Porosity, fraction	0.25
Reference pressure (kPa)	9100
Reference depth (m)	900
Storage Pressure (kPa)	15000
Total area (acre)	20000
Aquifer temperature (^{o}C)	33
Rock Compressibility (1/kPa)	1.0 E-08
Water Compressibility (1/kPa)	4.6 E-07

*The permeability data were distributed usig a geostatistical method (Krigging)

Based on the general stratigraphy in the sedimentary strata in this area, regional siliciclastic (e.g. sandstone) aquifer containing Calcite, Kaolinite and Anorthite formation minerals were identified at depth of 850 m for Mt.Simon.

The numerical model is based on some assumptions:

- CO_2 was injected at supercritical and gas phase conditions.
- Isothermal conditions were sustained during the injection and sequestration processes.

- Structural, solubility and mineral trapping processes were considered together.
- Porosity and permeability changes were ignored regarding the mineralization process.
- Adsorption of CO_2 on rock matrix was not taken into account during the storage of CO_2.
- No flow boundary condition was used around the confined aquifer.

The intra-aqueous chemical-equilibrium reactions and the mineral dissolution reactions are shown in Tables 7.2 and 7.3, respectively. The values of the rate constants k_β, reactive surface areas $\hat{A}_\beta$ and activation energies $E_{a\beta}$ were taken from literature [89]. The initial aqueous phase concentration and the mineral properties and initial volume fractions of minerals are also given in Table 7.4 and Table 7.5 respectively.

Table 7.2 Intra-aqueous chemical-equilibrium reactions [89]

	Reaction	**Chemical-equilibrium constants (log K_{eq}^{a})**
1	$H_2O = H^+ + OH^-$	-13.2631
2	CO_2 (aq) + $H_2O = H^+ + HCO_3^-$	-6.3221
3	$HCO_3^- = H^+ + CO_3^-$	-10.2342

Table 7.3 Mineral dissolution / precipitation reactions [89]

	Reactions	**log K_{eq}^{m} (50°C)**	**log k_β [mol/(m^2s)] at 25°C**	$\hat{A}_\beta$ **[m^2/m^3]**	**$E_{a\beta}$ [J/mol]**
4	Kaolinite + $6H^+$ =	5.4706	-13.0	17600	62,760
	$5H_2O + 2SiO_2 + 2Al^{+++}$				
5	Calcite + $H^+ = Ca^{++} + HCO_3^-$	1.3560	-8.79588	88	41,870
6	Anorthite + $8H^+$ =	23.0603	-12.0	88	67,830
	$Ca^{++} + 2Al^{+++} + 2SiO_2$(aq) + $4H_2O$				

Table 7.4 Mineral Properties [89]

Mineral	Chemical Formula	Molecular weight	Density (kg/m^3)	Volume fraction
Kaolinite	$Al_2Si_2O_5(OH)_4$	258.1616	2410	0.0176
Calcite	$CaCO_3$	100.0869	2710	0.0088
Anorthite	$CaAl_2Si_2O_8$	278.2082	2740	0.0088

For a field aquifer model, two successive cases (Runs 1a and 2a) were simulated. These cases have different aquifer pressures at the beginning of CO_2 injection. Table 7.5 summarizes some of the input data for these runs. For Run 2a, water was produced from the aquifer for 10 years to start with lower aquifer pressure at the beginning of simulation. By doing this, more CO_2 was planned to be sequestered in the aquifer. CO_2 was injected in gaseous phase for Run 2a since the pressure was decreased below the supercritical pressure of CO_2 (72 atm, 7295 kPa).

Table 7.5 Input parameters for a field aquifer model

Run ID		Initial Condition	Final Condition	CO_2 injection rate (sm^3/day/well)
	Pressure gradient	Brine 10.11 kPa/m (0.447 psi/ft)	Overburden 16.67 kPa/m (0.737 psi/ft)	
1a	Pressure at 900 m	9100 kPa	15000 kPa	220000
2a	Bottom hole pressure after water production	2800 kPa	15000 kPa	700000
Other properties	• Water salinity is 100000 ppm. • Aquifer temperature is 33 °C at 900 m depth. • Number of CO_2 injection well is 2. • Injection time is 30 years and simulation time is 200 years. • Variable permeability distribution in each layer and k_v / k_h is 0.1. • Number of grids [X*Y*Z, 35*31*3] is 3255. • Grid dimensions of runs 1a and 2a are given Table 7.6.			

Table 7.6 Grid Dimensions for a field scale aquifer model

Run		Field-Scale Aquifer Model (I)									
1a and 2a	**Grid Numbers**	**1**	**2**	**3**	**4**	**5**	**6**	**7**	**8**	**9**	**10***
	Grid Dimensions (m)	570	603	536	268	469	402	235	536	335	335
	Grid Numbers	**11**	**12**	**13**	**14**	**15**	**16**	**17**	**18**	**19**	**20**
	Grid Dimensions (m)	201	134	201	268	201	670	603	603	570	603
	Grid Numbers	**21**	**22***	**23**	**24**	**25**	**26**	**27**	**28**	**29**	**30**
	Grid Dimensions (m)	603	201	503	436	201	268	201	134	101	168
	Grid Numbers	**31**	**32**	**33**	**34**	**35**					
	Grid Dimensions (m)	369	335	201	603	570					
Run		**Field-Scale Aquifer Model (J)**									
1a and 2a	**Grid Numbers**	**1**	**2**	**3**	**4**	**5**	**6**	**7**	**8**	**9***	**10**
	Grid Dimensions (m)	335	570	603	637	603	570	704	67	134	67
	Grid Numbers	**11**	**12**	**13**	**14**	**15**	**16**	**17**	**18**	**19**	**20**
	Grid Dimensions (m)	536	134	168	335	101	168	704	670	235	536
	Grid Numbers	**21**	**22**	**23***	**24**	**25**	**26**	**27**	**28**	**29**	**30**
	Grid Dimensions (m)	268	570	201	335	402	402	268	603	570	670
	Grid Numbers	**31**									
	Grid Dimensions (m)	603									

* CO_2 Injector wells were located at grid blocks (10, 23) and (22, 9).

The reference pressure was 9100 kPa at the depth of 900m having 10.11 kPa/m pressure gradients for the brine (Figure 7.1). This was also the initial aquifer pressure for Run 1a. The aquifer pressure for Run 2a was determined to be 2800 kPa after 10 years of water production. Decreasing the aquifer pressure by water production caused injection of CO_2 below supercritical conditions. For both cases, the cap rock resistance pressure was taken as 15000 kPa using an overburden pressure gradient of 16.67 kPa/m at 900 m (Figure 7.1), which was considered as the highest pressure (final constraint) for the simulation. So, CO_2 injection had been ceased when the bottom-hole pressure for CO_2 injectors reached to 15000 kPa. There were two CO_2 injection wells namely CO_2-injector 1 and 2 and six water producers for the field aquifer model. CO_2-injector 1 was located at the high permeability region of the field. The permeabilities around CO_2-injector 2 well were lower. Location of wells and grid configuration for both cases for a field aquifer model are given in Figures 7.3 and 7.4 Grid thickness of the first layer was taken as 41 m, second layer as 30 m and third layer as 111 m. CO_2 was injected at the bottom of the aquifer (layer 3).

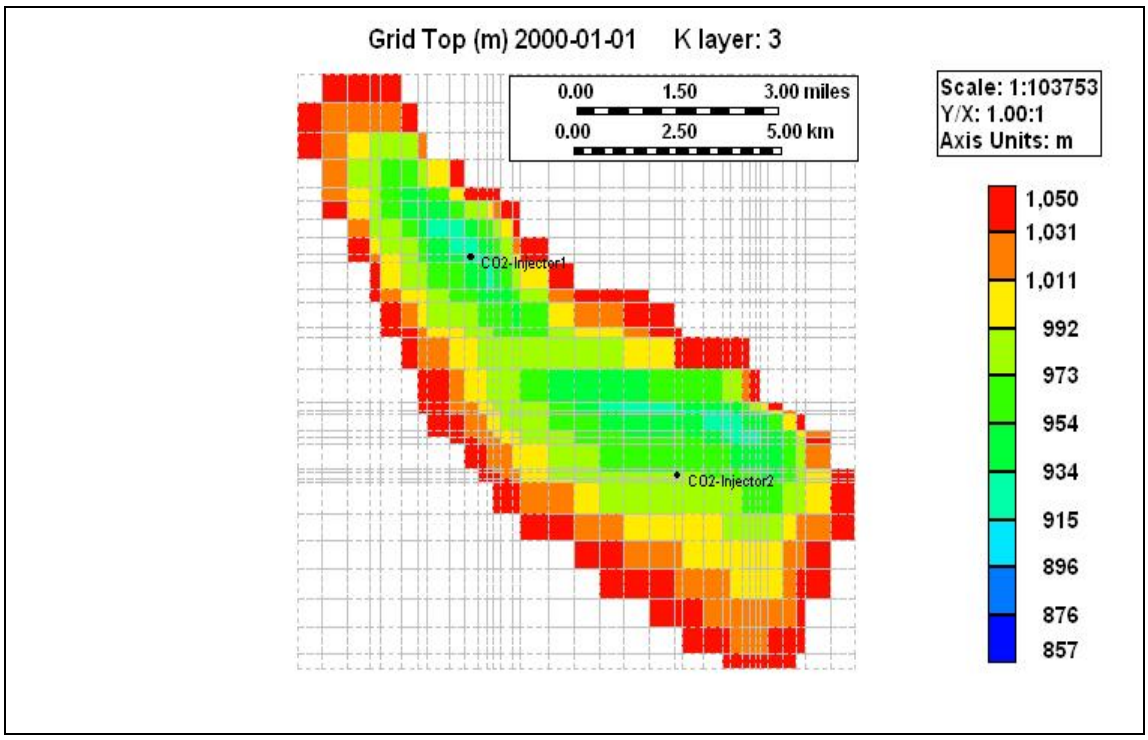

Figure 7.3 Map of Grid Top for layer 3 in 2-D view of field aquifer for Run 1a

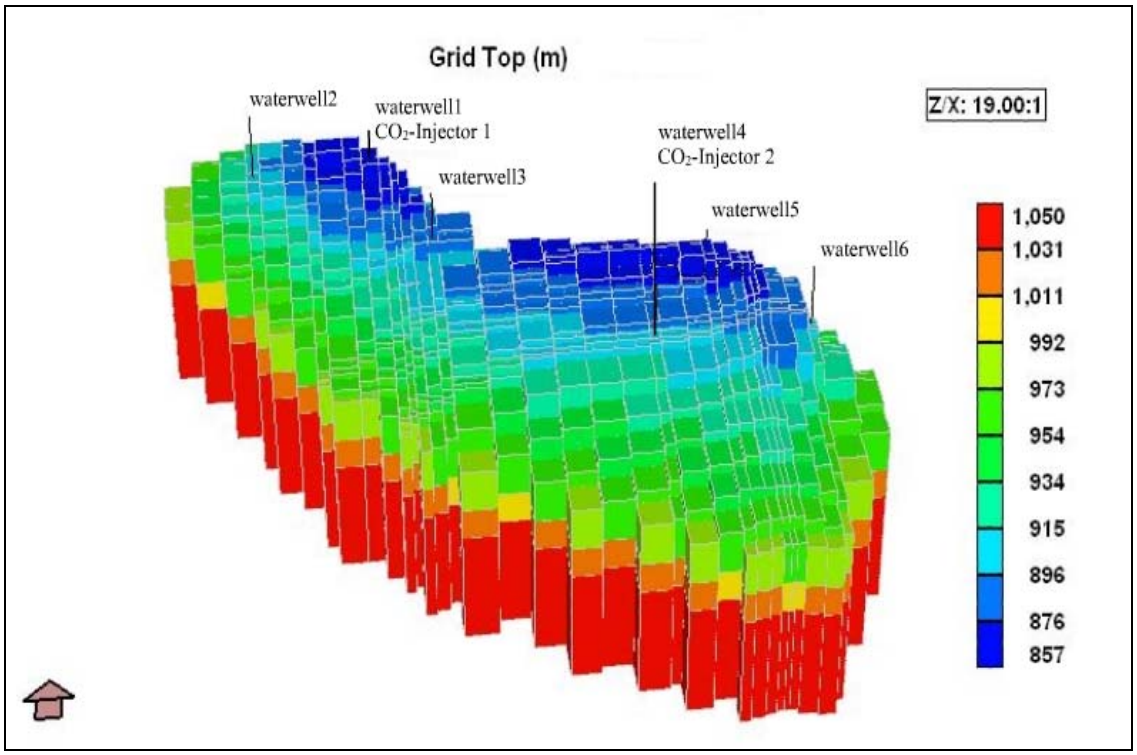

Figure 7.4 Map of Grid Top in 3-D view of field aquifer for Run 2a

7.1.2 Single Well Aquifer Model

In sensitivity analyses, a CO_2-injector well-1 was chosen and a radial aquifer model having three layers was used to analyze the effects of heterogeneity, injection rate, initial reservoir conditions and salinity on CO_2 sequestration process. Grid thickness graph of a radial aquifer model in 3-D and a cross section of grid thickness are given in Figures 7.5 and 7.6. The thickness of the first layer was 41 m, second layer was 30 m and third layer was 111 m. The conditions related to these runs are given in Tables 7.6, 7.7 and 7.8.

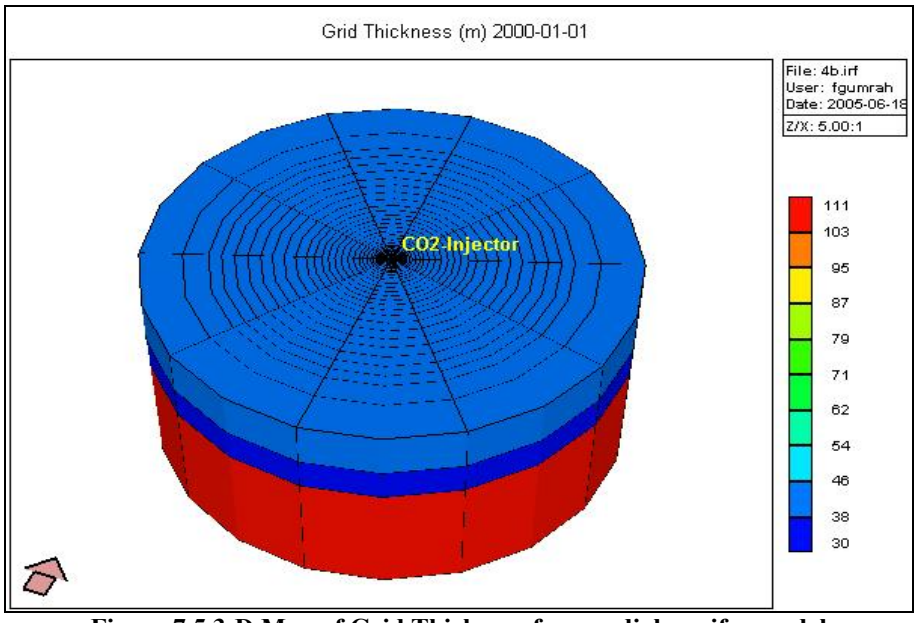

Figure 7.5 3-D Map of Grid Thickness for a radial aquifer model

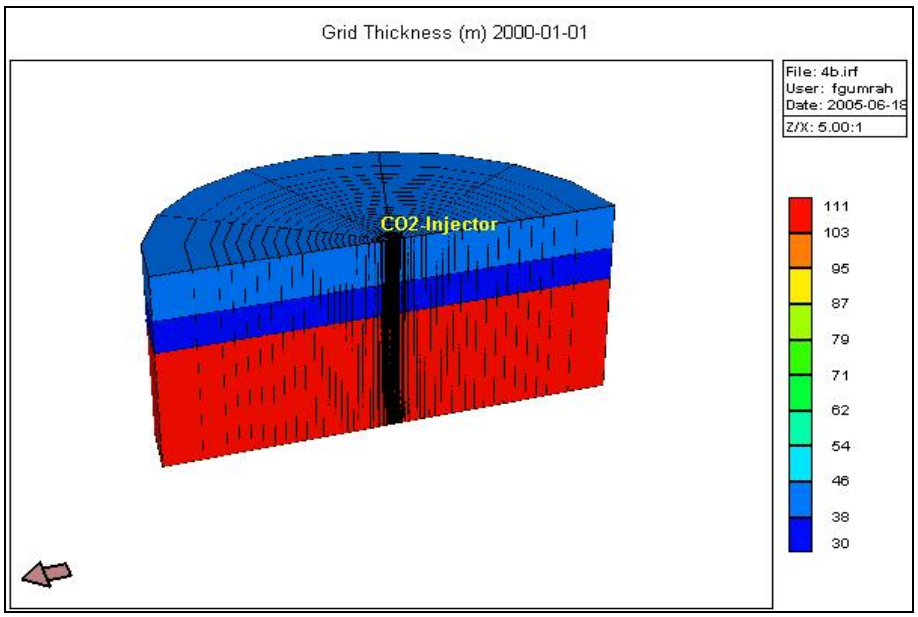

Figure 7.6 Cross Section of Grid Thickness for a radial aquifer model

Table 7.7 Input Parameters for Sensitivity Runs to examine the effect of heterogeneity on CO_2 sequestration in a radial aquifer model

Run ID	System	Layer permeability (md)			k_v / k_h	Grid properties
		1(top)	2(middle)	3 (bottom)		
3a	Homogeneous	150	150	150	1.0	Coarse(*)
4a	Homogeneous	150	150	150	1.0	Fine(*)
4b	Heterogeneous	150	150	150	0.1	Fine
4c	Heterogeneous	150	150	150	0.2	Fine
4d	Heterogeneous	150	150	150	0.3	Fine
		Constant permeability in each layer				
5b	Heterogeneous	112	45	150	0.1	Fine
5c	Heterogeneous	112	45	150	0.2	Fine
5d	Heterogeneous	112	45	150	0.3	Fine
6b	Heterogeneous	Variable permeability distribution in each layer			0.1	Fine
6c	Heterogeneous				0.2	Fine
6d	Heterogeneous				0.3	Fine
Other properties	• CO_2 injection rate is 40000 sm^3/day for each run. • Injection time is 13 years and the duration of simulation is 200 years. • Initial pressure is 9100 kPa and final pressure is 15000 kPa. • Water salinity is 100000 ppm. • Aquifer temperature is 33 °C at 900 m depth. (*) Grid dimensions are given in Table 7.10.					

Table 7.8 Input Parameters for Sensitivity Runs to examine the effect of CO_2 injection rate on CO_2 sequestration in a radial aquifer model

Run ID		Initial Condition	Final Condition	CO_2 injection rate (sm3/day)
	Pressure gradient	Brine 10.11 kPa/m (0.447 psi/ft)	Overburden 16.67 kPa/m (0.737 psi/ft)	
5b, 5c, 5d	Pressure at 900 m	9100 kPa	15000 kPa	40000
7b, 7c, 7d	Pressure at 900 m	9100 kPa	15000 kPa	20000
8b, 8c, 8d	Bottom hole pressure after water production	2800 kPa *	15000 kPa	40000
9b, 9c, 9d	Bottom hole pressure after water production	2800 kPa *	15000 kPa	80000
10b, 10c, 10d	Bottom hole pressure after water production	2800 kPa *	15000 kPa	20000
Other properties	• Water salinity is 100000 ppm. • Aquifer temperature is 33 °C at 900 m depth. • Aquifer properties of runs 7b, 7c and 7d are the same values as in runs 5b, 5c and 5d, respectively. • Aquifer properties of runs 8b, 8c and 8d are the same values as in runs 5b, 5c and 5d, respectively. • Aquifer properties of runs 9b, 9c and 9d are the same values as in runs 5b, 5c and 5d, respectively. • Aquifer properties of runs 10b, 10c and 10d are the same values as in runs 5b, 5c and 5d, respectively. *CO_2 was injected at gas phase till the supercritical CO_2 pressure was reached (7295kPa).			

Table 7.9 Input Parameters for Sensitivity Runs to examine the effect of salinity on CO_2 sequestration in a radial aquifer model

Run ID		Initial Condition	Final Condition	Salinity (ppm)
5b	Pressure at 900 m	Brine 9100 kPa	Overburden 15000 kPa	100000
11b	Pressure at 900 m	9100 kPa	15000 kPa	50000
12b	Pressure at 900 m	9100 kPa	15000 kPa	10000
Other properties	• CO_2 injection rate is 40000 sm^3/day for each run. • Injection time is 13 years and the duration of simulation is 200 years. • Aquifer temperature is 33 °C at 900 m depth. • Aquifer properties of runs 11b and 12b are the same values as in run 5b.			

Table 7.10 Grid Dimensions for a Single-well Aquifer Model

Run ID		Single-well Aquifer Model									
3a (Coarse)	**Grid Numbers**	**1**	**2**	**3**	**4**	**5**	**6**	**7**	**8**	**9**	**10**
	Grid Dimensions (m)	80	87.5	100	101	68	68	100	101	134	134
4a (Fine)	**Grid Numbers**	**1**	**2**	**3**	**4**	**5**	**6**	**7**	**8**	**9**	**10**
	Grid Dimensions (m)	1	1	1	1	1	2	2	2	2	2
	Grid Numbers	**11**	**12**	**13**	**14**	**15**	**16**	**17**	**18**	**19**	**20**
	Grid Dimensions (m)	3	3	3	3	3	5	5	5	5	5
	Grid Numbers	**21**	**22**	**23**	**24**	**25**	**26**	**27**	**28**	**29**	**30**
	Grid Dimensions (m)	5	10	10	15	15	15	20	22.5	25	25
	Grid Numbers	**31**	**32**	**33**	**34**	**35**	**36**	**37**	**38**	**39**	**40**
	Grid Dimensions (m)	25	25	30	30	41	44	45	45	50	50
	Grid Numbers	**41**	**41**	**43**	**44**						
	Grid Dimensions (m)	50	51	100	168						
8b (Fine)	**Grid Numbers**	**1**	**2**	**3**	**4**	**5**	**6**	**7**	**8**	**9**	**10**
	Grid Dimensions (m)	1	1	2	2	2	3	3	3	3	4
	Grid Numbers	**11**	**12**	**13**	**14**	**15**	**16**	**17**	**18**	**19**	**20**
	Grid Dimensions (m)	4	4	4	4	5	5	5	5	5	5
	Grid Numbers	**21**	**22**	**23**	**24**	**25**	**26**	**27**	**28**	**29**	**30**
	Grid Dimensions (m)	5	5	5	5	10	10	10	10	20	30
	Grid Numbers	**31**	**32**	**33**	**34**	**35**					
	Grid Dimensions (m)	30	50	50	100	300					

The grid dimensions for Runs 4c, 4d, 5b, 5c, 5d, 6b, 6c, 6d, 7b, 7c, 7d, 11b and 12b were taken same as the values of Run 4b. The grid dimensions for Runs 8c, 8d, 9b, 9c, 9d, 10b, 10c, and 10d were taken same as the values of Run 8b.

7.2 Data Preparation for CMG/GEM Simulator

The sample input data files for a field scale aquifer model (Run 1a) and a single well aquifer model (Run 5b) are given in Appendices A.1 and A.2 respectively.

CHAPTER 8

RESULTS AND DISCUSSION

8.1 Introduction

Two aquifer models, a field scale and a single well [91], were studied in a CMG simulator.

8.2 Results of a Field-Scale Aquifer Model

The simulation results of CO_2 injection histories for two cases without water production (Run 1a) and after water production (Run 2a) are shown in Figures 8.1 and 8.2 for Run 1a and Figures 8.3 and 8.4 for Run 2a. The maximum bottom-hole pressure of 15000 kPa for CO_2-Injectors 1 and 2 was reached after 30 years of CO_2 injection. The CO_2 injection was then ceased and CO_2 was kept in the aquifer for 200 years.

In Figures 8.1 and 8.2 for Run 1a, after 5 years from the date when CO_2 injection has been ceased, the well bottom-hole pressure for CO_2-Injector 1 was dropped to 14375 kPa because of the solubility of CO_2 in water and then the change in pressure drop was almost constant (14254 kPa) till the end of 200 years. For CO_2-Injector 2, the well bottom-hole pressure declined to 14813 kPa after 5 years from the date when CO_2 injection has been ceased and decreased to 14711 kPa at the end of 200 years due to the solubility of CO_2 in water.

In Figures 8.3 and 8.4 for Run 2a, after 3 years the well bottom-hole pressure for CO_2-Injector 1 was dropped to 14563 kPa and then the change in pressure drop was almost

stable (14320 kPa) through 200 years. For CO_2-Injector 2, well bottom-hole pressure reached at 14772 kPa at the end of 200 years.

The cumulative $2.40*10^9$ sm^3 of CO_2 was injected into an aquifer from the CO_2-Injector 1 at the end of simulation (Figure 8.1), whereas CO_2-Injector 2 injected $2.35*10^9$ sm^3 of cumulative CO_2 (Figure 8.2). Although CO_2 injection rates and injection durations for two injectors were same; the cumulative injected CO_2 amounts at reservoir conditions were different. The difference between these cumulative injected CO_2 amounts for two injectors might be attributed to permeability distribution around the injection wells. CO_2-Injector 1 was located at the high permeable region compared to CO_2-Injector 2. The well bottom-hole pressures for both injectors were also decreasing after the CO_2 injection had been stopped because of the fact that some of CO_2 were dissolved in water and some of CO_2 were precipitated with calcite minerals.

It is seen from Figures 8.3 and 8.4, the similar results of the first case, without water production, were also figured out for 10 years of water production case. The only difference between two cases was the cumulative injected CO_2 values. The decrease in aquifer pressure through water production leads to an increase in the amount of CO_2 injected as it was expected. After water production, approximately $7*10^9$ sm^3 of cumulative CO_2 was injected from two injectors at the end of injection period. In this case, since CO_2 was injected in gaseous phase, CO_2 filled up the aquifer first and then propagated through the aquifer.

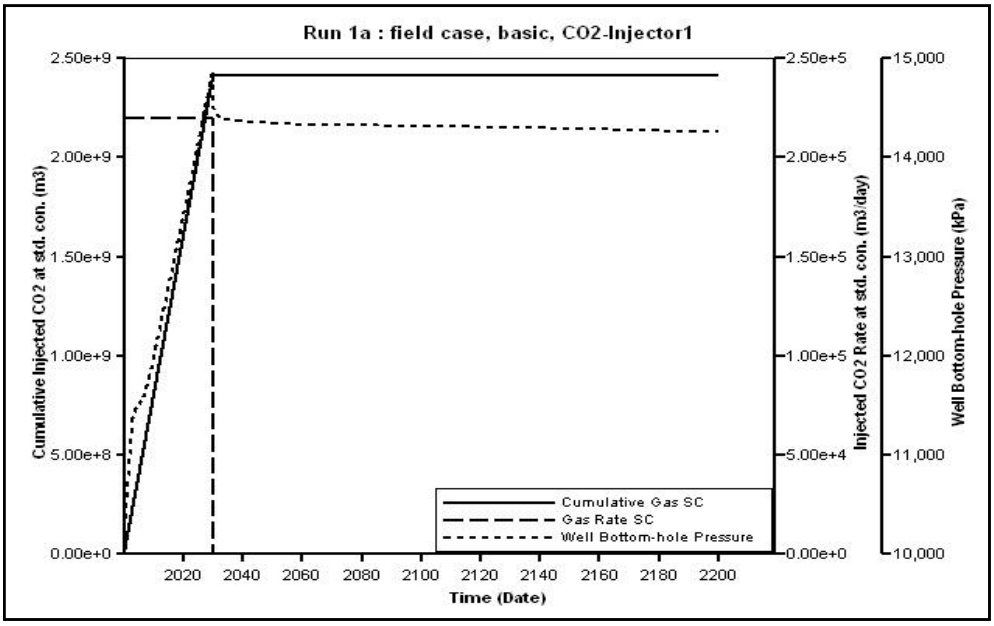

Figure 8.1 CO_2 Injection History for Run 1a: field case, CO_2-Injector 1 (CO_2 injection rate = 220000 sm^3/d)

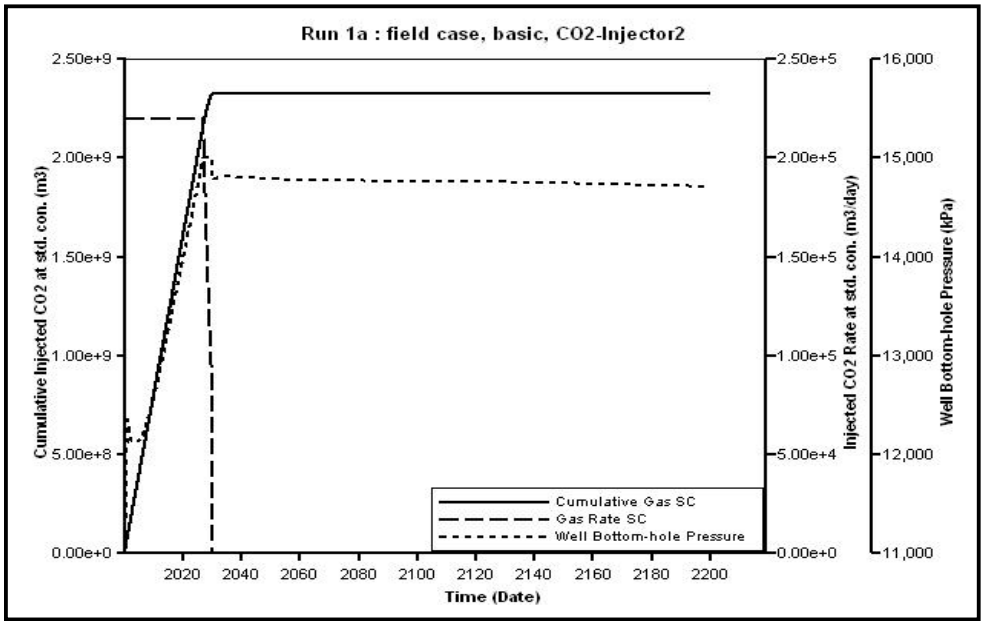

Figure 8.2 CO_2 Injection History for Run 1a: field case, CO_2-Injector 2 (CO_2 injection rate = 220000 sm^3/d)

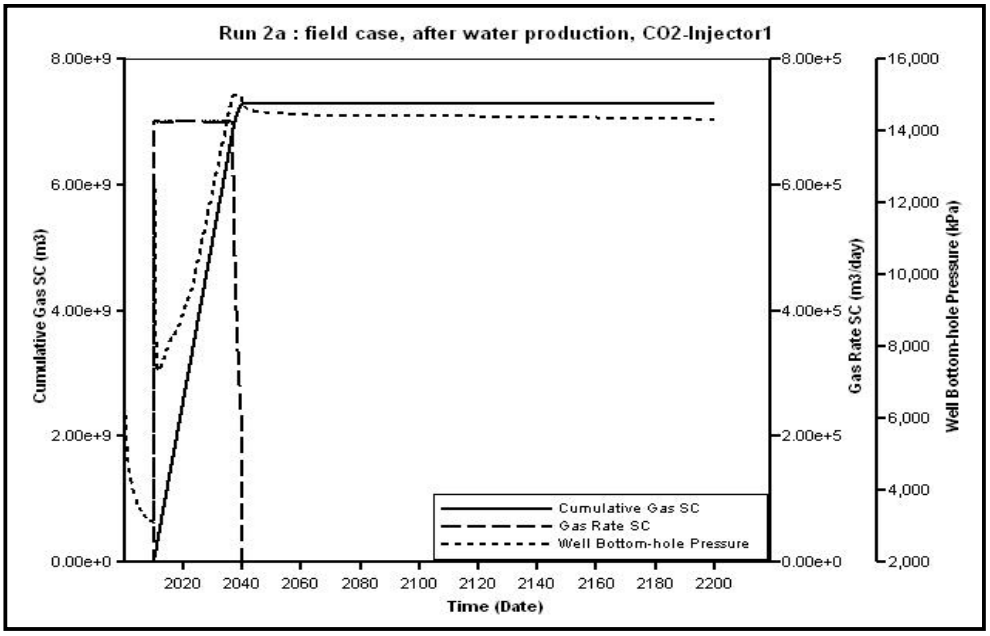

Figure 8.3 CO_2 Injection History for Run 2a: field case, CO_2-Injector 1 (CO_2 injection rate = 700000 sm^3/d)

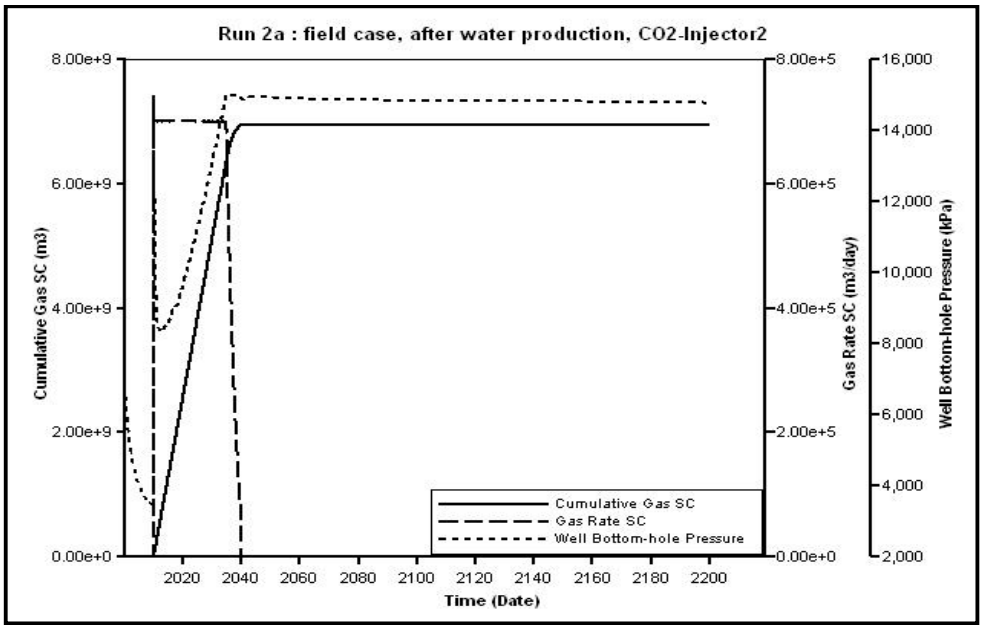

Figure 8.4 CO_2 Injection History for Run 2a: field case, CO_2-Injector 2 (CO_2 injection rate = 700000 sm^3/d)

In detail for two cases namely Run 1a and Run 2a, for both injectors at the injection well block, the plots of CO_2 saturation as a free gas, soluble CO_2 mole fraction in water and precipitated CO_2 as Calcite dissolution / precipitation, Kaolinite dissolution / precipitation and Anorthite dissolution / precipitation are indicated in Figures 8.5 through 8.24 for all three layers of the aquifer. In all plots, first layer was represented by solid line, dashed line stands for second layer and smaller dashed line indicates third layer of the aquifer. Related to above properties for all layers, 2-D maps were also demonstrated at three different simulation time namely 2040 in Appendix B.1 and 2100 in Appendix B.2 and 2200 in Figures 8.25 through 8.60. The simulation was started at 2000 and continued till 2200. Pressure distributions for Runs 1a and 2a were also given in Figures 8.61 through 8.84.

Figures 8.5 and 8.6 show the CO_2 saturation in free gas phase for CO_2-Injector 1 and CO_2-Injector 2, respectively. As indicated in both figures, CO_2 saturation increased in all layers until CO_2 injection has ceased (30 years). After 30 years, CO_2 saturation in layer 1 was increasing while in layers 2 and 3, there was a reduction in CO_2 saturation indicating free CO_2 has a tendency to rise. Since CO_2-Injector 2 was located in low permeable zone in all directions, CO_2 saturation in layer 1 for CO_2-Injector 2 was less than the saturation in layer 1 for CO_2-Injector 1 and CO_2 saturation in layer 3 for CO_2-Injector 2 was more than the value that CO_2-Injector 1 posses since free CO_2 has a tendency to rise within the aquifer. For Run 2a with 10 years of water production case (Figures 8.7 and 8.8) that CO_2 was injected in gaseous phase, after the water production (10 years), CO_2 saturation increased in all layers until CO_2 injection has been ceased (40 years). After 40 years, CO_2 saturation in layer 1 was increasing while in layers 2 and 3, there was a reduction in CO_2 saturation indicating free CO_2 has a tendency to rise.

Soluble CO_2 in water increased up to a value of 2.8 % of cummulative injected CO_2 for both injectors until injection has stopped (until 30 years) for both cases (Run 1a and 2a). After CO_2 injection has stopped, CO_2 mole fraction in water became stable at the same value till the end of simulation (200 years) (Figures 8.9, 8.10, 8.11 and 8.12).

Calcite dissolution / precipitation plots were constructed to investigate the precipitated CO_2, (Figures 8.13, 8.14, 8.15 and 8.16). In these Figures, (-) sign designates dissolution of Calcite minerals where as CO_2 precipitation with Calcite minerals is indicated by (+) sign. It can be seen from these figures that dissolution of Calcite mineral reached a value of - $4*10^9$ mole until 10 years for Run 1a (Figures 8.13 and 8.14). Then Calcite precipitation initiated and the rate of precipitation was increasing till the end of simulation (200 years). For Run 2a, the same tendencies on Calcite dissolution / precipitation plots were observed for both injectors as seen from Figures 8.15 and 8.16. Calcite precipitation mostly occured in layer 3 compared to precipitation in layers 1 and 2 for Runs 1a and 2a (Figures 8.28, 8.34, 8.40, 8.46, 8.52, 8.58) since most of the free and soluble CO_2 were identifed in layers 1 and 2. Decreasing the initial aquifer pressure by water production caused an increase in Calcite precipitation in all layers of the aquifer. Because, CO_2 was injected in gaseous phase in water production case which resulted in faster movement of CO_2 within the aquifer.

In Figures 8.17-8.20 Kaolinite dissolution / precipitation plots are given for both injectors. It was observed that Kaolinite precipitated in all three layers during the simulation period (200 years) for both cases. It was also seen that Kaolinite precipitation were much more in layer 3 compared to other two layers and Kaolinite precipitation decreased for Run 2a. For instance, $8.5 * 10^8$ mole of Kaolinite precipitated in layer 3 for Run 1a (Figures 8.17 and 8.18) where as $6 * 10^8$ mole of Kaolinite precipitated in layer 3 for Run 2a (Figures 8.19 and 8.20).

Anorthite dissolution / precipitation plots are given in Figures 8.21-8.24. Anorthite dissolved in all three layers during the simulation period (200 years) for both cases. Dissolution of Anorthite was mostly seen in layer 3 compared to other two layers and Anorthite dissolution declined for Run 2a. For example, $- 8 * 10^8$ mole of Anorthite dissolved in layer 3 for Run 1a (Figures 8.21 and 8.22) unlike $- 6 * 10^8$ mole of Anorthite dissolved in layer 3 Ror run 2a (Figures 8.23 and 8.24).

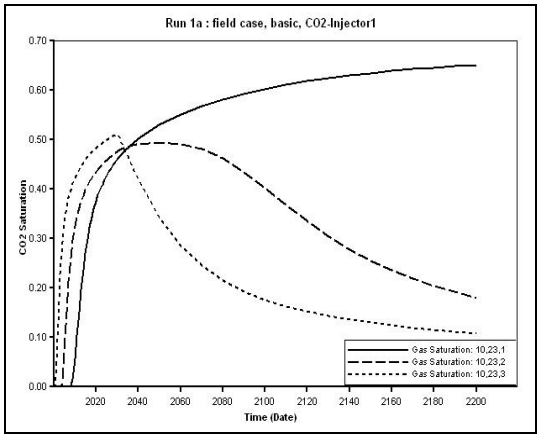

Figure 8.5 CO_2 Saturation for Run 1a: field case, CO_2-Injector 1

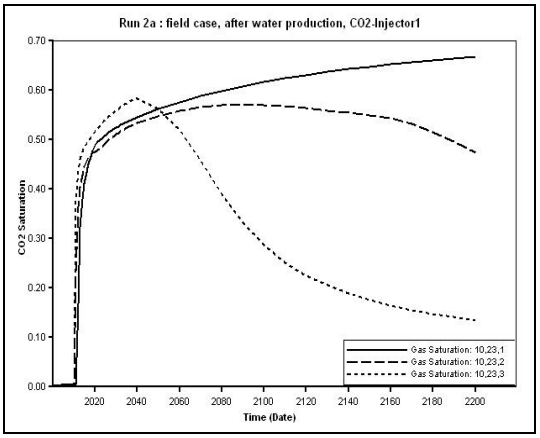

Figure 8.7 CO_2 Saturation for Run 2a: field case, CO_2-Injector 1

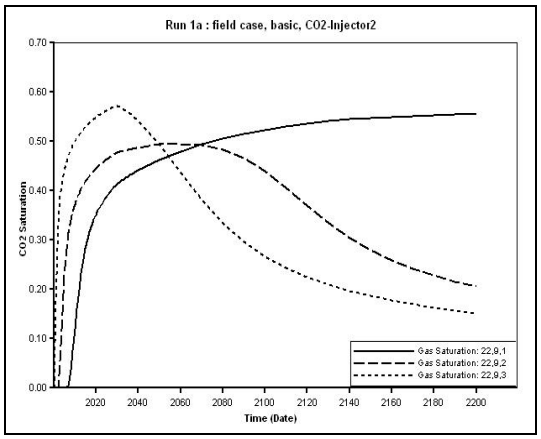

Figure 8.6 CO_2 Saturation for Run 1a: field case, CO_2-Injector 2

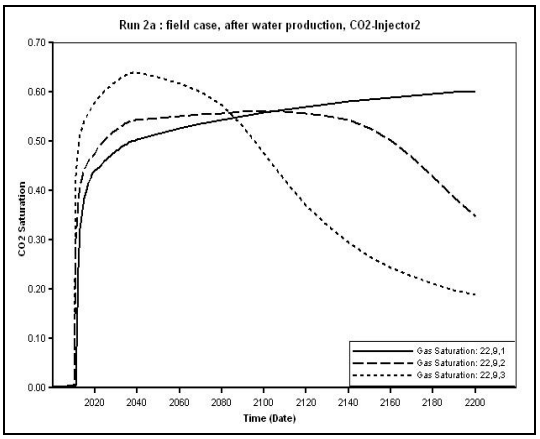

Figure 8.8 CO_2 Saturation for Run 2a: field case, CO_2-Injector 2

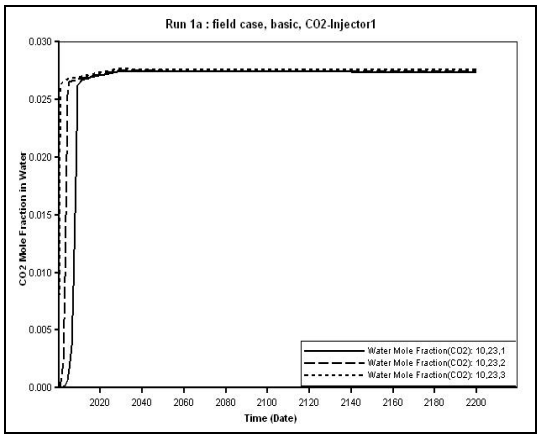

Figure 8.9 CO_2 Mole Fraction in Water for Run 1a: field case, CO_2-Injector 1

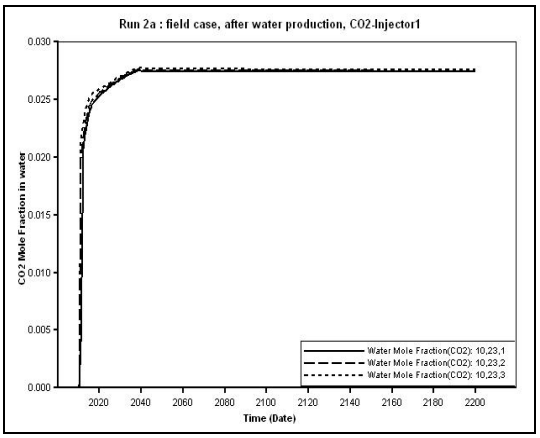

Figure 8.11 CO_2 Mole Fraction in Water for Run 2a: field case, CO_2-Injector 1

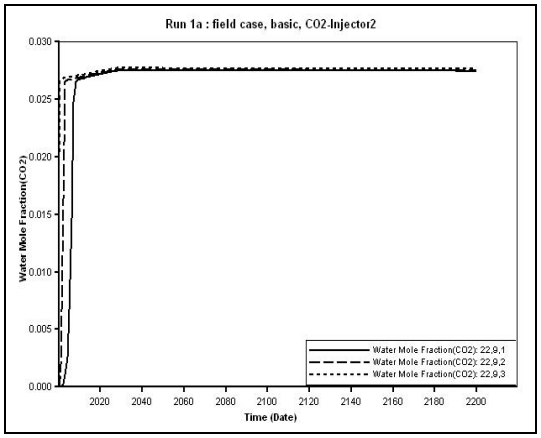

Figure 8.10 CO_2 Mole Fraction in Water for Run 1a: field case, CO_2-Injector 2

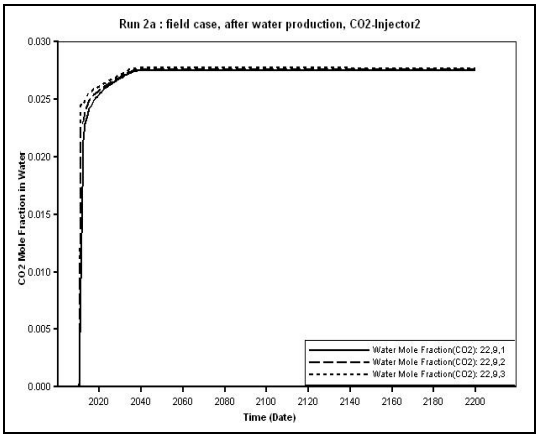

Figure 8.12 CO_2 Mole Fraction in Water for Run 2a: field case, CO_2-Injector 2

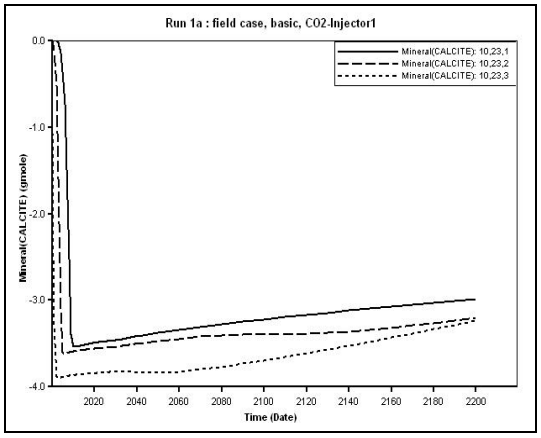

Figure 8.13 Calcite Dissolution / Precipitation for Run 1a: field case, CO_2-Injector 1

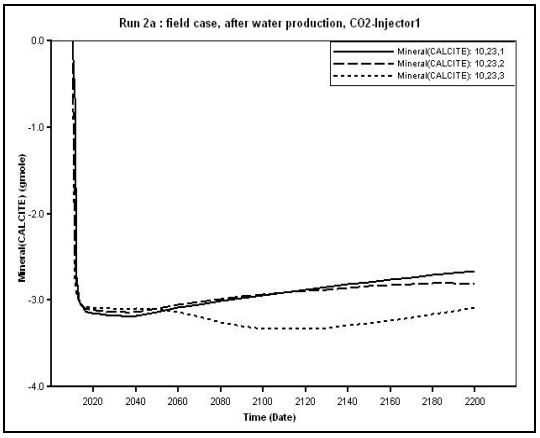

Figure 8.15 Calcite Dissolution / Precipitation for Run 2a: field case, CO_2-Injector 1

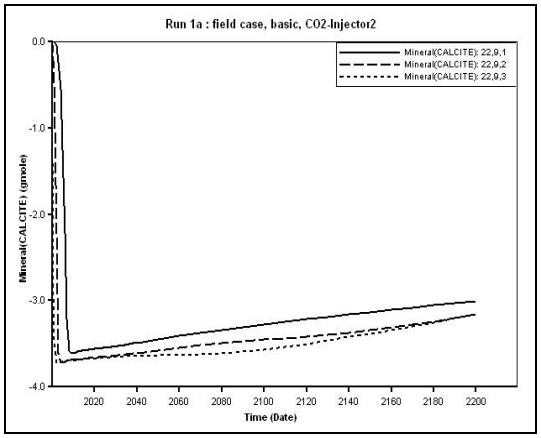

Figure 8.14 Calcite Dissolution / Precipitation for Run 1a: field case, CO_2-Injector 2

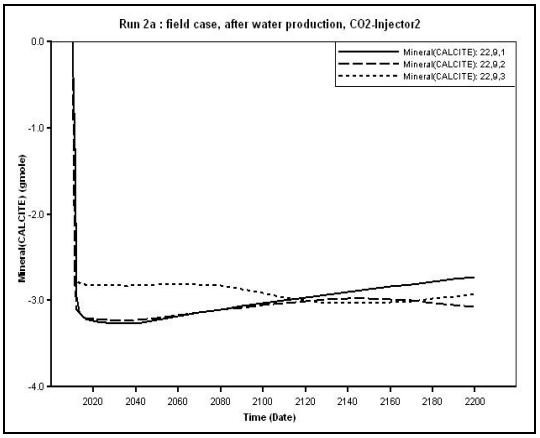

Figure 8.16 Calcite Dissolution / Precipitation for Run 2a: field case, CO_2-Injector 2

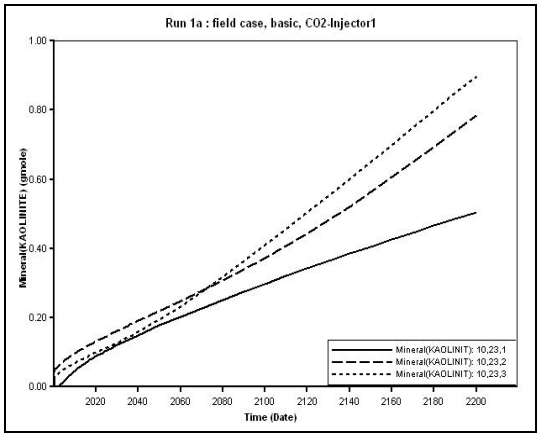

Figure 8.17 Kaolinite Dissolution / Precipitation for Run 1a: field case, CO_2-Injector 1

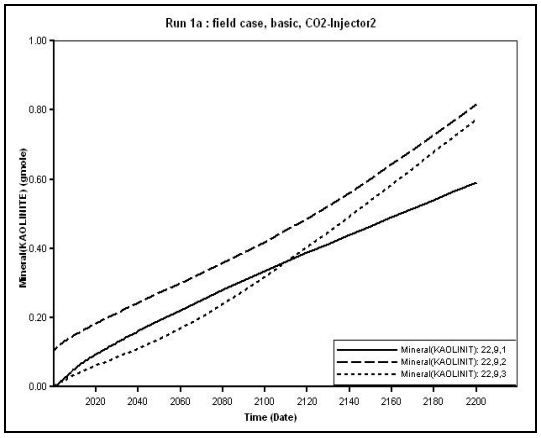

Figure 8.18 Kaolinite Dissolution / Precipitation for Run 1a: field case, CO_2-Injector 2

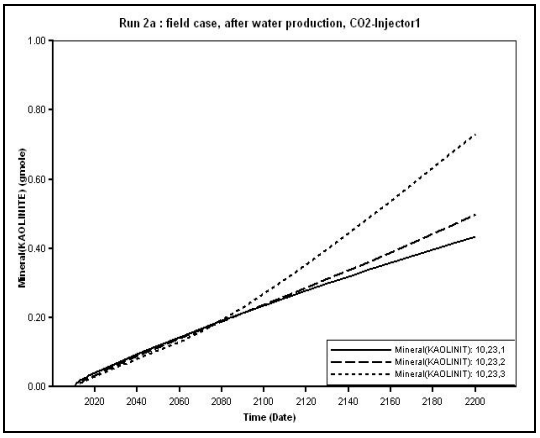

Figure 8.19 Kaolinite Dissolution / Precipitation for Run 2a: field case, CO_2-Injector 1

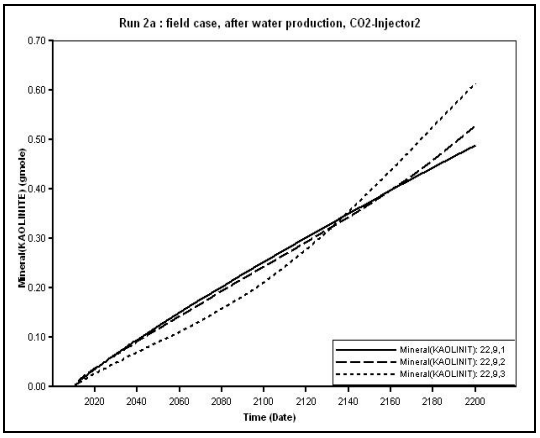

Figure 8.20 Kaolinite Dissolution / Precipitation for Run 2a: field case, CO_2 Injector 2

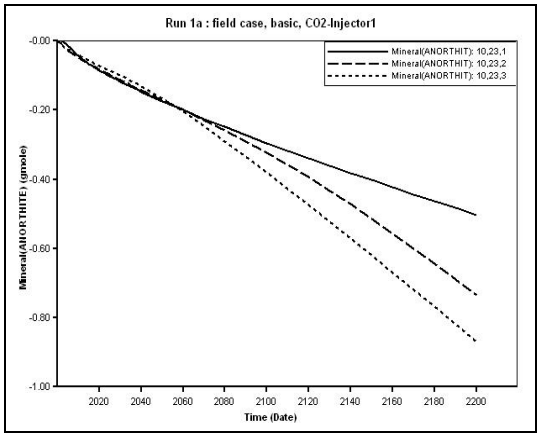

Figure 8.21 Anorthite Dissolution / Precipitation for Run 1a: field case, CO_2-Injector 1

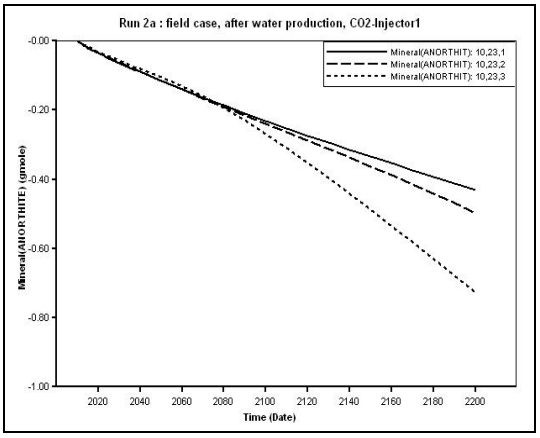

Figure 8.23 Anorthite Dissolution / Precipitation for Run 2a: field case, CO_2-Injector 1

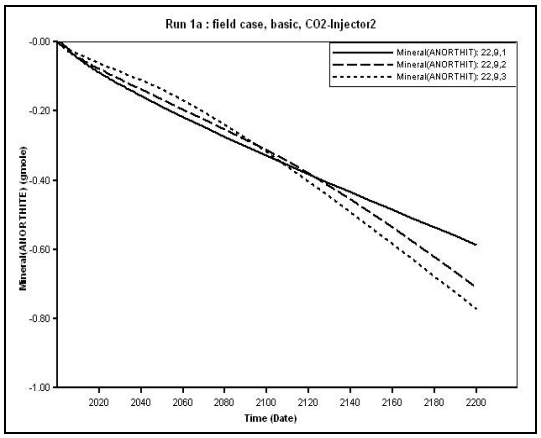

Figure 8.22 Anorthite Dissolution / Precipitation for Run 1a: field case, CO_2-Injector 2

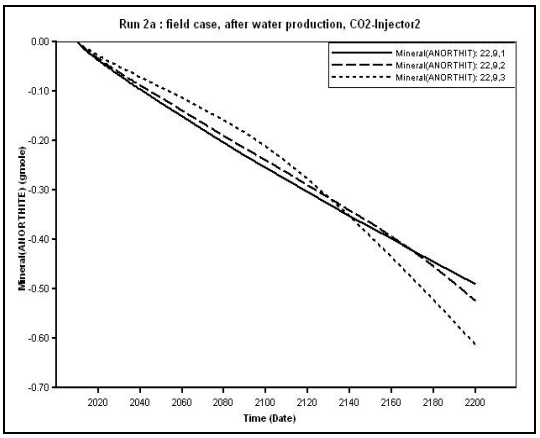

Figure 8.24 Anorthite Dissolution / Precipitation for Run 2a: field case, CO_2-Injector 2

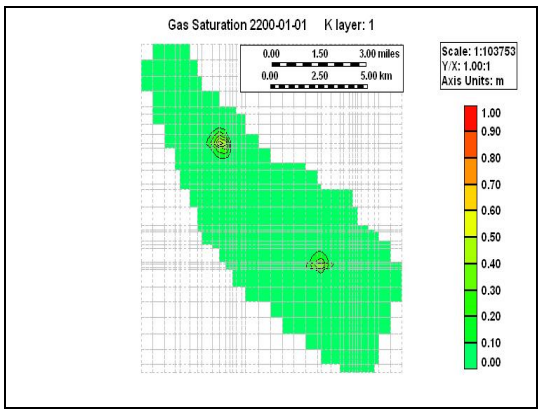

Figure 8.25 Map of CO2 Saturation at 2200(200 years) for Run 1a: field case, layer 1

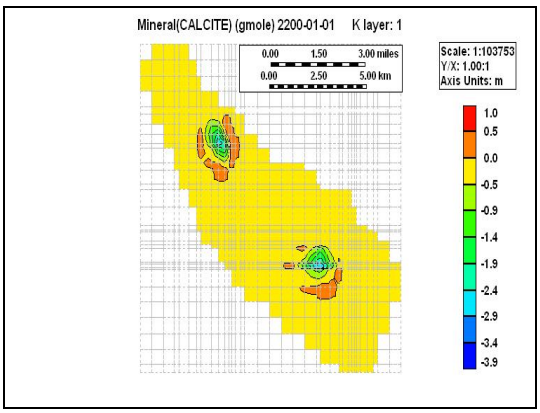

Figure 8.28 Map of Calcite Dissolution / Precipitation at 2200 (200 years) for Run 1a: field case, layer 1

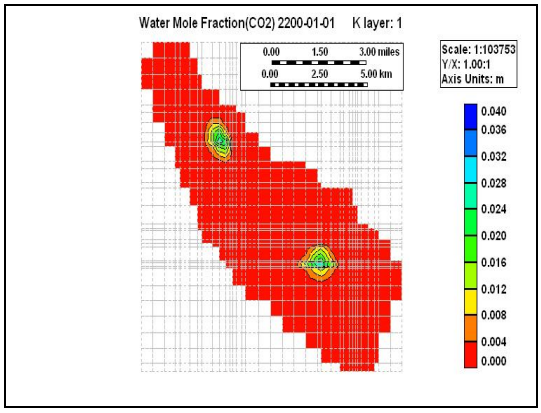

Figure 8.26 Map of CO_2 Mole Fraction in Water at 2200 (200 years) for Run 1a: field case, layer 1

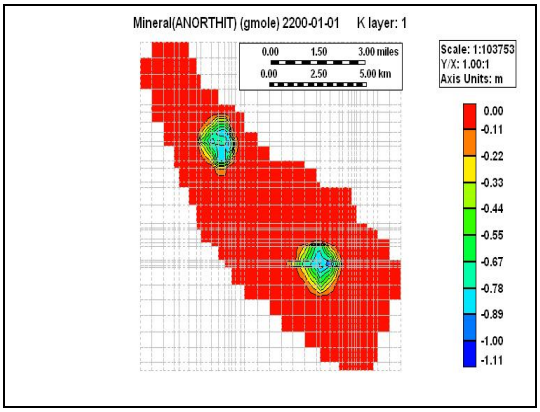

Figure 8.29 Map of Anorthite Dissolution / Precipitation at 2200 (200 years) for Run 1a: field case, layer 1

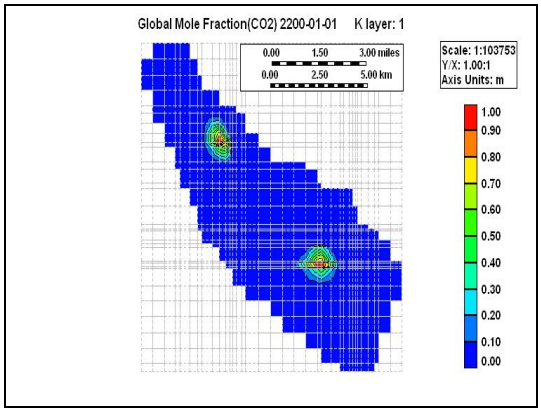

Figure 8.27 Map of CO_2 Global Mole Fraction at 2200 (200 years) for Run 1a: field case, layer 1

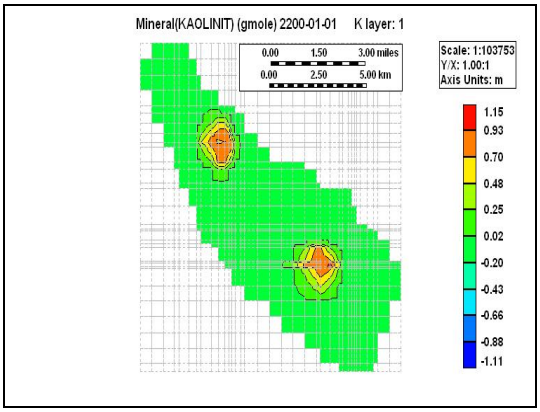

Figure 8.30 Map of Kaolinite Dissolution / Precipitation at 2200 (200 years) for Run 1a: field case, layer 1

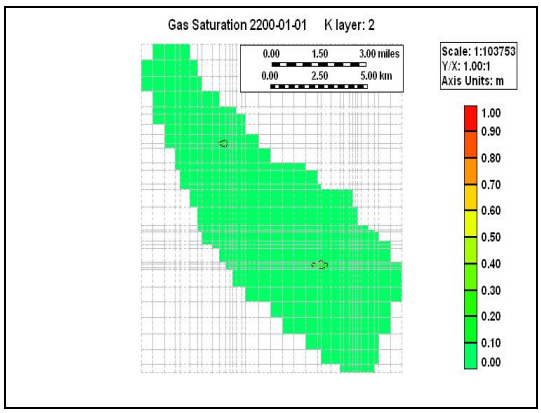

Figure 8.31 Map of CO_2 Saturation at 2200 (200 years) for Run 1a: field case, layer 2

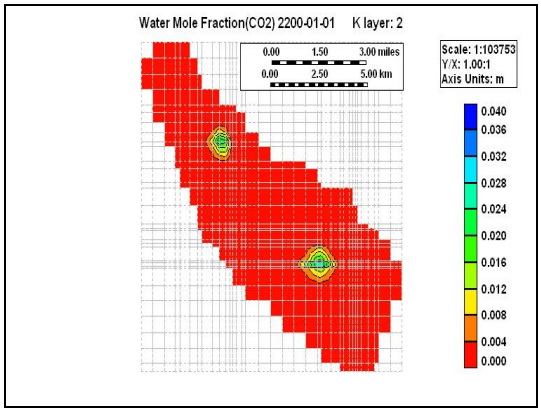

Figure 8.32 Map of CO_2 Mole Fraction in Water at 2200 (200 years) for Run 1a: field case, layer 2

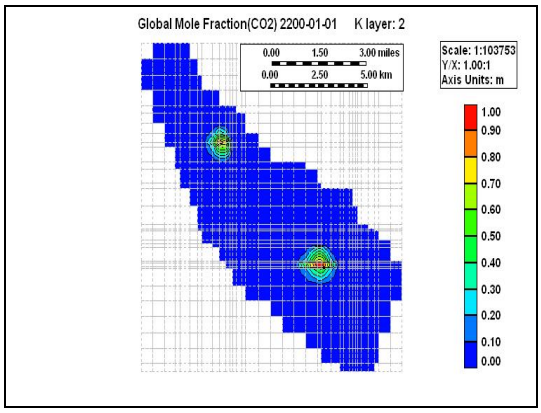

Figure 8.33 Map of CO_2 Global Mole Fraction at 2200 (200 years) for Run 1a: field case, layer 2

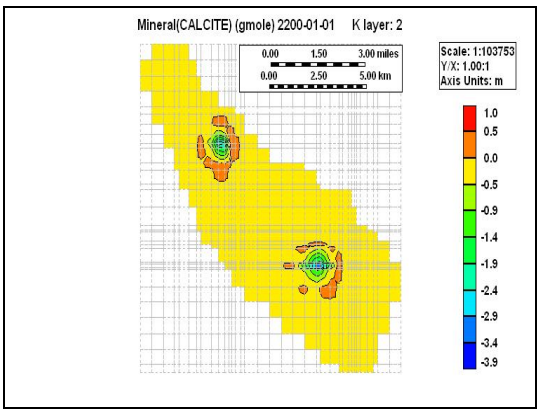

Figure 8.34 Map of Calcite Dissolution / Precipitation at 2200 (200 years) for Run 1a: field case, layer 2

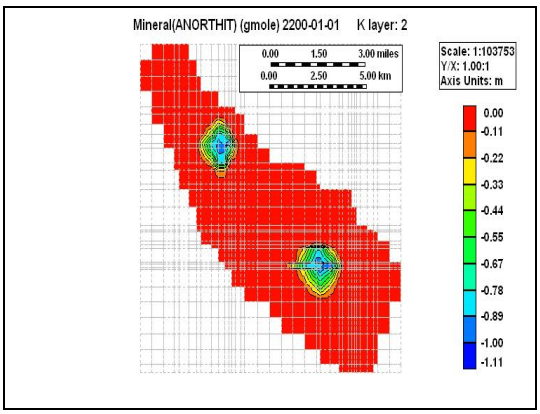

Figure 8.35 Map of Anorthite Dissolution / Precipitation at 2200 (200 years) for Run 1a: field case, layer 2

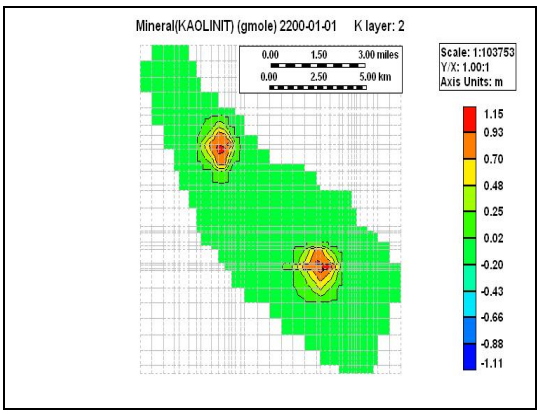

Figure 8.36 Map of Kaolinite Dissolution / Precipitation at 2200 (200 years) for Run 1a: field case, layer 2

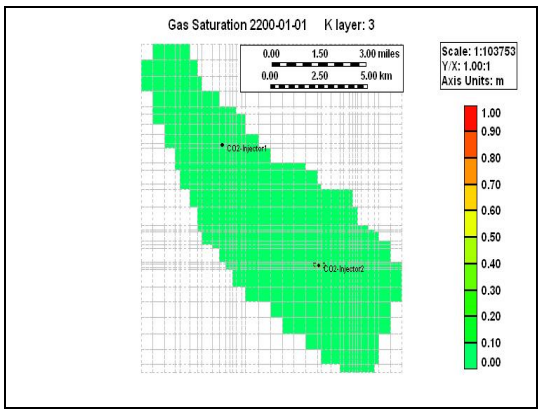

Figure 8.37 Map of CO_2 Saturation at 2200 (200 years) for Run 1a: field case, layer 3

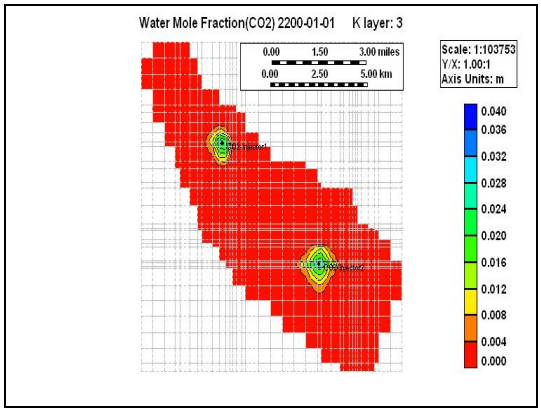

Figure 8.38 Map of CO_2 Mole Fraction in Water at 2200 (200 years) for Run 1a: field case, layer 3

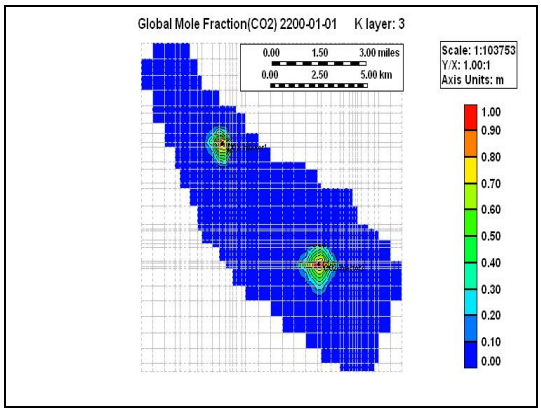

Figure 8.39 Map of CO_2 Global Mole Fraction at 2200 (200 years) for Run 1a: field case, layer 3

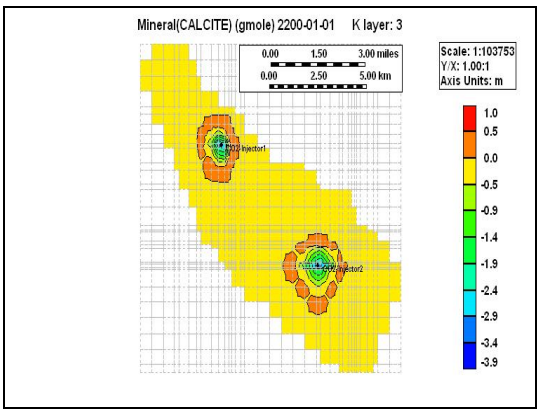

Figure 8.40 Map of Calcite Dissolution / Precipitation at 2200 (200 years) for Run 1a: field case, layer 3

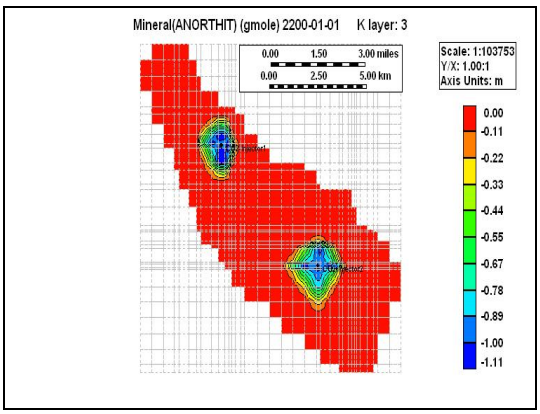

Figure 8.41 Map of Anorthite Dissolution / Precipitation at 2200 (200 years) for Run 1a: field case, layer 3

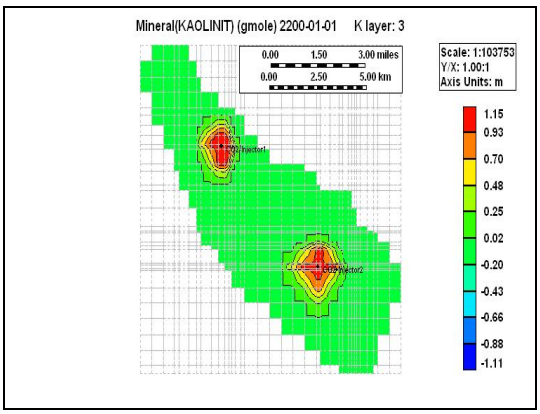

Figure 8.42 Map of Kaolinite Dissolution / Precipitation at 2200 (200 years) for Run 1a: field case, layer 3

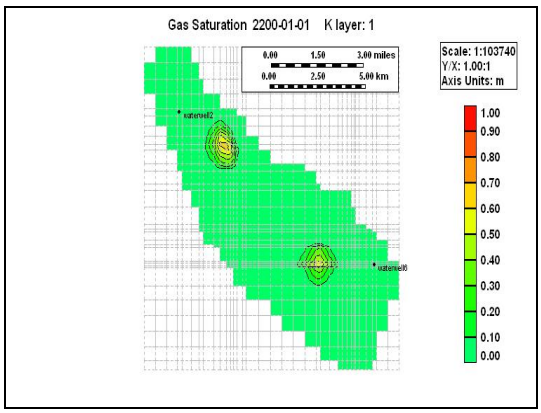

Figure 8.43 Map of CO_2 Saturation at 2200 (200 years) for Run 2a: field case, layer 1

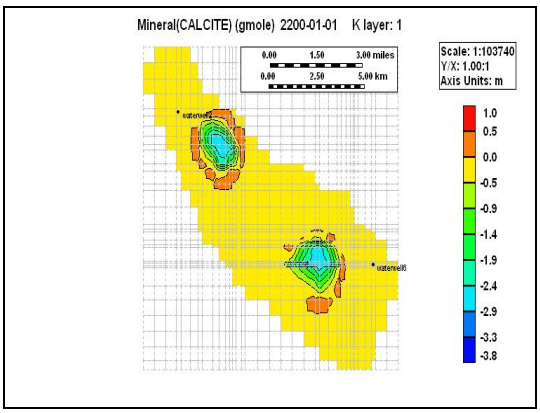

Figure 8.46 Map of Calcite Dissolution / Precipitation at 2200 (200 years) for Run 2a: field case, layer 1

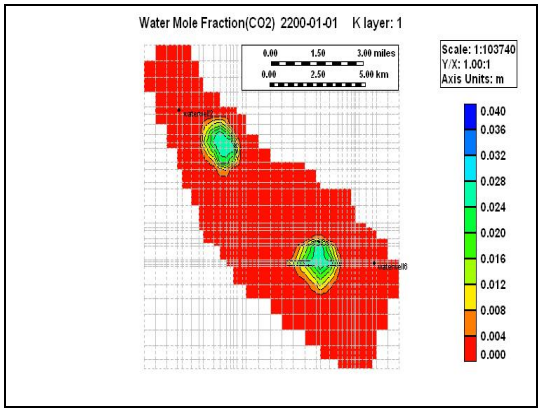

Figure 8.44 Map of CO_2 Mole Fraction in Water at 2200 (200 years) for Run 2a: field case, layer 1

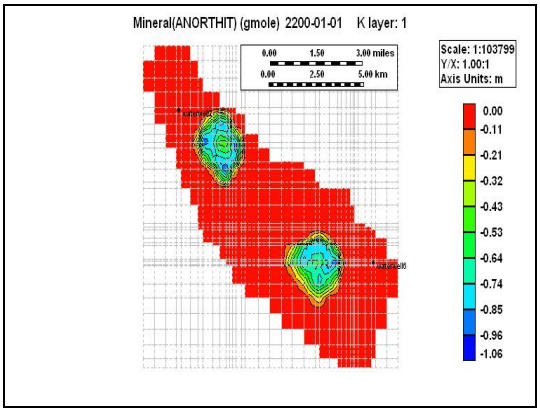

Figure 8.47 Map of Anorthite Dissolution / Precipitation at 2200 (200 years) for Run 2a: field case, layer 1

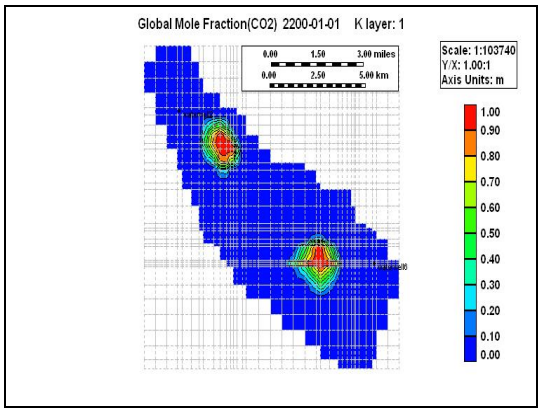

Figure 8.45 Map of CO_2 Global Mole Fraction at 2200 (200 years) for Run 2a: field case, layer 1

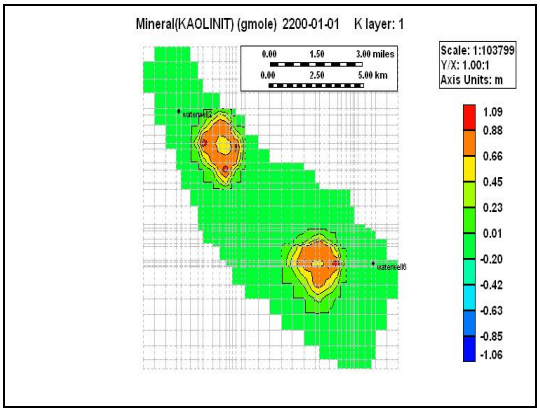

Figure 8.48 Map of Kaolinite Dissolution / Precipitation at 2200 (200 years) for Run 2a: field case, layer 1

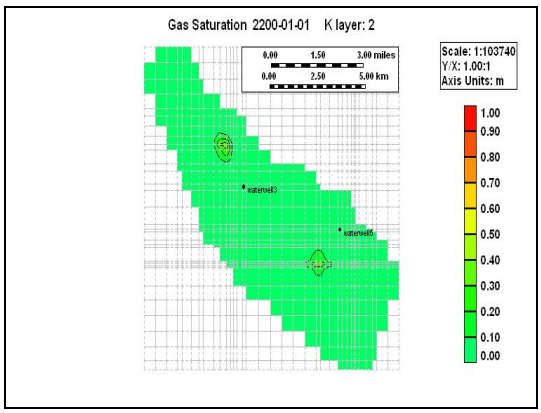

Figure 8.49 Map of CO_2 Saturation at 2200 (200 years) for Run 2a: field case, layer 2

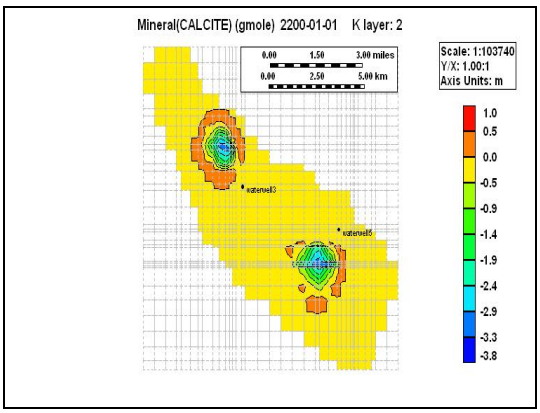

Figure 8.52 Map of Calcite Dissolution / Precipitation at 2200 (200 years) for Run 2a: field case, layer 2

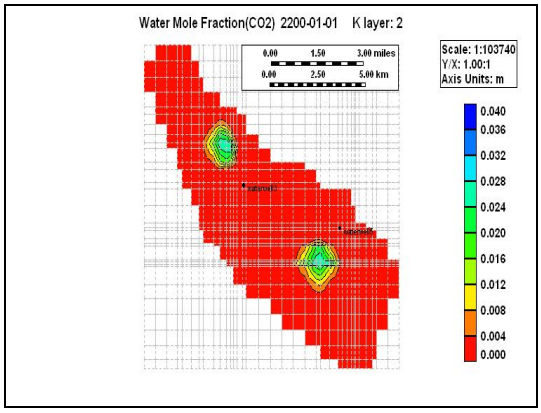

Figure 8.50 Map of CO_2 Mole Fraction in Water at 2200 (200 years) for Run 2a: field case, layer 2

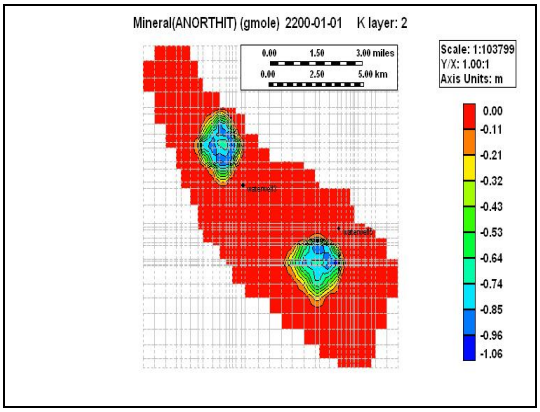

Figure 8.53 Map of Anorthite Dissolution / Precipitation at 2200 (200 years) for Run 2a: field case, layer 2

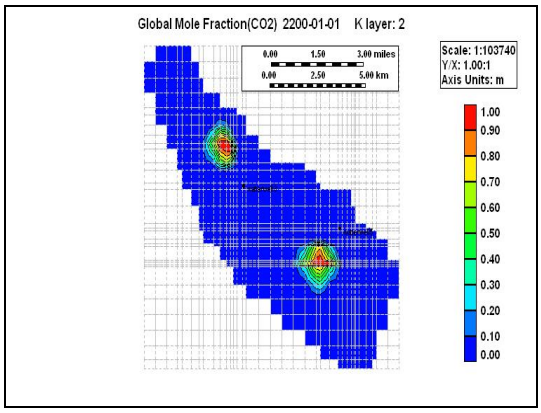

Figure 8.51 Map of CO_2 Global Mole Fraction at 2200 (200 years) for Run 2a: field case, layer 2

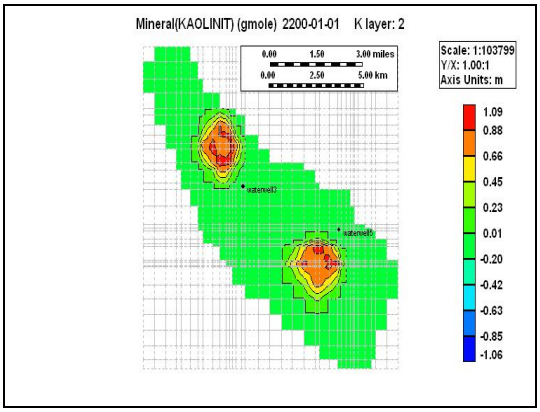

Figure 8.54 Map of Kaolinite Dissolution / Precipitation at 2200 (200 years) for Run 2a: field case, layer 2

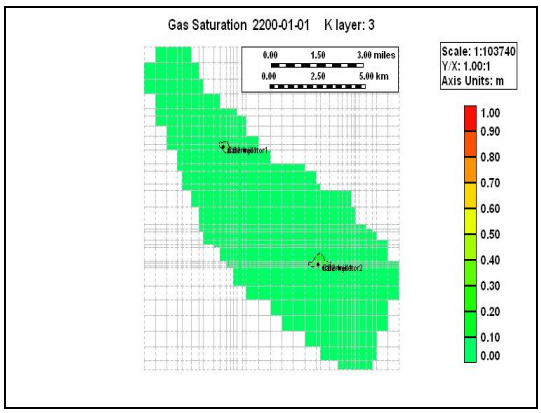

Figure 8.55 Map of CO_2 Saturation at 2200 (200 years) for Run 2a: field case, layer 3

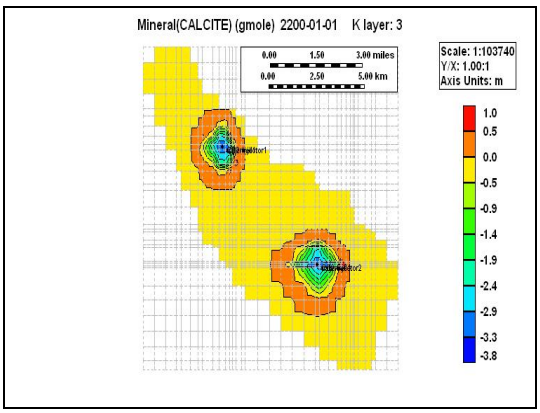

Figure 8.58 Map of Calcite Dissolution / Precipitation at 2200 (200 years) for Run 2a: field case, layer 3

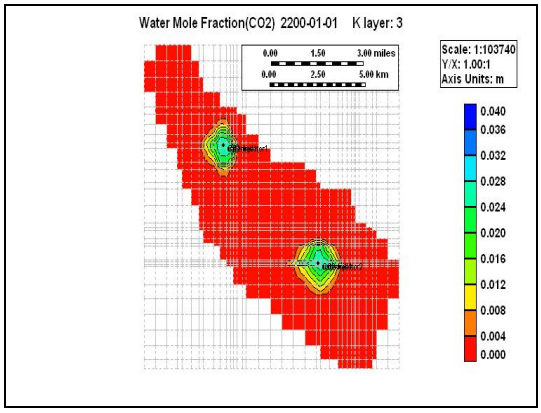

Figure 8.56 Map of CO_2 Mole Fraction in Water at 2200 (200 years) for Run 2a: field case, layer 3

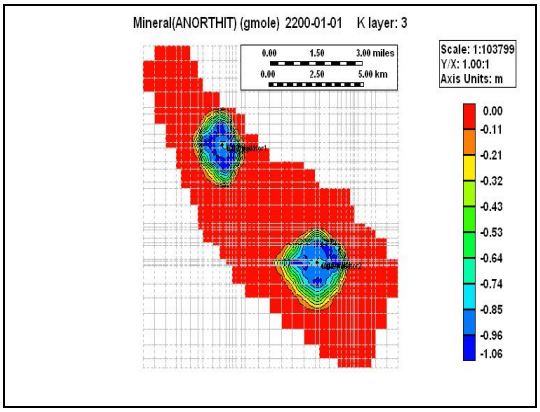

Figure 8.59 Map of Anorthite Dissolution / Precipitation at 2200 (200 years) for Run 2a: field case, layer 3

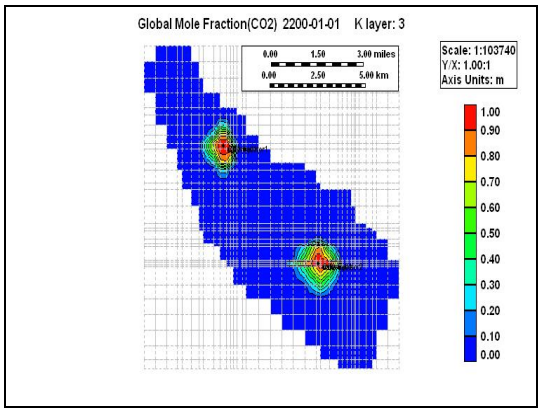

Figure 8.57 Map of CO_2 Global Mole Fraction at 2200 (200 years) for Run 2a: field case, layer 3

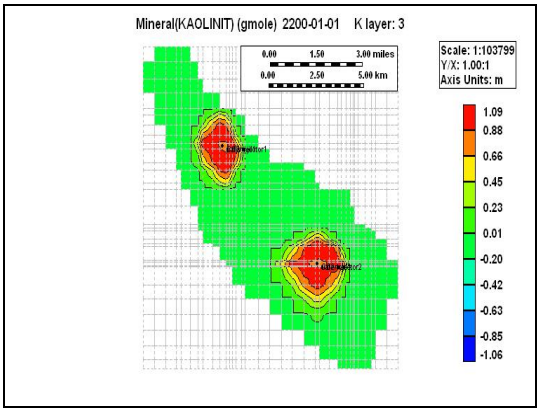

Figure 8.60 Map of Kaolinite Dissolution / Precipitation at 2200 (200 years) for Run 2a: field case, layer 3

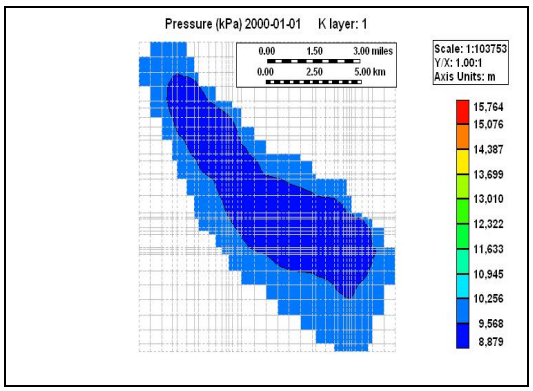

Figure 8.61 Pressure Distribution at layer 1 for field aquifer model, Run 1a at the beginning of the simulation (2000)

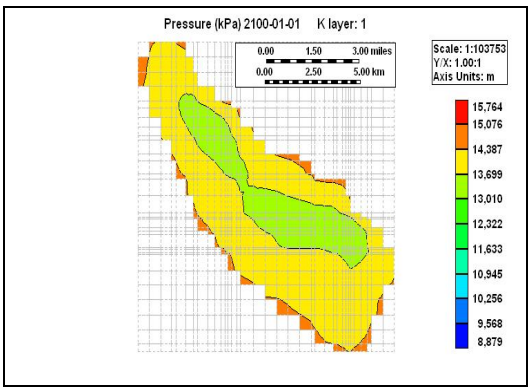

Figure 8.63 Pressure Distribution at layer 1 for field aquifer model, Run 1a after 100 years of the simulation (2100)

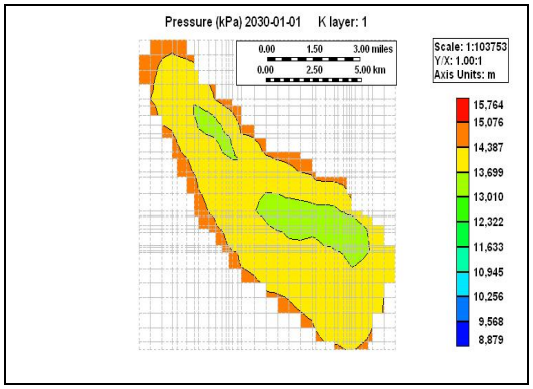

Figure 8.62 Pressure Distribution at layer 1 for field aquifer model, Run 1a after CO_2 injection has been ceased (2030)

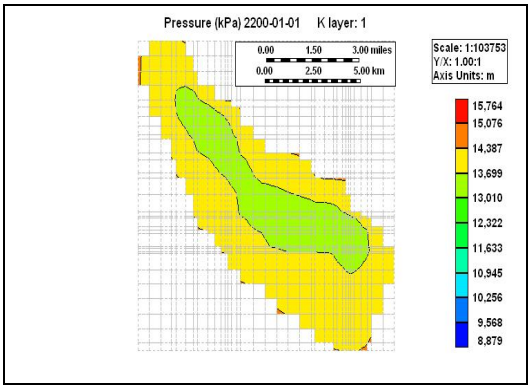

Figure 8.64 Pressure Distribution at layer 1 for field aquifer model, Run 1a at the end of the simulation (2200)

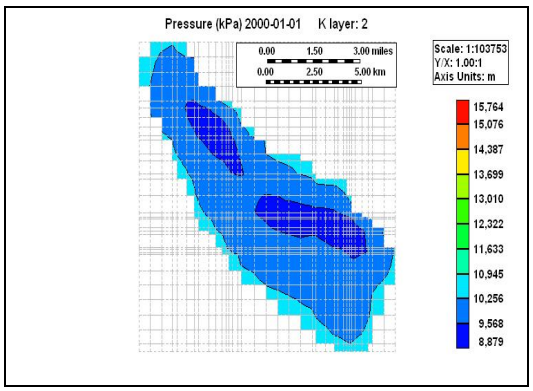

Figure 8.65 Pressure Distribution at layer 2 for field aquifer model, Run 1a at the beginning of the simulation (2000)

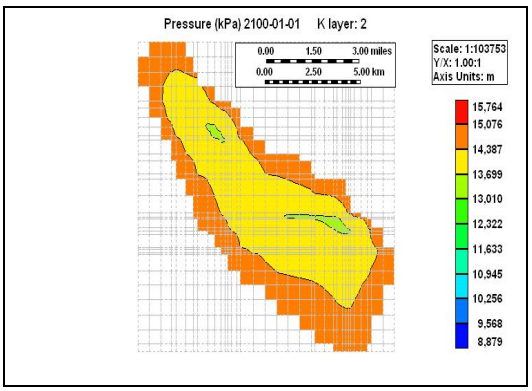

Figure 8.67 Pressure Distribution at layer 2 for field aquifer model, Run 1a after 100 years of the simulation (2100)

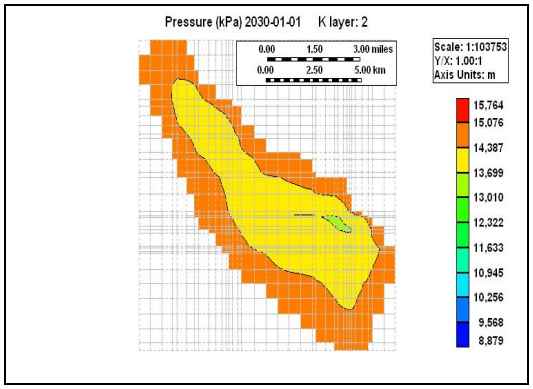

Figure 8.66 Pressure Distribution at layer 2 for field aquifer model, Run 1a after CO_2 injection has been ceased (2030)

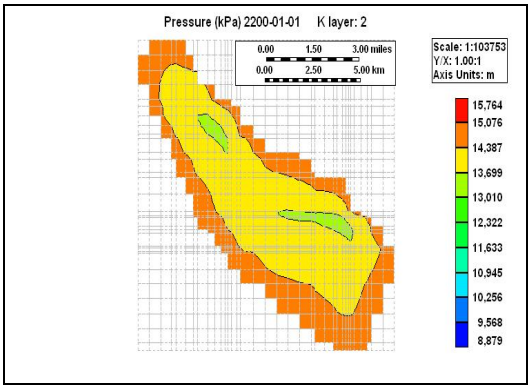

Figure 8.68 Pressure Distribution at layer 2 for field aquifer model, Run 1a at the end of the simulation (2200)

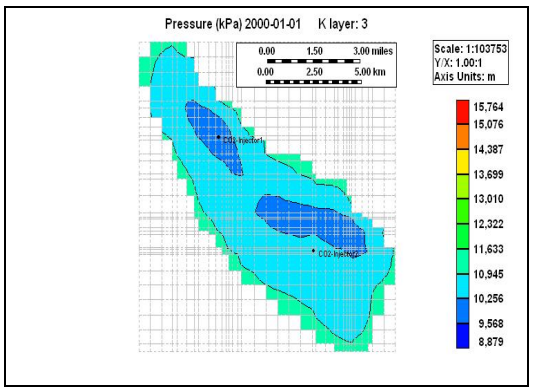

Figure 8.69 Pressure Distribution at layer 3 for field aquifer model, Run 1a at the beginning of the simulation (2000)

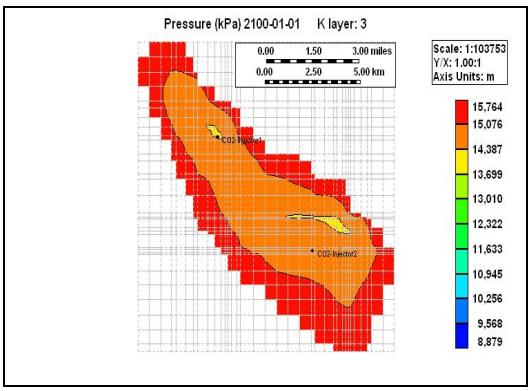

Figure 8.71 Pressure Distribution at layer 3 for field aquifer model, Run 1a after 100 years of the simulation (2100)

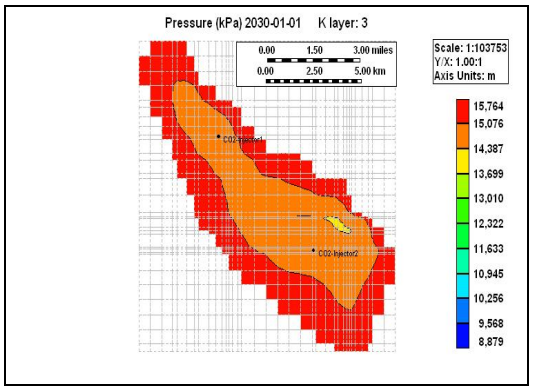

Figure 8.70 Pressure Distribution at layer 3 for field aquifer model, Run 1a after CO_2 injection has been ceased (2030)

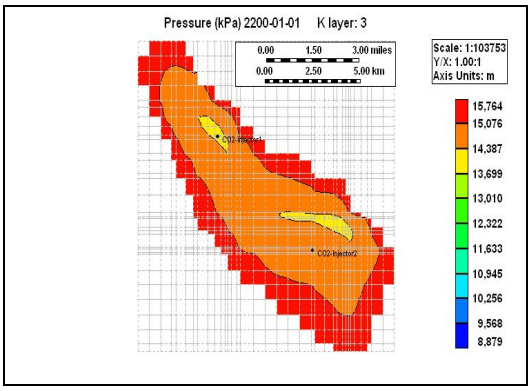

Figure 8.72 Pressure Distribution at layer 3 for field aquifer model, Run 1a at the end of the simulation (2200)

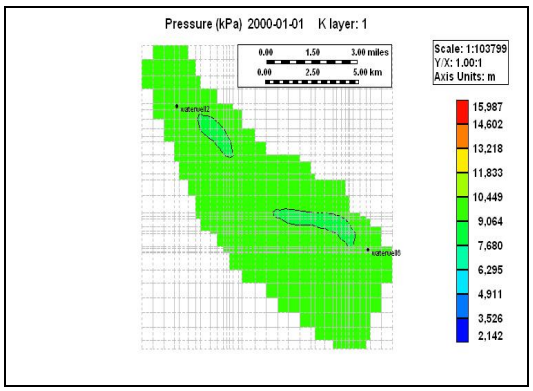

Figure 8.73 Pressure Distribution at layer 1 for field aquifer model, Run 2a at the beginning of the simulation (2000)

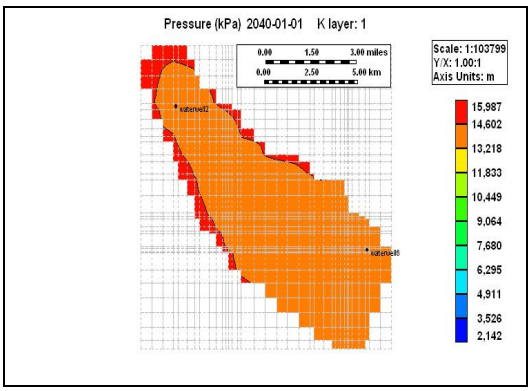

Figure 8.75 Pressure Distribution at layer 1 for field aquifer model, Run 2a after CO_2 injection has been ceased (2040)

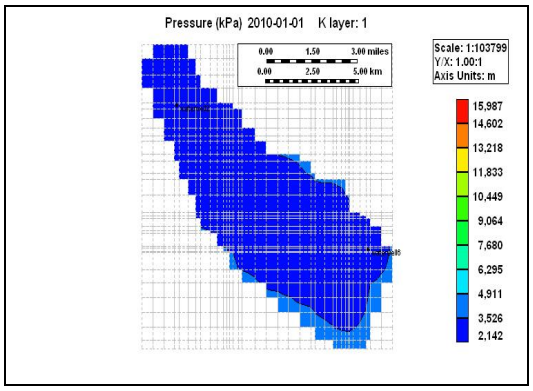

Figure 8.74 Pressure Distribution at layer 1 for field aquifer model, Run 2a after water production has been ceased (2010)

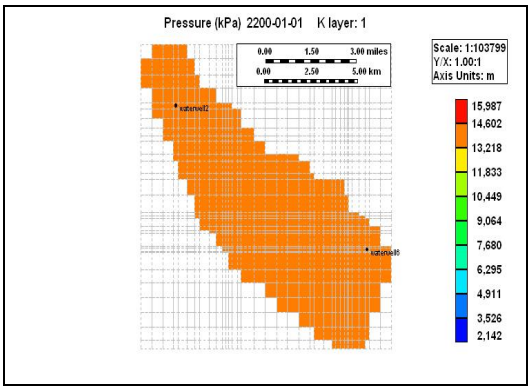

Figure 8.76 Pressure Distribution at layer 1 for field aquifer model, Run 2a at the end of the simulation (2200)

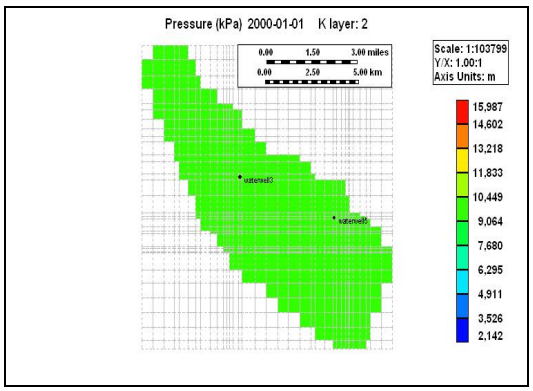

Figure 8.77 Pressure Distribution at layer 2 for field aquifer model, Run 2a at the beginning of the simulation (2000)

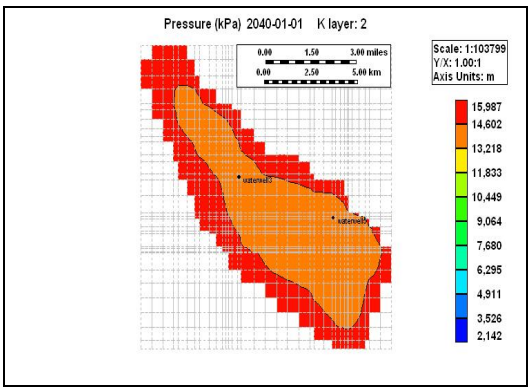

Figure 8.79 Pressure Distribution at layer 2 for field aquifer model, Run 2a after 40 years of the simulation (2040)

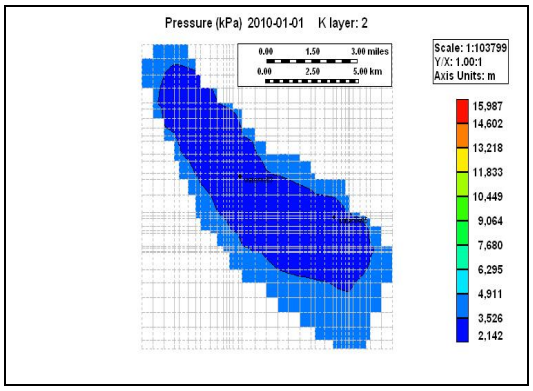

Figure 8.78 Pressure Distribution at layer 2 for field aquifer model, Run 2a after CO_2 injection has been ceased (2010)

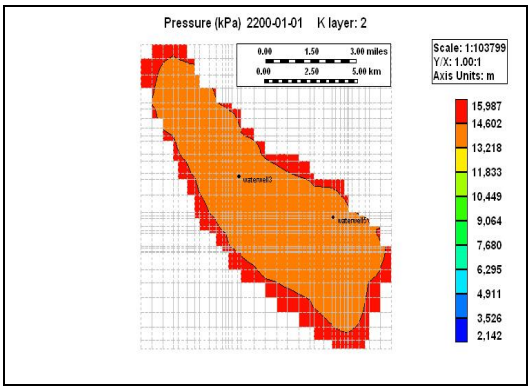

Figure 8.80 Pressure Distribution at layer 2 for field aquifer model, Run 2a at the end of the simulation (2200)

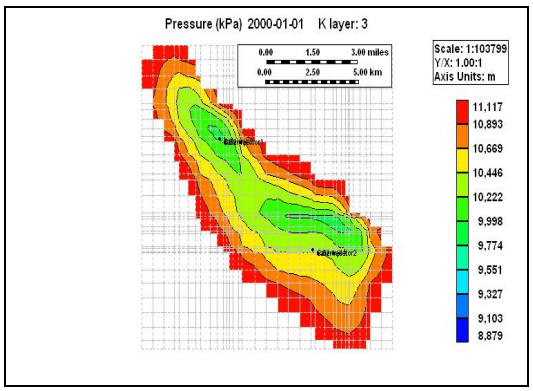

Figure 8.81 Pressure Distribution at layer 3 for field aquifer model, Run 2a at the beginning of the simulation (2000)

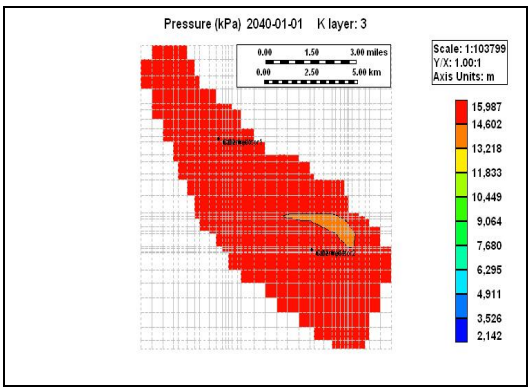

Figure 8.83 Pressure Distribution at layer 3 for field aquifer model, Run 2a after 40 years of the simulation (2040)

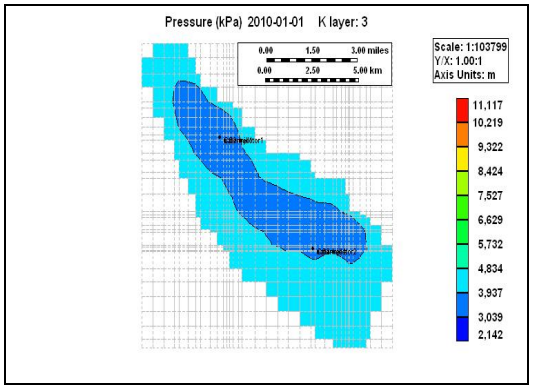

Figure 8.82 Pressure Distribution at layer 3 for field aquifer model, Run 2a after CO_2 injection has been ceased (2010)

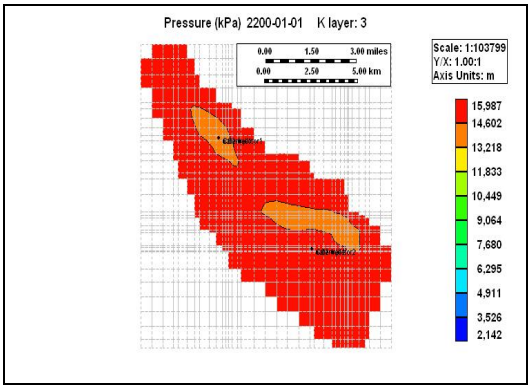

Figure 8.84 Pressure Distribution at layer 3 for field aquifer model, Run 2a at the end of the simulation (2200)

In a field aquifer model, CO_2 propagation in layer 1 for Runs 1a (without water production) and 2a (after water production) at injectors 1 and 2 are illustrated in Figures 8.85 through 8.90 and Tables 8.1 through 8.4. Figures 8.85 and 8.86 show CO_2 propagation in layer 1 along A-B direction for Runs 1a and 2a, respectively.

For Run 1a, CO_2 propagated in layer 1 at a distance of about 600 m at the end of 200 years. The relatively higher global mole fraction of CO_2 was observed around injector 1 when compared with that of injector 2 . This result was attributed to the presence of higher permeabilities around injector 1 (Figures 8.87 and 8.88 and Tables 8.1 and 8.2).

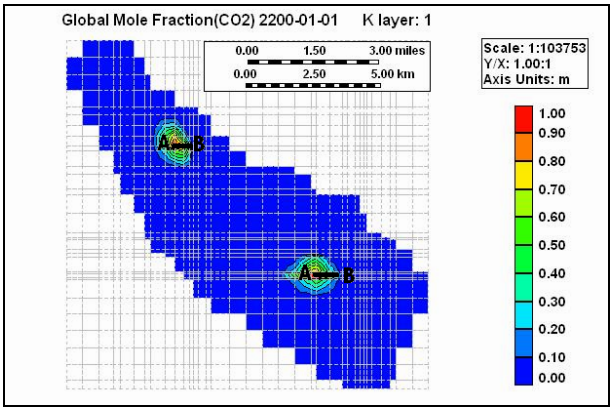

Figure 8.85 Map of CO_2 Global Mole Fraction at 2200 (200 years) for Run 1a: field case, layer 1

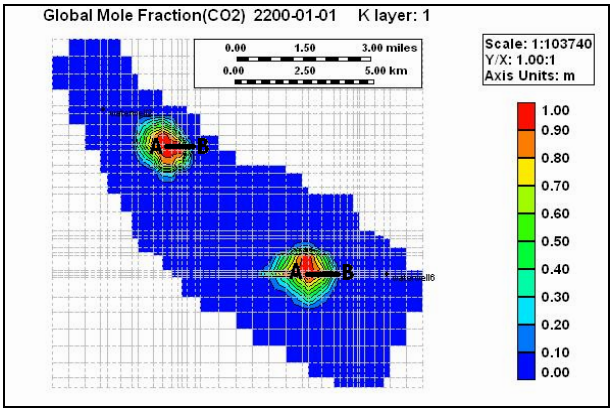

Figure 8.86 Map of CO_2 Global Mole Fraction at 2200 (200 years) for Run 2a: field case, layer 1

Table 8.1 Global Mole Fraction of CO_2 along A-B direction in layer 1 for Run 1a, field case, for injector 1

Date	2007	2008	2010	2015	2020	2025	2030	2035	2040	2200
Distance (m)	7 (years)	8	10	15	20	25	30	35	40	200
0.0	1.000	1.000	1.000	1.000	1.000	1.000	1.000	1.000	1.000	1.000
167.5	0.268	0.611	0.996	0.999	0.999	0.999	1.000	1.000	1.000	1.000
268.0	0.004	0.008	0.026	0.172	0.927	0.998	0.999	0.999	0.999	1.000
355.0	0.002	0.004	0.010	0.010	0.400	0.500	0.550	0.600	0.650	0.700
435.5	0.001	0.001	0.001	0.005	0.030	0.086	0.138	0.166	0.185	0.233
603.0	0.001	0.001	0.001	0.001	0.001	0.003	0.006	0.008	0.009	0.010

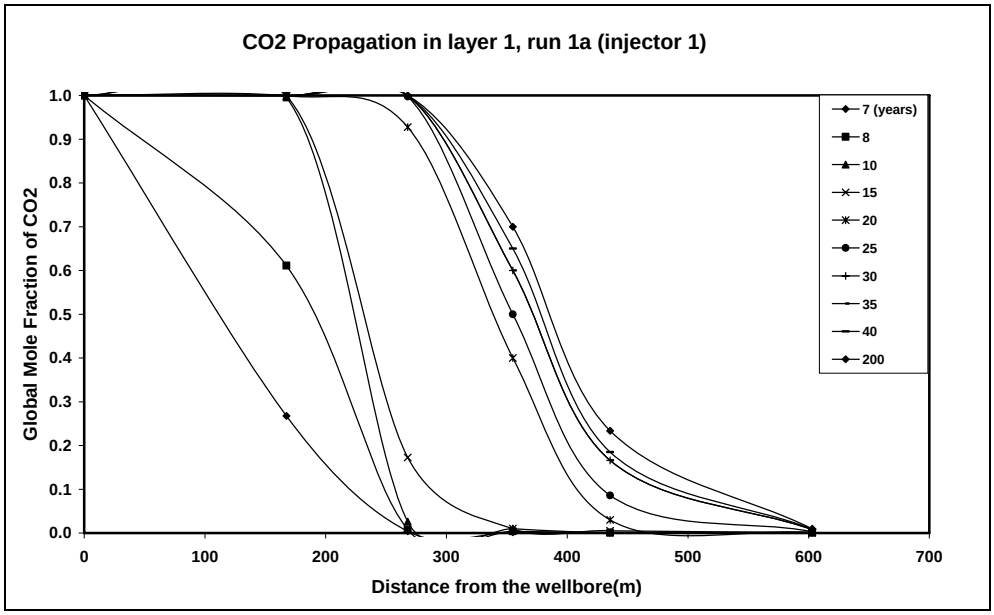

Figure 8.87 CO_2 Propagation in layer 1 for Run 1a along A-B direction, field case, for injector 1

Table 8.2 Global Mole Fraction of CO_2 along A-B direction in layer 1 for Run 1a, field case, for injector 2

Date	2005	2006	2007	2008	2010	2015	2020	2025	2030	2035	2040	2200
Distance (m)	5 (years)	6	7	8	10	15	20	25	30	35	40	200
0	1.000	1.000	1.000	1.000	1.000	1.000	1.000	1.000	1.000	1.000	1.000	1.000
167.5	0.198	0.467	0.915	0.992	0.998	0.999	0.999	0.999	0.999	0.999	0.999	1.000
268.0	0.002	0.003	0.005	0.008	0.014	0.054	0.179	0.382	0.684	0.937	0.988	0.999
435.5	0.001	0.001	0.001	0.001	0.001	0.001	0.002	0.005	0.010	0.011	0.012	0.174
603.0	0.001	0.001	0.001	0.001	0.001	0.001	0.001	0.001	0.001	0.001	0.001	0.001

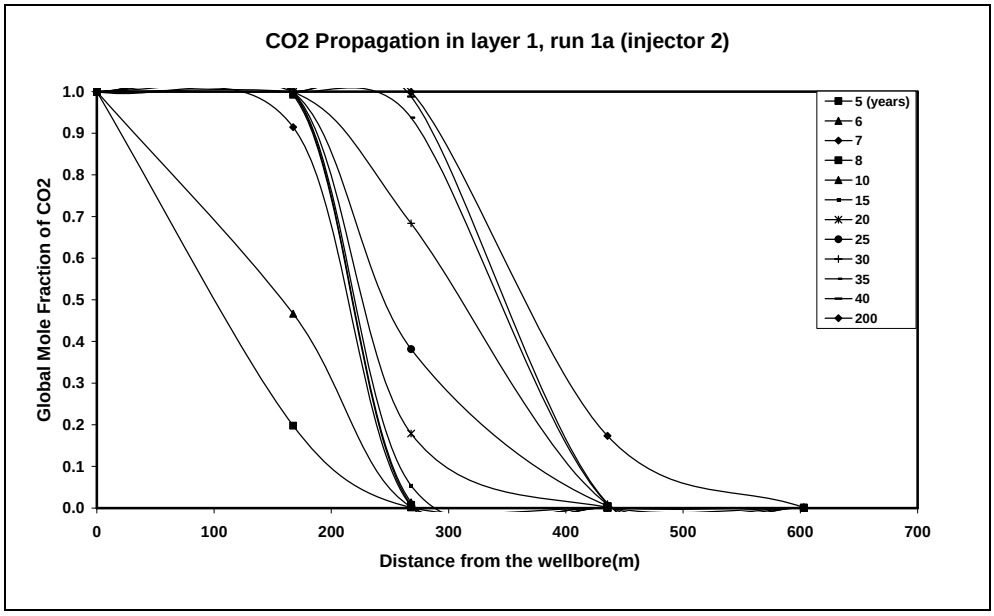

Figure 8.88 CO_2 Propagation in layer 1 for Run 1a along A-B direction, field case, for injector 2

The decrease in aquifer pressure after water production (Run 2a) resulted in more CO_2 propagation in layer 1. CO_2 propagated at a distance of about 835 m at the end of 200 years, (Figures 8.89 and 8.90, Tables 8.3 and 8.4). The relatively higher global mole fraction of CO_2 was observed around injector 1 because of having higher permeable region around it.

Table 8.3 Global Mole Fraction of CO_2 along A-B direction in layer 1 for Run 2a, field case, for injector 1

Date	2011	2012	2013	2014	2015	2016	2017	2020	2025	2030	2035	2040	2200
Distance (m)	11 (years)	12	13	14	15	16	17	20	25	30	35	40	200
0.0	1	1	1	1	1	1	1	1	1	1	1	1	1
167.5	0.231	0.991	0.996	0.997	0.998	0.998	0.998	0.999	0.999	1.000	1.000	1.000	1.000
268.0	0.005	0.068	0.378	0.954	0.994	0.997	0.998	0.998	0.999	0.999	1.000	1.000	1.000
435.5	0.002	0.003	0.015	0.058	0.149	0.319	0.650	0.995	0.998	0.999	0.999	0.999	1.000
603.0	0.002	0.002	0.002	0.003	0.006	0.011	0.018	0.065	0.088	0.217	0.553	0.987	0.999
837.5	0.002	0.002	0.002	0.001	0.001	0.001	0.001	0.002	0.003	0.006	0.014	0.025	0.049
938.0	0.002	0.002	0.001	0.001	0.001	0.001	0.001	0.001	0.001	0.001	0.001	0.001	0.002

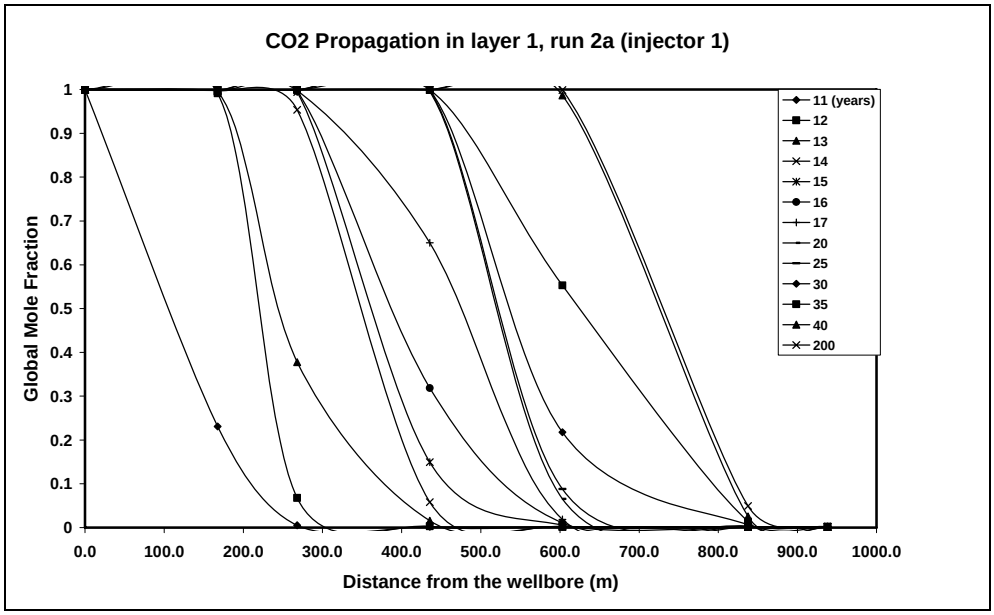

Figure 8.89 CO_2 Propagation in layer 1 for Run 2a along A-B direction, field case, for injector 1

Table 8.4 Global Mole Fraction of CO_2 along A-B direction in layer 1 for Run 2a, field case, for injector 2

Date	2011	2012	2013	2014	2015	2016	2017	2020	2025	2030	2035	2040	2200
Distance (m)	11 (years)	12	13	14	15	16	17	20	25	30	35	40	200
0.0	1	1	1	1	1	1	1	1	1	1	1	1	1
167.5	0.490	0.994	0.996	0.997	0.998	0.998	0.998	0.999	0.999	0.999	1.000	1.000	1.000
268.0	0.004	0.035	0.138	0.295	0.546	0.890	0.988	0.997	0.999	0.999	0.999	0.999	1.000
435.5	0.002	0.002	0.003	0.006	0.011	0.018	0.027	0.054	0.106	0.227	0.417	0.607	0.999
603.0	0.002	0.002	0.002	0.002	0.002	0.002	0.002	0.002	0.004	0.009	0.018	0.025	0.080
837.5	0.002	0.002	0.002	0.002	0.001	0.001	0.001	0.001	0.001	0.001	0.001	0.001	0.002

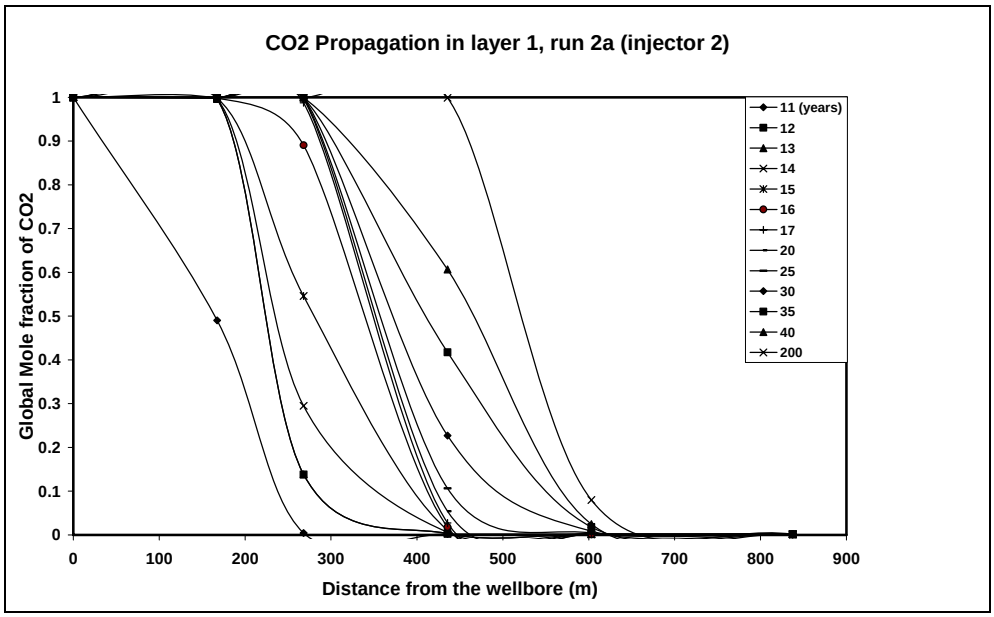

Figure 8.90 CO_2 Propagation in layer 1 for Run 2a along A-B direction, field case, for injector 2

8.3 Results of Single-well Aquifer Model

In a single-well aquifer model, 25 different scenarios (Runs 3a to 12b) whose conditions are given in Tables 7.6, 7.7 and 7.8 were performed to investigate grid refinement, effects of heterogeneity, injection rate, initial pressure conditions and salinity on CO_2 sequestration.

8.3.1 Grid Refinement

Grid dimension distributions for single-well aquifer model were illustrated in Table 7.10. There were 3 different grid configurations in our single-well aquifer model. Runs 3a and 4a were performed with coarse and fine grids configurations, respectively to obtain the convenient gridding configuration. Run 8b were performed with finer grid configuration than that of run 4a in order to produce less amount of water from the aquifer. CO_2 injection histories, CO_2 saturations, CO_2 mole fractions in water, Calcite dissolution / precipitation, Anorthite dissolution / precipitation, Kaolinite dissolution / precipitation graphs at the injection well block for Run 3a and 4a are given in Figures 8.91 through 8.102. By comparing these graphs for both Runs 3a and 4a, it was obtained that fine grid configurations were more appropriate than coarse grid representation. For instance, in CO_2 saturation versus time plots, it was observed that CO_2 saturation values for all three layers especially for layer 3 for Run 3a were lower than values that were observed for Run 4a which were considered as wrong saturation values for our simulation. It was thought that saturation values with coarse grid configuration case (Run 3a) were not representative for grid itself since grid dimesions were chosen as large enough around the wellbore. For instance, dimension of the first grid next to wellbore block was chosen as 80 m whereas wellbore radius was taken as 0.25 m for coarse grid configuration for Run 3a. Dimension of the first grid next to wellbore block was chosen as 0.5 m for Run 4a. After determining the grid configuration as they were in Run 4a, in order to examine effects of heterogeneity, injection rate, initial pressure conditions and salinity on CO_2 sequestration several runs were compared. Related to

these successive runs, assigned graphs plotted for the injection well blocks are demonstrated for each case particularly in C.1 through C.138 (Appendix C).

8.3.2 Effect of k_v/k_h ratio on CO_2 Saturation

The results of Runs (4a, 4b, 4c, 4d) and (5b, 5c, 5d) and (6b, 6c, 6d) were compared to examine the effect of k_v / k_h ratio on CO_2 saturation (Figures 8.103 through 8.111). It can be detected that the increase in k_v / k_h ratio caused an increase in CO_2 saturation in layer 1 unlike CO_2 saturation decreased with an increase in k_v / k_h ratio in layers 2 and 3 after the CO_2 injection had been stopped which indicated that CO_2 has a tendency to rise up.

8.3.3 Effect of Permeability Distribution on CO_2 Saturation

Figures 8.112 through 8.114 show the effect of permeability distribution on CO_2 sequestration process by examining the results of Runs 4b, 5b and 6b. The layer wise horizontal permeability distribution played an important role on CO_2 saturation compared to block wise horizontal permeability distribution. Because of the fact that CO_2 tended to move through upper layers immediately due to density difference, there was no significant change in CO_2 saturation between the constant horizontal permeability in each layer case (Run 5b) and variable horizontal permeability distribution in each layer case (Run 6b). However, a significant change was observed in CO_2 saturation between Runs 5b and 6b compared to a constant horizontal permeability (150 md) in whole layers of aquifer case (Run 4b). It can be perceived from Figures 8.226 through 8.228 that the decrease in horizontal permeability from bottom to top layers resulted in an increase in CO_2 saturation in layers 2 and 3 contrary to layer 1 after the CO_2 injection has been ceased.

8.3.4 Effect of CO_2 Injection Rate on on CO_2 Saturation

Figures 8.115 through 8.2117 were constructed to analyze the effect of CO_2 injection rate by comparing the results of Runs 5b and 7b. The increase in injection rate increased the CO_2 saturation in layers 2 and 3 after the injection had been ceased. There were no significant changes in layer 1 with increasing injection rate. But by comparing Runs 8b, 9b and 10b, different situation has been encountered. The increase in injection rate caused a decrease in CO_2 saturation in all three layers (Figures 8.118 through 8.120) after CO_2 injection has been stopped. This may be attributed to decreasing the initial aquifer pressure by producing water before CO_2 was injected which resulted an increase in CO_2 solubility in water with applying high pressure by injecting more CO_2. Solubility of CO_2 increases with increasing pressure [90].

8.3.5 Effect of Salinity on CO_2 Saturation

Finally, the results of Runs 5b, 11b and 12b were compared to determine the effect of salinity of the aquifer water on CO_2 sequestration. It can be seen from Figures 8.121 through 8.122 that the impact of salinity on CO_2 saturation was seen as insignificant. But the solubility of CO_2 in water will be affected by changes in salinity [90].

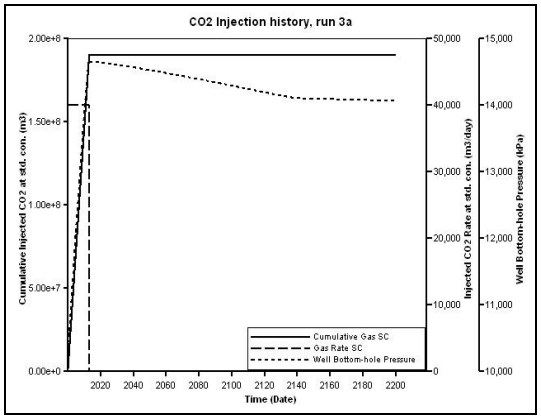

Figure 8.91 CO_2 Injection History for Run 3a: single-well case, (CO_2 injection rate = 40000 sm^3/d)

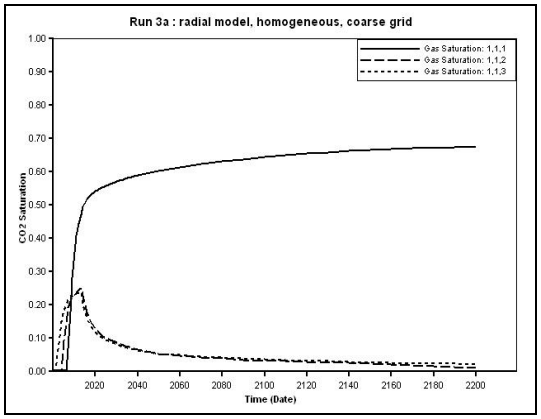

Figure 8.92 CO_2 Saturation for Run 3a: single-well case

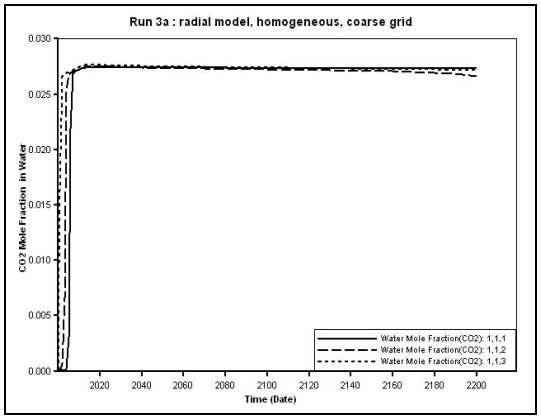

Figure 8.93 CO_2 Mole Fraction in Water for Run 3a: single-well case

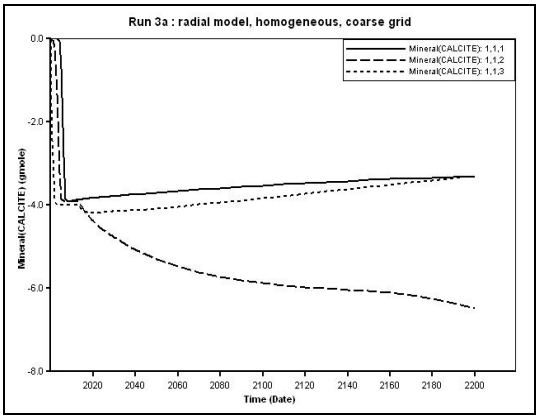

Figure 8.94 Calcite Dissolution / Precipitation for Run 3a: single-well case

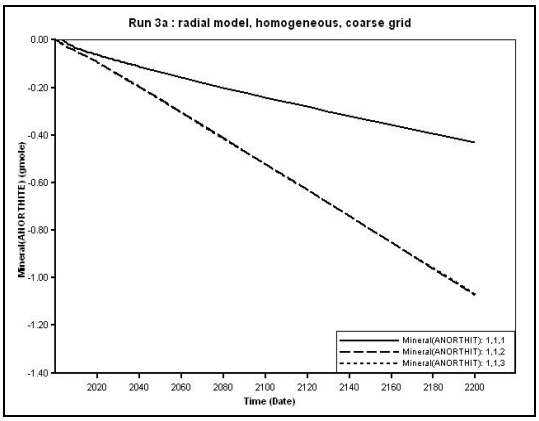

Figure 8.95 AnorthiteDissolution / Precipitation for Run 3a: single-well case

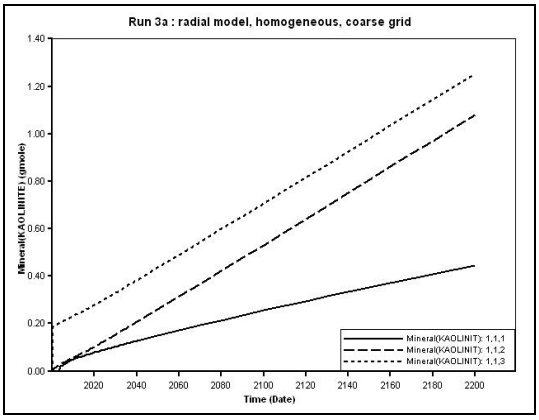

Figure 8.96 Kaolinite Dissolution / Precipitation for Run 3a: single-well case

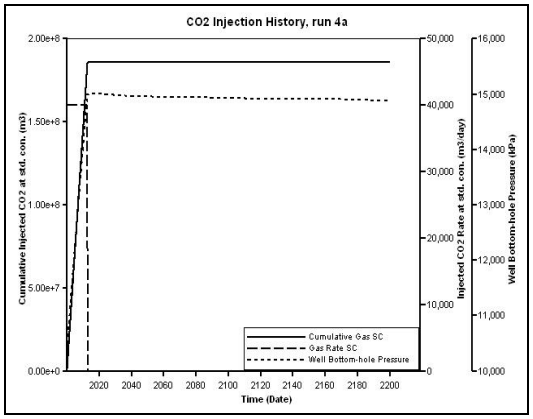

Figure 8.97 CO_2 Injection History for Run 4a: single-well case, (CO_2 injection rate = 40000 sm^3/d)

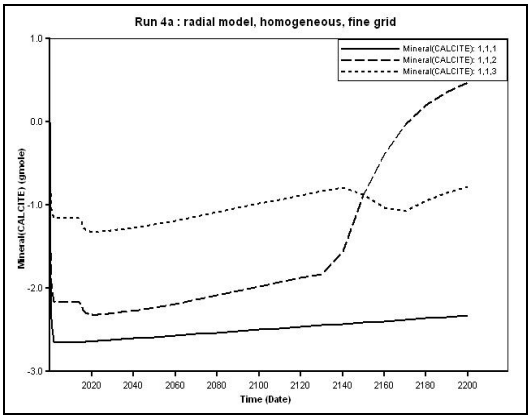

Figure 8.100 Calcite Dissolution / Precipitation for Run 4a: single-well case

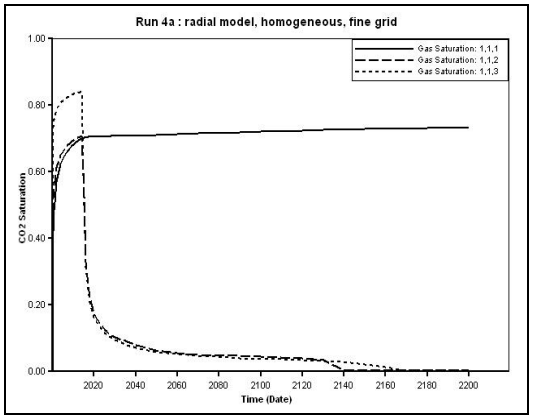

Figure 8.98 CO_2 Saturation for Run 4a: single-well case

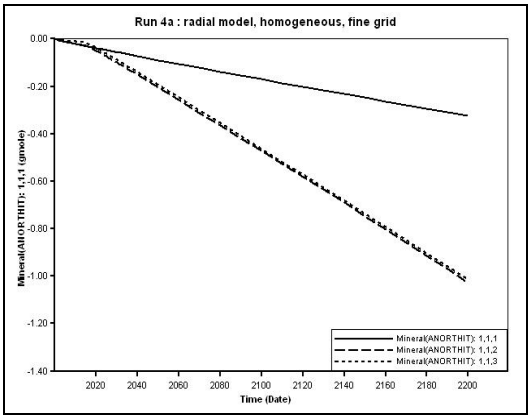

Figure 8.101 AnorthiteDissolution / Precipitation for Run 4a: single-well case

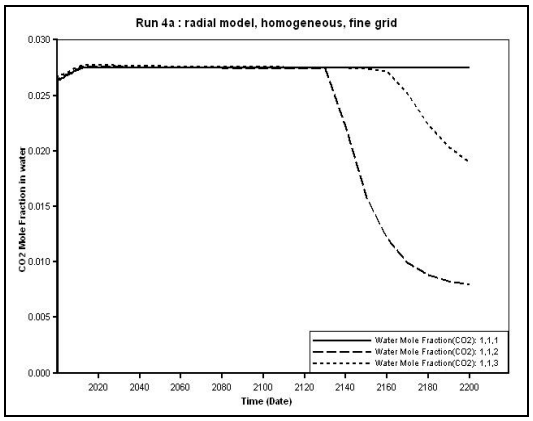

Figure 8.99 CO_2 Mole Fraction in Water for Run 4a: single-well case

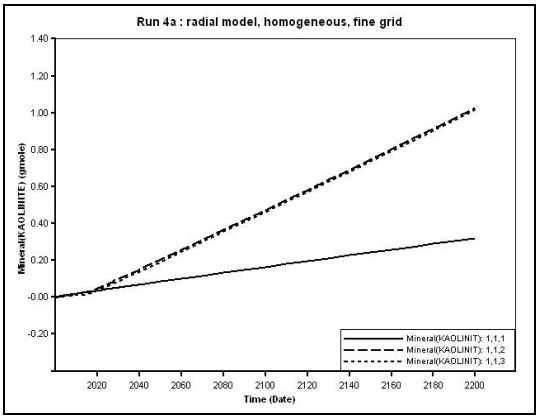

Figure 8.102 Kaolinite Dissolution / Precipitation for Run 4a: single-well case

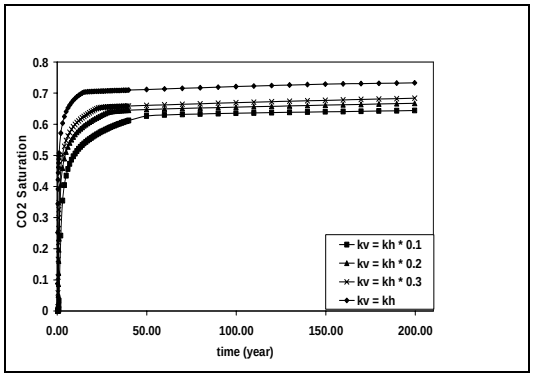

Figure 8.103 Effect of k_v / k_h ratio on CO_2 Saturation for Run 4a, 4b, 4c, 4d: radial model, layer 1

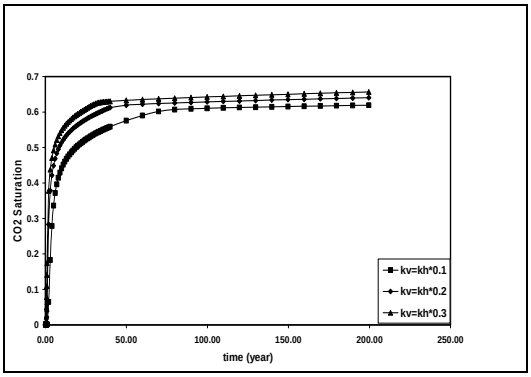

Figure 8.106 Effect of k_v / k_h ratio on CO_2 Saturation for Run 5b, 5c, 5d: radial model, layer 1

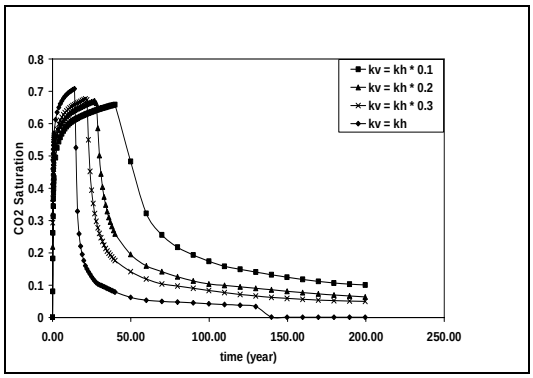

Figure 8.104 Effect of k_v / k_h ratio on CO_2 Saturation for Run 4a, 4b, 4c, 4d: radial model, layer 2

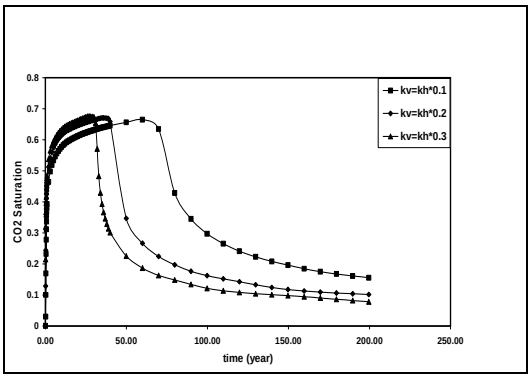

Figure 8.107 Effect of k_v / k_h ratio on CO_2 Saturation for Run 5b, 5c, 5d: radial model, layer 2

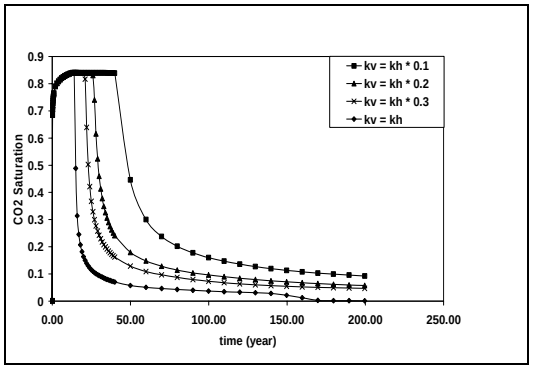

Figure 8.105 Effect of k_v / k_h ratio on CO_2 Saturation for Run 4a, 4b, 4c, 4d: radial model, layer 3

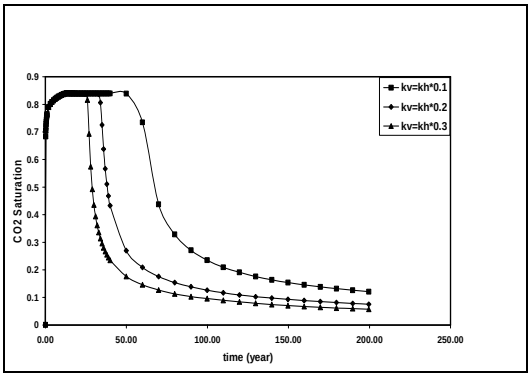

Figure 8.108 Effect of k_v / k_h ratio on CO_2 Saturation for Run 5b, 5c, 5d: radial model, layer 3

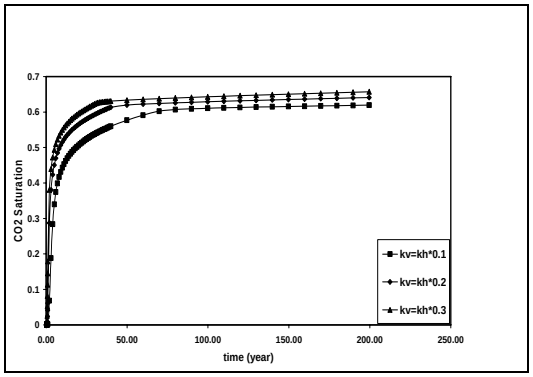

Figure 8.109 Effect of k_v / k_h ratio on CO_2 Saturation for Run 6b, 6c, 6d: radial model, layer 1

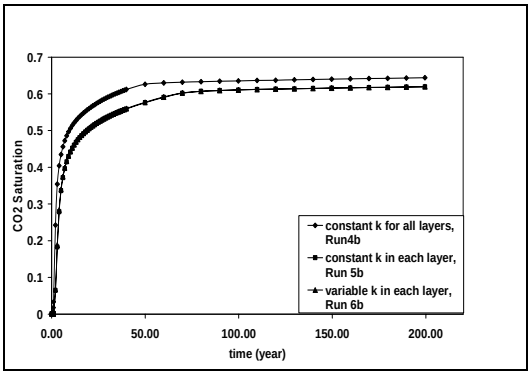

Figure 8.112 Effect of permeability distribution on CO_2 Saturation for Run 4b, 5b, 6b: radial model, k_v / k_h = 0.1 layer 1

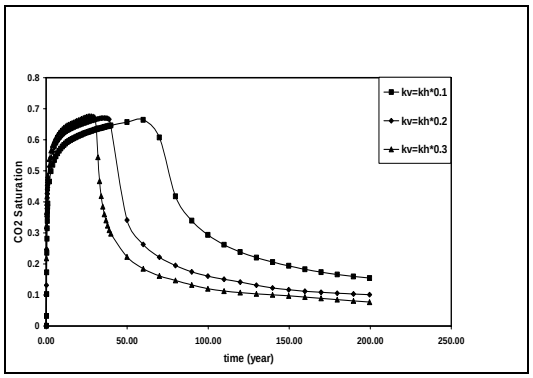

Figure 8.110 Effect of k_v / k_h ratio on CO_2 Saturation for Run 6b, 6c, 6d: radial model, layer 2

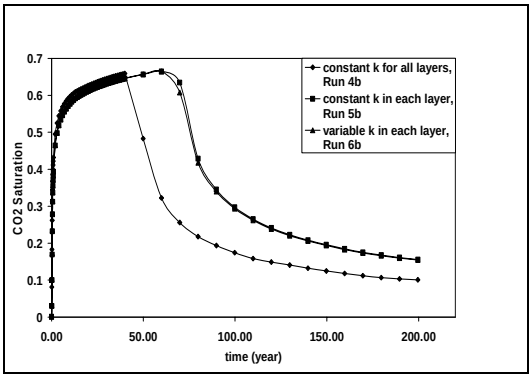

Figure 8.113 Effect of permeability distribution on CO_2 Saturation for Run 4b, 5b, 6b: radial model, k_v / k_h = 0.1 layer 2

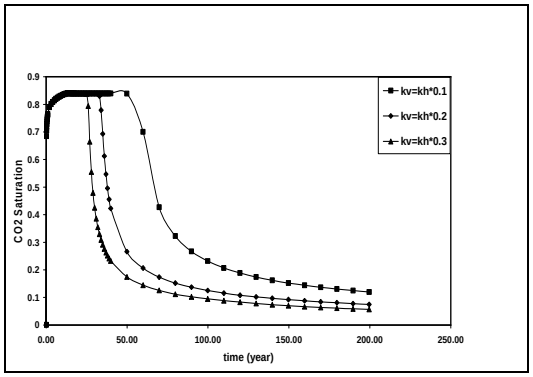

Figure 8.111 Effect of k_v / k_h ratio on CO_2 Saturation for Run 6b, 6c, 6d: radial model, layer 3

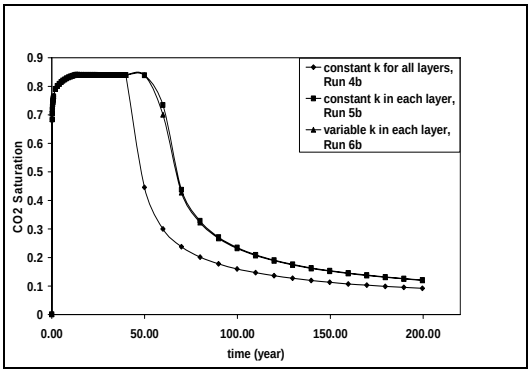

Figure 8.114 Effect of permeability distribution on CO_2 Saturation for Run 4b, 5b, 6b: radial model, k_v / k_h = 0.1 layer 3

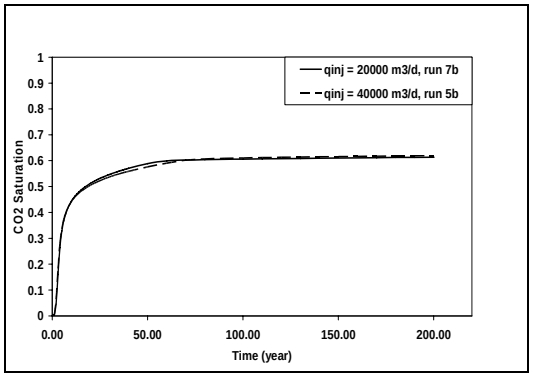

Figure 8.115 Effect of CO_2 injection rate on CO_2 Saturation for Run 5b, 7b: radial model, $k_v / k_h = 0.1$ layer 1

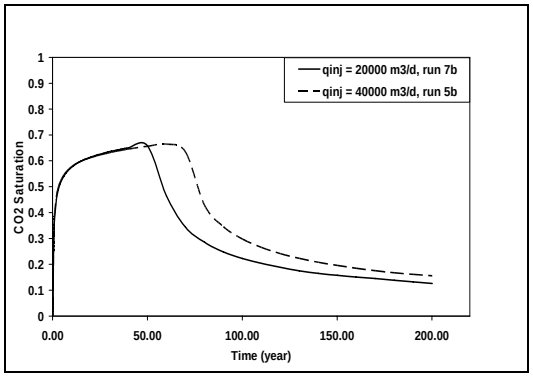

Figure 8.116 Effect of CO_2 injection rate on CO_2 Saturation for Run 5b, 7b: radial model, $k_v / k_h = 0.1$ layer 2

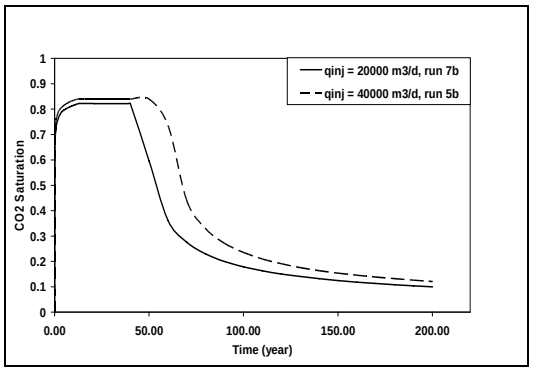

Figure 8.117 Effect of CO_2 injection rate on CO_2 Saturation for Run 5b, 7b: radial model, $k_v / k_h = 0.1$ layer 3

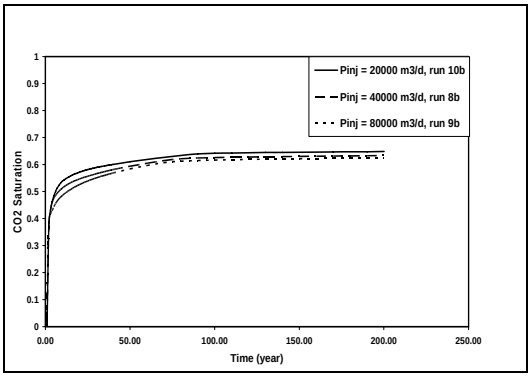

Figure 8.118 Effect of CO_2 injection rate on CO_2 Saturation for Run 8b, 9b, 10b: radial model, $k_v / k_h = 0.1$ layer 1

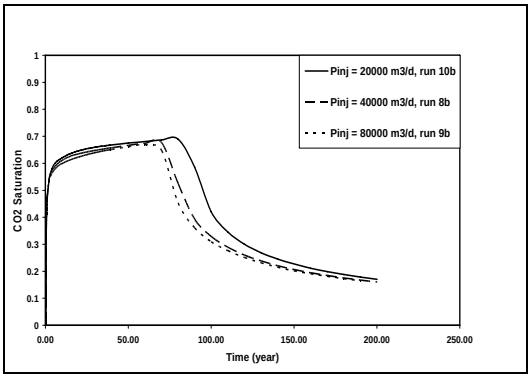

Figure 8.119 Effect of CO_2 injection rate on CO_2 Saturation for Run 8b, 9b, 10b: radial model, $k_v / k_h = 0.1$ layer 2

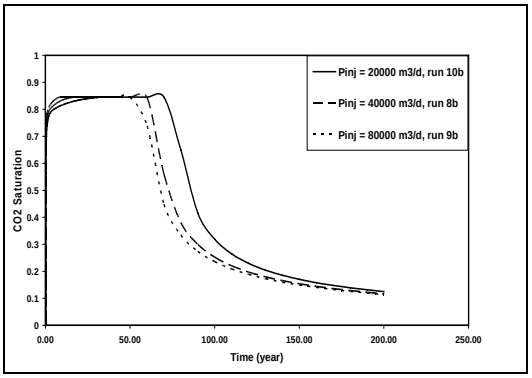

Figure 8.120 Effect of CO_2 injection rate on CO_2 Saturation for Run 8b, 9b, 10b: radial model, $k_v / k_h = 0.1$ layer 3

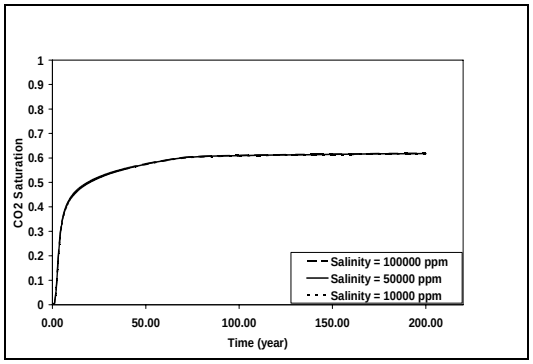

Figure 8.121 Effect of salinity on CO_2 Saturation for Runs 5b, 11b and 12b: radial model, $k_v / k_h = 0.1$ layer 1

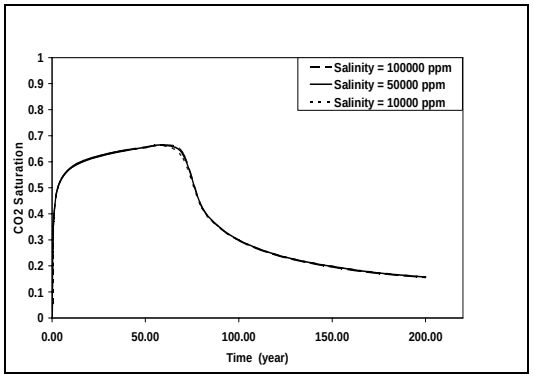

Figure 8.122 Effect of salinity on CO_2 Saturation for Runs 5b, 11b and 12b: radial model, $k_v / k_h = 0.1$ layer 2

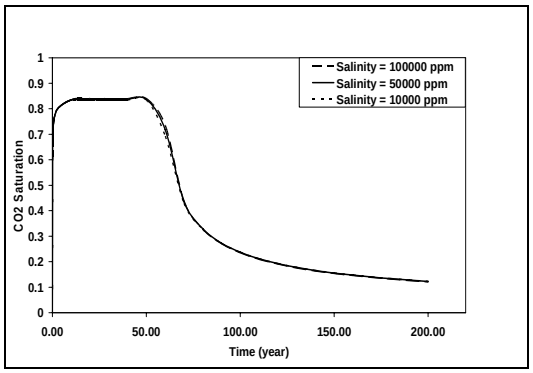

Figure 8.123 Effect of salinity on CO_2 Saturation for Runs 5b, 11b and 12b: radial model, $k_v / k_h = 0.1$ layer 3

CO_2 Propagations in layer 1 along A-B direction (Figure 8.124) are demonstrated particularly in Figures 8.125 through 8.147 and in Tables D.1 through D.23 (Appendix D) for all successive runs 4b through 12b. It was observed from Figures 8.125 through 8.147 and in Tables D.1 through D.23 that CO_2 propagated at a distance between 135 m and 255 m at the end of simulation (200 years) for different cases.

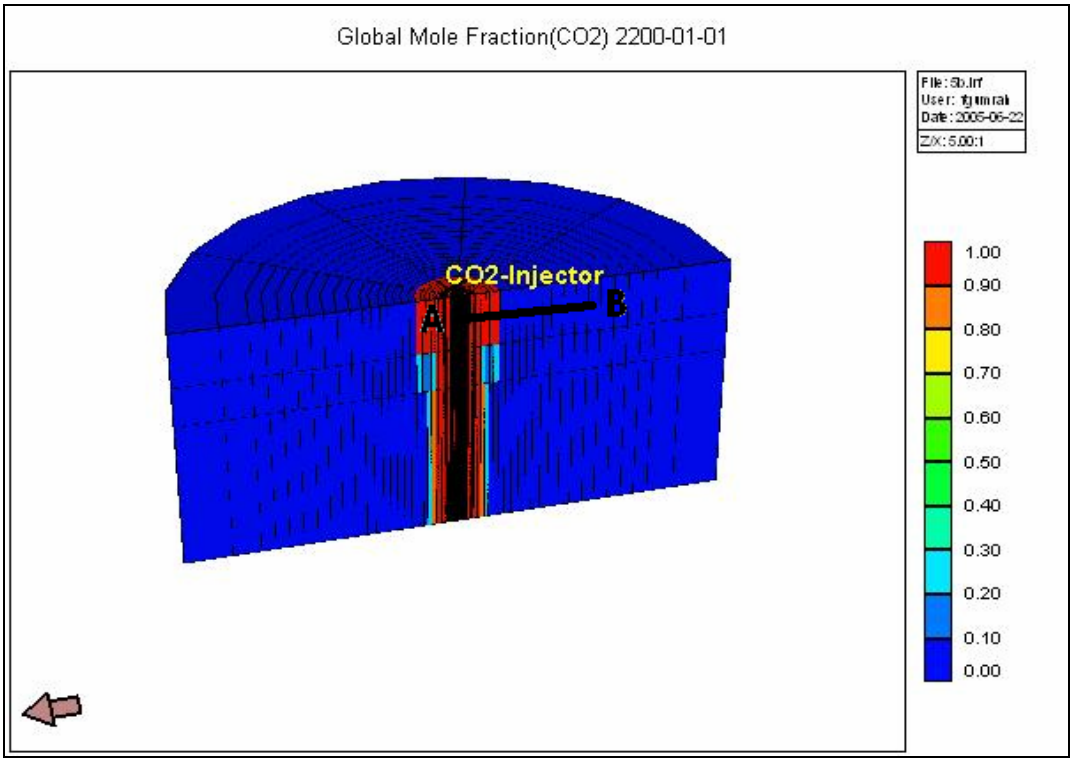

Figure 8.124Global Mole Fraction of CO_2 for run 5b, radial model

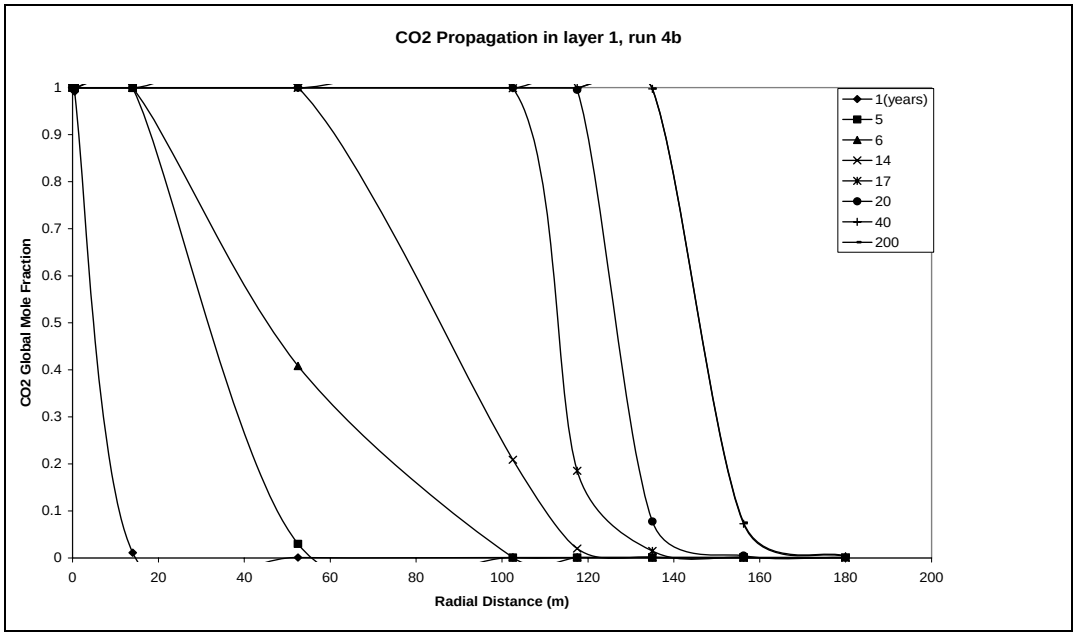

Figure 8.125 CO_2 Propagation in layer 1 for Run 4b, single-well model

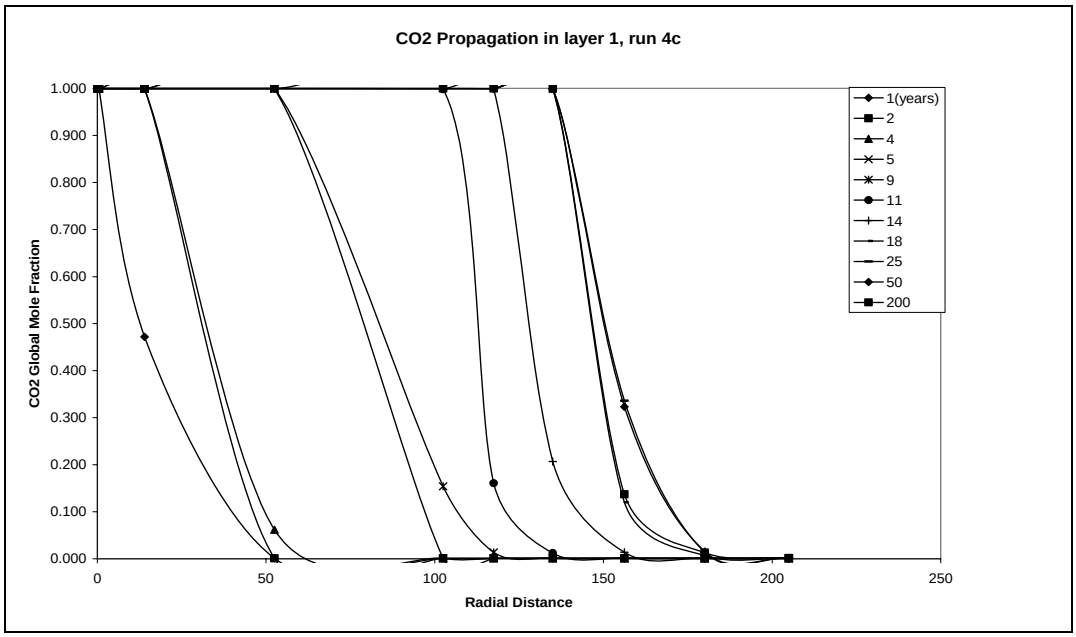

Figure 8.126 CO_2 Propagation in layer 1 for Run 4c, single-well model

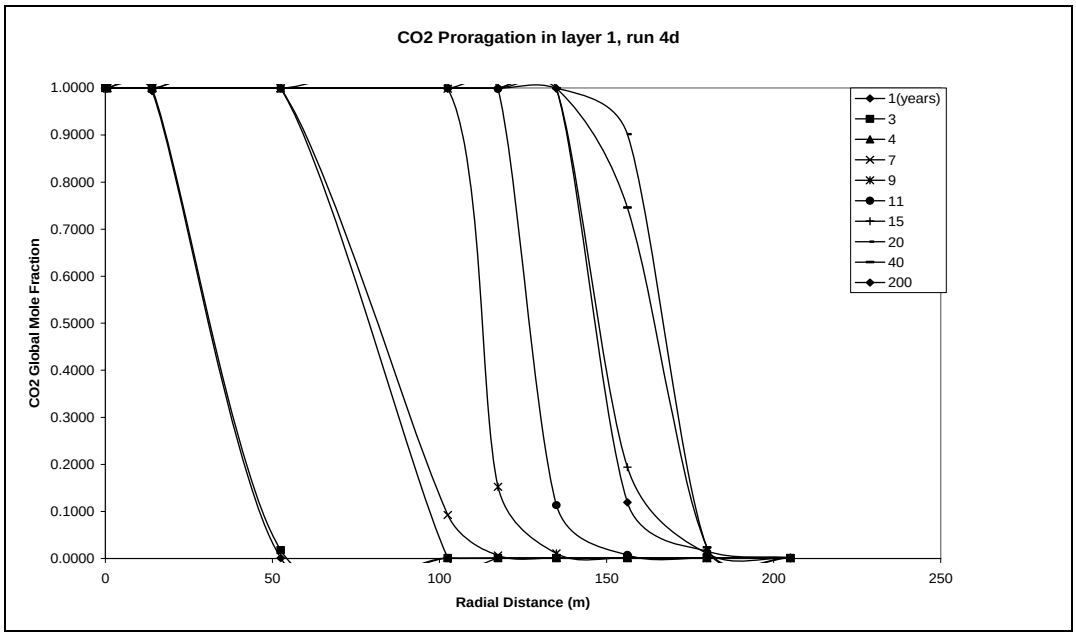

Figure 8.127 CO_2 Propagation in layer 1 for Run 4d, single-well model

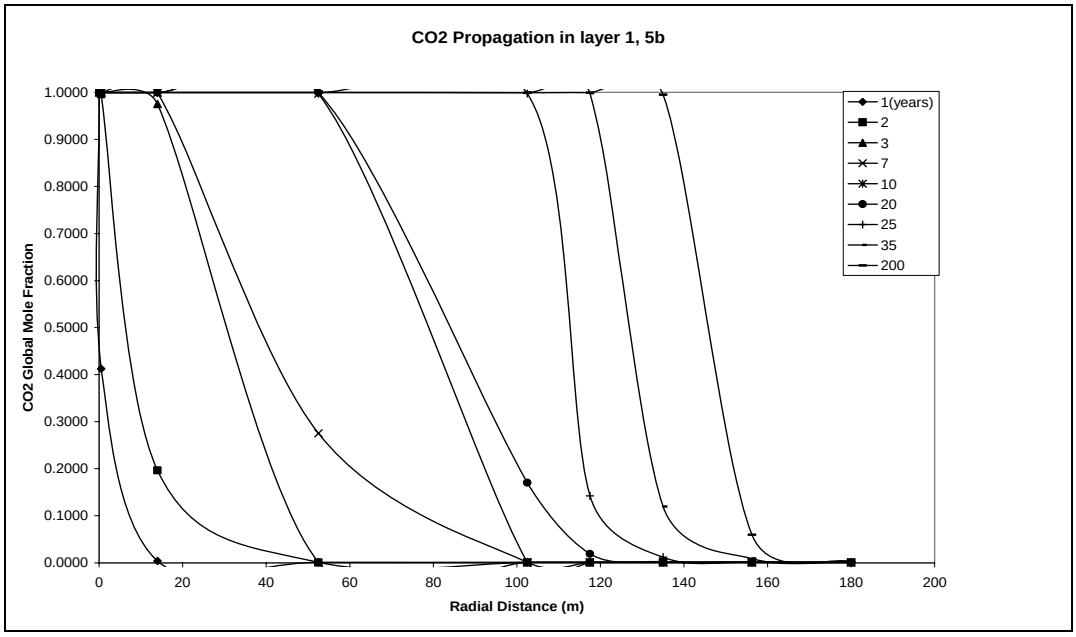

Figure 8.128 CO_2 Propagation in layer 1 for Run 5b, single-well model

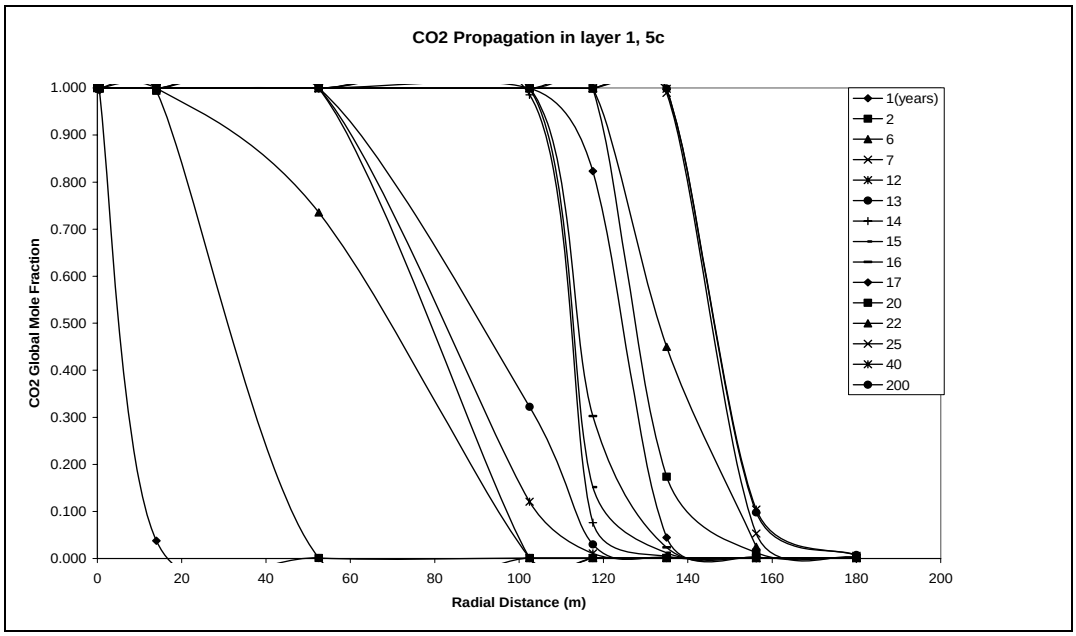

Figure 8.129 CO_2 Propagation in layer 1 for Run 5c, single-well model

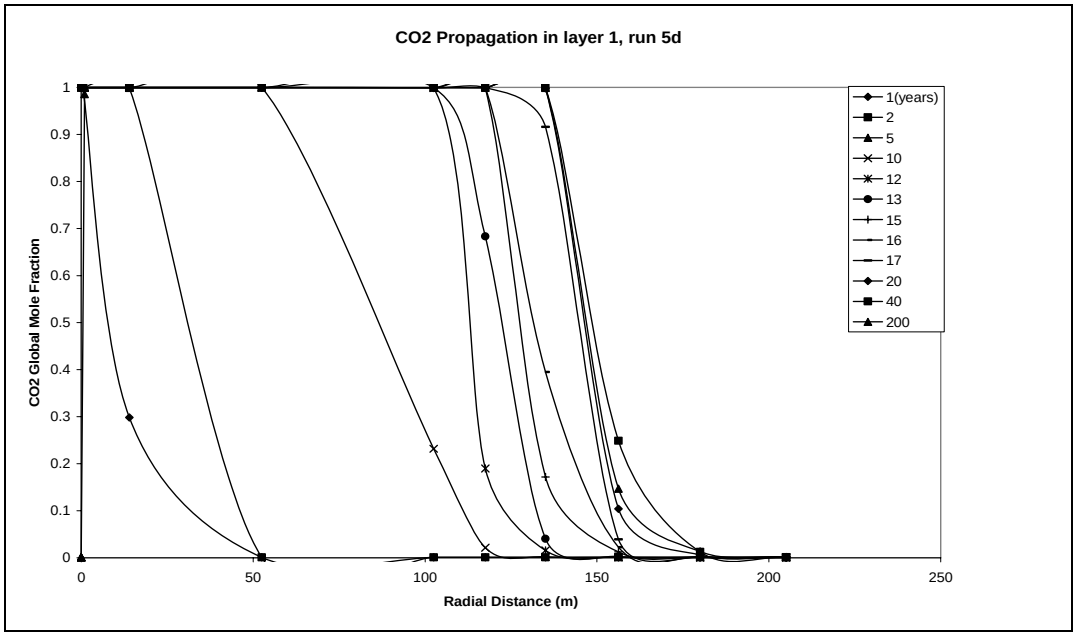

Figure 8.130 CO_2 Propagation in layer 1 for Run 5d, single-well model

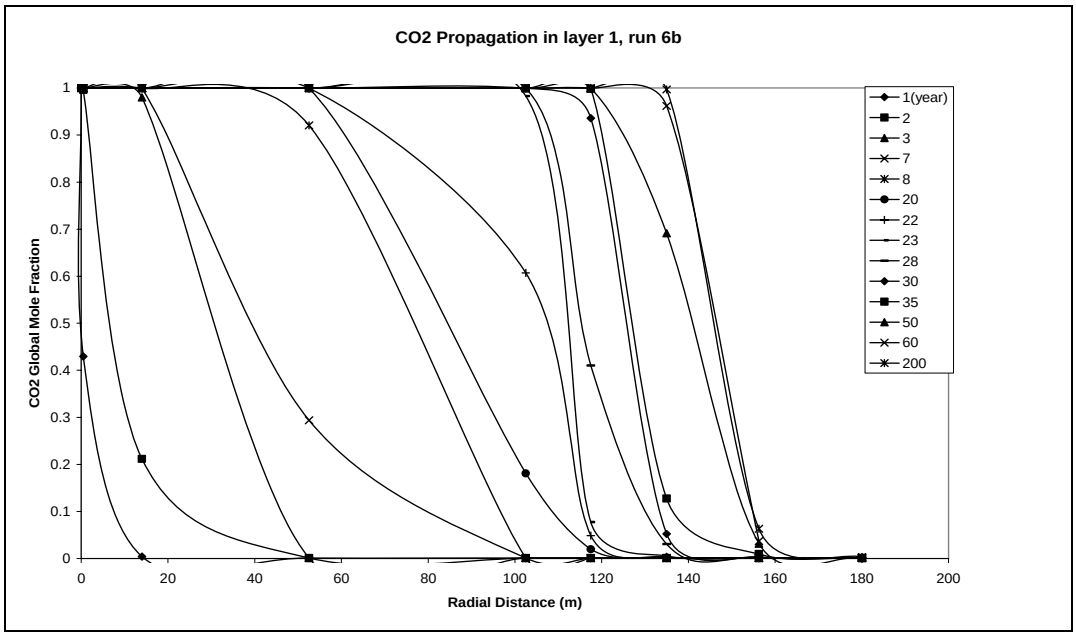

Figure 8.131 CO_2 Propagation in layer 1 for Run 6b, single-well model

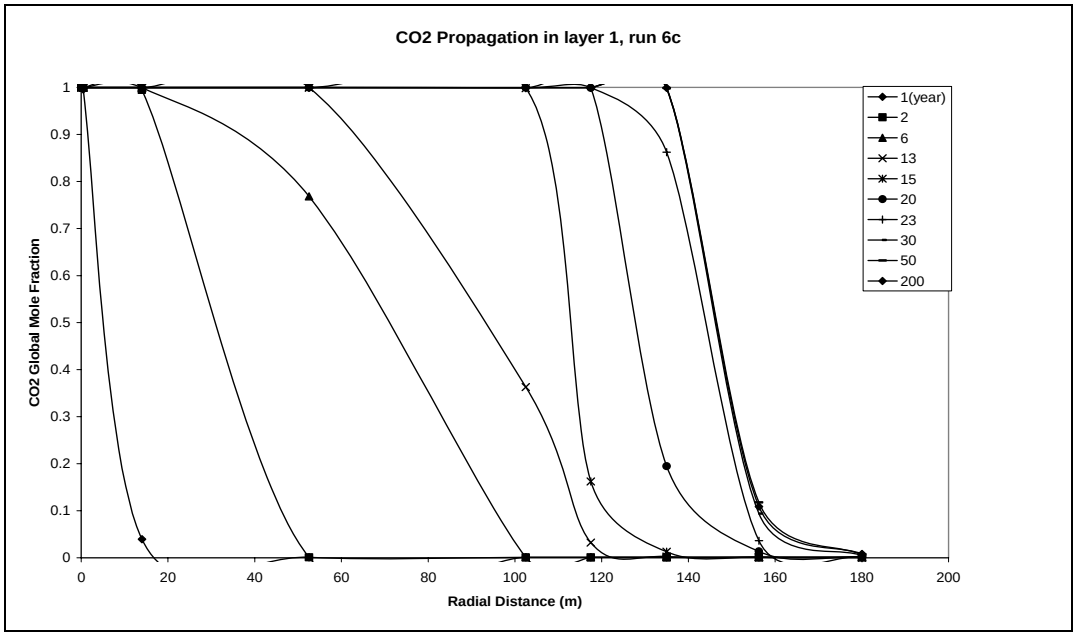

Figure 8.132 CO_2 Propagation in layer 1 for Run 6c, single-well model

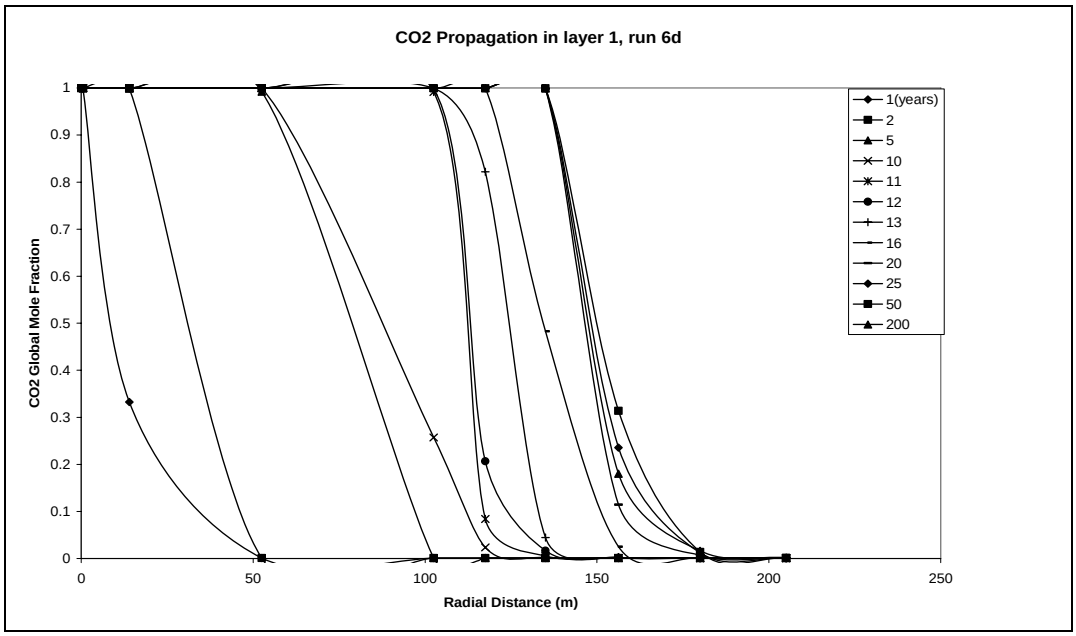

Figure 8.133 CO_2 Propagation in layer 1 for Run 6d, single-well model

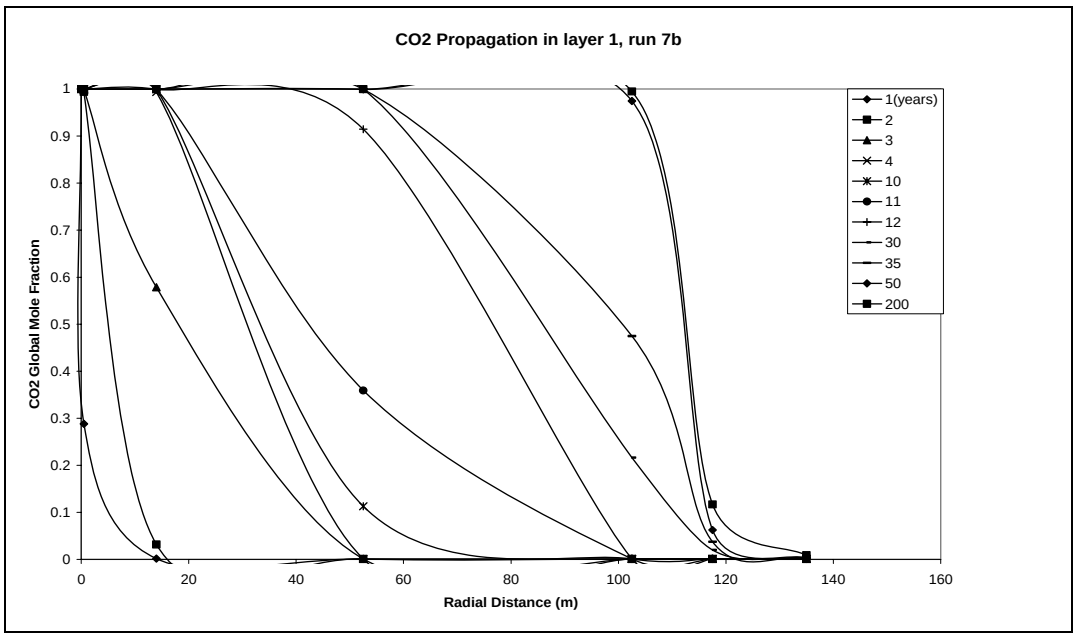

Figure 8.134 CO_2 Propagation in layer 1 for Run 7b, single-well model

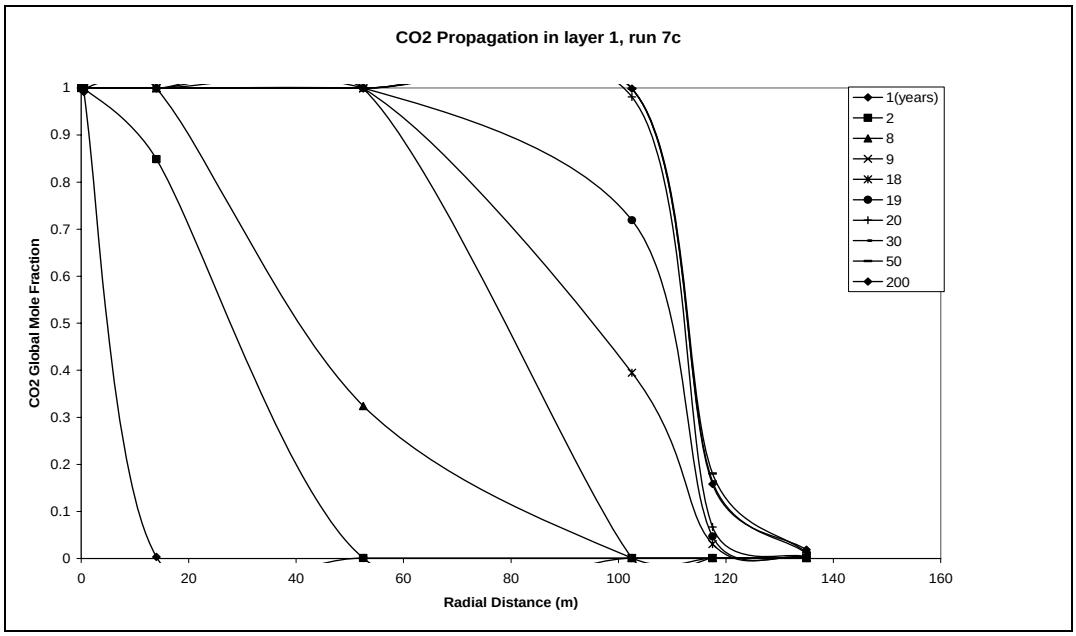

Figure 8.135 CO_2 Propagation in layer 1 for Run 7c, single-well model

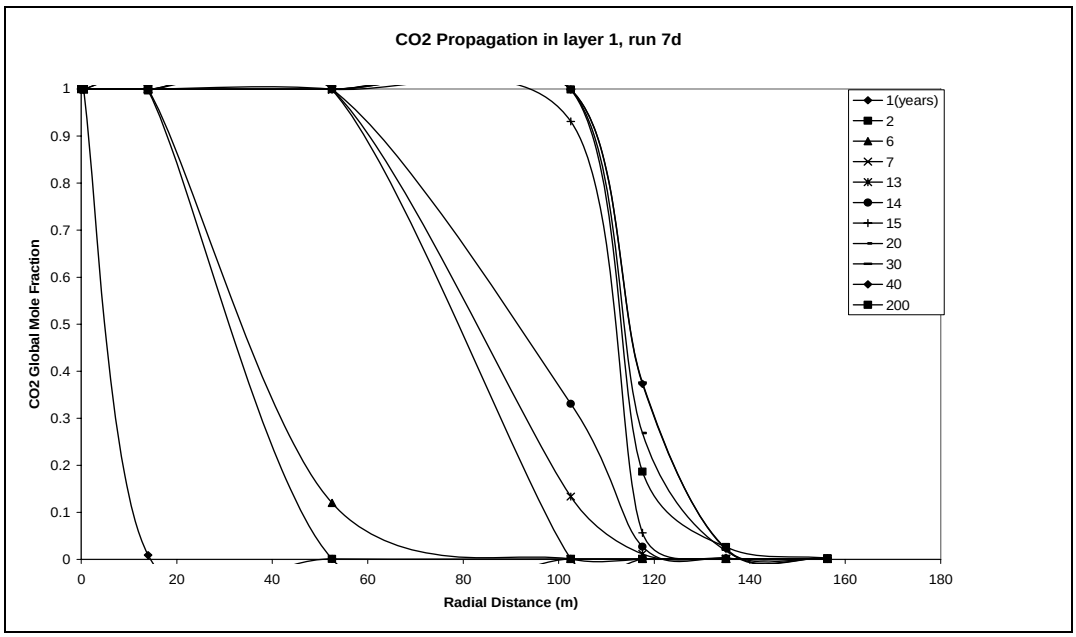

Figure 8.136 CO_2 Propagation in layer 1 for Run 7d, single-well model

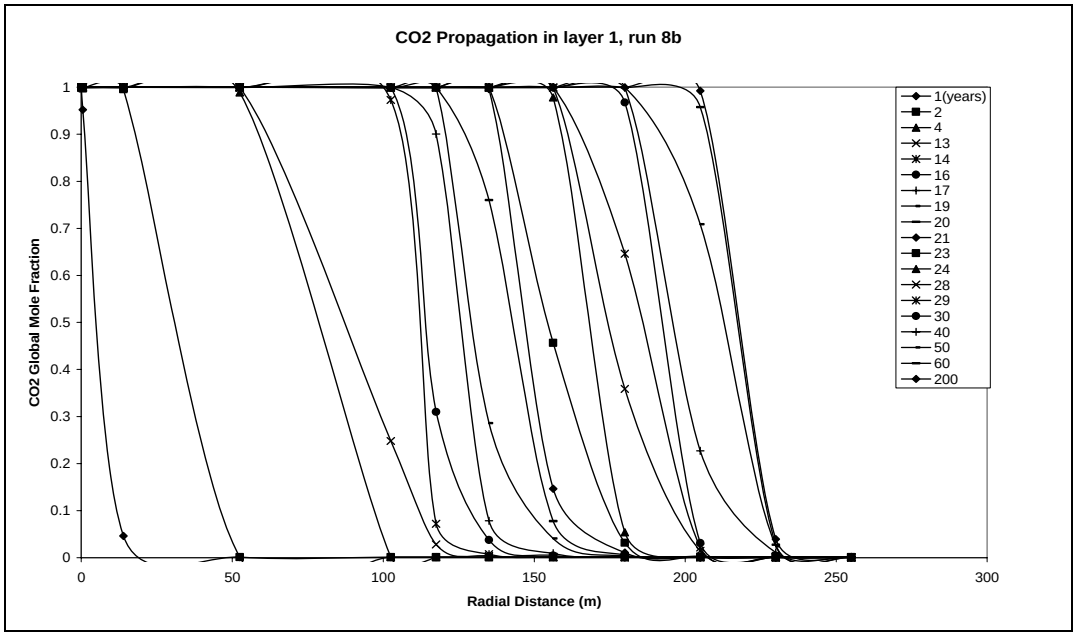

Figure 8.137 CO_2 Propagation in layer 1 for Run 8b, single-well model

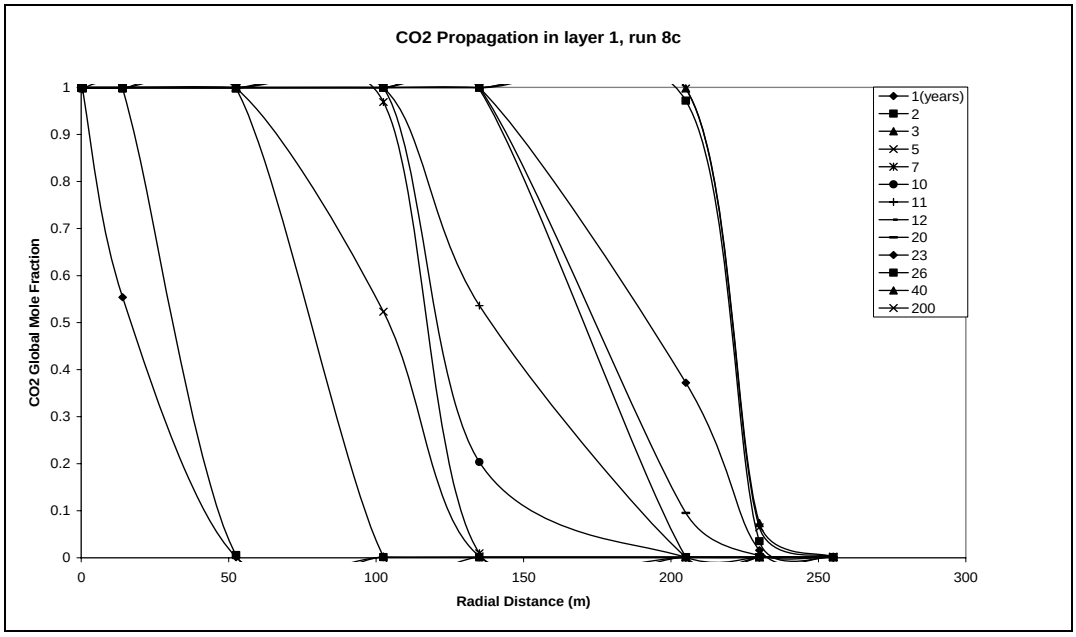

Figure 8.138 CO_2 Propagation in layer 1 for Run 8c, single-well model

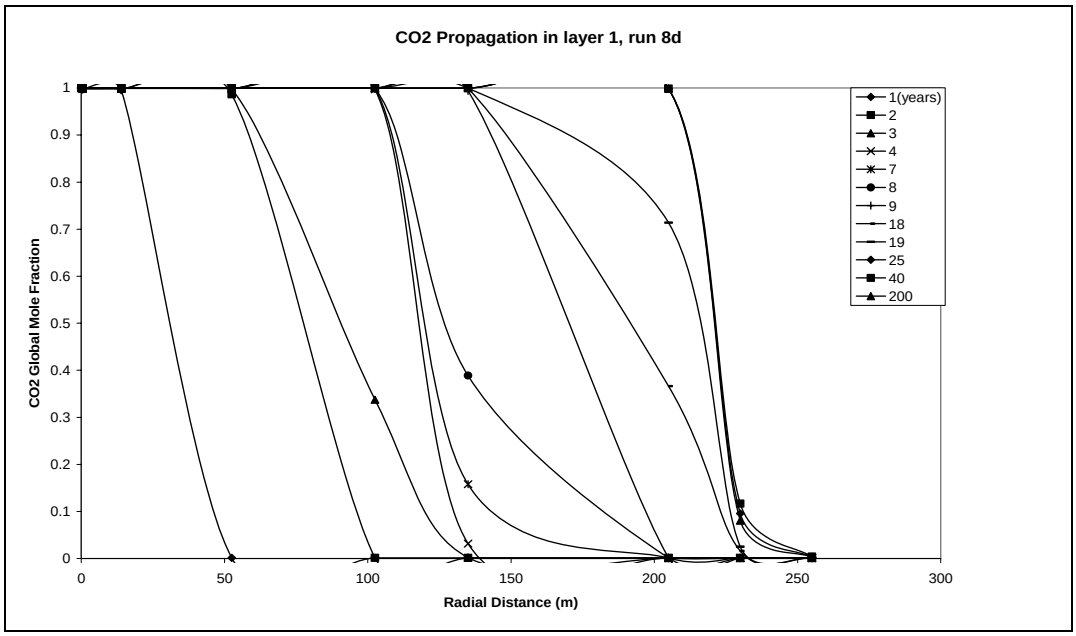

Figure 8.139 CO_2 Propagation in layer 1 for Run 8d, single-well model

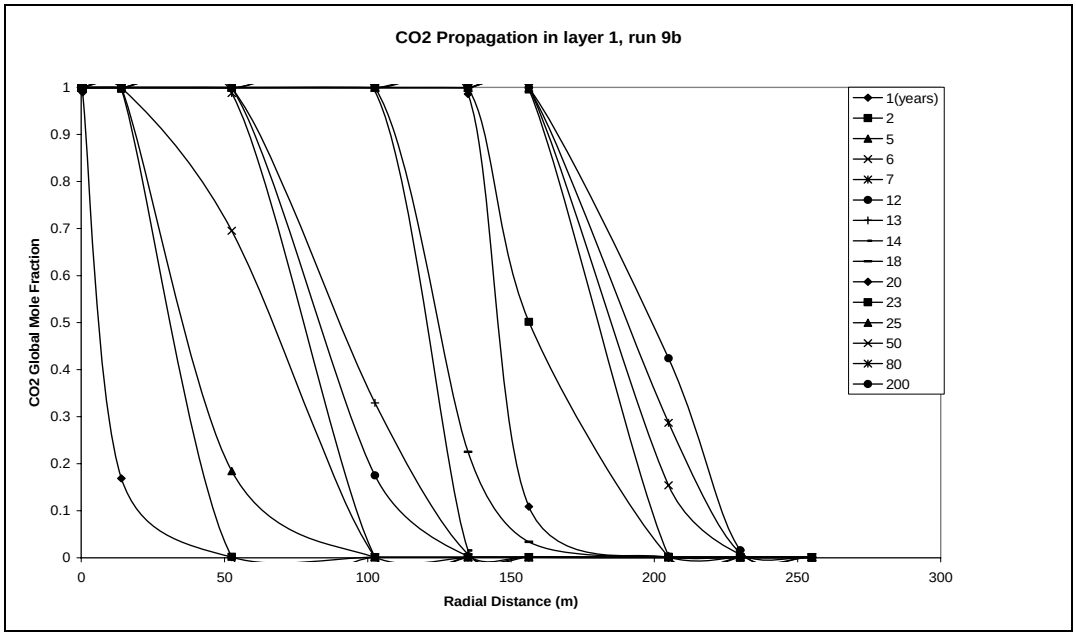

Figure 8.140 CO_2 Propagation in layer 1 for Run 9b, single-well model

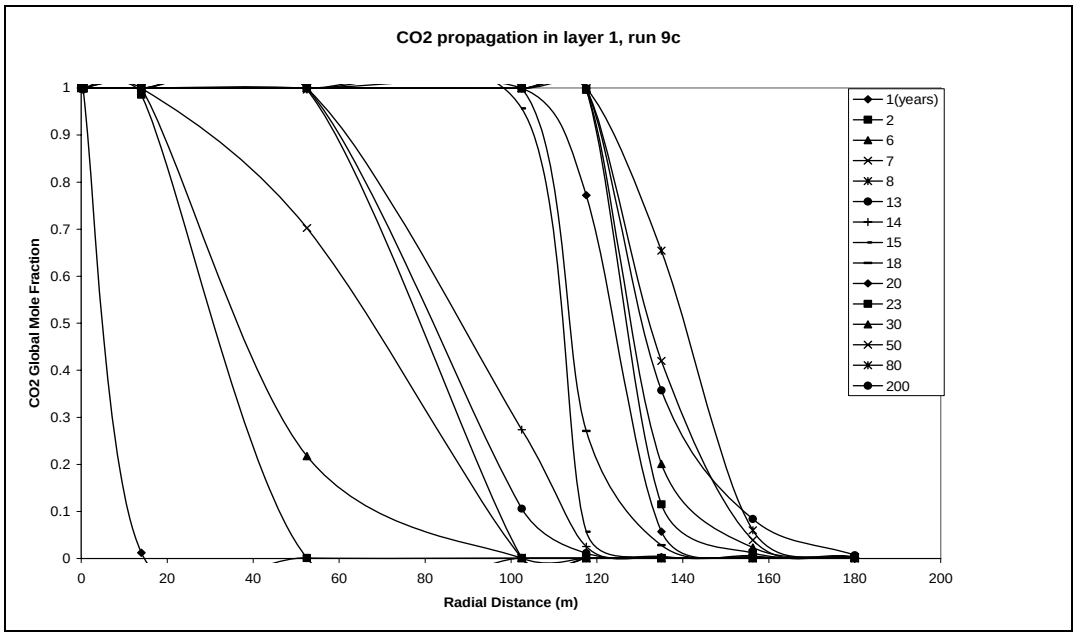

Figure 8.141 CO_2 Propagation in layer 1 for Run 9c, single-well model

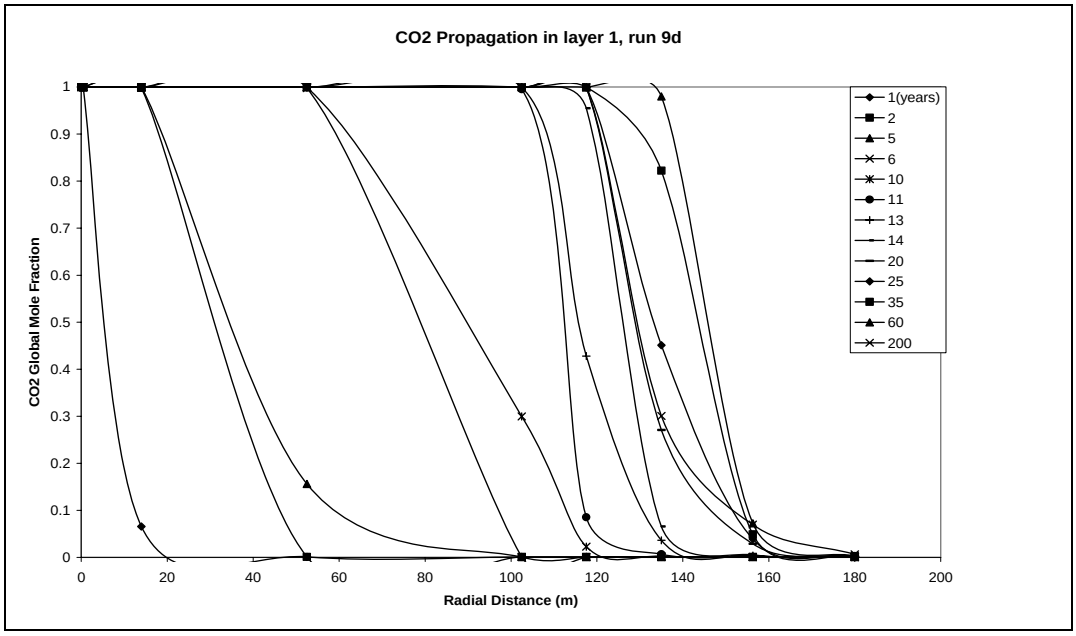

Figure 8.142 CO_2 Propagation in layer 1 for Run 9d, single-well model

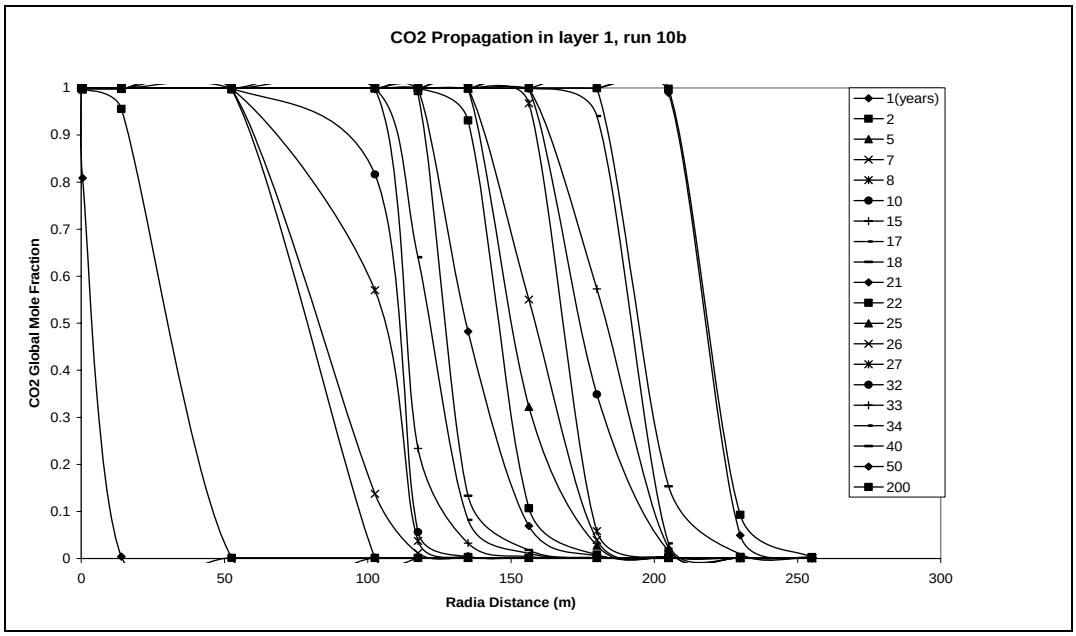

Figure 8.143 CO_2 Propagation in layer 1 for Run 10b, single-well model

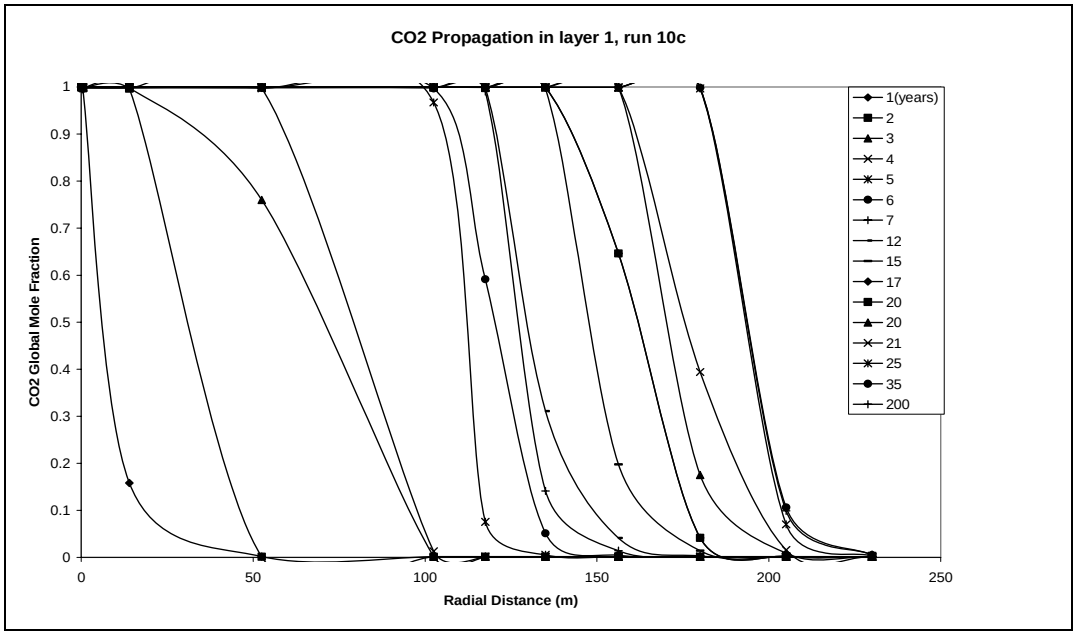

Figure 8.144 CO_2 Propagation in layer 1 for Run 10c, single-well model

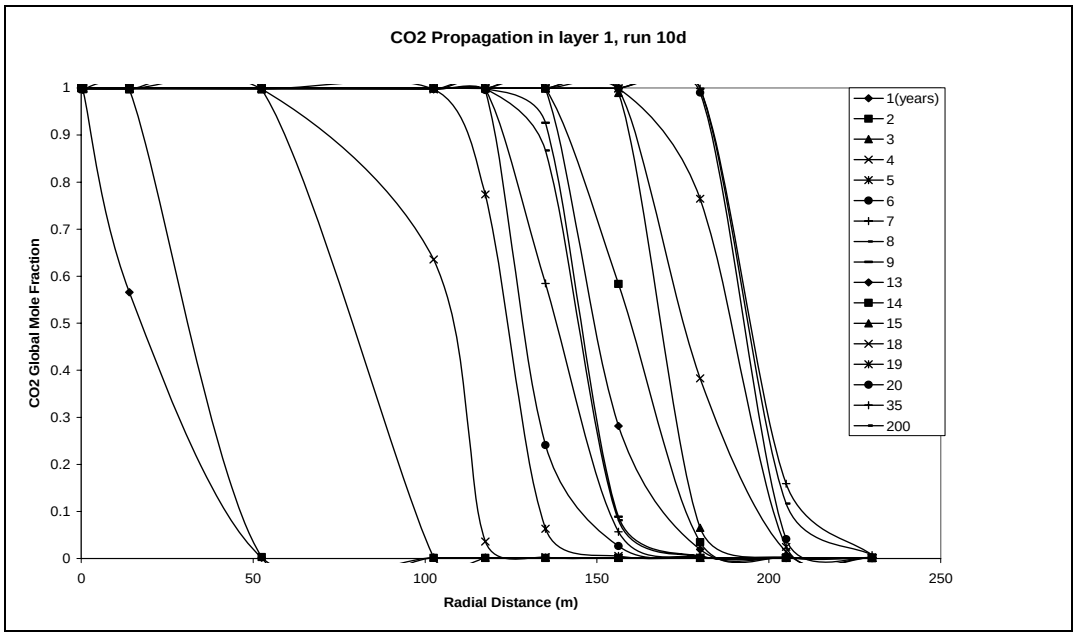

Figure 8.145 CO_2 Propagation in layer 1 for Run 10d, single-well model

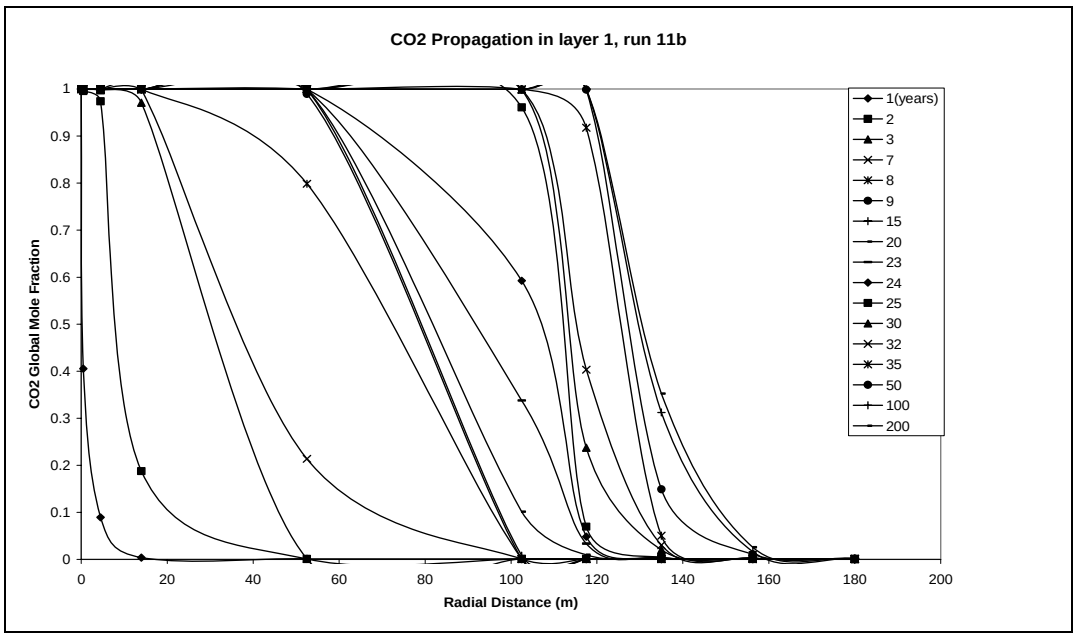

Figure 8.146 CO_2 Propagation in layer 1 for Run 11b, single-well model

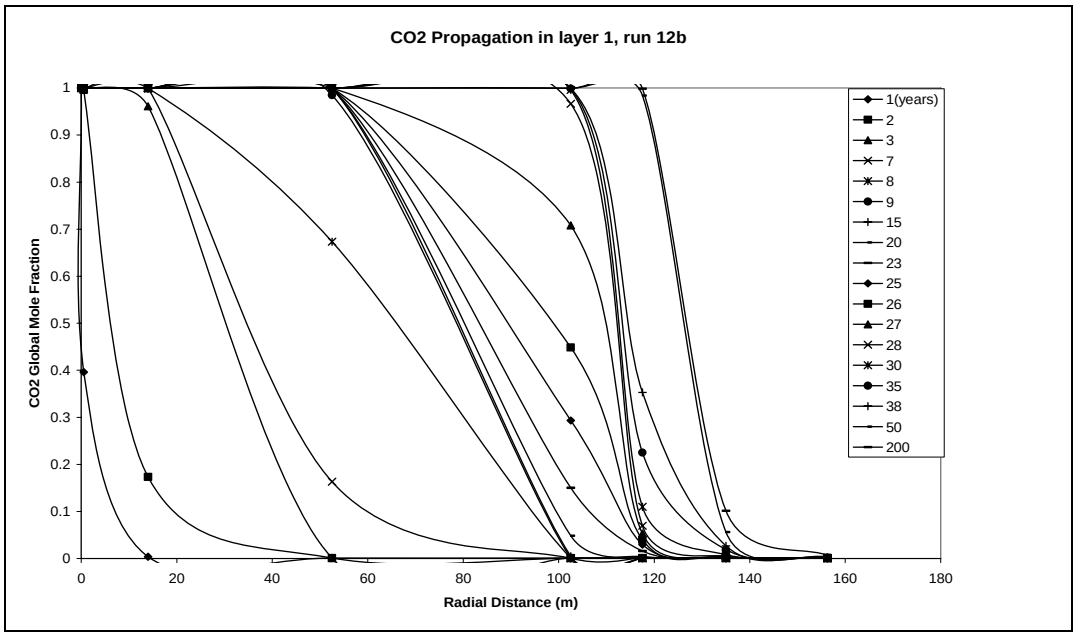

Figure 8.147 CO_2 Propagation in layer 1 for Run 12b, single-well model

Combining all these successive Runs 4b through 12b, Tables C.24 through C.26 (Appendix C) and Figures 8.148 through 8.151 were prepared at 6 different simulation times. In figures 8.148 and 8.149, Runs 4b, 4c, 4d and Runs 5b, 5c, 5d were compared in order to examine the effect of k_v/k_h ratio on CO_2 propagation at layer 1 respectively. Increasing k_v/k_h ratio caused an increase in CO_2 propagation at layer 1. Maximum CO_2 propagation was observed in Run 4d at 2025 (Figure 8.148) and Run 5d at 2050 (Figure 8.149). After reaching these maximum propagations, CO_2 propagations at layer 1 decreased which was attributed to the initialization of precipitation of Calcite minerals.

In Figure 8.150, the results of Runs 4b, 5b and 6b were compared to analyze the effect of permeability distribution on the propagation of CO_2 at layer 1. The higher global mole fraction of CO_2 that resulted in more CO_2 propagation was observed in constant permeability case (Run 4b) compared to the results of Runs 5b and 6b. There was not much more difference in propagation values between Runs 5b and 6b.

Comparing the results of Runs 8b, 9b and 10b, Figure 8.151 was constructed. Increasing CO_2 injection rate caused a decrease in the propagation of CO_2 which might be attributed to the increase in CO_2 solubility in water at higher pressures. The highest global mole fraction of CO_2 was observed at layer 1 for Run 10b (20000 sm^3/day of CO_2 injection rate).

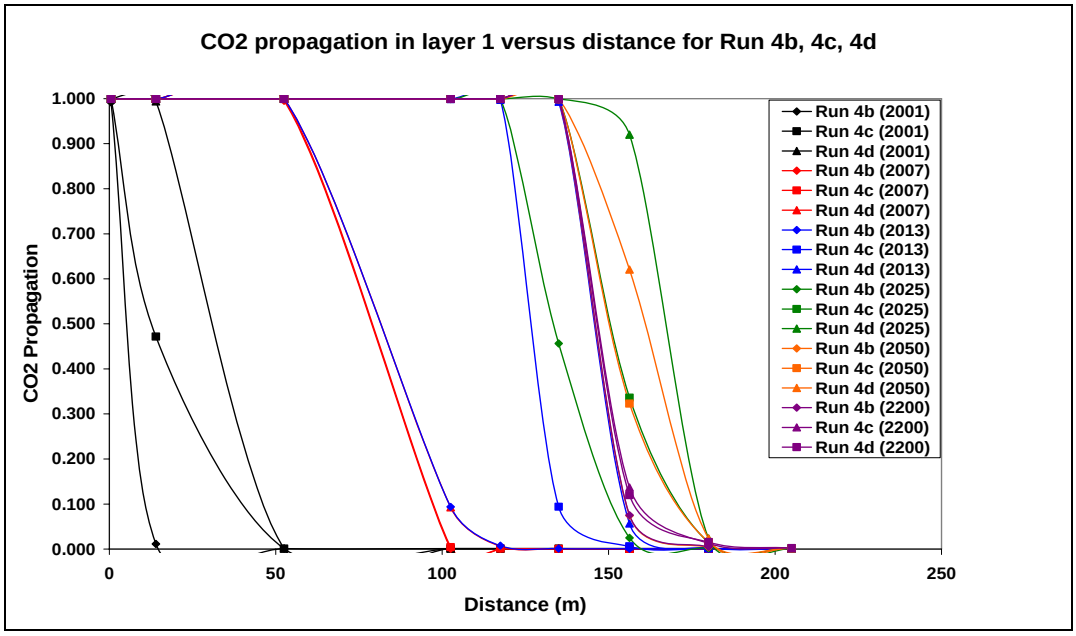

Figure 8.148 CO_2 Propagation in layer 1 for Runs 4b, 4c, 4d

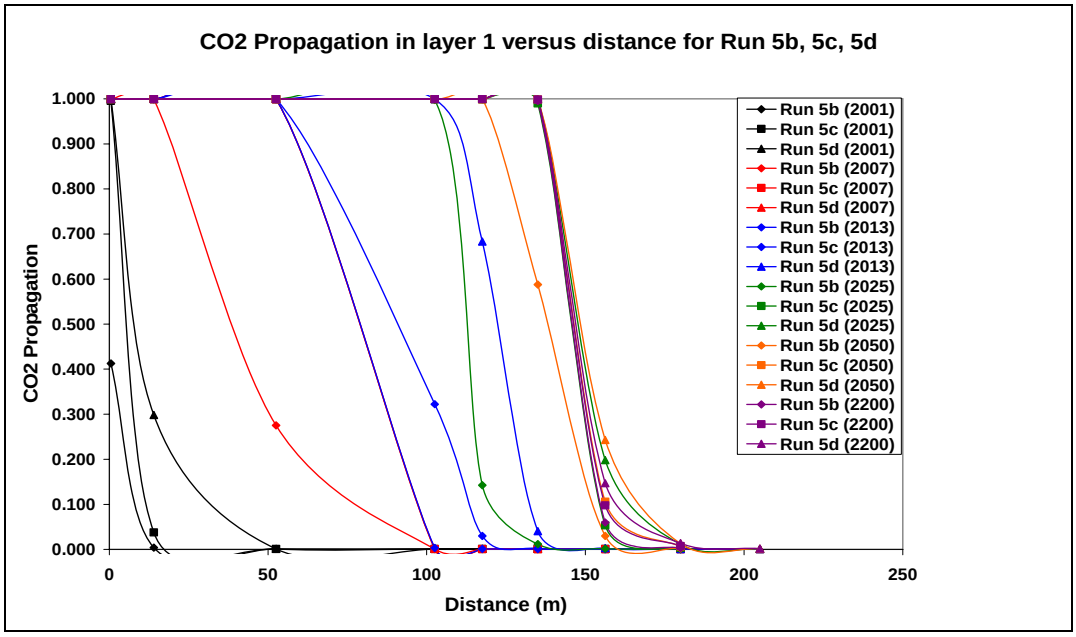

Figure 8.149 CO_2 Propagation in layer 1 for Runs 5b, 5c, 5d

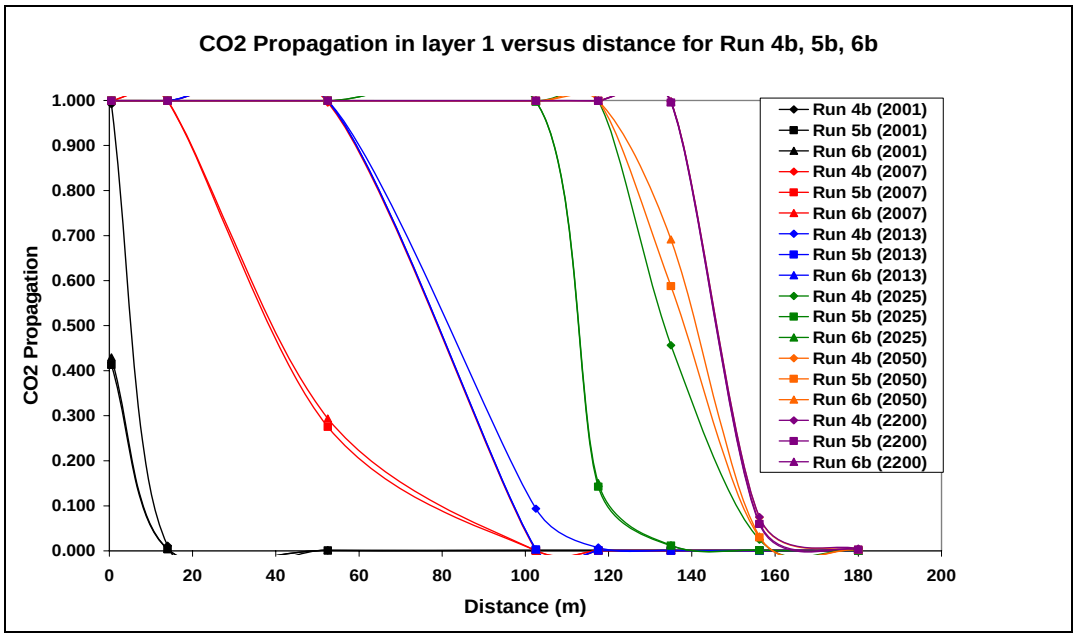

Figure 8.150 CO_2 Propagation in layer 1 for Runs 4b, 5b, 6b

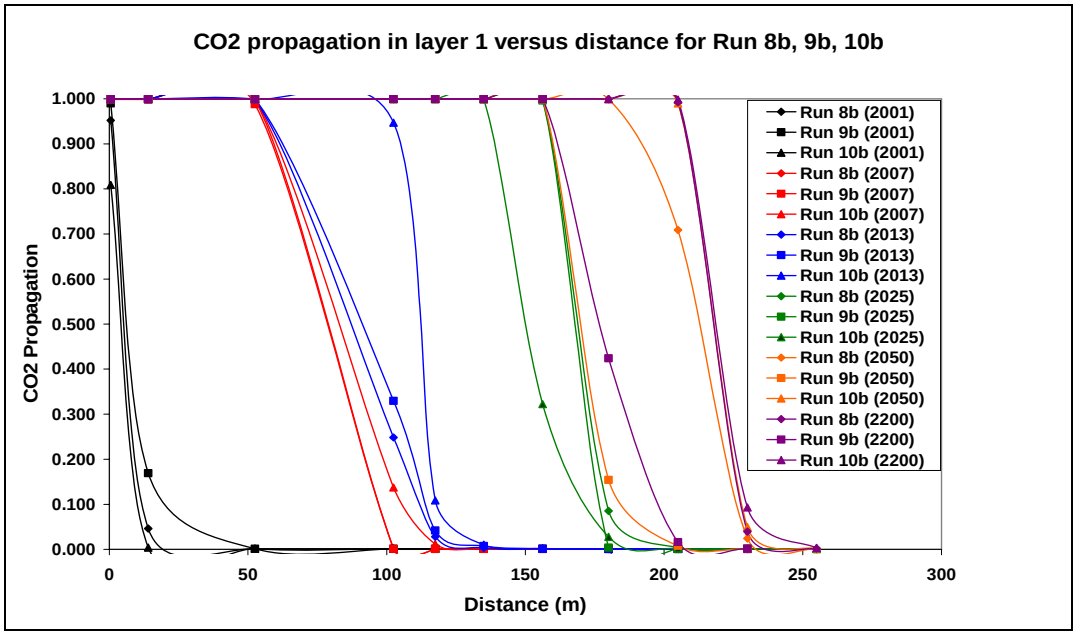

Figure 8.151 CO_2 Propagation in layer 1 for Runs 8b, 9b, 10b

CO_2 front velocity was also determined for Runs 5b (without water production) in Table 8.5 and Figure 8.152 and 8b (with water production) in Table 8.6 and Figure 8.153. CO_2 propagated faster with increasing velocity during CO_2 injection. After the CO_2 injection, CO_2 front velocity decreased. The front velocity was almost twice in Run 8b. The CO_2 supercritical pressure of 7295 kPa was reached after 2 years of CO_2 injection. CO_2 front reached to 14 meter for Run 8b and 0.5 meter for Run 5b after 2 years. This result was attributed to the faster movement of gas phase within the aquifer.

Table 8.5 CO_2 Front Velocity at 0.99 Global Mole Fraction of CO_2 for Run 5b

Global Mole Fraction of CO_2	x (m)	t (year)	x/t (m/year)
0.99	0.50	2	0.25
	14.00	7	2.00
	52.50	10	5.25
	102.50	25	4.10
	117.50	35	3.36
	135.00	200	0.68

*CO_2 injection was stopped at the year of 13.

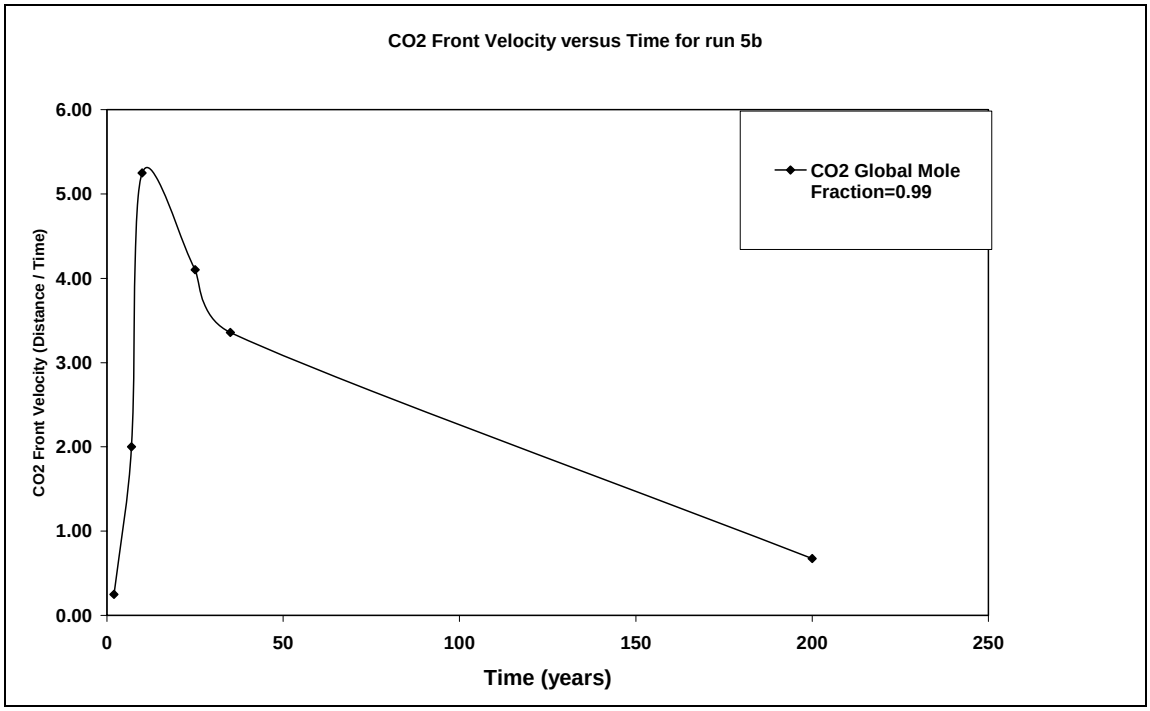

Figure 8.152 CO_2 Front Velocity at CO_2 Global Mole Fraction of 0.99 for Run 5b

Table 8.6 CO_2 Front Velocity at 0.99 Global Mole Fraction of CO_2 for Run 8b

Global Mole Fraction of CO_2	x (m)	t (year)	x/t
0.99	0.50	2	0.25
	14.00	2	7.00
	52.50	4	13.13
	102.50	16	6.41
	117.50	19	6.18
	135.00	21	6.43
	156.25	28	5.58
	180.00	40	4.50
	205.00	200	1.03

*CO_2 injection was stopped at the year of 20.

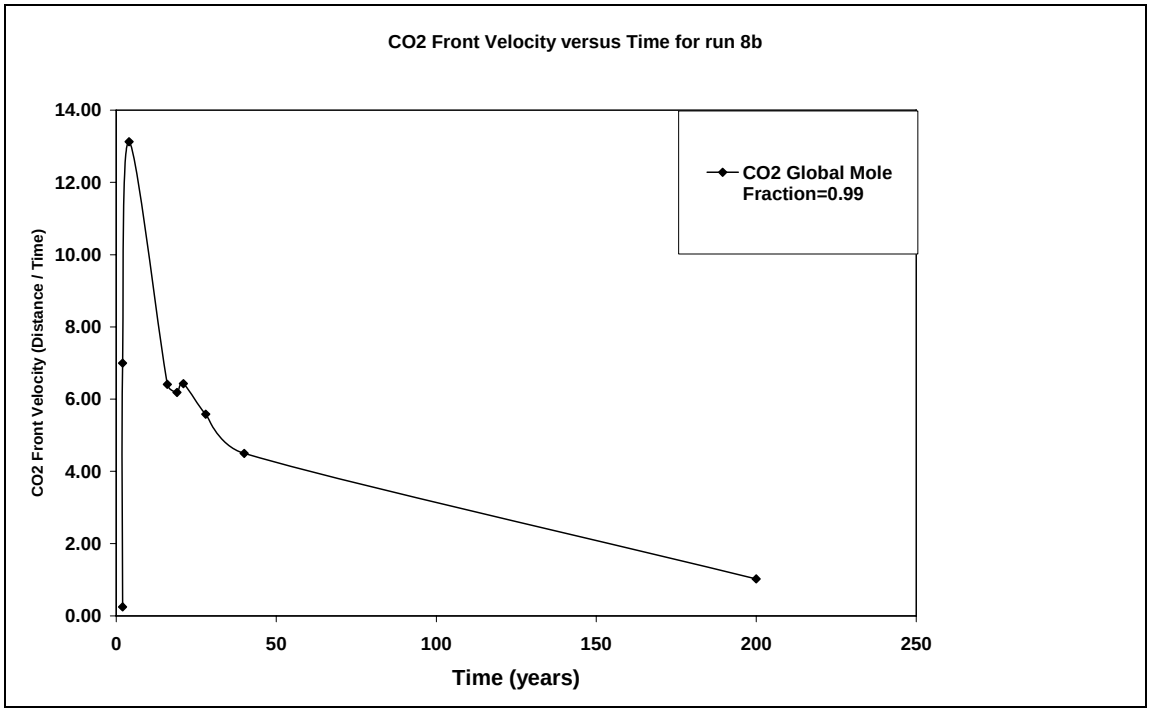

Figure 8.153 CO_2 Front Velocity at CO_2 Global Mole Fraction of 0.99 Run 8b

In order to examine CO_2 Saturation, CO_2 Mole Fraction in Water, Calcite Dissolution / Precipitation, Anorthite Dissolution / Precipitation, Kaolinite Dissolution / Precipitation and pressure distribution at other aquifer blocks rather than the injection well block, sample plots were illustrated for Runs 5b (without water production) and 8b (with water production) in Figures 8.154 through 8.189.

In Figures 8.154 through 8.159 for Run 5b, the similar behaviour of paramaters were observed for the grid block 52.5 m away from the injection well comparing with that of the injection well. The free CO_2 propagated in all three layers of the aquifer (Figure 8.154) having the highest saturation values at layer 1 comparing to layers 2 and 3. CO_2 solubility in water was almost same in all three layers (Figure 8.155). Calcite dissolution / precipitation, Anorthite dissolution, Kaolinite precipitation occurred in all three layers of the aquifer with the same tendency as for the injection well (Figures 8.157, 8.158 and 8.159). But, for the grid block 102.5 m away from the injection well, CO_2 saturation values at layers 2 and 3 were approaching to zero comparing to values at layer 1 (Figure 8.160) since CO_2 has a tendency to rise there. Similarly, CO_2 solubility in water at layer 1 was higher than the values of layers 2 and 3 (Figure 8.161). The rates of calcite precipitation at layers 2 and 3 were much higher than the rate of calcite precipitation at layer 1 (Figure 8.163). For the grid block 135 m away from the injection well, CO_2 saturation values at layer 1 started to decrease after 2170. CO_2 saturation values were already zero at layers 2 and 3 (Figure 8.166). In Figure 8.167, CO_2 solubility in water at layer 1 was higher than the values of layers 2 and 3. For layer 3, CO_2 solubility in water was zero at the distance 135 m away from the injection well. Calcite precipitation was higher at layer 3 than the values of other two layers (Figure 8.169).

For Run 8b, the similar results were observed comparing to the behavior of parameters for Run 5b. For the grid block 52.5 m away from the injection well, free CO_2 propagated in three layers having the highest saturation values at layer 1 comparing to layers 2 and 3 (Figure 8.172). CO_2 solubility in water was almost same in all three layers (Figure 8.173). Calcite dissolution / precipitation, anorthite dissolution, Kaolinite precipitation

occurred in all three layers of the aquifer with the same tendency as for the injection well (Figures 8.175, 8.176 and 8.177). For the grid block 135 m away from the injection well, CO_2 saturation values at layers 2 and 3 were approaching zero comparing to values of layer 1 (Figure 8.178) since CO_2 has a tendency to rise there. Similarly, CO_2 solubility in water at layer 1 was higher than the values for layers 2 and 3 (Figure 8.179). The rates of calcite precipitation at layers 2 and 3 were much higher than the rate of calcite precipitation at layer 1 (Figure 8.181). For the grid block 205 m away from the injection well, CO_2 saturation values at layer 1 started to decrease after 2150. CO_2 saturation values were already zero at layers 2 and 3 (Figure 8.184). In figure 8.185, CO_2 solubility in water at layer 1 was higher than the values of layers 2 and 3. For layer 3, CO_2 solubility in water was zero at the distance 205 m away from the injection well. Calcite precipitation was higher at layer 3 than the values of other two layers (Figure 8.187).

Pressure distributions for Runs 5b and 8b were demonstrated in Figures 8.190 through 8.201. The aquifer pressure increased to 15000 kPa starting from 9100 kPa for Run 5b till the CO_2 injection has been ceased. Then, the pressure decreased to 13500 kPa for layer 1, 14000 kPa for layer 2 and 14500 kPa for layer 3 at the end of the simulation (200 years) since CO_2 solubility in water increased in all three layers of the aquifer. For Run 8b, the aquifer pressure decreased to 2800 kPa by water production. Then CO_2 injection has been initiated causing an increase in aquifer pressure up to a value of 15000 kPa. After CO_2 injection has been stopped, aquifer pressure decreased to about 14000 kPa due to the availability of soluble CO_2 in water.

3-D view of CO_2 Saturation, CO_2 Global Mole Fraction, CO_2 Mole Fraction in Water, Calcite Dissolution / Precipitation, Anorthite Dissolution / Precipitation, Kaolinite Dissolution / Precipitation were also illustrated for Runs 5b (without water production) and Run 8b (with water production) at 3 different simulation times (2013, 2030 and 2200) in E.1 and E.2 (Appendix E).

For field and single-well aquifer model, cumulative injected CO_2 values are also indicated in Table 8.7 in order to examine the results of all Runs 1a through 12b.

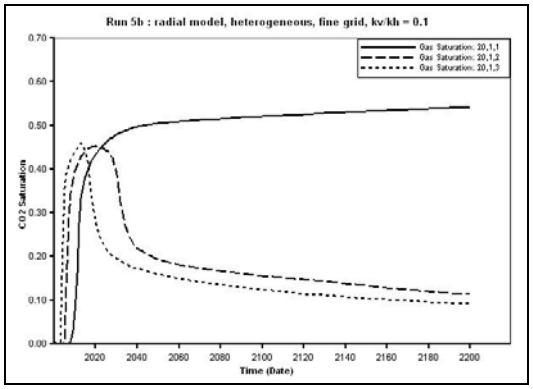

Figure 8.154 CO_2 Saturation at 52.5 m away from the injection well block along A-B direction for Run 5b

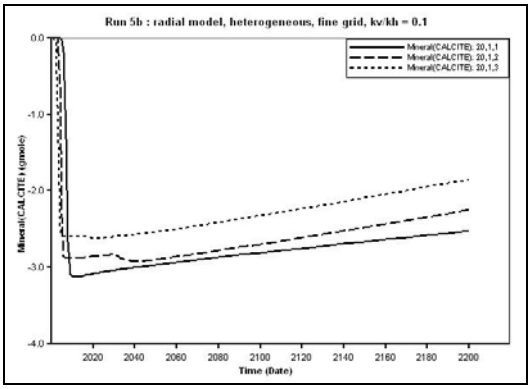

Figure 8.157 Calcite Dissolution/Precipitation at 52.5 m away from the injection well block along A-B direction for Run 5b

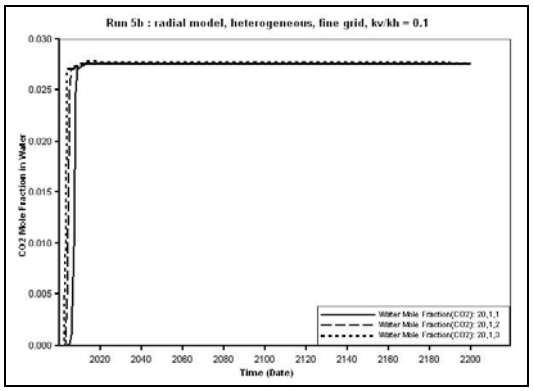

Figure 8.155 CO_2 Mole Fraction in water at 52.5 m away from the injection well block along A-B direction for Run 5b

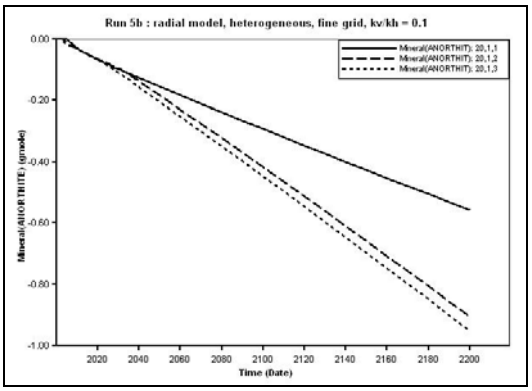

Figure 8.158 Anorthite Dissolution /Precipitation at 52.5 m away from the injection well block along A-B direction for Run 5b

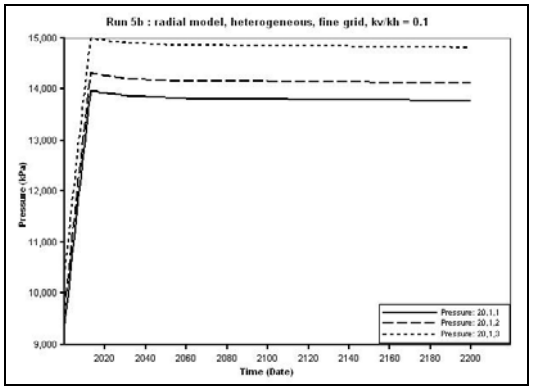

Figure 8.156 Pressure at 52.5 m away from the injection well block along A-B direction for Run 5b

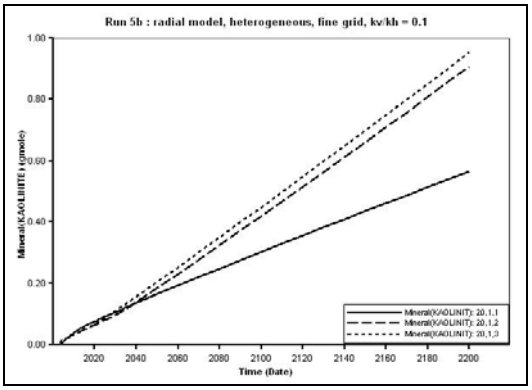

Figure 8.159 Kaolinite Dissolution /Precipitation at 52.5 m away from the injection well block along A-B direction for Run 5b

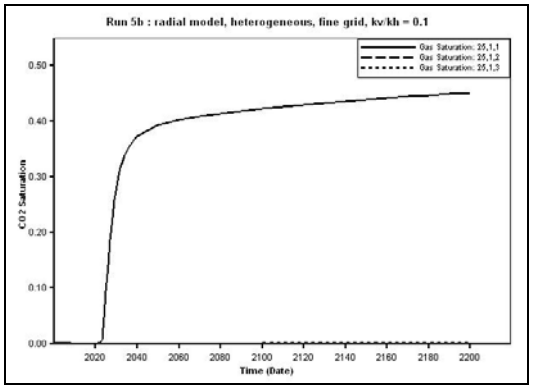

Figure 8.160 CO_2 Saturation at 102.5 m away from the injection well block along A-B direction for Run 5b

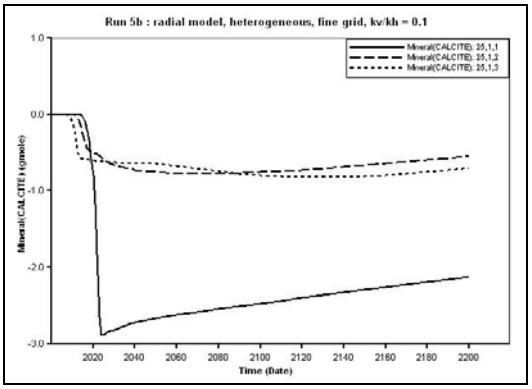

Figure 8.163 Calcite Dissolution/Precipitation at 102.5 m away from the injection well block along A-B direction for Run 5b

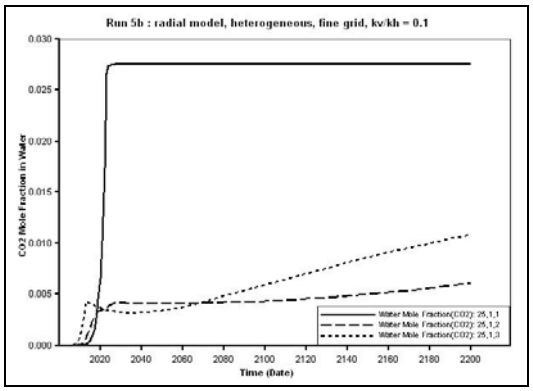

Figure 8.161 CO_2 Mole Fraction in water at 102.5 m away from the injection well block along A-B direction for Run 5b

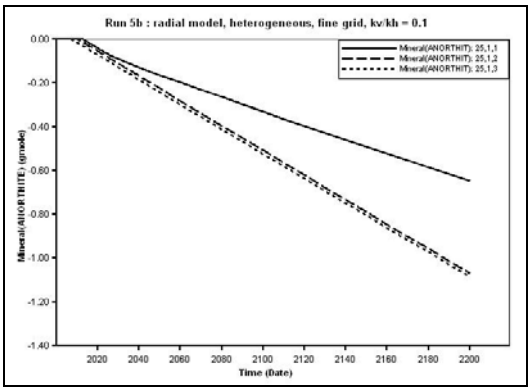

Figure 8.164 Anorthite Dissolution /Precipitation at 102.5 m away from the injection well block along A-B direction for Run 5b

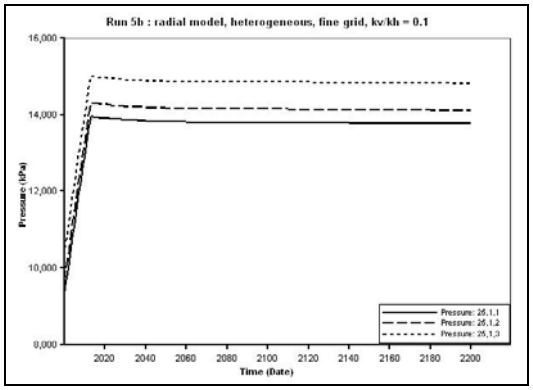

Figure 8.162 Pressure at 102.5 m away from the injection well block along A-B direction for Run 5b

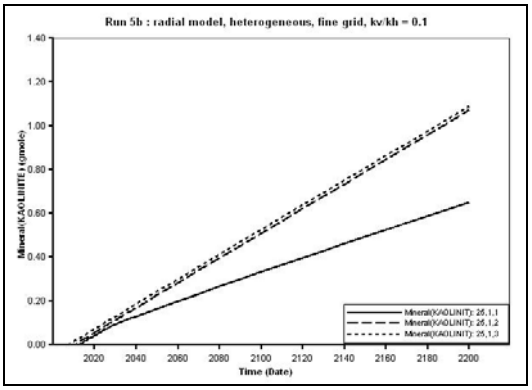

Figure 8.165 Kaolinite Dissolution /Precipitation at 102.5 m away from the injection well block along A-B direction for Run 5b

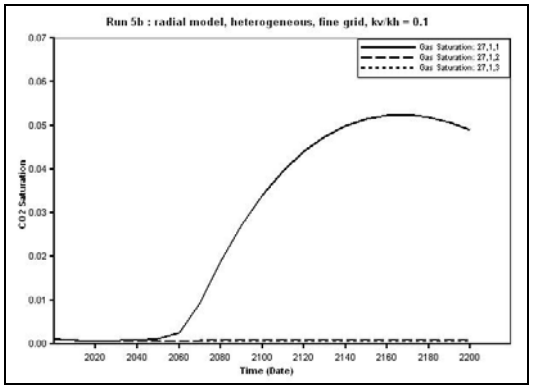

Figure 8.166 CO_2 Saturation at 135 m away from the injection well block along A-B direction for Run 5b

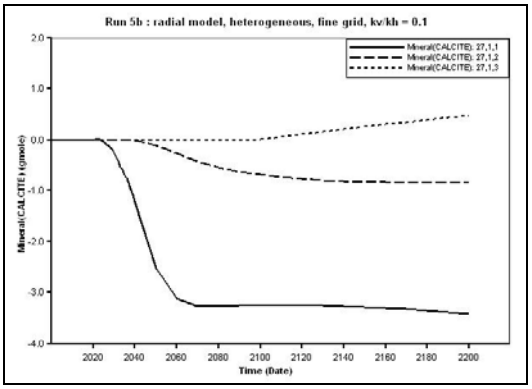

Figure 8.169 Calcite Dissolution/Precipitation at 135 m away from the injection well block along A-B direction for Run 5b

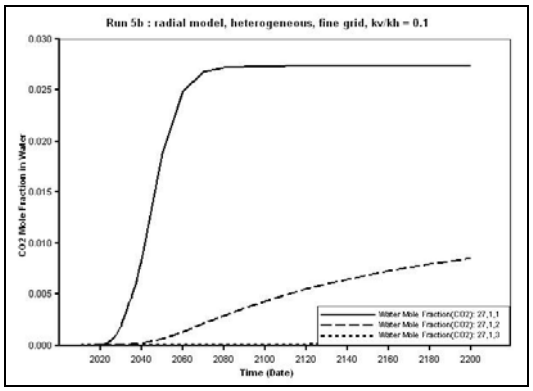

Figure 8.167 CO_2 Mole Fraction in water at 135 m away from the injection well block along A-B direction for Run 5b

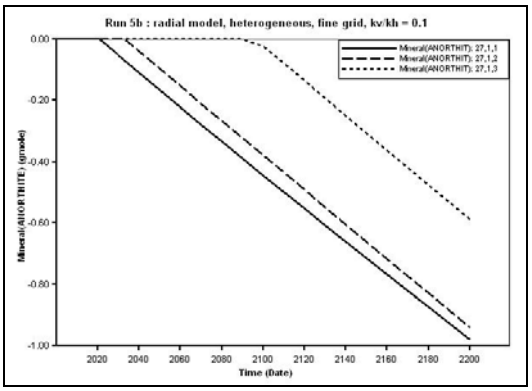

Figure 8.170 Anorthite Dissolution /Precipitation at 135 m away from the injection well block along A-B direction for Run 5b

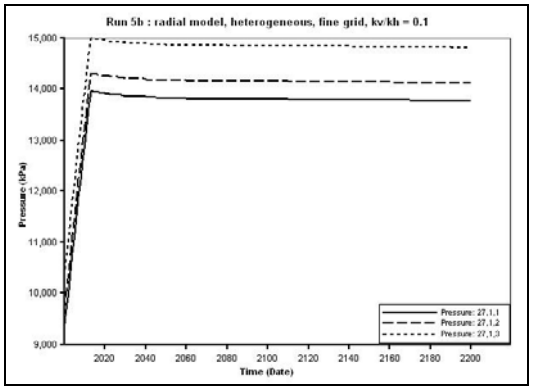

Figure 8.168 Pressure at 135 m away from the injection well block along A-B direction for Run 5b

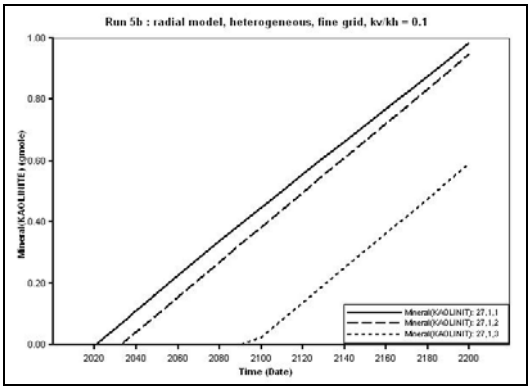

Figure 8.171 Kaolinite Dissolution /Precipitation at 135 m away from the injection well block along A-B direction for Run 5b

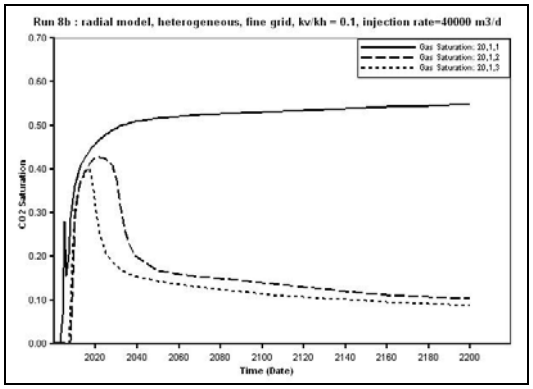

Figure 8.172 CO_2 Saturation at 52.5 m away from the injection well block along A-B direction for Run 8b

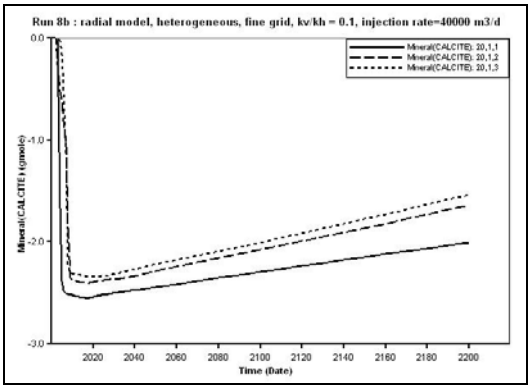

Figure 8.175 Calcite Dissolution/Precipitation at 52.5 m away from the injection well block along A-B direction for Run 8b

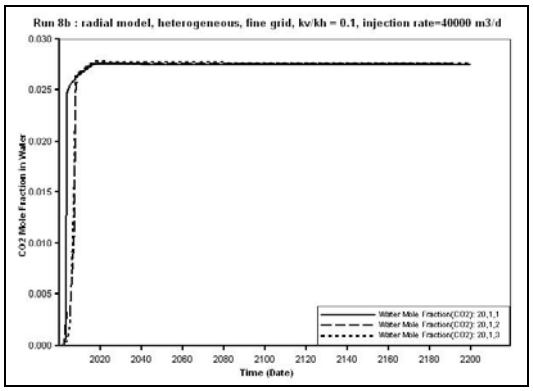

Figure 8.173 CO_2 Mole Fraction in water at 52.5 m away from the injection well block along A-B direction for Run 8b

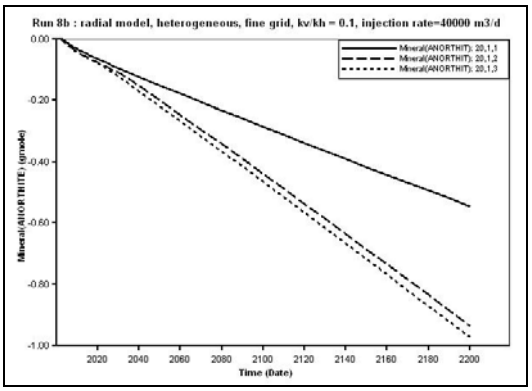

Figure 8.176 Anorthite Dissolution /Precipitation at 52.5 m away from the injection well block along A-B direction for Run 8b

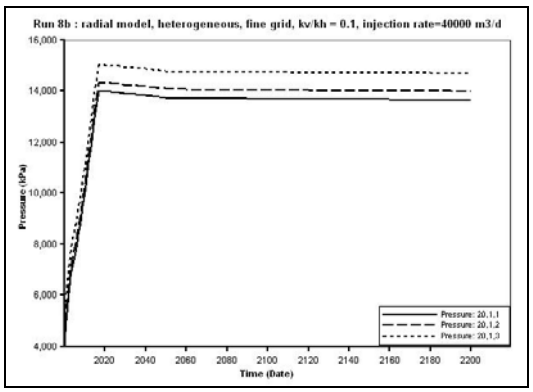

Figure 8.174 Pressure at 52.5 m away from the injection well block along A-B direction for Run 8b

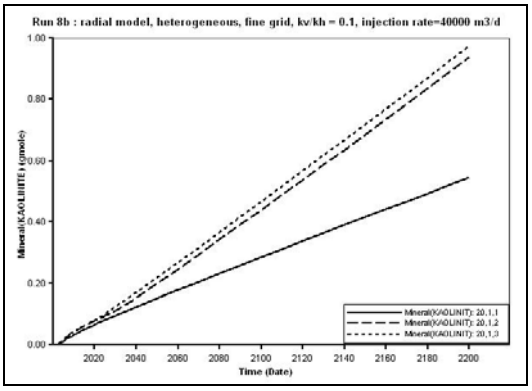

Figure 8.177 Kaolinite Dissolution /Precipitation at 52.5 m away from the injection well block along A-B direction for Run 8b

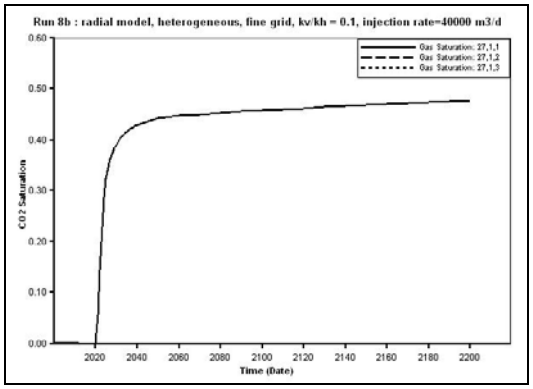

Figure 8.178 CO_2 Saturation at 135 m away from the injection well block along A-B direction for Run 8b

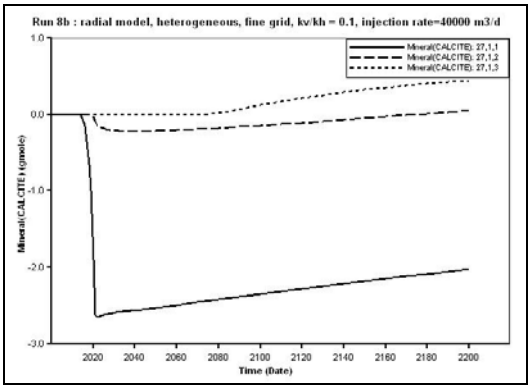

Figure 8.181 Calcite Dissolution/Precipitation at 135 m away from the injection well block along A-B direction for Run 8b

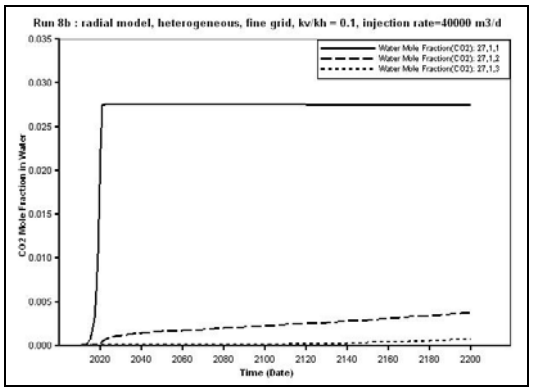

Figure 8.179 CO_2 Mole Fraction in water at 135 m away from the injection well block along A-B direction for Run 8b

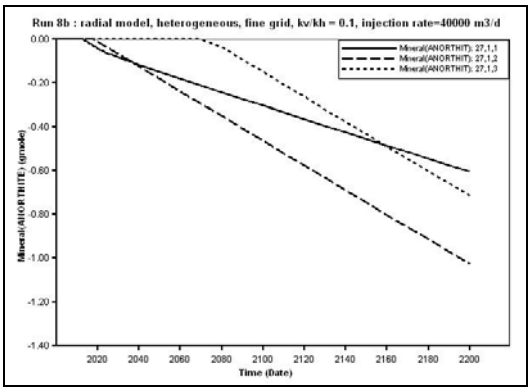

Figure 8.182 Anorthite Dissolution /Precipitation at 135 m away from the injection well block along A-B direction for Run 8b

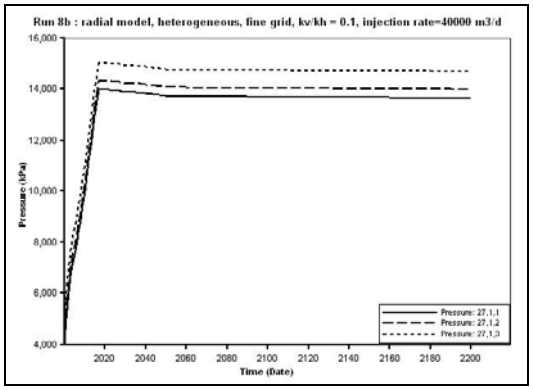

Figure 8.180 Pressure at 135 m away from the injection well block along A-B direction for Run 8b

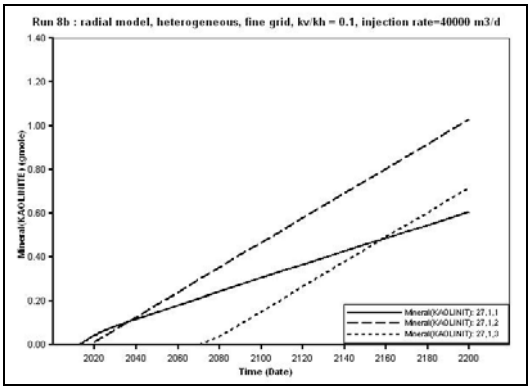

Figure 8.183 Kaolinite Dissolution /Precipitation at 135 m away from the injection well block along A-B direction for Run 8b

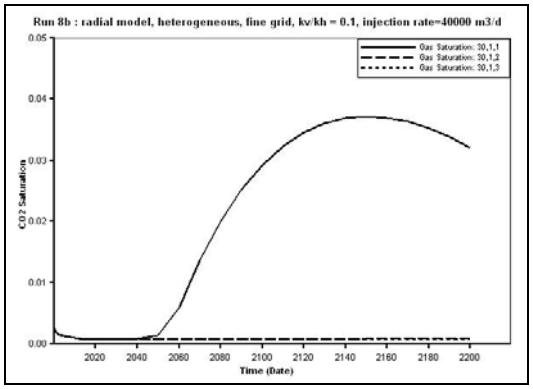

Figure 8.184 CO_2 Saturation at 205 m away from the injection well block along A-B direction for Run 8b

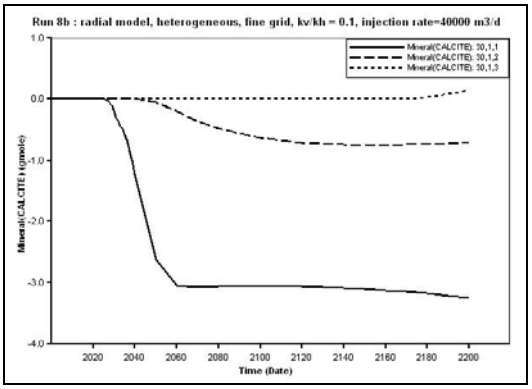

Figure 8.187 Calcite Dissolution/Precipitation at 205 m away from the injection well block along A-B direction for Run 8b

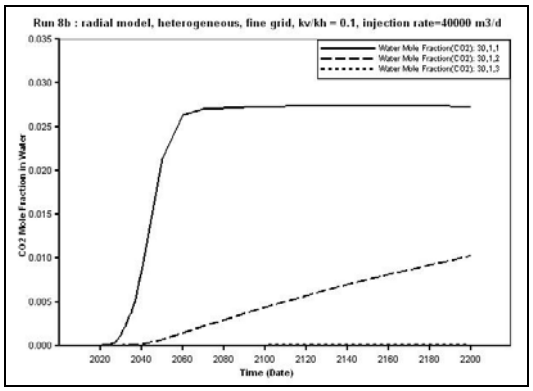

Figure 8.185 CO_2 Mole Fraction in water at 205 m away from the injection well block along A-B direction for Run 8b

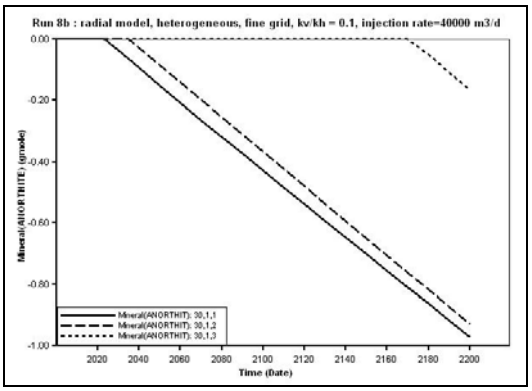

Figure 8.188 Anorthite Dissolution /Precipitation at 205 m away from the injection well block along A-B direction for Run 8b

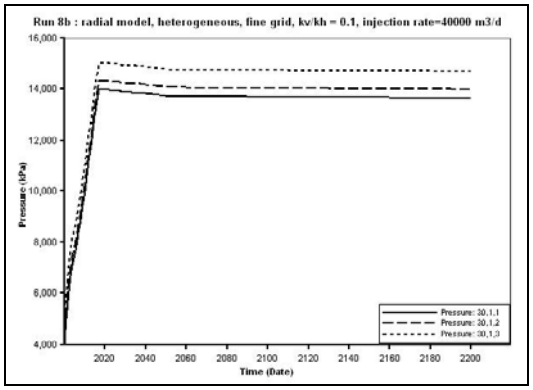

Figure 8.186 Pressure at 205 m away from the injection well block along A-B direction for Run 8b

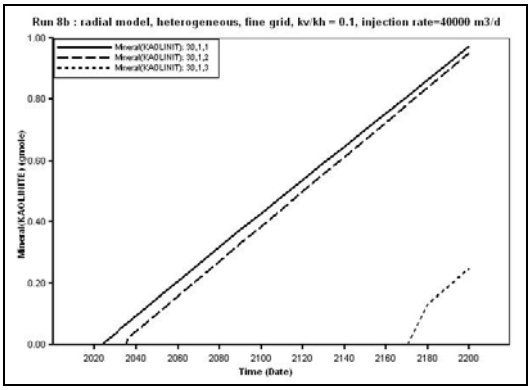

Figure 8.189 Kaolinite Dissolution /Precipitation at 205 m away from the injection well block along A-B direction for Run 8b

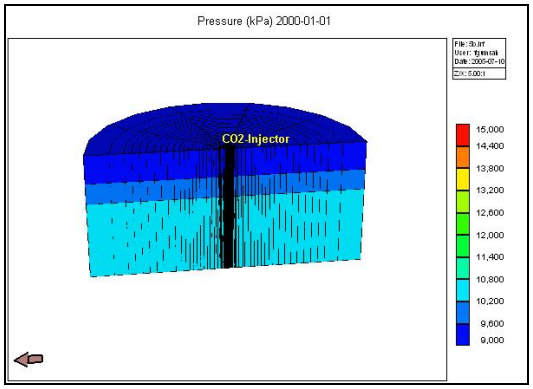

Figure 8.190 Pressure Distribution for single-well aquifer model, Run 5b at the beginning of the simulation (2000)

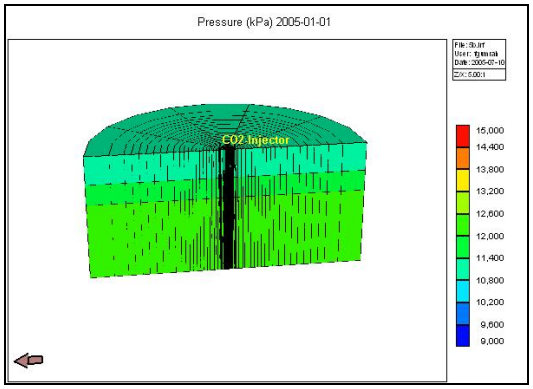

Figure 8.191 Pressure Distribution for single-well aquifer model, Run 5b after 5 years of the simulation (2005)

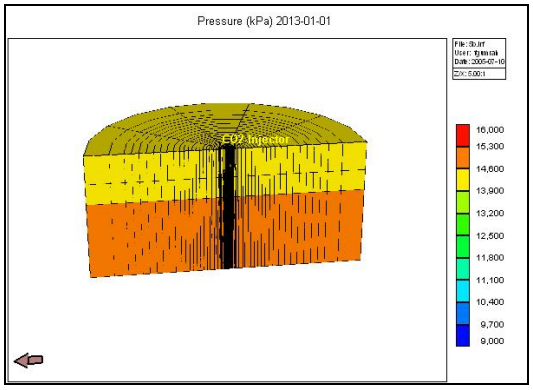

Figure 8.192 Pressure Distribution for single-well aquifer model, Run 5b after CO_2 injection has been ceased (2013)

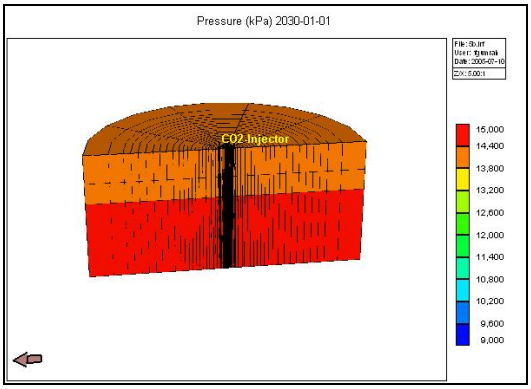

Figure 8.193 Pressure Distribution for single-well aquifer model, Run 5b after 30 years of the simulation (2030)

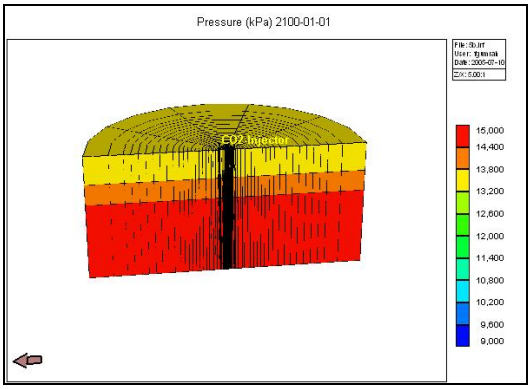

Figure 8.194 Pressure Distribution for single-well aquifer model, Run 5b after 100 years of the simulation (2100)

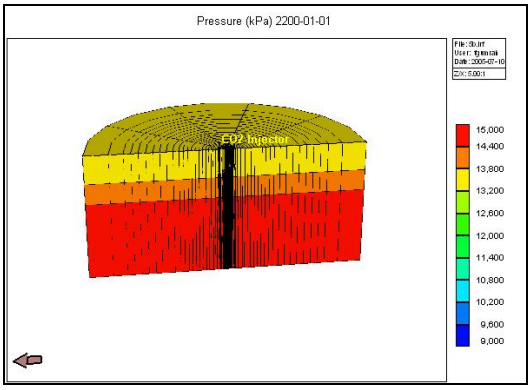

Figure 8.195 Pressure Distribution for single-well aquifer model, Run 5b at the end of the simulation (2200)

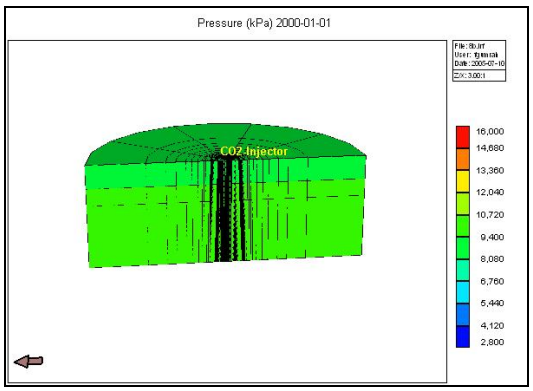

Figure 8.196 Pressure Distribution for single-well aquifer model, Run 8b at the beginning of the simulation (2000)

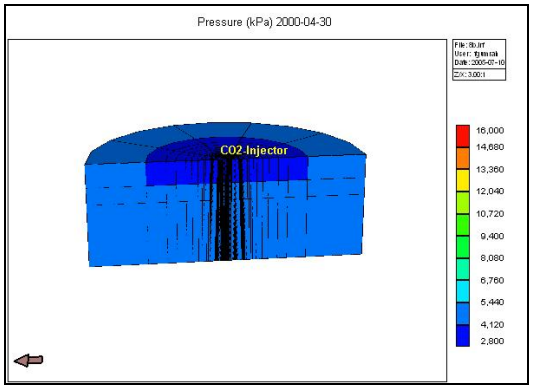

Figure 8.197 Pressure Distribution for single-well aquifer model, Run 8b after water production (2000-4)

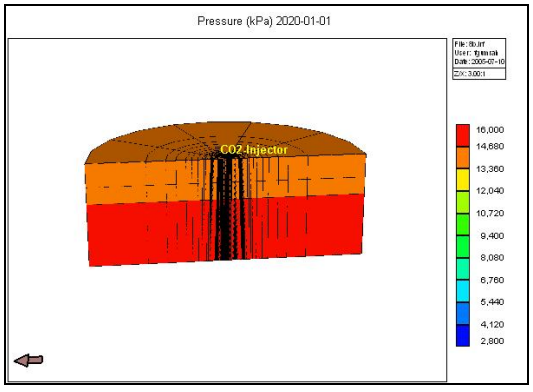

Figure 8.198 Pressure Distribution for single-well aquifer model, Run 8b after CO_2 injection has been ceased (2020)

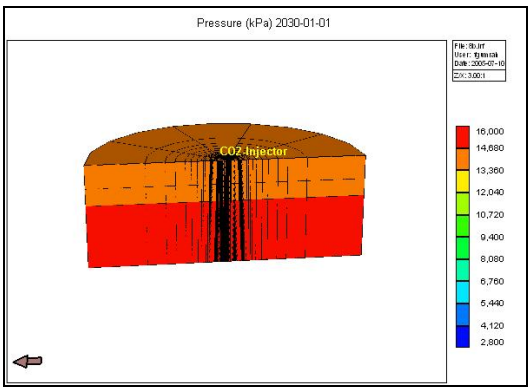

Figure 8.199 Pressure Distribution for single-well aquifer model, Run 8b after 30 years of the simulation (2030)

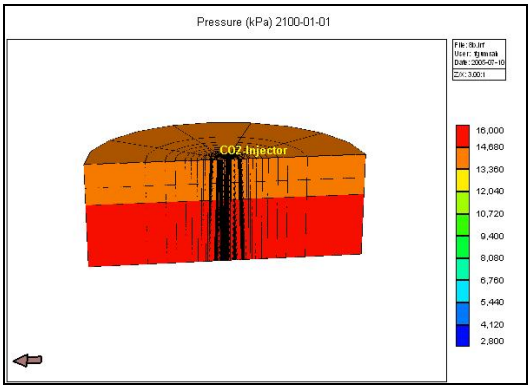

Figure 8.200 Pressure Distribution for single-well aquifer model, Run 8b after 100 years of the simulation (2100)

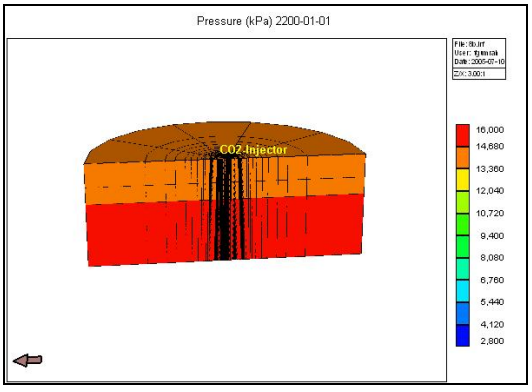

Figure 8.201 Pressure Distribution for single-well aquifer model, Run 8b at the end of the simulation (2200)

In order to see the effects of perforation interval on CO_2 saturation, additional Runs 5e (without water production) and 8e (with water production) were performed. Aquifer properties of Runs 5e and 8e were same as that of Runs 5b and 8b respectively. The only difference between these runs were the perforation intervals. In Runs 5e and 8e, CO_2 was injected through all layers of the aquifer. The results of Runs 5b and 5e (without water production) and Runs 8b and 8e (with water production) are given in Figures 8.202 through 8.207. It was observed from Figures 8.202 and 8.205 that CO_2 saturation values at layer 1 for Runs 5e and 8e (all layers perforated) were higher than the values for Runs 5b and 8b respectively. In Figures 8.203 and 8.206, similar saturation trends were observed for layer 2. For instance, CO_2 saturation values at layer 2 were higher for Runs 5e and 8e than the CO_2 saturation values for Runs 5b and 8b respectively before the CO_2 injection has been ceased. But, after the CO_2 injection has been stopped, CO_2 saturation values at layer 2 were higher for Runs 5b and 8b than the CO_2 saturation values for Runs 5e and 8e respectively which may be attributed to that CO_2 has a tendency to rise within the aquifer layers. For Runs 5e and 8e, even if CO_2 was injected through all layers, CO_2 saturation values at layer 3 were almost zero comparing with the saturation values for Runs 5b and 8b. This situation can be attributed to the difference between the injection rates shared by each three layer of the aquifer Figures 8.204 and 8.207.

Related to Runs 5e and 8e, CO_2 injection histories, CO_2 saturation, CO_2 Mole Fraction in Water, Calcite Dissolution / Precipitation, Anorthite Dissolution / Precipitation, Kaolinite Dissolution / Precipitation plots were also illustrated seperately in Appendix F.

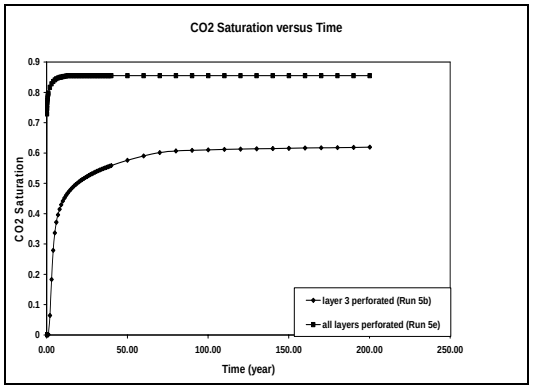

Figure 8.202 Effect of perforation interval on CO_2 Saturation for Run 5b, 5e: radial model, $k_v / k_h = 0.1$ layer 1

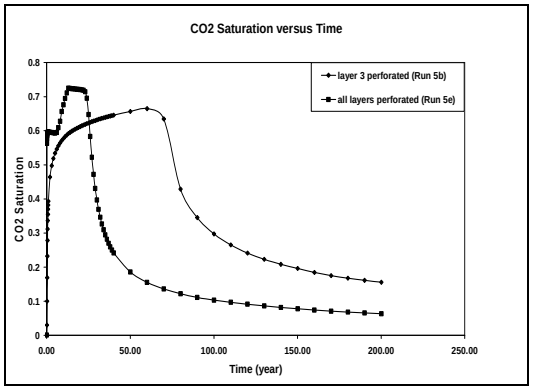

Figure 8.203 Effect of perforation interval on CO_2 Saturation for Run 5b, 5e: radial model, $k_v / k_h = 0.1$ layer 2

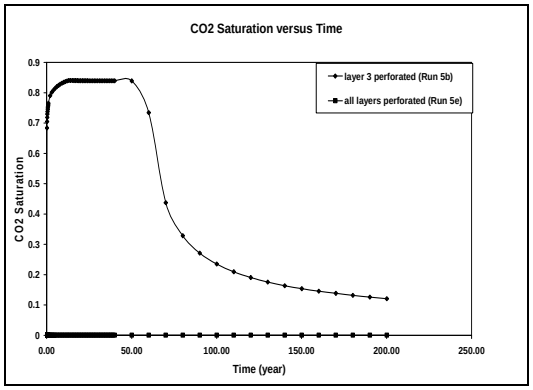

Figure 8.204 Effect of perforation interval on CO_2 Saturation for Run 5b, 5e: radial model, $k_v / k_h = 0.1$ layer 3

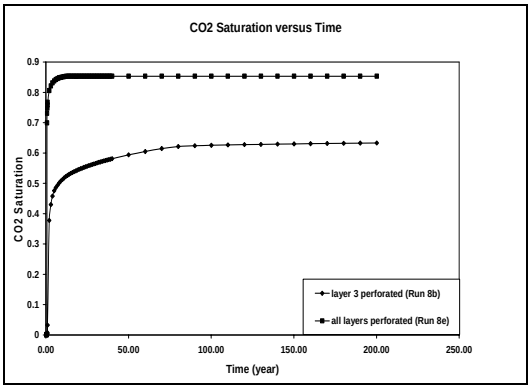

Figure 8.205 Effect of perforation interval on CO_2 Saturation for Run 8b, 8e: radial model, $k_v / k_h = 0.1$ layer 1

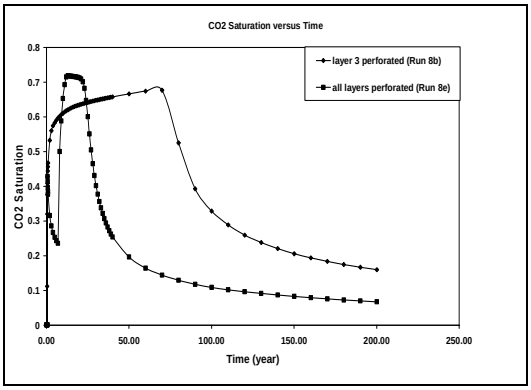

Figure 8.206 Effect of perforation interval on CO_2 Saturation for Run 8b, 8e: radial model, $k_v / k_h = 0.1$ layer 2

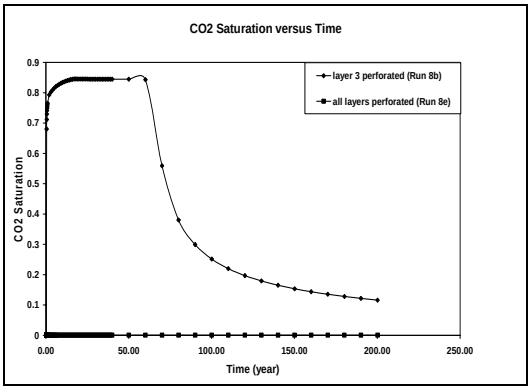

Figure 8.207 Effect of perforation interval on CO_2 Saturation for Run 8b, 8e: radial model, $k_v / k_h = 0.1$ layer 3

Table 8.7 Cumulative Injected CO_2 amounts for field and single-well aquifer models

Run ID		Injected CO_2 Phase State	CO_2 Injection rate (m^3/day)	Pore Volume (m^3)	Injection time (years)	Cum Inj. CO_2 ($10^6 m^3$) at res. con.		Cum Inj. CO_2 $*10^9$(mole) at res. con.		Cum Inj. CO_2 (PV %)	
	Field-Scale Aquifer Model										
						CO_2 Injector-1	CO_2 Injector-2	CO_2 Injector-1	CO_2 Injector-2	CO_2 Injector-1	CO_2 Injector-2
1a		Supercritical	220,000	3,680,430,791	30	6.00	5.70	102	98.8	0.16	0.15
2a		Supercritical	700,000	3,680,430,791	30	31.40	24.80	309	295	0.85	0.67
	Single-well Aquifer Model										
3a	**Grid dimension**	Supercritical	40,000	135,398,220	13	0.47		8.06		0.35	Coarse
4a		Supercritical	40,000	137,632,707	13	0.46		7.89		0.33	Fine
4b	**Constant Permeability in entire aquifer**	Supercritical	40,000	137,632,707	13	0.46		7.94		0.33	Fine
4c		Supercritical	40,000	137,632,707	13	0.46		7.91		0.33	Fine
4d		Supercritical	40,000	137,632,707	13	0.46		7.90		0.33	Fine
5b	**Constant Permeability in each layer of aquifer**	Supercritical	40,000	137,632,707	13	0.46		7.99		0.34	Fine
5c		Supercritical	40,000	137,632,707	13	0.46		7.92		0.33	Fine
5d		Supercritical	40,000	137,632,707	13	0.46		7.93		0.33	Fine
6b	**Variable Permeability in each layer of aquifer**	Supercritical	40,000	137,632,707	13	0.46		8.00		0.34	Fine
6c		Supercritical	40,000	137,632,707	13	0.46		7.92		0.33	Fine
6d		Supercritical	40,000	137,632,707	13	0.46		7.94		0.33	Fine
7b	**Injection Rate (Constant Permeability in each layer of aquifer)**	Supercritical	20,000	137,632,707	13	0.24		4.03		0.18	Fine
7c		Supercritical	20,000	137,632,707	13	0.24		4.03		0.18	Fine
7d		Supercritical	20,000	137,632,707	13	0.24		4.03		0.18	Fine
8b	**After water Production (Constant Permeability in each layer of aquifer)**	Gaseous	40,000	68,020,407	20	0.88		10.2		1.30	Fine
8c		Gaseous	40,000	68,020,407	20	0.87		10.2		1.27	Fine
8d		Gaseous	40,000	68,020,407	20	0.86		10.1		1.26	Fine
9b	**Injection Rate after water Production (Constant Permeability in each layer of aquifer)**	Gaseous	80,000	68,020,407	20	0.89		10.3		1.31	Fine
9c		Gaseous	80,000	68,020,407	20	0.33		5.53		0.48	Fine
9d		Gaseous	80,000	68,020,407	20	0.32		5.48		0.48	Fine
10b	**Injection Rate after water Production (Constant Permeability in each layer of aquifer)**	Gaseous	20,000	68,020,407	20	0.87		10.2		1.28	Fine
10c		Gaseous	20,000	68,020,407	20	0.62		6.10		0.91	Fine
10d		Gaseous	20,000	68,020,407	20	0.61		6.10		0.90	Fine
11b	**Salinity (Constant Permeability in each layer of aquifer)**	Supercritical	40,000	137,632,707	13	0.42		7.21		0.30	Fine
12b		Supercritical	40,000	137,632,707	13	0.38		6.53		0.28	Fine

CHAPTER 9

CONCLUSIONS

A case study was studied by using CMG / GEM compositional simulator to simulate CO_2 sequestration in a deep saline aquifer. Sensitivity analyses were performed in order to examine the effects of parameters such as vertical to horizontal permeability ratio, aquifer pressure conditions, CO_2 injection rate and salinity on CO_2 sequestration process.

The following conclusions can be drawn from the results of field-scale and single-well aquifer models studied in this project:

1. The CO_2 bubble displaced the formation water with an immiscible behavior. During and after the displacement, the gravitational effects caused CO_2 to rise and accumulate under the cap rock.

2. The higher amounts of CO_2 were injected by decreasing the aquifer pressure by water production. First, CO_2 filled up aquifer volume evacuated by water production and then it propagated through the aquifer layers.

3. Vertical to horizontal permeability ratio and initial aquifer pressure conditions were the most dominating parameters affecting CO_2 saturation at injection well block in each layer. The increase in vertical to horizontal permeability ratio caused an increase in CO_2 saturation in top layer where as CO_2 saturation decreased with an increase in k_v / k_h ratio in middle and bottom layers after the CO_2 injection had been ceased which indicated that CO_2 has a tendency to rise up.

4. CO_2 injection rate affected CO_2 saturation mostly in middle and bottom layers since CO_2 was injected through bottom layer of the aquifer at the injection well block. The increase in injection rate caused an increase in CO_2 saturation in middle and bottom layers with an insignificant effect on CO_2 saturation values in top layer without water production case where as CO_2 saturation in all layers with water production case decreased by increasing injection rate after the CO_2 injection has been ceased. For instance, at 2050, CO_2 saturation on layer 3 was 0.8 for higher injection rate (q = 40000 m^3/day) where as at the same simulation time, CO_2 saturation on layer 3 was 0.65 for lower injection rate (q = 20000 m^3/day) for without water production case. For with water production case, at 2100, CO_2 saturation on layer 3 was 0.35 for lower injection rate (q = 20000 m^3/day), 0.28 for the 40000 m^3/day injection rate and 0.25 for the higher injection rate (q = 80000 m^3/day). This result might be attributed to the increase in the solubility of CO_2 in water at higher pressures via higher injection rates and also the injection of gaseous CO_2 in water production case.

5. Horizontal permeability distribution was also an important factor affecting the propagation of CO_2 in top layer since CO_2 rose up after it has been injected. But the constant layer-wise permeability distribution caused significant changes in CO_2 saturation at the injection well block. CO_2 saturation values were different in the case of constant permeability in entire aquifer than the case of constant permeability values in each layer while changing in layer-wise. However, CO_2 saturation values were not significantly different in the case of constant permeability values in each layer while changing in layer-wise than variable permeability in each layer case.

6. Calcite precipitation mostly occured in bottom layer compared to precipitations in top and middle layers for a field-scale and single-well aquifer models . Decreasing the initial aquifer pressure by water production caused an increase in calcite precipitation in all layers of the aquifer at the injection well block due to the injection of gaseous CO_2.

7. Kaolinite precipitation and Anorthite dissolution were mostly seen in bottom layer compared to top and middle layers. The precipitation of Kaolinite and dissolution of Anorthite were lower with water production case than that of without water production case.

8. Salinity of the aquifer water has insignificant effect on free CO_2 saturation since the solubility of CO_2 did not change much in the rang of studied salinity.

9. Vertical to horizontal permeability ratio, injection rate and initial aquifer pressure were the factors affected the propagation of CO_2. Decreasing the initial aquifer pressure by water production and increasing vertical to horizontal permeability ratio caused an increase in propagation of CO_2 along the top layer of the aquifer. The increase in injection rate caused an increase in CO_2 propagation along the top layer of the aquifer for without water production case where as it caused a decrease in CO_2 propagation with water production case.

10. CO_2 saturation values at top layer for runs with all layers perforated were higher than the values for runs with only bottom layers perforated. CO_2 saturation values at middle layer were higher for runs with all layers perforated than the CO_2 saturation values for runs with only bottom layers perforated before the CO_2 injection has been ceased. After the CO_2 injection has been stopped, CO_2 saturation values at middle layer were higher for runs with only bottom layers perforated than the CO_2 saturation values for runs with all layers perforated which may be attributed to that CO_2 has a tendency to rise within the aquifer layers. For runs with all layers perforated, even if CO_2 was injected through all layers, CO_2 saturation values at bottom layer were almost zero comparing with the saturation values for runs with only bottom layers perforated. This situation can be attributed to the difference between the injection rates shared by each three layer of the aquifer.

11. For without water production case, for the grid block 52.5 m away from the injection well comparing with that of the injection well, the similar behaviour of paramaters were observed. The free CO_2 propagated in all three layers of the aquifer having the highest saturation values at top layer comparing to middle and bottom layers. CO_2 solubility in water was almost same in all layers of the aquifer. Calcite dissolution / precipitation, Anorthite dissolution, Kaolinite precipitation occurred in all layers of the aquifer with the same tendency as for the injection well. For the grid block 102.5 m away from the injection well, CO_2 saturation values at middle and bottom layers were approaching to zero comparing to values at top layer since CO_2 has a tendency to rise up to the top layer. CO_2 solubility in water at top layer was higher than the values of middle and bottom layers. The rates of calcite precipitation at middle and bottom layers were much higher than the rate of calcite precipitation at top layer. For the grid block 135 m away from the injection well, CO_2 saturation values at top layer started to decrease after 2170. CO_2 saturation values were already zero at middle and bottom layers. CO_2 solubility in water at top layer was higher than the values of middle and bottom layers. For top layer, CO_2 solubility in water was zero at the distance 135 m away from the injection well. Calcite precipitation was higher at bottom layer than the values of other two layers.

12. For with water production case, for the grid block 52.5 m away from the injection well, free CO_2 propagated in all layers having the highest saturation values at top layer comparing to middle and bottom layers. CO_2 solubility in water was almost same in all layers. Calcite dissolution / precipitation, anorthite dissolution, Kaolinite precipitation occurred in all layers of the aquifer with the same tendency as for the injection well. For the grid block 135 m away from the injection well, CO_2 saturation values at middle and bottom layers were approaching zero comparing to values of top layer since CO_2 has a tendency to rise there. CO_2 solubility in water at top layer was higher than the values for middle and bottom layers. The rates of calcite precipitation at middle and bottom layers were much higher than the rate of calcite precipitation at top layer. For the grid block 205 m away from the injection well,

CO_2 saturation values at top layer started to decrease after 2150. CO_2 saturation values were already zero at middle and bottom layers. CO_2 solubility in water at top layer was higher than the values of middle and bottom layers. For top layer, CO_2 solubility in water was zero at the distance 205 m away from the injection well. Calcite precipitation was higher at bottom layer than the values of other two layers.

13. The cumulative injected CO_2 in percentage of pore volumes changed between 0.15 and 1.3 that indicated the importance of the aquifer parameters on the amount of sequestered CO_2.

14. Changes in permeability due to the mineralization were not considered in this study. It was observed that the amount of Anorthite dissolution, Kaolinite and Calcite precipitations were higher. Therefore the change in permeability that might be resulted due to mineralization should be considered in future studies.

REFERENCES

1. Houghton, J.T., Ding, Y., Griggs, D.J. Noguer, M., van der Linden, P.J. and Dai, X.: "Climate Change 2001: The Scientific Basis," (2001) Cambridge University Press.

2. Wigley, T.M.L., Richels, R. and Edmonds, J.A.: "Economic and Environmental Choices in the Stabilization of Atmospheric CO_2 Concentrations," Nature, Vol. 379 (1996) 240-243.

3. Ennis-King, J. and Paterson, L.: "Engineering Aspects of Geological Sequestration of Carbon Dioxide," paper SPE 77809, 2002.

4. Hendricks, C. A. and Blok, K.: "Underground Storage of Carbon Dioxide," Energy Convers. Mgmt, Vol. 36 (1995) 539-542.

5. Gunter, W.D., Wong, S., Cheel, D.B. and Sjostrom, G.: "Large CO_2 Sinks: Their Role in the Mitigation of Greenhouse Gases From and International, National (Canadian) and Provincial (Alberta) Perspective," Applied Energy, Vol. 61 (1998) 209-227.

6. Bachu, S., Gunter, W.D. and Perkins, E.H.: "Carbon Dioxide Disposal," Aquifer Disposal of Carbon Dioxide, Brian Hitchon Editor, Geoscience Publishing Ltd., Edmonton, Alberta (1996) 11-22.

7. Hitchon, B., Gunter, W.D., Gentziz, T. and Bailey, R.T.: "Sedimentary Basins and Greenhouse Gases: A Serendipitous Association," Energy Convers. Mgmt, Vol. 40 (1999) 825-843.

8. Tanaka, S., Koide, H. and Sasagawa, A.: "Possibility of Underground CO_2 Sequestration in Japan," Energy Convers. Mgmt, Vol. 36 (1995) 527-530.

9. Koide, H.G., Tazaki, Y., Noguchi, Y., Iijima, M., Ito, K., Shindo, Y.: "Subterranean containment and long-term storage of carbon dioxide in unused aquifers and depleted natural gas reservoirs," Energy Convers. Mgmt. (1992) 33, 619.

10. Koide, H.G., Tazaki, Y., Noguchi, Y., Iijima, M., Ito, K. and Shindo, Y.: "Carbon Dioxide Injection into Useless Aquifers and Recovery of Natural Gas Dissolved in Fossil Water," Energy Convers. Mgmt, Vol.34 (1993) 921-924.

11. Krom, T.D., Jacobsen, F.L. and Ipsen, K.H.: "Aquifer Based Carbon Dioxide Disposal in Denmark: Capacities, Feasibilities, Implications and State of Readiness," Energy Convers. Mgmt, Vol.34 (1993) 933-940.

12. Baklid, A., Korbol, R. and Owren, G.: "Sleipner Vest CO_2 Disposal, CO_2 Injection into a Shallow Underground Aquifer," paper SPE 36600, Proceedings 1996 SPE Annual Technical Conference and Exhibition, Denver, Colorado, 6-9 October 1996.

13. Kongsjorden, H., Karstad, O. and Torp, T.A.: "Saline Aquifer Storage of Carbon Dioxide in the Sleipner Project," Waste Management, Vol.17 (1997) 303-308.

14. Chadwick, R.A., Zweigel, P., Gregersen, U., Kirby, G.A., Holloway, S. and Johannessen, P.N.: "Geological Characterization of CO_2 Storage Sites: Lesson From Sleipner, Northern North Sea." Proceedings 6^{th} Greenhouse Gas Technologies Conference (GHGT6), Kyoto, Japan, 1-4 October 2002.

15. Emberley, S., Hutchron, I., Shevalier, M., Durocher, K., Gunter, W.D. and Perkins, E.H.: "Geochemical Monitoring of Fluid-Rock Interaction and CO_2 Storage at the Weyburn CO_2-Injection Enhanced Oil Recovery Site, Saskatchewan, Canada," Proceedings 6th Greenhouse Gas Technologies Conference (GHGT6), Kyoto, Japan, 1-4 October 2002.

16. van der Meer, L.G.H.: "CO_2 Storage in the Subsurface," Proceedings 6th Greenhouse Gas Technologies Conference (GHGT6), Kyoto, Japan, 1-4 October 2002.

17. Nghiem, L.: "A code gem-ghg_200319d.exe of Compositional Simulator for Carbon Dioxide Sequestration," Computer Modeling Group Ltd, 2003.

18. Crowley, T.J.: "Causes of Climate Change Over the Past 100 Years," Science, Vol. 289 (2000) 270–277.

19. Alley R.B., Marotzke J., Nordhaus W.D., Overpeck J.T. and Peteet D.M.: "Abrupt Climate Change," *Science,* Vol. 299 (2003) 2005–2010.

20. Karl T.R. and Trenberth K.E.: "Modern Global Climate Change," Science, Vol .302 (2003) 1719–1723.

21. Energy Inf. Adm. 2001. Annual energy review 2000. *Rep. DOE/EIA-03842001*, US Dep. Energy, Washington, DC.

22. Intergovernmental panel on climate change (IPCC), IPCC third assessment report on climate change. Cambridge: Cambridge University Press; 2001.

23. US Environ. Prot. Agency. 2002. Inventory of U.S. greenhouse gas emissions and sinks: 1990–2000. *Rep. EPA 430-R-02–003*, Off. Atmos. Programs, Washington, DC.

24. US EIA (1997) 'Six greenhouse gases', Fact sheet US Delegation to the 3rd Conf. of the Parties, United Nations Committee on Climate Change, Kyoto, Japan, Dec. 5, 1997. http://www.state.gov/global/oes/fs sixgas cop.html, May 2005.

25. US EPA (2001a) 'Global warming'. http://www.epa.gov/globalwarming/emissions/national/ghgintro.html, May 2005.

26. Ledley, T.S., Sundquist, E.T., Schwartz, S.E., Hall, D.K., Fellows, J.D., Killeen, T.L.: "Climate Change and Greenhouse Gases, EOS," Transactions Am. Geoph. Union, Vol. 80 (1999) No. 39, pp. 453-458.

27. Watson RT. *Climate Change 2001: Synthesis Report. Assess. Rep.* Intergov. Panel Clim. Change. Cambridge, UK/New York: Cambridge Univ. Press 2001.

28. Intergovernmental Panel on Climate Change, 2000. Special Report on Land Use, Land-Use Change and Forestry. Cambridge University Press, Cambridge.

29. Intergovernmental Panel on Climate Change Working Group I, 1995. The Science of Climate Change. Cambridge University Press, Cambridge.

30. Jepma, C., Munasinghe, M., 'Climate Change Policy. New York, NY: Cambridge University Press; 1998. p. 331.

31. Bajura, R.A., The role of carbon dioxide sequestration in the long term energy future. In: Fifth International Greenhouse Gas Technologies Conference, Cairns, Australia, Collingwood. VIC, AU: CSIRO Publishing; 2001. pp. 52-8.

32. IEA, 2000. CO2 Emissions From Fuel Combustion 1971–1998. International Energy Agency, Paris.

33. Galeotti, M., Lanza, A.: "Richer and Cleaner, A study on carbon dioxide emissions in developing countries". Energy Policy, Vol 27 (1999) 565–573.

34. Bryant E. Climate process and change. Cambridge, UK: Cambridge University Press; 1997. p.209.

35. Grimston, M.C., Karakoussis, V., Fouquet, R., van der Vorst, R., Pearson, P., Leach, M.; 'The European and global potential of carbon dioxide sequestration in tackling climate change,' Climate Policy 1 (2001) 155–171.

36. Chandler, W., Schaeffer, R., Dadi, Z., Shukla, P.R., Tudela, F., Davidson, O. and Alpan, S.: "Climate Change Mitigation in Developing Countries," October 2002.

37. Akçasoy, K., Önder, F. and Güven, S.: "Statistical Evaluation of Greenhouse Gas Emissions of Turkey Between the Years of 1970 and 2010," State Institute of Statistics, Environmental Statistics Division, Ankara, Turkey.

38. Akçasoy, K., and Önder, F.: "Methodology on Greenhouse Gas Emissions Used by Turkey," State Institute of Statistics, Environmental Statistics Division, Ankara, Turkey.

39. Intergovernmental Panel on Climate Change, 1997. Greenhouse Gas Inventory Reference Manual, Revised 1996 IPCC Guidelines for National Greenhouse Gas Inventories. OECD, IEA.

40. Nguyen, D.N., "Carbon Dioxide Geological Sequestration: Technical and Economical Reviews"; paper SPE 81199, March 2003.

41. Nobles, J., Stancik, J., "Purifying food-grade, naturally occuring CO_2," Oil & Gas Journal, December 1983.

42. Ennis-King, J., Paterson, L.: "Engineering aspects of geological sequestration of carbon dioxide," paper SPE 77809, 2002.

43. West, J., "*Line will move 240 MMcfd of CO_2*," The Oil and Gas Journal, November 1971.

44. Farris, C., "Unusual Design Factors for Supercritical CO_2 Pipelines," Energy Progress, September 1983.

45. Socolow, R. (Ed.), "Fuels Decarbonisation and Carbon Sequestration: Report of a Workshop", Report 302 (1997) Princeton University/Center for Energy and Environmental Studies.

46. Ribeiro, J., Henry, B., "Carbon Dioxide Disposal and Storage Techniques. European Commission (DG XVIII)", (1995) Brussels.

47. Hendricks, C.A., "Carbon dioxide removal from coal-fired power plants" Ph.D. thesis (1994), Department of Science, Technology and Society, Utrecht University, The Netherlands.

48. Klara, S., Srivastava, R.D., McIlvried, H.G., " Integrated collaborative technology development program for CO_2 sequestration in geologic formations: United States department of energy R&D," Energy Conversion and Management (2003) 44, 2699-2712.

49. Bachu, S., "Sequestration of CO_2 in geological media: criteria and approach for site selection in response to climate change," Energy Conversion and Management (2000) 41, 953-970.

50. Gunter, W.D., Wiwchar, B., Perkins, E.H.: "Aquifer Disposal of CO_2- rich Gases: extension of the time scale of experiment for CO_2-sequestering reactions by geochemical modeling," Mineralogy and Petrology (1997) 59: 121-140.

51. Holloway, S., Savage, D.: "The potential for aquifer disposal of carbon dioxide in the UK," Energy Convers Mgmt. (1993) Vol.34 925-932.

52. Blunt, M., Fayers, F.J., Orr, F.M., "Carbon dioxide in enhanced oil recovery," Energy Convers Mgmt (1993) Vol. 34 1197-204.

53. Koide, H.G., Tazaki, Y., Noguchi, Y., Iijima, M., Ito, K., Shindo, Y.: "Subterranean containment and long-term storage of carbon dioxide in unused aquifers and depleted natural gas reservoirs," Energy Convers. Mgmt. (1992) 33, 619.

54. Van der Meer, L.G.H., "Investigations Regarding the Storage of Carbon dioxide in Aquifers in the Netherlands," Energy Convers. Mgmt. (1992) 33, 611-618.

55. Bachu, S., Gunter, W.D., and Perkins, E.H.: "Aquifer Disposal of CO_2: Hydrodynamic and Mineral Trapping"; Energy Conversion Management, (1994) 35, 269-279.

56. Law, D.H-S. Bachu, S.: "Hydro geological and numerical analysis of CO_2 disposal in deep saline aquifers in the Alberta sedimentary basin," Energy Convers. Mgmt. (1996) 37, 1167-1174.

57. Van der Meer, L.G.H.: "The Conditions Limiting CO_2 Storage in Aquifers," Energy Convers. Mgmt. (1993) 34, 956-966.

58. Kharaka, Y.K., Gunter, W.D., Aggarwal, P.K., Perkins, E.H., DeBraal, J.D., "SOLMINEQ.88: A computer program for geochemical modelling of water-rock reactions" U.S. Geol.Surv. Water-Resources Investigations (1988). Report 88-4227, Menlo Park.

59. Perkins, E.H., (1980). A reinvestigation of the theoretical basis for the calculation of mass transfer in geochemical processes involving aqueous solutions. MSc. Thesis, University of British Columbia, Vancouver.

60. Holloway, S., Van der Straaten, R.: "The Joule II Project, the Underground Disposal of Carbon Dioxide," Energy Convers. Mgmt. (1995) 36, 519-522.

61. Holt, T., Jensen, J.L. and Lindeberg, E.: "Underground Storage of CO_2 in Aquifers and Oil Reservoirs," Energy Convers. Mgmt. (1995) 36, 535-538.

62. Bergman, P.D., Winter, E. M.: "Disposal of Carbon Dioxide in Aquifers in the U.S.," Energy Convers. Mgmt. (1995) 36,523-526.

63. ChemicalLogicLtd., http://www.chemicalogic.com/download/co2_phase_diagram.pdf, May 2005.

64. Holloway, S., Savage, D.: "The potential for aquifer disposal of carbon dioxide in the UK," Energy Convers Mgmt. (1993) 34, 925-932.

65. Hendricks, C. A., Blok, K.: "Underground Storage of Carbon Dioxide," Energy Convers. Mgmt. (1993) 34, 949-957.

66. Koide, H.G., Tazaki, Y., Noguchi, Y., Iijima, M., Ito, K., Shindo, Y.: "Underground storage of carbon dioxide in depleted natural gas reservoirs and useless aquifers," Engineering Geology (1993) 34, 175-179.

67. Honor, J.S., "Origin of saline fluids in sedimentary basins. In: Geofluids: Origin, Migration, and Evolution of Fluids in Sedimentary Basins (ed J. Parnell), Geological Society of London Special Publication, 78, 151-74.

68. Bachu, S., Adams, J.J., "Equations of state for basin geofluids: algorithm review and intercomparison for brines," Geofluids (2002) 2, 257-271.

69. McCain, W.D.Jr., "Reservoir fluid property correlations: state of the art," SPE Reservoir Engineering (1991), 6, 266-272.

70. Batzle, M., Wang, Z., "Seismic properties of pore fluids," Geophysics (1992), 57, 1396-1408.

71. Kestin, J., Khalifa, H.E., Correia, R.J., "Tables of dynamic and kinematic viscosity of aqueous KCl solutions in the temperature range 25-150 °C and the pressure range 0.1-35 MPa," Journal of Physical Chemistry Reference Data (1981a), 10, 57-70.

72. Gunter, W. D., Perkins, E. H., and Mccann, T. J., "Aquifer Disposal of CO_2- rich Gases: Reaction Design for Added Capacity"; Energy Conversion and Management (1993) Volume 34, Issues 9-11, pp. 941-948.

73. Gunter, W. D., Bachu, S., Law, D.H-S. 'Technical and Economic Feasibility of CO_2 Disposal in Aquifers within the Alberta Sedimentary Basin, CANADA', Energy Convers. Mgmt. (1996) 37, 1135-1142.

74. Gunter, W.D., Bachu, S., Perkins, E.H., Undershultz, J.R., Wiwchar, B., Yuan, L.P., Berhane, M., Cotterill, D., Central Alberta: "CO_2 disposal into Alberta Basins-Phase II: Hydrogeological and mineralogical characterization of Mannville Group strata in Lake Wabamun area & water-rock interactions due to CO_2 injection into Glauconitic Sandstone aquifer" (1994), Alberta Geological Survey Open File Report 1994-17, 125 pages + appendicies.

75. Gunter, W.D., Bird, G.W., "CO_2 Production in tar sands reservoirs under in situ steam temperatures: reactive calcite dissolution," Chemical Geology (1988), 70, 301-311.

76. Sverdrup, H.U., Warfvinge, P., "Weathering of primary silicate minerals in the natural soil environment in relation to a chemical weathering model," Water Air Soil Poll (1988), 38, 387-408.

77. Weir, G.J., White, S.P. and Kissling, W.M.: "Reservoir Storage and Containment of Greenhouse Gases," Energy Convers. Mgmt (1995) 36, 6-9.

78. Van der Meer, L.G.H., "Computer Modeling of Underground CO_2 Storage," Energy Convers. Mgmt. (1996) 37, 1155-1160.

79. Pruess, K., Garcia, J. E., 'Flow Instabilities during Injection of CO_2 into Saline Aquifers', Proceedings, TOUGH Symposium 2003, Lawrence Berkeley National Laboratory, Berkeley, California, May 12-14, 2003.

80. Nguyen, D.N. and Allinson, W.G.: "The Economics of CO_2 Capture and Geological Storage"; SPE 77810, October 2002.

81. Schmidt, C.E., Klara, S., Srivastava, R.D., "DOE Carbon Sequestration Program-US Department of Energy Proceeding of the Electric Utilities Environmental Conference" 2002, Tucson, Arizona.

82. Lindeberg, E. : "Escape of CO_2 From Aquifers"; Energy Convers. Mgmt, Vol. 38. (1997) 235-240.

83. Pruess, K., Xu, T., Apps, J. and Garcia, J.: "Numerical Modeling of Aquifer Disposal of CO_2," SPE 66537, 2001.

84. Doughty, C. and Pruess, K.: "Modeling Supercritical CO_2 Injection in Heterogeneous Porous Media," Proceedings, TOUGH Symposium 2003, Lawrence Berkeley National Laboratory, Berkeley, California, 2003.

85. Katz and Coats: "Underground Storage of Fluids," Malloy Lithographing, Inc., 1968.

86. Nghiem, L., Sammon, P., Grabenstetter, J. and Ohkuma, H.: "Modeling CO_2 Storage in Aquifers with a Fully-Coupled Geochemical EOS Compositional Simulator," SPE 89474, 2004.

87. Computer Modeling Group (CMG): "GEM, Advanced Compositional Reservoir Simulator, Version 2004 User's Guide," 2004.

88. Katz, D. and Lee, R.: "Natural Gas Engineering: Production and Storage," McGraw-Hill International Editions, Chemical Engineering Series, 1990.

89. Nghiem, L.: "Compositional Simulator for CO_2 Sequestration: Part 2," Computer Modelling Group, June 2003.

90. Dirik, I., Altintas, A., Bulbul, S., Gumrah, F.: "Analytical Modeling of CO_2 Sequestration in Saline Aquifers"; Canadian International Petroleum Conference (55^{th} Annual Technical Meeting) Calgary, Alberta, Canada, 2004.

91. Basbug, B., Gumrah, F. and Oz: "Simulating the Effects of Deep Saline Aquifer Properties on CO_2 Sequestration"; Canadian International Petroleum Conference (56^{th} Annual Technical Meeting) Calgary, Alberta, Canada, 2005.

APPENDIX A

SAMPLE INPUT DATA FOR FIELD AND SINGLE-WELL AQUIFER MODELS

A.1 Input Data for a field aquifer model (Run 1a)

RESULTS SIMULATOR GEM

**** ------- Input/Output ----------**

```
*FILENAMES *OUTPUT *SRFOUT *RESTARTOUT *INDEXOUT *MAINRESULTSOUT
**INDEXIN 'basic.irf'
*INUNIT *SI
*INTERRUPT *INTERACTIVE
*RANGECHECK *ON
*XDR *ON
*REWIND   3
*MAXERROR  20
*WRST *TIME

*WPRN *WELL  *TIME
*WPRN *GRID  *TIME
*WPRN *ITER  *BRIEF

*WSRF *WELL 1
*WSRF *GRID *TIME

*DIARY *CHANGES

*OUTPRN *WELL *BRIEF
*OUTPRN *GRID *NONE
*OUTPRN *RES *NONE


*OUTSRF *GRID *SW *SG *PRES *DENW *DENG
        *Z 'CO2' *W 'CO2'
        *MOLALITY 'CO2' *MOLALITY 'H+' *MOLALITY 'Ca++'
        *MOLALITY 'SiO2(aq)' *MOLALITY 'Al+++' *MOLALITY 'OH-'
        *MOLALITY 'CO3--' *MOLALITY 'HCO3-' *MINERAL 'CALCITE'
        *MINERAL 'KAOLINIT' *MINERAL 'ANORTHIT'
*OUTSRF *RES *ALL
```

**RESTART 4730

** ---------- **Grid** ----------

RESULTS AXES-DIRECTIONS 1. 1. 1.
*GRID *VARI 35 31 3
*KDIR DOWN
*DI *IVAR 570. 603. 536. 268. 469. 402. 235. 536. 335. 335. 201. 134.
201. 268. 201. 670. 603. 603. 570. 603. 603. 201. 503. 436.
201. 268. 201. 134. 101. 168. 369. 335. 201. 603. 570.

*DJ *JVAR 335. 570. 603. 637. 603. 570. 704. 67. 134. 67. 536.
134. 168. 335. 101. 168. 704. 670. 235. 536. 268. 570.
201. 335. 402. 402. 268. 603. 570. 670. 603.

*DK *KVAR 41. 30. 111.

*DTOP
1010 1010 1010 1010 1010 1010 1010 1010 1010 1010 1010 1010 1010 1010 1010 1010 1010 1010
1010 1010 1010 1010 1010 1010 1010 979 976 973 970 970 970 976 979 1010 1010 1010
1010 1010 1010 1010 1010 1010 1010 1010 1010 1010 1010 1010 1010 1010 1010 1010 1010 1010
1010 1010 1010 1010 1010 976 967 964 958 956 955 955 956 961 970 979 1010 1010
1010 1010 1010 1010 1010 1010 1010 1010 1010 1010 1010 1010 1010 1010 1010 1010 1010 1010
1010 1010 1010 976 972 964 952 946 946 946 946 946 946 947 956 967 1010 1010
1010 1010 1010 1010 1010 1010 1010 1010 1010 1010 1010 1010 1010 1010 1010 1010 1010 1010
1010 979 972 964 956 947 943 941 936 933 933 933 933 939 952 961 973 1010
1010 1010 1010 1010 1010 1010 1010 1010 1010 1010 1010 1010 1010 1010 1010 1010 1010 1010
972 964 953 949 943 939 933 927 926 924 923 923 926 933 947 956 972 1010
1010 1010 1010 1010 1010 1010 1010 1010 1010 1010 1010 1010 1010 1010 1010 979 964
949 941 936 933 933 930 926 921 918 915 912 912 912 918 933 946 956 972
1010 1010 1010 1010 1010 1010 1010 1010 1010 1010 1010 1010 976 972 964 955 941
924 918 918 917 917 914 912 909 903 901 897 894 892 892 903 915 933 964
1010 1010 1010 1010 1010 1010 1010 1010 1010 1010 979 973 967 961 953 939 930
912 909 909 909 906 906 903 900 894 892 888 885 882 883 886 903 933 964
1010 1010 1010 1010 1010 1010 1010 1010 1010 1010 973 967 964 953 949 936 921
911 906 903 903 903 903 900 897 894 891 885 883 882 882 885 903 933 964
1010 1010 1010 1010 1010 1010 1010 1010 1010 1010 972 967 956 952 946 933 917
909 901 901 901 900 900 895 892 891 888 882 879 877 880 885 903 933 964
1010 1010 1010 1010 1010 1010 1010 1010 1010 972 964 956 952 943 936 924 911 903
897 894 894 894 892 891 888 882 877 874 872 868 879 888 918 949 1010
1010 1010 1010 1010 1010 1010 1010 1010 973 964 953 947 941 933 926 915 906 897
891 885 886 891 888 879 875 860 857 857 857 865 879 885 918 979 1010
1010 1010 1010 1010 1010 1010 1010 979 970 956 949 943 936 932 924 912 903 894
885 882 882 885 882 875 857 857 857 857 857 875 882 888 933 949 1010
1010 1010 1010 1010 1010 1010 1010 972 964 952 943 936 933 921 915 909 895 888
879 875 875 875 866 857 857 857 866 875 879 882 888 933 964 1010 1010
1010 1010 1010 1010 1010 1010 979 967 955 943 936 930 924 915 912 903 891 882
866 857 857 857 857 857 857 866 882 885 888 903 933 949 1010 1010 1010
1010 1010 1010 1010 1010 1010 976 964 952 941 933 930 921 912 911 903 888 879
863 857 857 866 866 866 869 879 888 903 918 933 964 1010 1010 1010 1010
1010 1010 1010 1010 1010 1010 972 961 943 933 926 921 912 911 903 895 882 872
875 882 891 888 888 888 903 918 949 964 979 979 1010 1010 1010 1010 1010
1010 1010 1010 1010 1010 972 956 941 933 924 915 911 911 911 903 903 903 903
918 933 933 964 979 976 979 979 979 1010 1010 1010 1010 1010 1010 1010 1010 1010

1010 1010 1010 1010 979 964 941 933 924 914 906 903 897 891 891 891 918 933
936 956 964 979 1010 1010 1010 1010 1010 1010 1010 1010 1010 1010 1010 1010 1010
1010 1010 1010 1010 972 949 933 921 911 903 895 892 891 885 882 888 933 949
956 964 976 1010 1010 1010 1010 1010 1010 1010 1010 1010 1010 1010 1010 1010 1010
1010 1010 1010 979 956 933 923 911 895 888 882 882 875 875 888 915 952 973
973 979 1010 1010 1010 1010 1010 1010 1010 1010 1010 1010 1010 1010 1010 1010 1010
1010 1010 1010 964 939 918 906 895 885 875 866 857 866 885 903 933 964 1010
1010 1010 1010 1010 1010 1010 1010 1010 1010 1010 1010 1010 1010 1010 1010 1010 1010
1010 1010 972 949 926 906 895 882 866 857 857 875 882 903 927 964 1010 1010
1010 1010 1010 1010 1010 1010 1010 1010 1010 1010 1010 1010 1010 1010 1010 1010 1010
1010 1010 964 933 917 903 888 875 857 857 875 882 888 912 943 972 1010 1010
1010 1010 1010 1010 1010 1010 1010 1010 1010 1010 1010 1010 1010 1010 1010 1010 1010
1010 1010 941 921 903 888 875 857 857 875 885 895 903 933 964 1010 1010 1010
1010 1010 1010 1010 1010 1010 1010 1010 1010 1010 1010 1010 1010 1010 1010 1010 1010
1010 964 933 911 900 882 872 875 885 903 918 933 949 964 979 1010 1010 1010
1010 1010 1010 1010 1010 1010 1010 1010 1010 1010 1010 1010 1010 1010 1010 1010 1010
1010 956 924 911 895 882 880 894 927 964 976 979 979 1010 1010 1010 1010 1010
1010 1010 1010 1010 1010 1010 1010 1010 1010 1010 1010 1010 1010 1010 1010 1010 1010
1010 952 918 909 897 895 903 933 964 1010 1010 1010 1010 1010 1010 1010 1010 1010
1010 1010 1010 1010 1010 1010 1010 1010 1010 1010 1010 1010 1010 1010 1010 1010 1010 1010
1010
979 952 930 915 915 920 941 1010 1010 1010 1010 1010 1010 1010 1010 1010 1010 1010
1010 1010 1010 1010 1010 1010 1010 1010 1010 1010 1010 1010 1010 1010 1010 1010 1010 1010
1010
979 956 943 941 943 964 1010 1010 1010 1010 1010 1010 1010 1010 1010 1010 1010 1010
1010 1010 1010 1010 1010 1010 1010 1010 1010 1010 1010 1010 1010 1010 1010 1010 1010 1010
1010
1010 972 964 964 979 1010 1010 1010 1010 1010 1010 1010 1010 1010 1010 1010 1010 1010
1010 1010 1010 1010 1010 1010 1010 1010 1010 1010 1010 1010 1010 1010 1010 1010 1010 1010
1010

*NULL IJK
1:1 1:28 1:3 0
1:1 31:31 1:3 0
2:2 1:25 1:3 0
3:3 1:22 1:3 0
4:4 1:20 1:3 0
5:5 1:18 1:3 0
6:6 31:31 1:3 0
6:6 1:17 1:3 0
7:7 30:31 1:3 0
7:7 1:14 1:3 0
8:8 29:31 1:3 0
8:8 1:12 1:3 0
9:9 29:31 1:3 0
9:9 1:11 1:3 0
10:10 28:31 1:3 0
10:10 1:10 1:3 0
11:11 28:31 1:3 0
11:11 1:7 1:3 0
12:12 28:31 1:3 0
12:12 1:7 1:3 0
13:13 28:31 1:3 0

13:13 1:6 1:3 0
14:14 27:31 1:3 0
14:14 1:6 1:3 0
15:15 27:31 1:3 0
15:15 1:6 1:3 0
16:16 25:31 1:3 0
16:16 1:5 1:3 0
17:17 23:31 1:3 0
17:17 1:5 1:3 0
18:18 22:31 1:3 0
18:18 1:4 1:3 0
19:19 22:31 1:3 0
19:19 1:3 1:3 0
20:20 22:31 1:3 0
20:20 1:3 1:3 0
21:21 21:31 1:3 0
21:21 1:2 1:3 0
22:22 20:31 1:3 0
22:22 1:2 1:3 0
23:23 19:31 1:3 0
23:23 1:1 1:3 0
24:24 19:31 1:3 0
24:24 1:1 1:3 0
25:25 19:31 1:3 0
26:26 19:31 1:3 0
27:27 19:31 1:3 0
28:28 18:31 1:3 0
29:29 18:31 1:3 0
30:30 17:31 1:3 0
31:31 17:31 1:3 0
32:32 16:31 1:3 0
33:33 15:31 1:3 0
33:33 1:1 1:3 0
34:34 14:31 1:3 0
34:34 1:3 1:3 0
35:35 1:5 1:3 0
35:35 11:31 1:3 0

*POR CON 0.25

MOD 1:1 1:28 1:3 = 0
1:1 31:31 1:3 = 0
2:2 1:25 1:3 = 0
3:3 1:22 1:3 = 0
4:4 1:20 1:3 = 0
5:5 1:18 1:3 = 0
6:6 31:31 1:3 = 0
6:6 1:17 1:3 = 0
7:7 30:31 1:3 = 0
7:7 1:14 1:3 = 0
8:8 29:31 1:3 = 0
8:8 1:12 1:3 = 0
9:9 29:31 1:3 = 0

9:9 1:11 1:3 = 0
10:10 28:31 1:3 = 0
10:10 1:10 1:3 = 0
11:11 28:31 1:3 = 0
11:11 1:7 1:3 = 0
12:12 28:31 1:3 = 0
12:12 1:7 1:3 = 0
13:13 28:31 1:3 = 0
13:13 1:6 1:3 = 0
14:14 27:31 1:3 = 0
14:14 1:6 1:3 = 0
15:15 27:31 1:3 = 0
15:15 1:6 1:3 = 0
16:16 25:31 1:3 = 0
16:16 1:5 1:3 = 0
17:17 23:31 1:3 = 0
17:17 1:5 1:3 = 0
18:18 22:31 1:3 = 0
18:18 1:4 1:3 = 0
19:19 22:31 1:3 = 0
19:19 1:3 1:3 = 0
20:20 22:31 1:3 = 0
20:20 1:3 1:3 = 0
21:21 21:31 1:3 = 0
21:21 1:2 1:3 = 0
22:22 20:31 1:3 = 0
22:22 1:2 1:3 = 0
23:23 19:31 1:3 = 0
23:23 1:1 1:3 = 0
24:24 19:31 1:3 = 0
24:24 1:1 1:3 = 0
25:25 19:31 1:3 = 0
26:26 19:31 1:3 = 0
27:27 19:31 1:3 = 0
28:28 18:31 1:3 = 0
29:29 18:31 1:3 = 0
30:30 17:31 1:3 = 0
31:31 17:31 1:3 = 0
32:32 16:31 1:3 = 0
33:33 15:31 1:3 = 0
33:33 1:1 1:3 = 0
34:34 14:31 1:3 = 0
34:34 1:3 1:3 = 0
35:35 1:5 1:3 = 0
35:35 11:31 1:3 = 0

*PERMI ALL
24*0 2*26.25 2*22.5 2*26.25 2*30. 25*0 26.25 30. 33.75 30. 26.25 3*30.
3*33.75 22*0 2*26.25 30. 33.75 2*37.5 33.75 37.5 33.75 37.5 2*41.25 37.5
20*0 4*30. 33.75 37.5 2*41.25 37.5 41.25 37.5 41.25 3*45. 30. 18*0 26.25
33.75 2*41.25 2*37.5 41.25 4*45. 48.75 52.5 2*56.25 48.75 30. 16*0 2*22.5
30. 41.25 2*45. 2*41.25 45. 48.75 2*52.5 48.75 52.5 56.25 2*60. 56.25 2*30.
12*0 2*26.25 2*22.5 26.25 33.75 45. 4*48.75 2*52.5 2*56.25 48.75 56.25
60. 2*63.75 60. 45. 30. 10*0 2*26.25 30. 33.75 2*37.5 33.75 37.5 45. 48.75

52.5 56.25 2*52.5 56.25 60. 2*56.25 60. 63.75 2*67.5 63.75 48.75 37.5 10*0
2*30. 2*37.5 2*41.25 37.5 41.25 45. 48.75 52.5 54.75 52.5 56.25 63.75 60.
56.25 60. 63.75 67.5 71.25 72.75 67.5 48.75 37.5 10*0 33.75 37.5 41.25
3*45. 41.25 2*45. 2*48.75 52.5 54. 3*52.5 2*56.25 60. 56.25 63.75 71.25
67.5 52.5 41.25 9*0 30. 37.5 41.25 2*45. 2*48.75 45. 41.25 45. 4*52.5 2*48.75
2*52.5 54. 56.25 60. 63.75 60. 56.25 33.75 9*0 30. 41.25 3*45. 3*48.75
45. 2*41.25 6*52.5 2*48.75 52.5 56.25 63.75 60. 52.5 37.5 30. 8*0 2*30.
45. 4*48.75 52.5 48.75 41.25 37.5 45. 4*48.75 52.5 2*48.75 45. 47.25 52.5
56.25 48.75 45. 33.75 30. 8*0 33.75 2*45. 52.5 2*56.25 2*52.5 45. 2*41.25
45. 48.75 3*45. 2*48.75 45. 2*52.5 60. 67.5 52.5 41.25 30. 8*0 37.5 41.25
48.75 52.5 56.25 63.75 2*60. 56.25 48.75 2*41.25 2*45. 3*41.25 45. 48.75
52.5 56.25 67.5 71.25 67.5 48.75 37.5 9*0 41.25 48.75 56.25 60. 56.25 67.5
60. 63.75 60. 52.5 3*45. 41.25 3*37.5 2*45. 48.75 2*63.75 75. 71.25 52.5
10*0 45. 52.5 56.25 2*60. 63.75 71.25 67.5 2*63.75 2*60. 56.25 45. 37.5
30. 33.75 2*41.25 45. 52.5 60. 71.25 67.5 10*0 48.75 52.5 56.25 63.75 60.
63.75 67.5 71.25 75. 71.25 75. 71.25 67.5 63.75 45. 33.75 26.25 3*30. 33.75
41.25 12*0 52.5 60. 67.5 71.25 75. 63.75 71.25 82.5 75. 78.75 81.75 78.75
71.25 63.75 52.5 41.25 2*30. 17*0 45. 82.5 78.75 82.5 2*86.25 82.5 86.25
82.5 78.75 71.25 82.5 2*63.75 48.75 41.25 30. 17*0 41.25 63.75 75. 87.
86.25 90. 75. 82.5 2*75. 71.25 60. 56.25 52.5 48.75 45. 37.5 18*0 52.5
71.25 82.5 90. 93.75 97.5 93.75 82.5 71.25 67.5 60. 48.75 41.25 33.75 20*0
48.75 60. 75. 90. 82.5 86.25 93.75 114. 70.5 2*71.25 60. 41.25 30. 21*0
45. 71.25 86.25 2*90. 82.5 86.25 101.25 82.5 78.75 75. 56.25 37.5 30. 21*0
41.25 75. 82.5 86.25 75. 67.5 56.25 67.5 78.75 75. 81. 63.75 41.25 21*0
60. 67.5 78.75 86.25 78.75 75. 71.25 60. 48.75 63.75 75. 71.25 75. 45.
21*0 56.25 71.25 84. 82.5 67.5 63.75 60. 45. 41.25 56.25 60. 45. 23*0 52.5
75. 78.75 71.25 63.75 52.5 45. 33.75 26*0 52.5 2*56.25 63.75 52.5 45. 48.75
28*0 41.25 48.75 41.25 45. 41.25 37.5 30*0 33.75 37.5 33.75 30. 54*0 2*10.5
2*9. 2*10.5 2*12. 25*0 10.5 12. 13.5 12. 10.5 3*12. 3*13.5 22*0 2*10.5
12. 13.5 2*15. 13.5 15. 13.5 15. 2*16.5 15. 20*0 4*12. 13.5 15. 2*16.5
15. 16.5 15. 16.5 3*18. 12. 18*0 10.5 13.5 2*16.5 2*15. 16.5 4*18. 19.5
21. 2*22.5 19.5 12. 16*0 2*9. 12. 16.5 2*18. 2*16.5 18. 19.5 2*21. 19.5
21. 22.5 2*24. 22.5 2*12. 12*0 2*10.5 2*9. 10.5 13.5 18. 4*19.5 2*21. 2*22.5
19.5 22.5 24. 2*25.5 24. 18. 12. 10*0 2*10.5 12. 13.5 2*15. 13.5 15. 18.
19.5 21. 22.5 2*21. 22.5 24. 2*22.5 24. 25.5 2*27. 25.5 19.5 15. 10*0 2*12.
2*15. 2*16.5 15. 16.5 18. 19.5 21. 21.9 21. 22.5 25.5 24. 22.5 24. 25.5
27. 28.5 29.1 27. 19.5 15. 10*0 13.5 15. 16.5 3*18. 16.5 2*18. 2*19.5 21.
21.6 3*21. 2*22.5 24. 22.5 25.5 28.5 27. 21. 16.5 9*0 12. 15. 16.5 2*18.
2*19.5 18. 16.5 18. 4*21. 2*19.5 2*21. 21.6 22.5 24. 25.5 24. 22.5 13.5
9*0 12. 16.5 3*18. 3*19.5 18. 2*16.5 6*21. 2*19.5 21. 22.5 25.5 24. 21.
15. 12. 8*0 2*12. 18. 4*19.5 21. 19.5 16.5 15. 18. 4*19.5 21. 2*19.5 18.
18.9 21. 22.5 19.5 18. 13.5 12. 8*0 13.5 2*18. 21. 2*22.5 2*21. 18. 2*16.5
18. 19.5 3*18. 2*19.5 18. 2*21. 24. 27. 21. 16.5 12. 8*0 15. 16.5 19.5
21. 22.5 25.5 2*24. 22.5 19.5 2*16.5 2*18. 3*16.5 18. 19.5 21. 22.5 27.
28.5 27. 19.5 15. 9*0 16.5 19.5 22.5 24. 22.5 27. 24. 25.5 24. 21. 3*18.
16.5 3*15. 2*18. 19.5 2*25.5 30. 28.5 21. 10*0 18. 21. 22.5 2*24. 25.5
28.5 27. 2*25.5 2*24. 22.5 18. 15. 12. 13.5 2*16.5 18. 21. 24. 28.5 27.
10*0 19.5 21. 22.5 25.5 24. 25.5 27. 28.5 30. 28.5 30. 28.5 27. 25.5 18.
13.5 10.5 3*12. 13.5 16.5 12*0 21. 24. 27. 28.5 30. 25.5 28.5 33. 30. 31.5
32.7 31.5 28.5 25.5 21. 16.5 2*12. 17*0 18. 33. 31.5 33. 2*34.5 33. 34.5
33. 31.5 28.5 33. 2*25.5 19.5 16.5 12. 17*0 16.5 25.5 30. 34.8 34.5 36.
30. 33. 2*30. 28.5 24. 22.5 21. 19.5 18. 15. 18*0 21. 28.5 33. 36. 37.5
39. 37.5 33. 28.5 27. 24. 19.5 16.5 13.5 20*0 19.5 24. 30. 36. 33. 34.5
37.5 45.6 28.2 2*28.5 24. 16.5 12. 21*0 18. 28.5 34.5 2*36. 33. 34.5 40.5

33. 31.5 30. 22.5 15. 12. 21*0 16.5 30. 33. 34.5 30. 27. 22.5 27. 31.5
30. 32.4 25.5 16.5 21*0 24. 27. 31.5 34.5 31.5 30. 28.5 24. 19.5 25.5 30.
28.5 30. 18. 21*0 22.5 28.5 33.6 33. 27. 25.5 24. 18. 16.5 22.5 24. 18.
23*0 21. 30. 31.5 28.5 25.5 21. 18. 13.5 26*0 21. 2*22.5 25.5 21. 18. 19.5
28*0 16.5 19.5 16.5 18. 16.5 15. 30*0 13.5 15. 13.5 12. 54*0 2*35. 2*30.
2*35. 2*40. 25*0 35. 40. 45. 40. 35. 3*40. 3*45. 22*0 2*35. 40. 45. 2*50.
45. 50. 45. 50. 2*55. 50. 20*0 4*40. 45. 50. 2*55. 50. 55. 50. 55. 3*60.
40. 18*0 35. 45. 2*55. 2*50. 55. 4*60. 65. 70. 2*75. 65. 40. 16*0 2*30.
40. 55. 2*60. 2*55. 60. 65. 2*70. 65. 70. 75. 2*80. 75. 2*40. 12*0 2*35.
2*30. 35. 45. 60. 4*65. 2*70. 2*75. 65. 75. 80. 2*85. 80. 60. 40. 10*0
2*35. 40. 45. 2*50. 45. 50. 60. 65. 70. 75. 2*70. 75. 80. 2*75. 80. 85.
2*90. 85. 65. 50. 10*0 2*40. 2*50. 2*55. 50. 55. 60. 65. 70. 73. 70. 75.
85. 80. 75. 80. 85. 90. 95. 97. 90. 65. 50. 10*0 45. 50. 55. 3*60. 55.
2*60. 2*65. 70. 72. 3*70. 2*75. 80. 75. 85. 95. 90. 70. 55. 9*0 40. 50.
55. 2*60. 2*65. 60. 55. 60. 4*70. 2*65. 2*70. 72. 75. 80. 85. 80. 75. 45.
9*0 40. 55. 3*60. 3*65. 60. 2*55. 6*70. 2*65. 70. 75. 85. 80. 70. 50. 40.
8*0 2*40. 60. 4*65. 70. 65. 55. 50. 60. 4*65. 70. 2*65. 60. 63. 70. 75.
65. 60. 45. 40. 8*0 45. 2*60. 70. 2*75. 2*70. 60. 2*55. 60. 65. 3*60. 2*65.
60. 2*70. 80. 90. 70. 55. 40. 8*0 50. 55. 65. 70. 75. 85. 2*80. 75. 65.
2*55. 2*60. 3*55. 60. 65. 70. 75. 90. 95. 90. 65. 50. 9*0 55. 65. 75. 80.
75. 90. 80. 85. 80. 70. 3*60. 55. 3*50. 2*60. 65. 2*85. 100. 95. 70. 10*0
60. 70. 75. 2*80. 85. 95. 90. 2*85. 2*80. 75. 60. 50. 40. 45. 2*55. 60.
70. 80. 95. 90. 10*0 65. 70. 75. 85. 80. 85. 90. 95. 100. 95. 100. 95.
90. 85. 60. 45. 35. 3*40. 45. 55. 12*0 70. 80. 90. 95. 100. 85. 95. 110.
100. 105. 109. 105. 95. 85. 70. 55. 2*40. 17*0 60. 110. 105. 110. 2*115.
110. 115. 110. 105. 95. 110. 2*85. 65. 55. 40. 17*0 55. 85. 100. 116. 115.
120. 100. 110. 2*100. 95. 80. 75. 70. 65. 60. 50. 18*0 70. 95. 110. 120.
125. 130. 125. 110. 95. 90. 80. 65. 55. 45. 20*0 65. 80. 100. 120. 110.
115. 125. 152. 94. 2*95. 80. 55. 40. 21*0 60. 95. 115. 2*120. 110. 115.
135. 110. 105. 100. 75. 50. 40. 21*0 55. 100. 110. 115. 100. 90. 75. 90.
105. 100. 108. 85. 55. 21*0 80. 90. 105. 115. 105. 100. 95. 80. 65. 85.
100. 95. 100. 60. 21*0 75. 95. 112. 110. 90. 85. 80. 60. 55. 75. 80. 60.
23*0 70. 100. 105. 95. 85. 70. 60. 45. 26*0 70. 2*75. 85. 70. 60. 65. 28*0
55. 65. 55. 60. 55. 50. 30*0 45. 50. 45. 40. 30*0

*PERMJ ALL
24*0 2*26.25 2*22.5 2*26.25 2*30. 25*0 26.25 30. 33.75 30. 26.25 3*30.
3*33.75 22*0 2*26.25 30. 33.75 2*37.5 33.75 37.5 33.75 37.5 2*41.25 37.5
20*0 4*30. 33.75 37.5 2*41.25 37.5 41.25 37.5 41.25 3*45. 30. 18*0 26.25
33.75 2*41.25 2*37.5 41.25 4*45. 48.75 52.5 2*56.25 48.75 30. 16*0 2*22.5
30. 41.25 2*45. 2*41.25 45. 48.75 2*52.5 48.75 52.5 56.25 2*60. 56.25 2*30.
12*0 2*26.25 2*22.5 26.25 33.75 45. 4*48.75 2*52.5 2*56.25 48.75 56.25
60. 2*63.75 60. 45. 30. 10*0 2*26.25 30. 33.75 2*37.5 33.75 37.5 45. 48.75
52.5 56.25 2*52.5 56.25 60. 2*56.25 60. 63.75 2*67.5 63.75 48.75 37.5 10*0
2*30. 2*37.5 2*41.25 37.5 41.25 45. 48.75 52.5 54.75 52.5 56.25 63.75 60.
56.25 60. 63.75 67.5 71.25 72.75 67.5 48.75 37.5 10*0 33.75 37.5 41.25
3*45. 41.25 2*45. 2*48.75 52.5 54. 3*52.5 2*56.25 60. 56.25 63.75 71.25
67.5 52.5 41.25 9*0 30. 37.5 41.25 2*45. 2*48.75 45. 41.25 45. 4*52.5 2*48.75
2*52.5 54. 56.25 60. 63.75 60. 56.25 33.75 9*0 30. 41.25 3*45. 3*48.75
45. 2*41.25 6*52.5 2*48.75 52.5 56.25 63.75 60. 52.5 37.5 30. 8*0 2*30.
45. 4*48.75 52.5 48.75 41.25 37.5 45. 4*48.75 52.5 2*48.75 45. 47.25 52.5
56.25 48.75 45. 33.75 30. 8*0 33.75 2*45. 52.5 2*56.25 2*52.5 45. 2*41.25
45. 48.75 3*45. 2*48.75 45. 2*52.5 60. 67.5 52.5 41.25 30. 8*0 37.5 41.25
48.75 52.5 56.25 63.75 2*60. 56.25 48.75 2*41.25 2*45. 3*41.25 45. 48.75

52.5 56.25 67.5 71.25 67.5 48.75 37.5 9*0 41.25 48.75 56.25 60. 56.25 67.5
60. 63.75 60. 52.5 3*45. 41.25 3*37.5 2*45. 48.75 2*63.75 75. 71.25 52.5
10*0 45. 52.5 56.25 2*60. 63.75 71.25 67.5 2*63.75 2*60. 56.25 45. 37.5
30. 33.75 2*41.25 45. 52.5 60. 71.25 67.5 10*0 48.75 52.5 56.25 63.75 60.
63.75 67.5 71.25 75. 71.25 75. 71.25 67.5 63.75 45. 33.75 26.25 3*30. 33.75
41.25 12*0 52.5 60. 67.5 71.25 75. 63.75 71.25 82.5 75. 78.75 81.75 78.75
71.25 63.75 52.5 41.25 2*30. 17*0 45. 82.5 78.75 82.5 2*86.25 82.5 86.25
82.5 78.75 71.25 82.5 2*63.75 48.75 41.25 30. 17*0 41.25 63.75 75. 87.
86.25 90. 75. 82.5 2*75. 71.25 60. 56.25 52.5 48.75 45. 37.5 18*0 52.5
71.25 82.5 90. 93.75 97.5 93.75 82.5 71.25 67.5 60. 48.75 41.25 33.75 20*0
48.75 60. 75. 90. 82.5 86.25 93.75 114. 70.5 2*71.25 60. 41.25 30. 21*0
45. 71.25 86.25 2*90. 82.5 86.25 101.25 82.5 78.75 75. 56.25 37.5 30. 21*0
41.25 75. 82.5 86.25 75. 67.5 56.25 67.5 78.75 75. 81. 63.75 41.25 21*0
60. 67.5 78.75 86.25 78.75 75. 71.25 60. 48.75 63.75 75. 71.25 75. 45.
21*0 56.25 71.25 84. 82.5 67.5 63.75 60. 45. 41.25 56.25 60. 45. 23*0 52.5
75. 78.75 71.25 63.75 52.5 45. 33.75 26*0 52.5 2*56.25 63.75 52.5 45. 48.75
28*0 41.25 48.75 41.25 45. 41.25 37.5 30*0 33.75 37.5 33.75 30. 54*0 2*10.5
2*9. 2*10.5 2*12. 25*0 10.5 12. 13.5 12. 10.5 3*12. 3*13.5 22*0 2*10.5
12. 13.5 2*15. 13.5 15. 13.5 15. 2*16.5 15. 20*0 4*12. 13.5 15. 2*16.5
15. 16.5 15. 16.5 3*18. 12. 18*0 10.5 13.5 2*16.5 2*15. 16.5 4*18. 19.5
21. 2*22.5 19.5 12. 16*0 2*9. 12. 16.5 2*18. 2*16.5 18. 19.5 2*21. 19.5
21. 22.5 2*24. 22.5 2*12. 12*0 2*10.5 2*9. 10.5 13.5 18. 4*19.5 2*21. 2*22.5
19.5 22.5 24. 2*25.5 24. 18. 12. 10*0 2*10.5 12. 13.5 2*15. 13.5 15. 18.
19.5 21. 22.5 2*21. 22.5 24. 2*22.5 24. 25.5 2*27. 25.5 19.5 15. 10*0 2*12.
2*15. 2*16.5 15. 16.5 18. 19.5 21. 21.9 21. 22.5 25.5 24. 22.5 24. 25.5
27. 28.5 29.1 27. 19.5 15. 10*0 13.5 15. 16.5 3*18. 16.5 2*18. 2*19.5 21.
21.6 3*21. 2*22.5 24. 22.5 25.5 28.5 27. 21. 16.5 9*0 12. 15. 16.5 2*18.
2*19.5 18. 16.5 18. 4*21. 2*19.5 2*21. 21.6 22.5 24. 25.5 24. 22.5 13.5
9*0 12. 16.5 3*18. 3*19.5 18. 2*16.5 6*21. 2*19.5 21. 22.5 25.5 24. 21.
15. 12. 8*0 2*12. 18. 4*19.5 21. 19.5 16.5 15. 18. 4*19.5 21. 2*19.5 18.
18.9 21. 22.5 19.5 18. 13.5 12. 8*0 13.5 2*18. 21. 2*22.5 2*21. 18. 2*16.5
18. 19.5 3*18. 2*19.5 18. 2*21. 24. 27. 21. 16.5 12. 8*0 15. 16.5 19.5
21. 22.5 25.5 2*24. 22.5 19.5 2*16.5 2*18. 3*16.5 18. 19.5 21. 22.5 27.
28.5 27. 19.5 15. 9*0 16.5 19.5 22.5 24. 22.5 27. 24. 25.5 24. 21. 3*18.
16.5 3*15. 2*18. 19.5 2*25.5 30. 28.5 21. 10*0 18. 21. 22.5 2*24. 25.5
28.5 27. 2*25.5 2*24. 22.5 18. 15. 12. 13.5 2*16.5 18. 21. 24. 28.5 27.
10*0 19.5 21. 22.5 25.5 24. 25.5 27. 28.5 30. 28.5 30. 28.5 27. 25.5 18.
13.5 10.5 3*12. 13.5 16.5 12*0 21. 24. 27. 28.5 30. 25.5 28.5 33. 30. 31.5
32.7 31.5 28.5 25.5 21. 16.5 2*12. 17*0 18. 33. 31.5 33. 2*34.5 33. 34.5
33. 31.5 28.5 33. 2*25.5 19.5 16.5 12. 17*0 16.5 25.5 30. 34.8 34.5 36.
30. 33. 2*30. 28.5 24. 22.5 21. 19.5 18. 15. 18*0 21. 28.5 33. 36. 37.5
39. 37.5 33. 28.5 27. 24. 19.5 16.5 13.5 20*0 19.5 24. 30. 36. 33. 34.5
37.5 45.6 28.2 2*28.5 24. 16.5 12. 21*0 18. 28.5 34.5 2*36. 33. 34.5 40.5
33. 31.5 30. 22.5 15. 12. 21*0 16.5 30. 33. 34.5 30. 27. 22.5 27. 31.5
30. 32.4 25.5 16.5 21*0 24. 27. 31.5 34.5 31.5 30. 28.5 24. 19.5 25.5 30.
28.5 30. 18. 21*0 22.5 28.5 33.6 33. 27. 25.5 24. 18. 16.5 22.5 24. 18.
23*0 21. 30. 31.5 28.5 25.5 21. 18. 13.5 26*0 21. 2*22.5 25.5 21. 18. 19.5
28*0 16.5 19.5 16.5 18. 16.5 15. 30*0 13.5 15. 13.5 12. 54*0 2*35. 2*30.
2*35. 2*40. 25*0 35. 40. 45. 40. 35. 3*40. 3*45. 22*0 2*35. 40. 45. 2*50.
45. 50. 45. 50. 2*55. 50. 20*0 4*40. 45. 50. 2*55. 50. 55. 50. 55. 3*60.
40. 18*0 35. 45. 2*55. 2*50. 55. 4*60. 65. 70. 2*75. 65. 40. 16*0 2*30.
40. 55. 2*60. 2*55. 60. 65. 2*70. 65. 70. 75. 2*80. 75. 2*40. 12*0 2*35.
2*30. 35. 45. 60. 4*65. 2*70. 2*75. 65. 75. 80. 2*85. 80. 60. 40. 10*0
2*35. 40. 45. 2*50. 45. 50. 60. 65. 70. 75. 2*70. 75. 80. 2*75. 80. 85.

2*90. 85. 65. 50. 10*0 2*40. 2*50. 2*55. 50. 55. 60. 65. 70. 73. 70. 75.
85. 80. 75. 80. 85. 90. 95. 97. 90. 65. 50. 10*0 45. 50. 55. 3*60. 55.
2*60. 2*65. 70. 72. 3*70. 2*75. 80. 75. 85. 95. 90. 70. 55. 9*0 40. 50.
55. 2*60. 2*65. 60. 55. 60. 4*70. 2*65. 2*70. 72. 75. 80. 85. 80. 75. 45.
9*0 40. 55. 3*60. 3*65. 60. 2*55. 6*70. 2*65. 70. 75. 85. 80. 70. 50. 40.
8*0 2*40. 60. 4*65. 70. 65. 55. 50. 60. 4*65. 70. 2*65. 60. 63. 70. 75.
65. 60. 45. 40. 8*0 45. 2*60. 70. 2*75. 2*70. 60. 2*55. 60. 65. 3*60. 2*65.
60. 2*70. 80. 90. 70. 55. 40. 8*0 50. 55. 65. 70. 75. 85. 2*80. 75. 65.
2*55. 2*60. 3*55. 60. 65. 70. 75. 90. 95. 90. 65. 50. 9*0 55. 65. 75. 80.
75. 90. 80. 85. 80. 70. 3*60. 55. 3*50. 2*60. 65. 2*85. 100. 95. 70. 10*0
60. 70. 75. 2*80. 85. 95. 90. 2*85. 2*80. 75. 60. 50. 40. 45. 2*55. 60.
70. 80. 95. 90. 10*0 65. 70. 75. 85. 80. 85. 90. 95. 100. 95. 100. 95.
90. 85. 60. 45. 35. 3*40. 45. 55. 12*0 70. 80. 90. 95. 100. 85. 95. 110.
100. 105. 109. 105. 95. 85. 70. 55. 2*40. 17*0 60. 110. 105. 110. 2*115.
110. 115. 110. 105. 95. 110. 2*85. 65. 55. 40. 17*0 55. 85. 100. 116. 115.
120. 100. 110. 2*100. 95. 80. 75. 70. 65. 60. 50. 18*0 70. 95. 110. 120.
125. 130. 125. 110. 95. 90. 80. 65. 55. 45. 20*0 65. 80. 100. 120. 110.
115. 125. 152. 94. 2*95. 80. 55. 40. 21*0 60. 95. 115. 2*120. 110. 115.
135. 110. 105. 100. 75. 50. 40. 21*0 55. 100. 110. 115. 100. 90. 75. 90.
105. 100. 108. 85. 55. 21*0 80. 90. 105. 115. 105. 100. 95. 80. 65. 85.
100. 95. 100. 60. 21*0 75. 95. 112. 110. 90. 85. 80. 60. 55. 75. 80. 60.
23*0 70. 100. 105. 95. 85. 70. 60. 45. 26*0 70. 2*75. 85. 70. 60. 65. 28*0
55. 65. 55. 60. 55. 50. 30*0 45. 50. 45. 40. 30*0

*PERMK ALL
24*0 2*2.625 2*2.25 2*2.625 2*3. 25*0 2.625 3. 3.375 3. 2.625 3*3. 3*3.375
22*0 2*2.625 3. 3.375 2*3.75 3.375 3.75 3.375 3.75 2*4.125 3.75 20*0 4*3.
3.375 3.75 2*4.125 3.75 4.125 3.75 4.125 3*4.5 3. 18*0 2.625 3.375 2*4.125
2*3.75 4.125 4*4.5 4.875 5.25 2*5.625 4.875 3. 16*0 2*2.25 3. 4.125 2*4.5
2*4.125 4.5 4.875 2*5.25 4.875 5.25 5.625 2*6. 5.625 2*3. 12*0 2*2.625
2*2.25 2.625 3.375 4.5 4*4.875 2*5.25 2*5.625 4.875 5.625 6. 2*6.375 6.
4.5 3. 10*0 2*2.625 3. 3.375 2*3.75 3.375 3.75 4.5 4.875 5.25 5.625 2*5.25
5.625 6. 2*5.625 6. 6.375 2*6.75 6.375 4.875 3.75 10*0 2*3. 2*3.75 2*4.125
3.75 4.125 4.5 4.875 5.25 5.475 5.25 5.625 6.375 6. 5.625 6. 6.375 6.75
7.125 7.275 6.75 4.875 3.75 10*0 3.375 3.75 4.125 3*4.5 4.125 2*4.5 2*4.875
5.25 5.4 3*5.25 2*5.625 6. 5.625 6.375 7.125 6.75 5.25 4.125 9*0 3. 3.75
4.125 2*4.5 2*4.875 4.5 4.125 4.5 4*5.25 2*4.875 2*5.25 5.4 5.625 6. 6.375
6. 5.625 3.375 9*0 3. 4.125 3*4.5 3*4.875 4.5 2*4.125 6*5.25 2*4.875 5.25
5.625 6.375 6. 5.25 3.75 3. 8*0 2*3. 4.5 4*4.875 5.25 4.875 4.125 3.75
4.5 4*4.875 5.25 2*4.875 4.5 4.725 5.25 5.625 4.875 4.5 3.375 3. 8*0 3.375
2*4.5 5.25 2*5.625 2*5.25 4.5 2*4.125 4.5 4.875 3*4.5 2*4.875 4.5 2*5.25
6. 6.75 5.25 4.125 3. 8*0 3.75 4.125 4.875 5.25 5.625 6.375 2*6. 5.625
4.875 2*4.125 2*4.5 3*4.125 4.5 4.875 5.25 5.625 6.75 7.125 6.75 4.875
3.75 9*0 4.125 4.875 5.625 6. 5.625 6.75 6. 6.375 6. 5.25 3*4.5 4.125 3*3.75
2*4.5 4.875 2*6.375 7.5 7.125 5.25 10*0 4.5 5.25 5.625 2*6. 6.375 7.125
6.75 2*6.375 2*6. 5.625 4.5 3.75 3. 3.375 2*4.125 4.5 5.25 6. 7.125 6.75
10*0 4.875 5.25 5.625 6.375 6. 6.375 6.75 7.125 7.5 7.125 7.5 7.125 6.75
6.375 4.5 3.375 2.625 3*3. 3.375 4.125 12*0 5.25 6. 6.75 7.125 7.5 6.375
7.125 8.25 7.5 7.875 8.175 7.875 7.125 6.375 5.25 4.125 2*3. 17*0 4.5 8.25
7.875 8.25 2*8.625 8.25 8.625 8.25 7.875 7.125 8.25 2*6.375 4.875 4.125
3. 17*0 4.125 6.375 7.5 8.7 8.625 9. 7.5 8.25 2*7.5 7.125 6. 5.625 5.25
4.875 4.5 3.75 18*0 5.25 7.125 8.25 9. 9.375 9.75 9.375 8.25 7.125 6.75
6. 4.875 4.125 3.375 20*0 4.875 6. 7.5 9. 8.25 8.625 9.375 11.4 7.05 2*7.125
6. 4.125 3. 21*0 4.5 7.125 8.625 2*9. 8.25 8.625 10.125 8.25 7.875 7.5

5.625 3.75 3. 21*0 4.125 7.5 8.25 8.625 7.5 6.75 5.625 6.75 7.875 7.5 8.1
6.375 4.125 21*0 6. 6.75 7.875 8.625 7.875 7.5 7.125 6. 4.875 6.375 7.5
7.125 7.5 4.5 21*0 5.625 7.125 8.4 8.25 6.75 6.375 6. 4.5 4.125 5.625 6.
4.5 23*0 5.25 7.5 7.875 7.125 6.375 5.25 4.5 3.375 26*0 5.25 2*5.625 6.375
5.25 4.5 4.875 28*0 4.125 4.875 4.125 4.5 4.125 3.75 30*0 3.375 3.75 3.375
3. 54*0 2*1.05 2*0.9 2*1.05 2*1.2 25*0 1.05 1.2 1.35 1.2 1.05 3*1.2 3*1.35
22*0 2*1.05 1.2 1.35 2*1.5 1.35 1.5 1.35 1.5 2*1.65 1.5 20*0 4*1.2 1.35
1.5 2*1.65 1.5 1.65 1.5 1.65 3*1.8 1.2 18*0 1.05 1.35 2*1.65 2*1.5 1.65
4*1.8 1.95 2.1 2*2.25 1.95 1.2 16*0 2*0.9 1.2 1.65 2*1.8 2*1.65 1.8 1.95
2*2.1 1.95 2.1 2.25 2*2.4 2.25 2*1.2 12*0 2*1.05 2*0.9 1.05 1.35 1.8 4*1.95
2*2.1 2*2.25 1.95 2.25 2.4 2*2.55 2.4 1.8 1.2 10*0 2*1.05 1.2 1.35 2*1.5
1.35 1.5 1.8 1.95 2.1 2.25 2*2.1 2.25 2.4 2*2.25 2.4 2.55 2*2.7 2.55 1.95
1.5 10*0 2*1.2 2*1.5 2*1.65 1.5 1.65 1.8 1.95 2.1 2.19 2.1 2.25 2.55 2.4
2.25 2.4 2.55 2.7 2.85 2.91 2.7 1.95 1.5 10*0 1.35 1.5 1.65 3*1.8 1.65
2*1.8 2*1.95 2.1 2.16 3*2.1 2*2.25 2.4 2.25 2.55 2.85 2.7 2.1 1.65 9*0
1.2 1.5 1.65 2*1.8 2*1.95 1.8 1.65 1.8 4*2.1 2*1.95 2*2.1 2.16 2.25 2.4
2.55 2.4 2.25 1.35 9*0 1.2 1.65 3*1.8 3*1.95 1.8 2*1.65 6*2.1 2*1.95 2.1
2.25 2.55 2.4 2.1 1.5 1.2 8*0 2*1.2 1.8 4*1.95 2.1 1.95 1.65 1.5 1.8 4*1.95
2.1 2*1.95 1.8 1.89 2.1 2.25 1.95 1.8 1.35 1.2 8*0 1.35 2*1.8 2.1 2*2.25
2*2.1 1.8 2*1.65 1.8 1.95 3*1.8 2*1.95 1.8 2*2.1 2.4 2.7 2.1 1.65 1.2 8*0
1.5 1.65 1.95 2.1 2.25 2.55 2*2.4 2.25 1.95 2*1.65 2*1.8 3*1.65 1.8 1.95
2.1 2.25 2.7 2.85 2.7 1.95 1.5 9*0 1.65 1.95 2.25 2.4 2.25 2.7 2.4 2.55
2.4 2.1 3*1.8 1.65 3*1.5 2*1.8 1.95 2*2.55 3. 2.85 2.1 10*0 1.8 2.1 2.25
2*2.4 2.55 2.85 2.7 2*2.55 2*2.4 2.25 1.8 1.5 1.2 1.35 2*1.65 1.8 2.1 2.4
2.85 2.7 10*0 1.95 2.1 2.25 2.55 2.4 2.55 2.7 2.85 3. 2.85 3. 2.85 2.7
2.55 1.8 1.35 1.05 3*1.2 1.35 1.65 12*0 2.1 2.4 2.7 2.85 3. 2.55 2.85 3.3
3. 3.15 3.27 3.15 2.85 2.55 2.1 1.65 2*1.2 17*0 1.8 3.3 3.15 3.3 2*3.45
3.3 3.45 3.3 3.15 2.85 3.3 2*2.55 1.95 1.65 1.2 17*0 1.65 2.55 3. 3.48
3.45 3.6 3. 3.3 2*3. 2.85 2.4 2.25 2.1 1.95 1.8 1.5 18*0 2.1 2.85 3.3 3.6
3.75 3.9 3.75 3.3 2.85 2.7 2.4 1.95 1.65 1.35 20*0 1.95 2.4 3. 3.6 3.3
3.45 3.75 4.56 2.82 2*2.85 2.4 1.65 1.2 21*0 1.8 2.85 3.45 2*3.6 3.3 3.45
4.05 3.3 3.15 3. 2.25 1.5 1.2 21*0 1.65 3. 3.3 3.45 3. 2.7 2.25 2.7 3.15
3. 3.24 2.55 1.65 21*0 2.4 2.7 3.15 3.45 3.15 3. 2.85 2.4 1.95 2.55 3.
2.85 3. 1.8 21*0 2.25 2.85 3.36 3.3 2.7 2.55 2.4 1.8 1.65 2.25 2.4 1.8
23*0 2.1 3. 3.15 2.85 2.55 2.1 1.8 1.35 26*0 2.1 2*2.25 2.55 2.1 1.8 1.95
28*0 1.65 1.95 1.65 1.8 1.65 1.5 30*0 1.35 1.5 1.35 1.2 54*0 2*3.5 2*3.
2*3.5 2*4. 25*0 3.5 4. 4.5 4. 3.5 3*4. 3*4.5 22*0 2*3.5 4. 4.5 2*5. 4.5
5. 4.5 5. 2*5.5 5. 20*0 4*4. 4.5 5. 2*5.5 5. 5.5 5. 5.5 3*6. 4. 18*0 3.5
4.5 2*5.5 2*5. 5.5 4*6. 6.5 7. 2*7.5 6.5 4. 16*0 2*3. 4. 5.5 2*6. 2*5.5
6. 6.5 2*7. 6.5 7. 7.5 2*8. 7.5 2*4. 12*0 2*3.5 2*3. 3.5 4.5 6. 4*6.5 2*7.
2*7.5 6.5 7.5 8. 2*8.5 8. 6. 4. 10*0 2*3.5 4. 4.5 2*5. 4.5 5. 6. 6.5 7.
7.5 2*7. 7.5 8. 2*7.5 8. 8.5 2*9. 8.5 6.5 5. 10*0 2*4. 2*5. 2*5.5 5. 5.5
6. 6.5 7. 7.3 7. 7.5 8.5 8. 7.5 8. 8.5 9. 9.5 9.7 9. 6.5 5. 10*0 4.5 5.
5.5 3*6. 5.5 2*6. 2*6.5 7. 7.2 3*7. 2*7.5 8. 7.5 8.5 9.5 9. 7. 5.5 9*0
4. 5. 5.5 2*6. 2*6.5 6. 5.5 6. 4*7. 2*6.5 2*7. 7.2 7.5 8. 8.5 8. 7.5 4.5
9*0 4. 5.5 3*6. 3*6.5 6. 2*5.5 6*7. 2*6.5 7. 7.5 8.5 8. 7. 5. 4. 8*0 2*4.
6. 4*6.5 7. 6.5 5.5 5. 6. 4*6.5 7. 2*6.5 6. 6.3 7. 7.5 6.5 6. 4.5 4. 8*0
4.5 2*6. 7. 2*7.5 2*7. 6. 2*5.5 6. 6.5 3*6. 2*6.5 6. 2*7. 8. 9. 7. 5.5
4. 8*0 5. 5.5 6.5 7. 7.5 8.5 2*8. 7.5 6.5 2*5.5 2*6. 3*5.5 6. 6.5 7. 7.5
9. 9.5 9. 6.5 5. 9*0 5.5 6.5 7.5 8. 7.5 9. 8. 8.5 8. 7. 3*6. 5.5 3*5. 2*6.
6.5 2*8.5 10. 9.5 7. 10*0 6. 7. 7.5 2*8. 8.5 9.5 9. 2*8.5 2*8. 7.5 6. 5.
4. 4.5 2*5.5 6. 7. 8. 9.5 9. 10*0 6.5 7. 7.5 8.5 8. 8.5 9. 9.5 10. 9.5
10. 9.5 9. 8.5 6. 4.5 3.5 3*4. 4.5 5.5 12*0 7. 8. 9. 9.5 10. 8.5 9.5 11.
10. 10.5 10.9 10.5 9.5 8.5 7. 5.5 2*4. 17*0 6. 11. 10.5 11. 2*11.5 11.

```
        11.5 11. 10.5 9.5 11. 2*8.5 6.5 5.5 4. 17*0 5.5 8.5 10. 11.6 11.5 12. 10.
        11. 2*10. 9.5 8. 7.5 7. 6.5 6. 5. 18*0 7. 9.5 11. 12. 12.5 13. 12.5 11.
        9.5 9. 8. 6.5 5.5 4.5 20*0 6.5 8. 10. 12. 11. 11.5 12.5 15.2 9.4 2*9.5
        8. 5.5 4. 21*0 6. 9.5 11.5 2*12. 11. 11.5 13.5 11. 10.5 10. 7.5 5. 4. 21*0
        5.5 10. 11. 11.5 10. 9. 7.5 9. 10.5 10. 10.8 8.5 5.5 21*0 8. 9. 10.5 11.5
        10.5 10. 9.5 8. 6.5 8.5 10. 9.5 10. 6. 21*0 7.5 9.5 11.2 11. 9. 8.5 8.
        6. 5.5 7.5 8. 6. 23*0 7. 10. 10.5 9.5 8.5 7. 6. 4.5 26*0 7. 2*7.5 8.5 7.
        6. 6.5 28*0 5.5 6.5 5.5 6. 5.5 5. 30*0 4.5 5. 4.5 4. 30*0


*CPOR  MATRIX   1.E-08
*PRPOR MATRIX   1000.

** ---------- Fluid Model ----------

*MODEL   *PR
*NC    2    2
*TRES         33.000
*PVC3  1.2000000E+00
*COMPNAME
          'CO2     '    'C1      '
*SG       8.1800000E-01  3.0000000E-01
*TB       -7.8450000E+01 -1.6145000E+02
*PCRIT     7.2800000E+01  4.5400000E+01
*VCRIT     9.4000000E-02  9.9000000E-02
*TCRIT     3.0420000E+02  1.9060000E+02
*AC        2.2500000E-01  8.0000000E-03
*MW        4.4010000E+01  1.6043000E+01
*HCFLAG    0  0  ** 0
*BIN
    1.0300000E-01
*VSHIFT
    0.0000000E+00  0.0000000E+00
*VISCOR *HZYT
*MIXVC     1.0000000E+00
*VISVC
    9.4000000E-02  9.9000000E-02
*VISCOEFF
    1.0230000E-01  2.3364000E-02  5.8533000E-02 -4.0758000E-02  9.3324000E-03
*OMEGA
    4.5723553E-01  4.5723553E-01
*OMEGB
    7.7796074E-02  7.7796074E-02
*PCHOR
    7.8000000E+01  7.7000000E+01
*HENRYC
    1.9510547E+05  0.0
*REFPH
    9.4000000E+03  9.4000000E+03
*VINFINITY
    3.5089333E-02  3.5242646E-02
*YAQU-RATE-CUTOFF
1.0E-4 100.0
```

```
*DER-CHEM-EQUIL *ANALYTICAL
*DER-REACT-RATE *ANALYTICAL

*ACTIVITY-MODEL *B-DOT
*SALINITY 0.1
*AQUEOUS-DENSITY *ROWE-CHOU
*AQUEOUS-VISCOSITY *KESTIN

*NC-AQUEOUS 7
*COMPNAME-AQUEOUS
'H+' 'Ca++' 'SiO2(aq)' 'Al+++' 'OH-' 'HCO3-' 'CO3--'
*MW-AQUEOUS
1.0079
40.0800
60.0843
26.9815
17.0073
61.0171
60.0092

*ION-SIZE-AQUEOUS
9.0 6.0 -0.5 9.0 3.5 4.5 4.5
*CHARGE-AQUEOUS
1 2 0 3 -1 -1 -2

*NC-MINERAL 3
*COMPNAME-MINERAL
'CALCITE' 'KAOLINIT' 'ANORTHIT'
*MW-MINERAL
100.0869
258.1616
278.2082

*MASSDENSITY-MINERAL
2710.00
2410.00
2740.00

*N-RATE-REACT 3
*N-CHEM-EQUIL 3

**REACTION NO. 1: H2O = H+ + OH-
*STOICHIOMETRY
0 0 -1 1 0 0 0 1 0 0
0 0 0
*CONCENTRATION-ORDER
0.0 0.0 0.0 1.0 0.0 0.0 0.0 1.0 0.0 0.0
0.0 0.0 0.0
*LOG-CHEM-EQUIL-CONST -13.2631

**REACTION NO. 2: CO2 + H2O = H+ + HCO3--
*STOICHIOMETRY
-1 0 -1 1 0 0 0 0 1 0
 0 0 0
```

```
*CONCENTRATION-ORDER
-1.0 0.0 0.0 1.0 0.0 0.0 0.0 0.0 1.0 0.0
 0.0 0.0 0.0
*LOG-CHEM-EQUIL-CONST -6.3221

**REACTION NO. 3: CO2 + H2O = 2H+ + CO3--
*STOICHIOMETRY
-1 0 -1 2 0 0 0 0 0 1
 0 0 0
*CONCENTRATION-ORDER
-1.0 0.0 0.0 2.0 0.0 0.0 0.0 0.0 0.0 1.0
 0.0 0.0 0.0
*LOG-CHEM-EQUIL-CONST -16.5563

**REACTION NO. 4:  CALCITE + H+ = (Ca++) + (HCO3-)
*STOICHIOMETRY
0 0 0 -1 1 0 0 0 1 0
-1 0 0
*REACTIVE-SURFACE-AREA 88.0
*ACTIVATION-ENERGY 41870.0
*REF-TEMP-RATE-CONST 25.0
*LOG-CHEM-EQUIL-CONST 1.3560
*TST-PARAM1 1.0
*TST-PARAM2 1.0
*LOG-TST-RATE-CONSTANT -8.79588

**REACTION NO. 5:  KAOLINITE + 6(H+) = 5(H2O) + 2SiO2(aq) + 2(Al+++)
*STOICHIOMETRY
0 0 5 -6 0 2 2 0 0 0
0 -1 0
*REACTIVE-SURFACE-AREA 17600.0
*ACTIVATION-ENERGY 62760.0
*REF-TEMP-RATE-CONST 25.0
*LOG-CHEM-EQUIL-CONST 5.4706
*TST-PARAM1 1.0
*TST-PARAM2 1.0
*LOG-TST-RATE-CONSTANT -13.00

**REACTION NO. 6:  ANORTHITE + 8H+ = 4(H2O) + (Ca++) + 2[SiO2(aq)] + 2(Al++)
*STOICHIOMETRY
0 0 4 -8 1 2 2 0 0 0
0 0 -1
*REACTIVE-SURFACE-AREA 088.0
*ACTIVATION-ENERGY 67830.0
*REF-TEMP-RATE-CONST 25.0
*LOG-CHEM-EQUIL-CONST 23.0603
*TST-PARAM1 1.0
*TST-PARAM2 1.0
*LOG-TST-RATE-CONSTANT -12.0

*ANNIH-MATRIX
 1.0   0.0   0.0   0.0   0.0   0.0   0.0   0.0   1.0   1.0
 0.0   1.0   0.0   0.0   0.0   0.0   0.0   0.0   0.0   0.0
 0.0   0.0   1.0   0.0   0.0   0.0   0.0   1.0   1.0   1.0
```

```
 0.0   0.0   0.0   1.0   0.0   0.0   0.0  -1.0  -1.0  -2.0
 0.0   0.0   0.0   0.0   1.0   0.0   0.0   0.0   0.0   0.0
 0.0   0.0   0.0   0.0   0.0   1.0   0.0   0.0   0.0   0.0
 0.0   0.0   0.0   0.0   0.0   0.0   1.0   0.0   0.0   0.0

*PHASEID *GAS
*SOLUBILITY
*CW   4.6E-07
*REFPW 9100.0
*OGW_FLASH *NO_H2OVAP
**COMPONENT 2 IS A TRACE COMPONENT
*TRACE-COMP 2
**DIFFUSION COEFFICIENT IN CM2/S
*DIFFC-AQU 2.0E-05 0.0
*PERM-VS-POR 1
*DERIVATIVE_METHOD *NUMERALL

** ---------- Rock Fluid ----------
*ROCKFLUID
*RPT 1  *DRAINAGE
*SWT
0.000000  0.000000  0.000000  0.000000
0.050000  0.000000  0.000000  0.000000
0.100000  0.000000  0.000000  0.000000
0.150000  0.000010  0.000000  0.000000
0.200000  0.000150  0.000000  0.000000
0.250000  0.000770  0.000000  0.000000
0.300000  0.002440  0.000000  0.000000
0.350000  0.005950  0.000000  0.000000
0.400000  0.012350  0.000000  0.000000
0.450000  0.022870  0.000000  0.000000
0.500000  0.039020  0.000000  0.000000
0.550000  0.062500  0.000000  0.000000
0.600000  0.095260  0.000000  0.000000
0.650000  0.139470  0.000000  0.000000
0.700000  0.197530  0.000000  0.000000
0.750000  0.272070  0.000000  0.000000
0.800000  0.365950  0.000000  0.000000
0.850000  0.482250  0.000000  0.000000
0.900000  0.624300  0.000000  0.000000
0.950000  0.795620  0.000000  0.000000
1.000000  1.000000  0.000000  0.000000
*SGT
0.000000  0.000000  0.000000  0.000000
0.050000  0.000080  0.000000  0.000000
0.100000  0.000680  0.000000  0.000000
0.150000  0.002330  0.000000  0.000000
0.200000  0.005610  0.000000  0.000000
0.250000  0.011140  0.000000  0.000000
0.300000  0.019610  0.000000  0.000000
0.350000  0.031740  0.000000  0.000000
0.400000  0.048370  0.000000  0.000000
0.450000  0.070420  0.000000  0.000000
0.500000  0.098940  0.000000  0.000000
```

```
0.550000  0.136180  0.000000  0.000000
0.600000  0.180650  0.000000  0.000000
0.650000  0.232750  0.000000  0.000000
0.700000  0.307520  0.000000  0.000000
0.750000  0.395200  0.000000  0.000000
0.800000  0.506570  0.000000  0.000000
0.850000  0.655620  0.000000  0.000000
0.900000  0.954430  0.000000  0.000000
0.950000  0.977220  0.000000  0.000000
1.000000  1.000000  0.000000  0.000000
*KROIL *STONE2 *SWSG

** ---------- Initial ----------

*INITIAL
*VERTICAL *BLOCK_CENTER *WATER_GAS
*NREGIONS 1
*ZOIL   0.001 0.999
*ZGAS  0.001 0.999
*REFDEPTH      900.
*REFPRES       9100.
*DWGC          100.
*SWOC          0.999

*CONCENTRATION-AQUEOUS *MOL/KG_H2O
  1.000000D-07   9.118492D-05
  2.345433D-08   2.317806D-11   5.456322D-07   2.489299D-02   1.170273D-05

*VOLUMEFRACTION-MINERAL
0.0088 0.0176 0.0088

** ---------- Numerical ----------

*NUMERICAL
  *NORM *PRESS 1500.
  *NORM *SATUR  0.10
  *NORM *GMOLAR 0.10
  *CONVERGE *MAXRES  1.e-4
*DTMIN 1.E-06

** ---------- Recurrent ----------

*RUN

*DATE 2000 01 01
*DTWELL 1.
*AIMWELL *WELLNN

*WELL  1 'CO2-Injector1'
*INJECTOR 'CO2-Injector1'
*INCOMP SOLVENT  1 0
*OPERATE *MAX *STG 2.2E+05 CONT
*OPERATE *MAX *BHP 15000. CONT
  *GEOMETRY K 0.2 0.37 1. 0.
```

```
  *PERF GEO   'CO2-Injector1'
      10 23 3 1. OPEN FLOW-FROM 'SURFACE'

*WELL  2 'CO2-Injector2'
*INJECTOR 'CO2-Injector2'
*INCOMP SOLVENT  1 0
*OPERATE *MAX *STG 2.2E+05 CONT
*OPERATE *MAX *BHP  15000.
  *GEOMETRY K 0.2 0.37 1. 0.
  *PERF GEO   'CO2-Injector2'
          22 9 3 1. OPEN FLOW-FROM 'SURFACE'


 *DTMAX 10.
DATE 2000 02 29
DATE 2000 03 31
DATE 2000 04 30
DATE 2000 05 31
DATE 2000 06 30
DATE 2000 07 31
DATE 2000 08 31
DATE 2000 09 30
DATE 2000 10 31
DATE 2000 11 30
DATE 2001 01 01
DATE 2002 01 01
DATE 2003 01 01
DATE 2004 01 01
DATE 2005 01 01
DATE 2006 01 01
DATE 2007 01 01
DATE 2008 01 01
DATE 2009 01 01
DATE 2010 01 01
DATE 2011 01 01
DATE 2012 01 01
DATE 2013 01 01
DATE 2014 01 01
DATE 2015 01 01
DATE 2016 01 01
DATE 2017 01 01
DATE 2018 01 01
DATE 2019 01 01
DATE 2020 01 01
DATE 2021 01 01
DATE 2022 01 01
DATE 2023 01 01
DATE 2024 01 01
DATE 2025 01 01
DATE 2026 01 01
DATE 2027 01 01
DATE 2028 01 01
DATE 2029 01 01
DATE 2030 01 01
```

```
*SHUTIN 1
*SHUTIN 2
DATE 2031 01 01
*DTMAX 30.
DATE 2032 01 01
DATE 2033 01 01
DATE 2034 01 01
DATE 2035 01 01
DATE 2036 01 01
DATE 2037 01 01
DATE 2038 01 01
DATE 2039 01 01
DATE 2040 01 01
DATE 2050 01 01
DATE 2060 01 01
DATE 2070 01 01
DATE 2080 01 01
DATE 2090 01 01
DATE 2100 01 01
DATE   2110   1   1
DATE   2120   1   1
DATE   2130   1   1
DATE   2140   1   1
DATE   2150   1   1
DATE   2160   1   1
DATE   2170   1   1
DATE   2180   1   1
DATE   2190   1   1
DATE   2200   1   1
*STOP
```

A.2 Input Data for Single-well Aquifer Model (run 5b)

RESULTS SIMULATOR GEM

**** ------- Input/Output ----------**

```
*FILENAMES *OUTPUT *SRFOUT *RESTARTOUT *INDEXOUT *MAINRESULTSOUT
**INDEXIN 'rad.irf'
*INUNIT *SI
*INTERRUPT *INTERACTIVE
*RANGECHECK *ON
*XDR *ON
*REWIND   3
*MAXERROR  20
*WRST *TIME

*WPRN *WELL  *TIME
*WPRN *GRID  *TIME
*WPRN *ITER  *BRIEF
```

```
*WSRF *WELL 1
*WSRF *GRID *TIME

*DIARY *CHANGES

*OUTPRN *WELL *BRIEF
*OUTPRN *GRID *NONE
*OUTPRN *RES *NONE

*OUTSRF *GRID *SW *SG *PRES *DENW *DENG
          *Z 'CO2' *W 'CO2'
          *MOLALITY 'CO2' *MOLALITY 'H+' *MOLALITY 'Ca++'
          *MOLALITY 'SiO2(aq)' *MOLALITY 'Al+++' *MOLALITY 'OH-'
          *MOLALITY 'CO3--' *MOLALITY 'HCO3-' *MINERAL 'CALCITE'
          *MINERAL 'KAOLINIT' *MINERAL 'ANORTHIT'
*OUTSRF *RES *ALL

**RESTART 4730


** ---------- Grid ----------

*GRID *RADIAL 44 10 3 *RW 0.0762
*KDIR DOWN
*DI *IVAR  1. 1. 1. 1. 1. 2. 2. 2. 2. 2. 3. 3. 3. 3. 3. 5. 5. 5. 5. 5. 5. 10. 10.
             15. 15. 15. 20. 22.5 25. 25. 25. 25. 30. 30. 41. 44. 45. 45. 50. 50. 50. 51. 100. 168.
*DJ *cON 36

*DK *KVAR 41. 30. 111.

*DTOP 440*900.
*POR CON 0.25
*PERMI *KVAR 112. 45. 150.
*PERMJ EQUALSI
*PERMK EQUALSI * 0.1
*CPOR  MATRIX   1.E-08
*PRPOR MATRIX   1000.

** ---------- Fluid Model ----------

*MODEL   *PR
*NC    2    2
*TRES  33.000
*PVC3  1.2000000E+00
*COMPNAME
          'CO2     '    'C1      '
*SG       8.1800000E-01  3.0000000E-01
*TB       -7.8450000E+01 -1.6145000E+02
*PCRIT     7.2800000E+01  4.5400000E+01
*VCRIT     9.4000000E-02  9.9000000E-02
*TCRIT     3.0420000E+02  1.9060000E+02
*AC        2.2500000E-01  8.0000000E-03
*MW        4.4010000E+01  1.6043000E+01
```

```
*HCFLAG    0  0  ** 0
*BIN
    1.0300000E-01
*VSHIFT
    0.0000000E+00  0.0000000E+00
*VISCOR *HZYT
*MIXVC     1.0000000E+00
*VISVC
    9.4000000E-02  9.9000000E-02
*VISCOEFF
    1.0230000E-01  2.3364000E-02  5.8533000E-02 -4.0758000E-02  9.3324000E-03
*OMEGA
    4.5723553E-01  4.5723553E-01
*OMEGB
    7.7796074E-02  7.7796074E-02
*PCHOR
    7.8000000E+01  7.7000000E+01
*HENRYC
    1.9510547E+05  0.0
*REFPH
    9.4000000E+03  9.4000000E+03
*VINFINITY
    3.5089333E-02  3.5242646E-02
*YAQU-RATE-CUTOFF
1.0E-4 100.0

*DER-CHEM-EQUIL *ANALYTICAL
*DER-REACT-RATE *ANALYTICAL

*ACTIVITY-MODEL *B-DOT
*SALINITY 0.1
*AQUEOUS-DENSITY *ROWE-CHOU
*AQUEOUS-VISCOSITY *KESTIN

*NC-AQUEOUS 7
*COMPNAME-AQUEOUS
'H+' 'Ca++' 'SiO2(aq)' 'Al+++' 'OH-' 'HCO3-' 'CO3--'
*MW-AQUEOUS
1.0079
40.0800
60.0843
26.9815
17.0073
61.0171
60.0092

*ION-SIZE-AQUEOUS
9.0 6.0 -0.5 9.0 3.5 4.5 4.5
*CHARGE-AQUEOUS
1 2 0 3 -1 -1 -2

*NC-MINERAL 3
*COMPNAME-MINERAL
'CALCITE' 'KAOLINIT' 'ANORTHIT'
```

```
*MW-MINERAL
100.0869
258.1616
278.2082

*MASSDENSITY-MINERAL
2710.00
2410.00
2740.00

*N-RATE-REACT 3
*N-CHEM-EQUIL 3

**REACTION NO. 1: H2O = H+ + OH-
*STOICHIOMETRY
0 0 -1 1 0 0 0 1 0 0
0 0 0
*CONCENTRATION-ORDER
0.0 0.0 0.0 1.0 0.0 0.0 0.0 1.0 0.0 0.0
0.0 0.0 0.0
*LOG-CHEM-EQUIL-CONST -13.2631

**REACTION NO. 2: CO2 + H2O = H+ + HCO3--
*STOICHIOMETRY
-1 0 -1 1 0 0 0 0 1 0
 0 0 0
*CONCENTRATION-ORDER
-1.0 0.0 0.0 1.0 0.0 0.0 0.0 0.0 1.0 0.0
 0.0 0.0 0.0
*LOG-CHEM-EQUIL-CONST -6.3221

**REACTION NO. 3: CO2 + H2O = 2H+ + CO3--
*STOICHIOMETRY
-1 0 -1 2 0 0 0 0 0 1
 0 0 0
*CONCENTRATION-ORDER
-1.0 0.0 0.0 2.0 0.0 0.0 0.0 0.0 0.0 1.0
 0.0 0.0 0.0
*LOG-CHEM-EQUIL-CONST -16.5563

**REACTION NO. 4:  CALCITE + H+ = (Ca++) + (HCO3-)
*STOICHIOMETRY
0 0 0 -1 1 0 0 0 1 0
-1 0 0
*REACTIVE-SURFACE-AREA 88.0
*ACTIVATION-ENERGY 41870.0
*REF-TEMP-RATE-CONST 25.0
*LOG-CHEM-EQUIL-CONST 1.3560
*TST-PARAM1 1.0
*TST-PARAM2 1.0
*LOG-TST-RATE-CONSTANT -8.79588

**REACTION NO. 5:  KAOLINITE + 6(H+) = 5(H2O) + 2SiO2(aq) + 2(Al+++)
*STOICHIOMETRY
```

0 0 5 -6 0 2 2 0 0 0
0 -1 0
*REACTIVE-SURFACE-AREA 17600.0
*ACTIVATION-ENERGY 62760.0
*REF-TEMP-RATE-CONST 25.0
*LOG-CHEM-EQUIL-CONST 5.4706
*TST-PARAM1 1.0
*TST-PARAM2 1.0
*LOG-TST-RATE-CONSTANT -13.00

**REACTION NO. 6: ANORTHITE + 8H+ = 4(H2O) + (Ca++) + 2[SiO2(aq)] + 2(Al++)
*STOICHIOMETRY
0 0 4 -8 1 2 2 0 0 0
0 0 -1
*REACTIVE-SURFACE-AREA 088.0
*ACTIVATION-ENERGY 67830.0
*REF-TEMP-RATE-CONST 25.0
*LOG-CHEM-EQUIL-CONST 23.0603
*TST-PARAM1 1.0
*TST-PARAM2 1.0
*LOG-TST-RATE-CONSTANT -12.0

*ANNIH-MATRIX
 1.0 0.0 0.0 0.0 0.0 0.0 0.0 0.0 1.0 1.0
 0.0 1.0 0.0 0.0 0.0 0.0 0.0 0.0 0.0 0.0
 0.0 0.0 1.0 0.0 0.0 0.0 0.0 1.0 1.0 1.0
 0.0 0.0 0.0 1.0 0.0 0.0 0.0 -1.0 -1.0 -2.0
 0.0 0.0 0.0 0.0 1.0 0.0 0.0 0.0 0.0 0.0
 0.0 0.0 0.0 0.0 0.0 1.0 0.0 0.0 0.0 0.0
 0.0 0.0 0.0 0.0 0.0 0.0 1.0 0.0 0.0 0.0

*PHASEID *GAS
*SOLUBILITY
*CW 4.6E-07
*REFPW 9100.0
*OGW_FLASH *NO_H2OVAP
**COMPONENT 2 IS A TRACE COMPONENT
*TRACE-COMP 2
**DIFFUSION COEFFICIENT IN CM2/S
*DIFFC-AQU 2.0E-05 0.0
*PERM-VS-POR 1
*DERIVATIVE_METHOD *NUMERALL

**** ---------- Rock Fluid ----------**
*ROCKFLUID
*RPT 1 *DRAINAGE
*SWT
0.000000 0.000000 0.000000 0.000000
0.050000 0.000000 0.000000 0.000000
0.100000 0.000000 0.000000 0.000000
0.150000 0.000010 0.000000 0.000000
0.200000 0.000150 0.000000 0.000000
0.250000 0.000770 0.000000 0.000000
0.300000 0.002440 0.000000 0.000000

```
0.350000  0.005950  0.000000  0.000000
0.400000  0.012350  0.000000  0.000000
0.450000  0.022870  0.000000  0.000000
0.500000  0.039020  0.000000  0.000000
0.550000  0.062500  0.000000  0.000000
0.600000  0.095260  0.000000  0.000000
0.650000  0.139470  0.000000  0.000000
0.700000  0.197530  0.000000  0.000000
0.750000  0.272070  0.000000  0.000000
0.800000  0.365950  0.000000  0.000000
0.850000  0.482250  0.000000  0.000000
0.900000  0.624300  0.000000  0.000000
0.950000  0.795620  0.000000  0.000000
1.000000  1.000000  0.000000  0.000000
*SGT
0.000000  0.000000  0.000000  0.000000
0.050000  0.000080  0.000000  0.000000
0.100000  0.000680  0.000000  0.000000
0.150000  0.002330  0.000000  0.000000
0.200000  0.005610  0.000000  0.000000
0.250000  0.011140  0.000000  0.000000
0.300000  0.019610  0.000000  0.000000
0.350000  0.031740  0.000000  0.000000
0.400000  0.048370  0.000000  0.000000
0.450000  0.070420  0.000000  0.000000
0.500000  0.098940  0.000000  0.000000
0.550000  0.136180  0.000000  0.000000
0.600000  0.180650  0.000000  0.000000
0.650000  0.232750  0.000000  0.000000
0.700000  0.307520  0.000000  0.000000
0.750000  0.395200  0.000000  0.000000
0.800000  0.506570  0.000000  0.000000
0.850000  0.655620  0.000000  0.000000
0.900000  0.954430  0.000000  0.000000
0.950000  0.977220  0.000000  0.000000
1.000000  1.000000  0.000000  0.000000
*KROIL *STONE2 *SWSG

** ---------- Initial ----------

*INITIAL
*VERTICAL *BLOCK_CENTER *WATER_GAS
*NREGIONS 1
*ZOIL   0.001 0.999
*ZGAS  0.001 0.999
*REFDEPTH      900.
*REFPRES       9100.
*DWGC          100.
*SWOC          0.999

*CONCENTRATION-AQUEOUS *MOL/KG_H2O
  1.000000D-07   9.118492D-05
  2.345433D-08   2.317806D-11   5.456322D-07   2.489299D-02   1.170273D-05
```

```
*VOLUMEFRACTION-MINERAL
0.0088 0.0176 0.0088

** ---------- Numerical ----------

*NUMERICAL
  *NORM *PRESS 1000.
  *NORM *SATUR  0.30
  *NORM *GMOLAR 0.10
  *CONVERGE *MAXRES  1.e-4
*DTMIN 1.E-10

** ---------- Recurrent ----------

*RUN

*DATE 2000 01 01
*DTWELL 0.01
*AIMWELL *WELLNN
*WELL  1 'CO2-Injector'
*INJECTOR 'CO2-Injector'
*INCOMP SOLVENT  1 0
*OPERATE *MAX *STG  4.E+04 CONT
*OPERATE *MAX *BHP 1.5E+04
  *GEOMETRY *K 0.0762 0.37 1. 0.
  *PERF GEO   'CO2-Injector'
      1 1 3 1. OPEN FLOW-FROM 'SURFACE'

 *DTMAX 10.
DATE 2000 02 29
DATE 2000 03 31
DATE 2000 04 30
DATE 2000 05 31
DATE 2000 06 30
DATE 2000 07 31
DATE 2000 08 31
DATE 2000 09 30
DATE 2000 10 31
DATE 2000 11 30
DATE 2001 01 01
DATE 2002 01 01
DATE 2003 01 01
DATE 2004 01 01
DATE 2005 01 01
DATE 2006 01 01
DATE 2007 01 01
DATE 2008 01 01
DATE 2009 01 01
DATE 2010 01 01
DATE 2011 01 01
DATE 2012 01 01
DATE 2013 01 01
*SHUTIN 1
*DTMAX 30.
```

```
DATE 2014 01 01
DATE 2015 01 01
DATE 2016 01 01
DATE 2017 01 01
DATE 2018 01 01
DATE 2019 01 01
DATE 2020 01 01
DATE 2021 01 01
DATE 2022 01 01
DATE 2023 01 01
DATE 2024 01 01
DATE 2025 01 01
DATE 2026 01 01
DATE 2027 01 01
DATE 2028 01 01
DATE 2029 01 01
DATE 2030 01 01
*DTMAX 60.
DATE 2031 01 01
DATE 2032 01 01
DATE 2033 01 01
DATE 2034 01 01
DATE 2035 01 01
DATE 2036 01 01
DATE 2037 01 01
DATE 2038 01 01
DATE 2039 01 01
DATE 2040 01 01
DATE 2050 01 01
DATE 2060 01 01
DATE 2070 01 01
DATE 2080 01 01
DATE 2090 01 01
DATE 2100 01 01
DATE   2110   1   1
DATE   2120   1   1
DATE   2130   1   1
DATE   2140   1   1
DATE   2150   1   1
DATE   2160   1   1
DATE   2170   1   1
DATE   2180   1   1
DATE   2190   1   1
DATE   2200   1   1
*STOP
```

APPENDIX B

B.1. 2-D Map of CO_2 saturation as a free gas, soluble CO_2 mole fraction in water and precipitated CO_2 as Calcite dissolution / precipitation, CO_2 Global Mole Fraction, Kaolinite dissolution / precipitation and Anorthite dissolution / precipitation for 2040 years for Runs 1a and 2a, field case

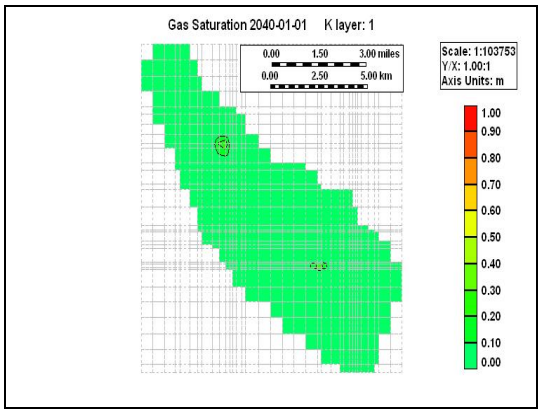

Figure B.1 Map of CO_2 Saturation at 2040 (40 years) for Run 1a: field case, layer 1

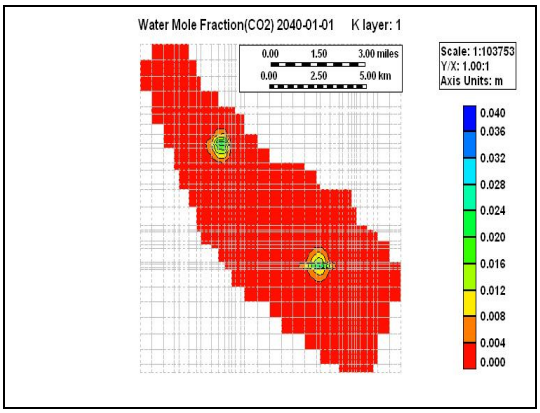

Figure B.2 Map of CO_2 Mole Fraction in Water at 2040 (40 years) for Run 1a: field case, layer 1

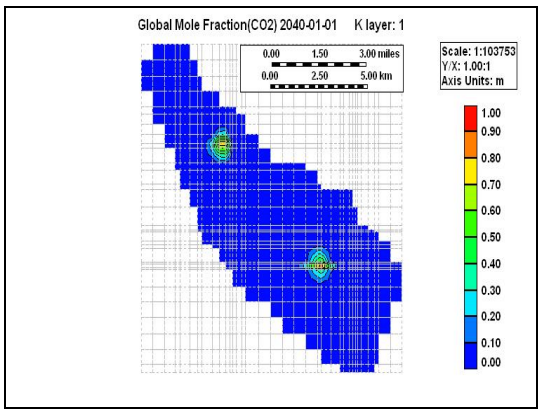

Figure B.3 Map of CO_2 Global Mole Fraction at 2040 (40 years) for Run 1a: field case, layer 1

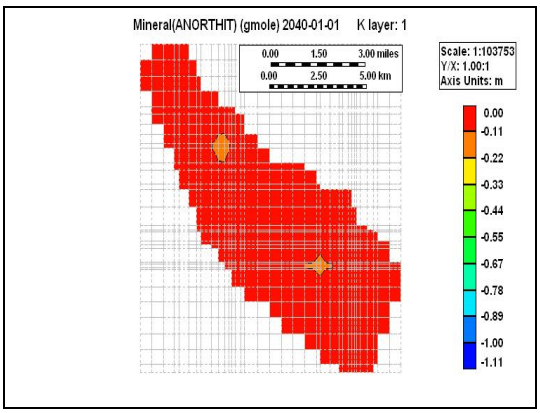

Figure B.5 Map of Anorthite Dissolution / Precipitation at 2040 (40 years) for Run 1a: field case, layer 1

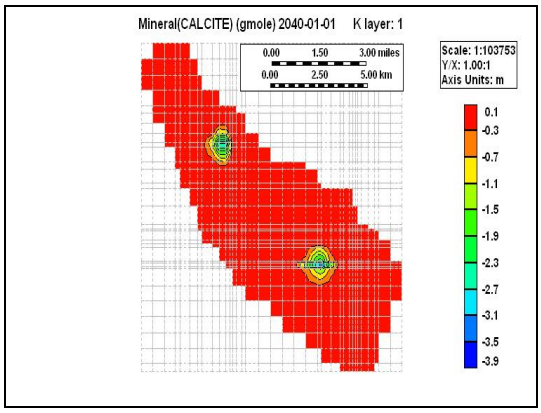

Figure B.4 Map of Calcite Dissolution / Precipitation at 2040 (40 years) for Run 1a: field case, layer 1

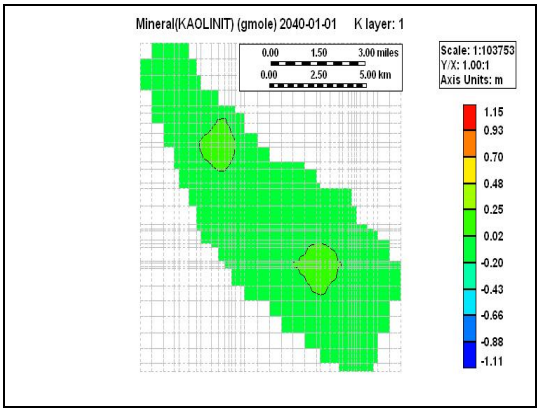

Figure B.6 Map of Kaolinite Dissolution / Precipitation at 2040 (40 years) for Run 1a: field case, layer 1

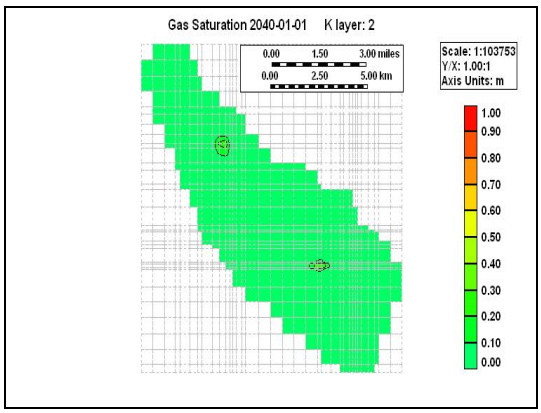

Figure B.7 Map of CO_2 Saturation at 2040 (40 years) for Run 1a: field case, layer 2

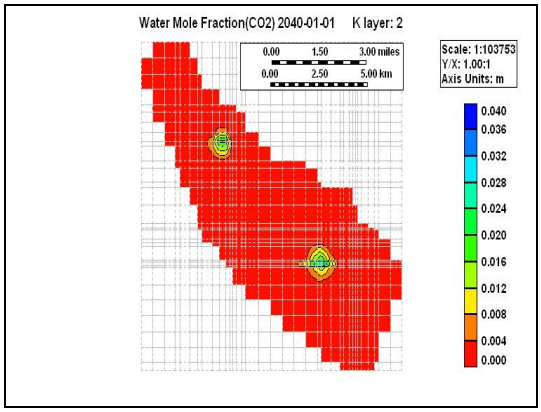

Figure B.8 Map of CO_2 Mole Fraction in Water at 2040 (40 years) for Run 1a: field case, layer 2

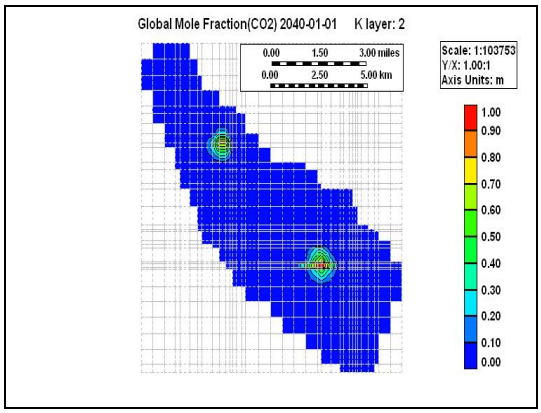

Figure B.9 Map of CO_2 Global Mole Fraction at 2040 (40 years) for Run 1a: field case, layer 2

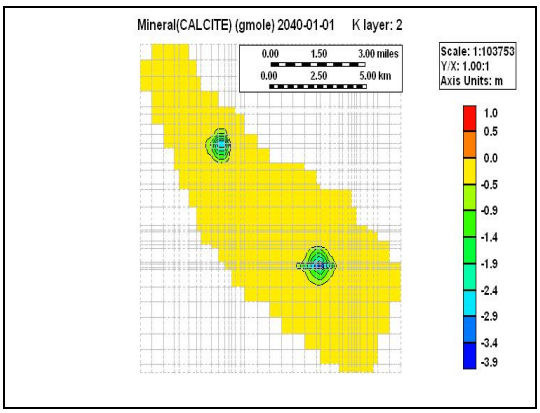

Figure B.10 Map of Calcite Dissolution / Precipitation at 2040 (40 years) for Run 1a: field case, layer 2

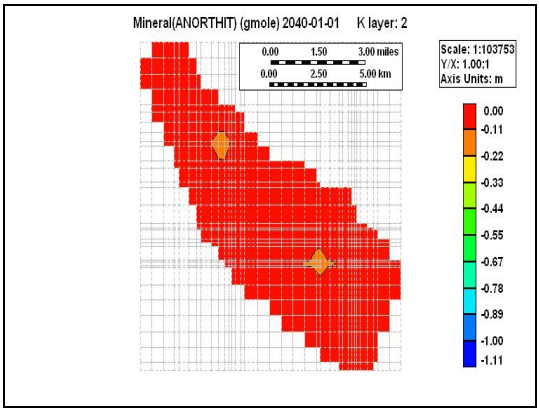

Figure B.11 Map of Anorthite Dissolution / Precipitation at 2040 (40 years) for Run 1a: field case, layer 2

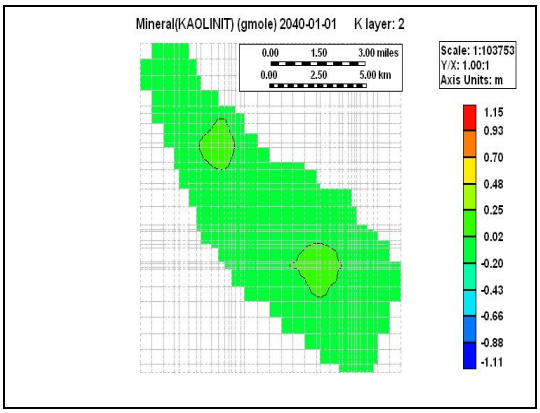

Figure B.12 Map of Kaolinite Dissolution / Precipitation at 2040 (40 years) for Run 1a: field case, layer 2

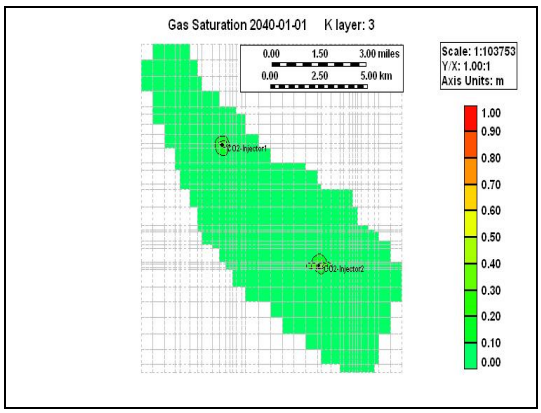

Figure B.13 Map of CO_2 Saturation at 2040 (40 years) for Run 1a: field case, layer 3

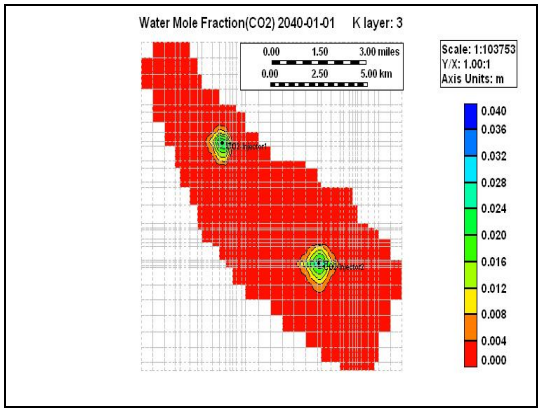

Figure B.14 Map of CO_2 Mole Fraction in Water at 2040 (40 years) for Run 1a: field case, layer 3

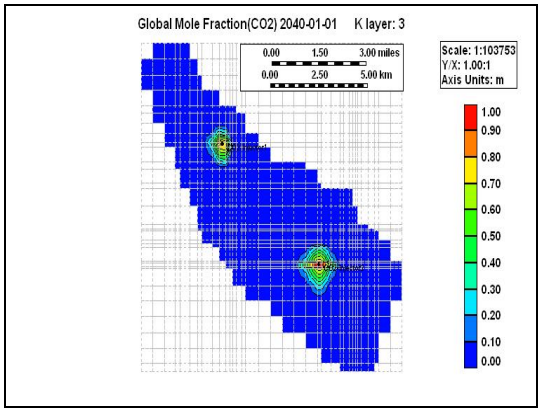

Figure B.15 Map of CO_2 Global Mole Fraction at 2040 (40 years) for Run 1a: field case, layer 3

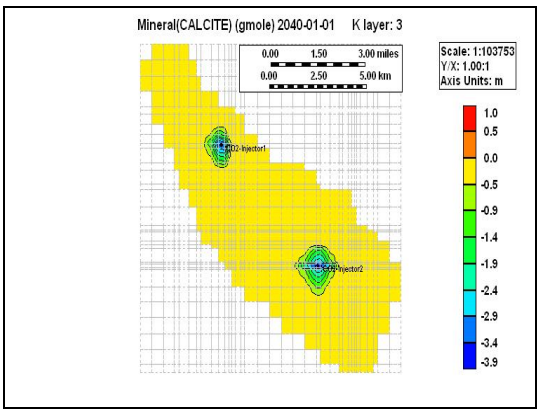

Figure B.16 Map of Calcite Dissolution / Precipitation at 2040 (40 years) for Run 1a: field case, layer 3

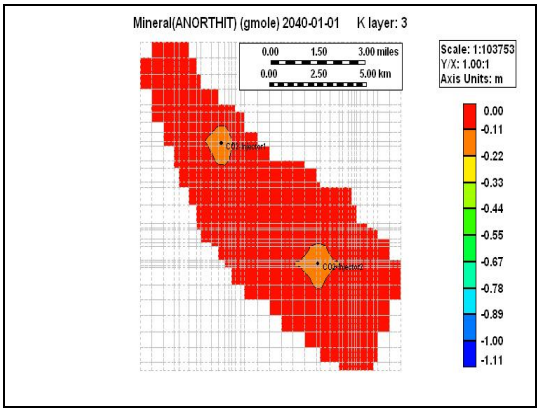

Figure B.17 Map of Anorthite Dissolution / Precipitation at 2040 (40 years) for Run 1a: field case, layer 3

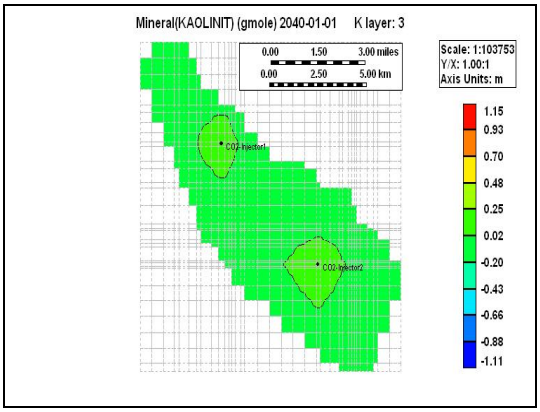

Figure B.18 Map of Kaolinite Dissolution / Precipitation at 2040 (40 years) for Run 1a: field case, layer 3

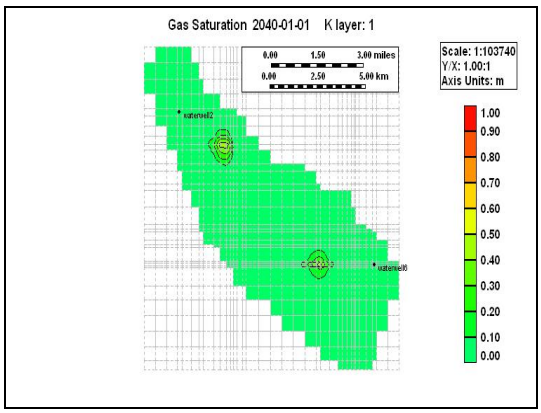

Figure B.19 Map of CO_2 Saturation at 2040 (40 years) for Run 2a: field case, layer 1

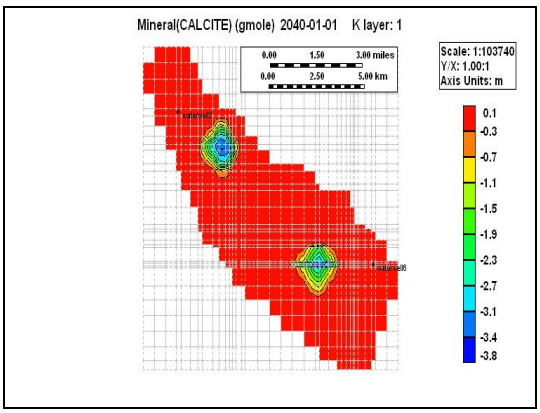

Figure B.22 Map of Calcite Dissolution / Precipitation at 2040 (40 years) for Run 2a: field case, layer 1

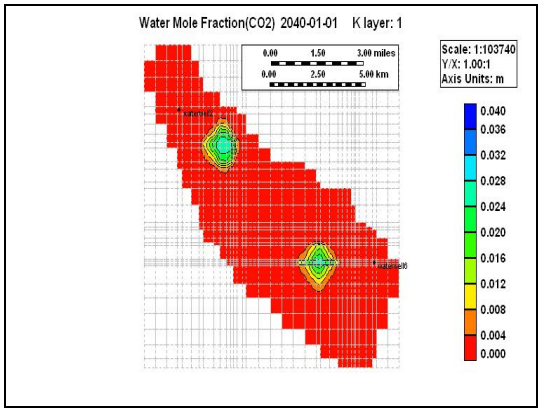

Figure B.20 Map of CO_2 Mole Fraction in Water at 2040 (40 years) for Run 2a: field case, layer 1

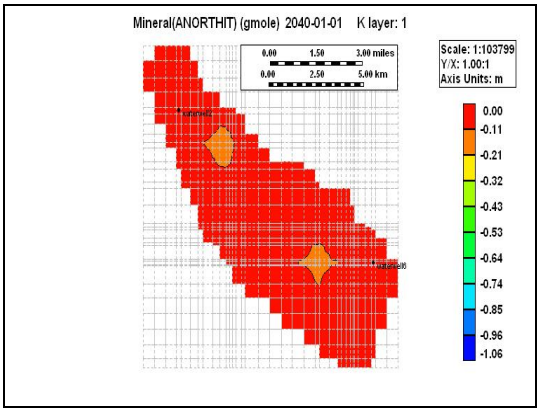

Figure B.23 Map of Anorthite Dissolution / Precipitation at 2040 (40 years) for Run 2a: field case, layer 1

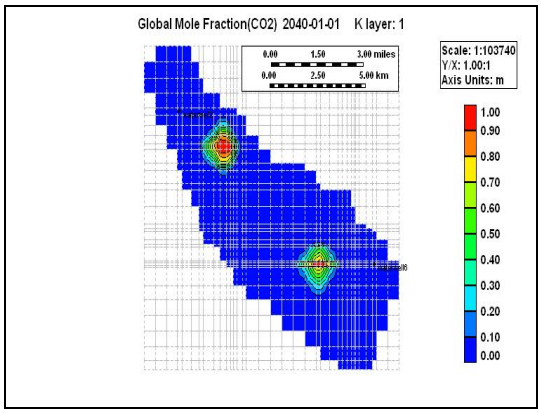

Figure B.21 Map of CO_2 Global Mole Fraction at 2040 (40 years) for Run 2a: field case, layer 1

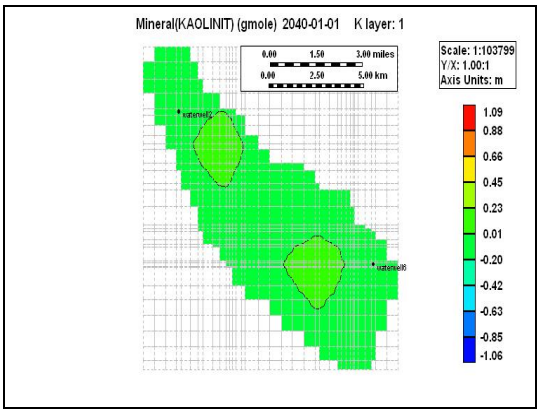

Figure B.24 Map of Kaolinite Dissolution / Precipitation at 2040 (40 years) for Run 2a: field case, layer 1

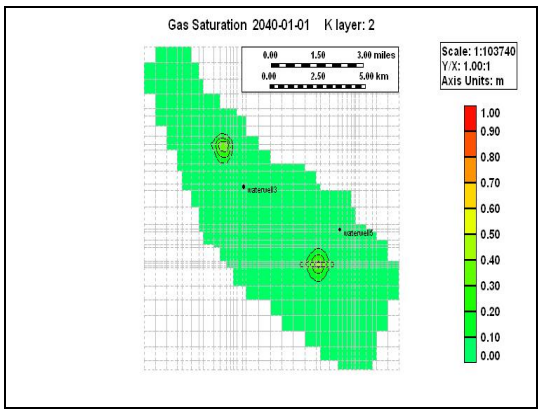

Figure B.25 Map of CO_2 Saturation at 2040 (40 years) for Run 2a: field case, layer 2

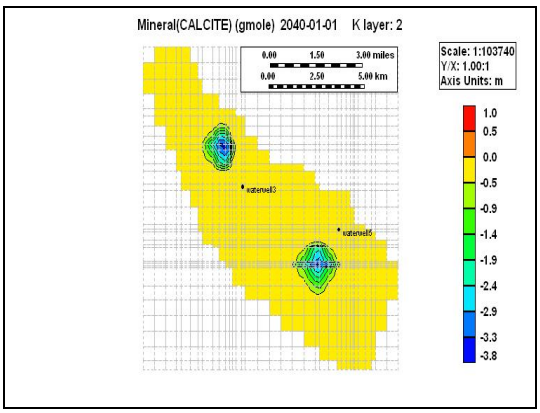

Figure B.28 Map of Calcite Dissolution / Precipitation at 2040 (40 years) for Run 2a: field case, layer 2

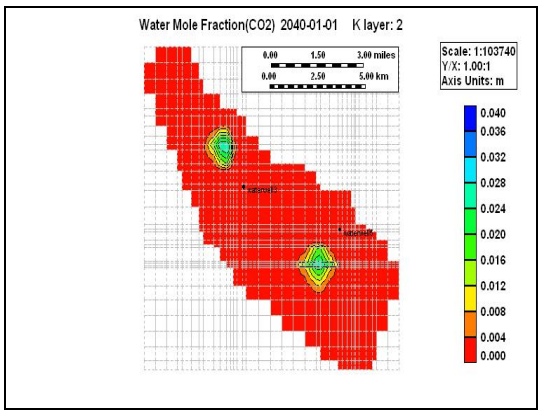

Figure B.26 Map of CO_2 Mole Fraction in Water at 2040 (40 years) for Run 2a: field case, layer 2

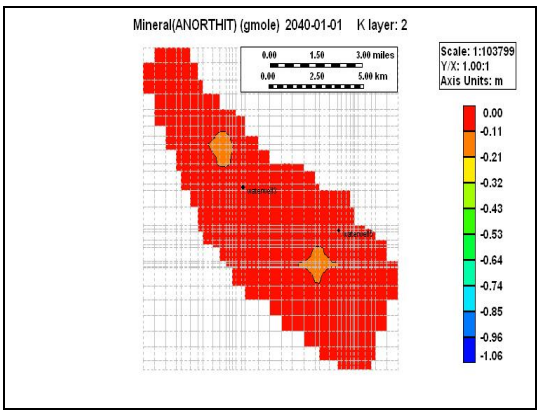

Figure B.29 Map of Anorthite Dissolution / Precipitation at 2040 (40 years) for Run 2a: field case, layer 2

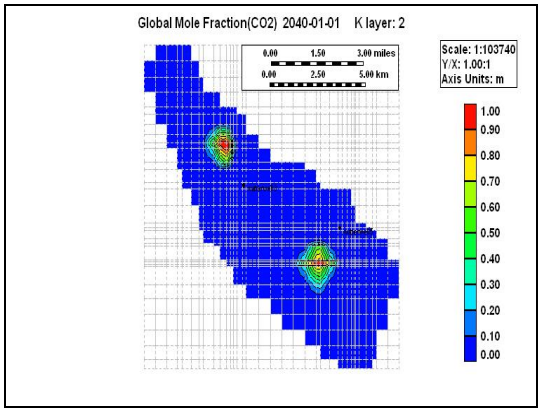

Figure B.27 Map of CO_2 Global Mole Fraction at 2040 (40 years) for Run 2a: field case, layer 2

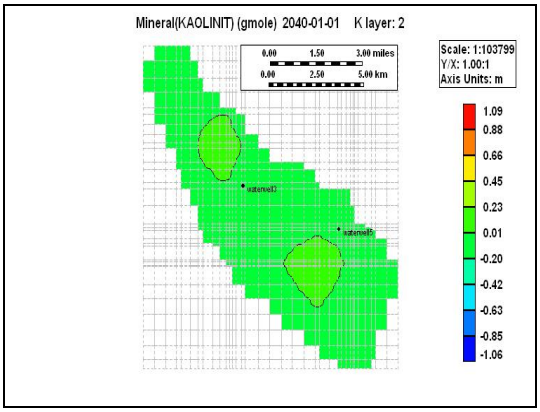

Figure B.30 Map of Kaolinite Dissolution / Precipitation at 2040 (40 years) for Run 2a: field case, layer 2

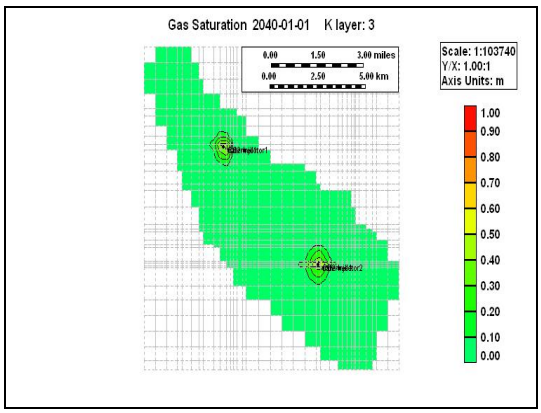

Figure B.31 Map of CO_2 Saturation at 2040 (40 years) for Run 2a: field case, layer 3

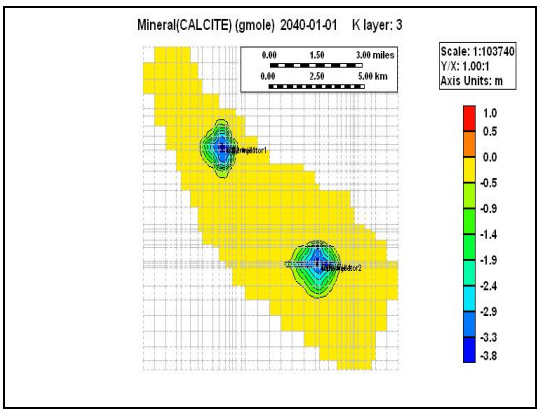

Figure B.34 Map of Calcite Dissolution / Precipitation at 2040 (40 years) for Run 2a: field case, layer 3

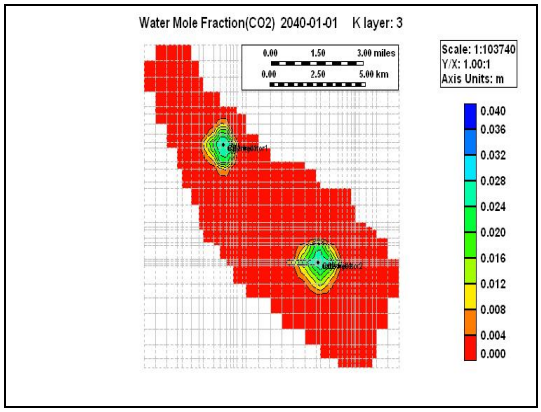

Figure B.32 Map of CO_2 Mole Fraction in Water at 2040 (40 years) for Run 2a: field case, layer 3

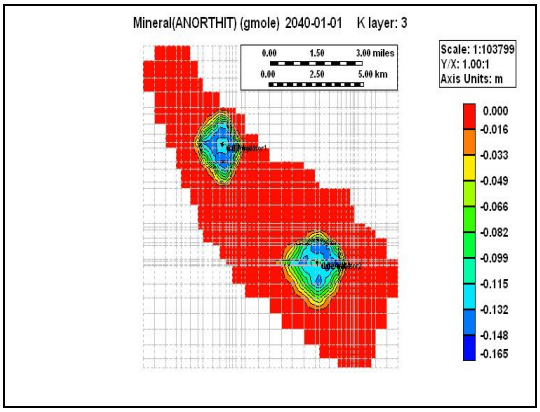

Figure B.35 Map of Anorthite Dissolution / Precipitation at 2040 (40 years) for Run 2a: field case, layer 3

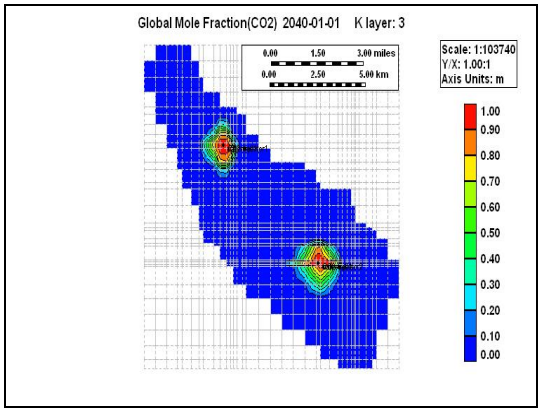

Figure B.33 Map of CO_2 Global Mole Fraction at 2040 (40 years) for Run 2a: field case, layer 3

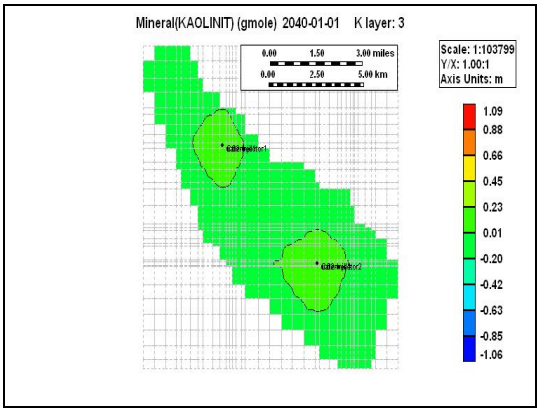

Figure B.36 Map of Kaolinite Dissolution / Precipitation at 2040 (40 years) for Run 2a: field case, layer 3

B.2 2-D Map of CO_2 saturation as a free gas, soluble CO_2 mole fraction in water and precipitated CO_2 as Calcite dissolution / precipitation, CO_2 Global Mole Fraction Kaolinite dissolution / precipitation and Anorthite dissolution / precipitation for 2100 years for Runs 1a and 2a, fieldcase.

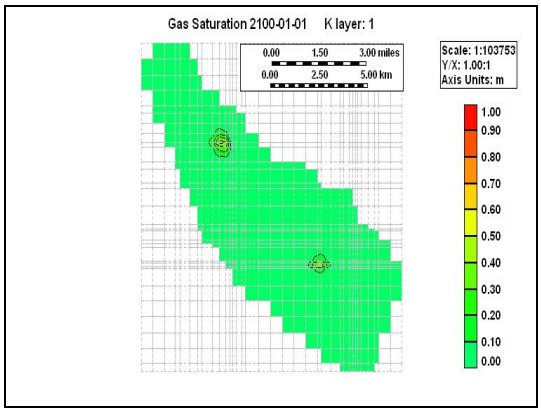

Figure B.37 Map of CO_2 Saturation at 2100 (100 years) for Run 1a: field case, layer 1

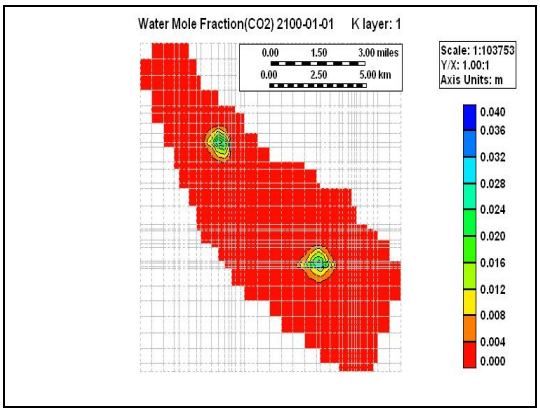

Figure B.38 Map of CO_2 Mole Fraction in Water at 2100 (100 years) for Run 1a: field case, layer 1

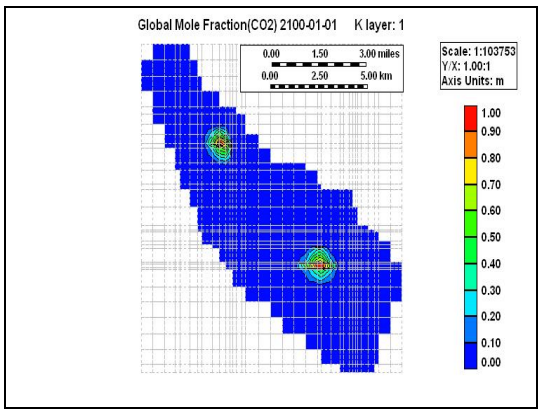

Figure B.39 Map of CO_2 Global Mole Fraction at 2100 (100 years) for Run 1a: field case, layer 1

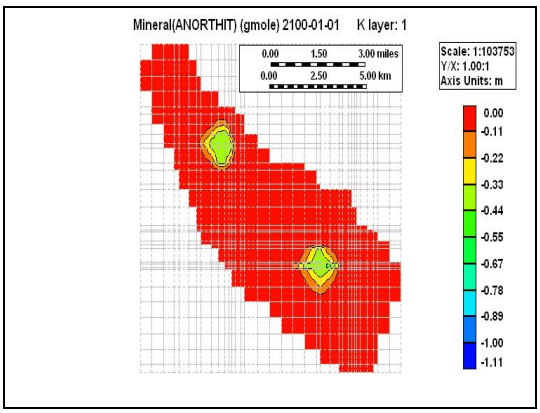

Figure B.41 Map of Anorthite Dissolution / Precipitation at 2100 (100 years) for Run 1a: field case, layer 1

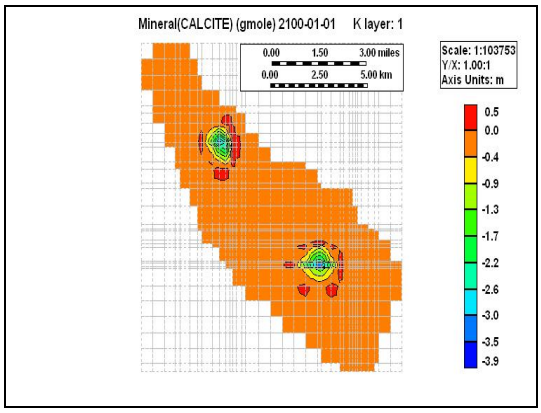

Figure B.40 Map of Calcite Dissolution / Precipitation at 2100 (100 years) for Run 1a: field case, layer 1

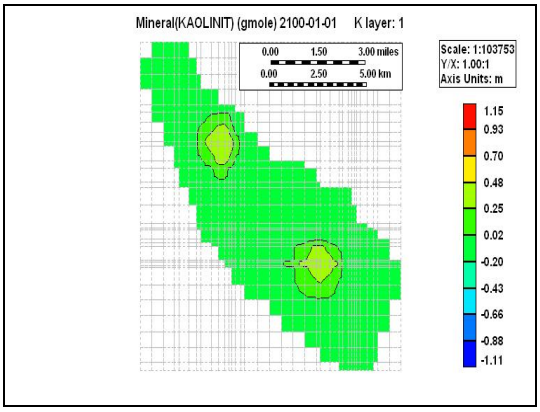

Figure B.42 Map of Kaolinite Dissolution / Precipitation at 2100 (100 years) for Run 1a: field case, layer 1

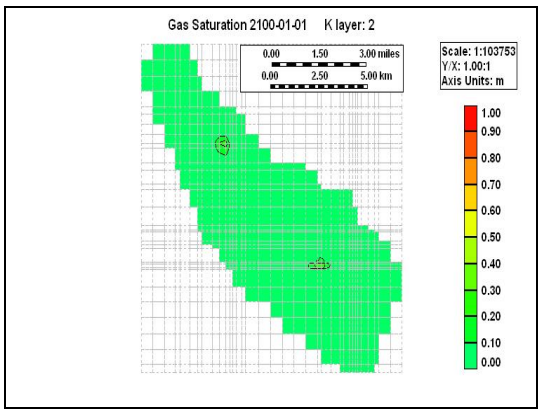

Figure B.43 Map of CO_2 Saturation at 2100 (100 years) for Run 1a: field case, layer 2

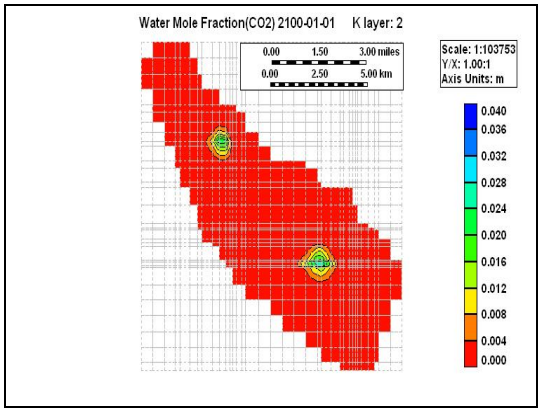

Figure B.44 Map of CO_2 Mole Fraction in Water at 2100 (100 years) for Run 1a: field case, layer 2

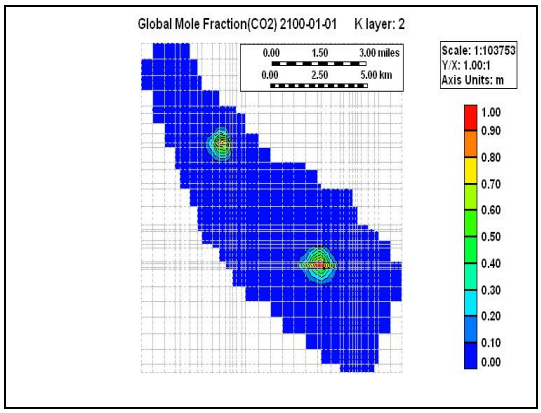

Figure B.45 Map of CO_2 Global Mole Fraction at 2100 (100 years) for Run 1a: field case, layer 2

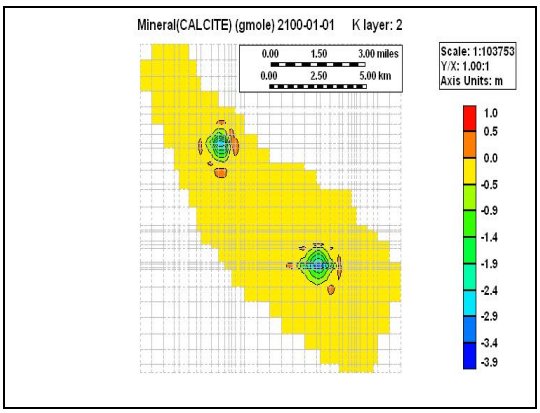

Figure B.46 Map of Calcite Dissolution / Precipitation at 2100 (100 years) for Run 1a: field case, layer 2

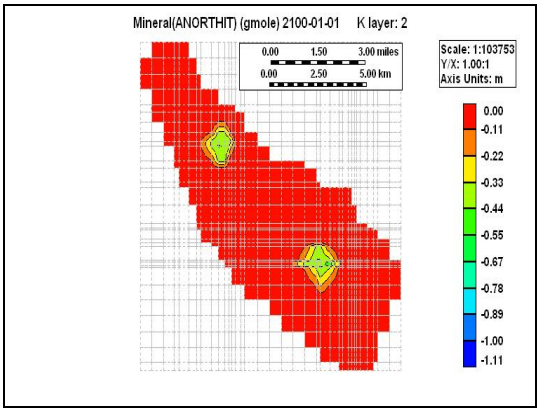

Figure B.47 Map of Anorthite Dissolution / Precipitation at 2100 (100 years) for Run 1a: field case, layer 2

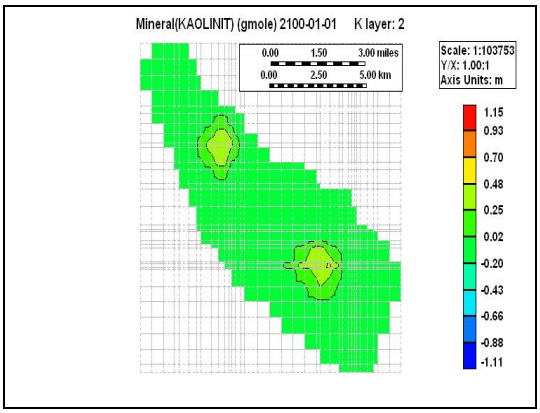

Figure B.48 Map of Kaolinite Dissolution / Precipitation at 2100 (100 years) for Run 1a: field case, layer 2

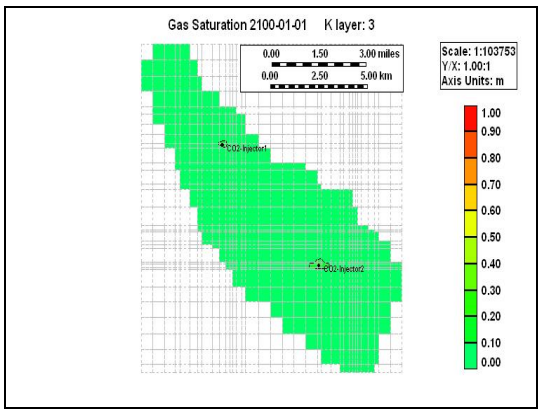

Figure B.49 Map of CO_2 Saturation at 2100 (100 years) for Run 1a: field case, layer 3

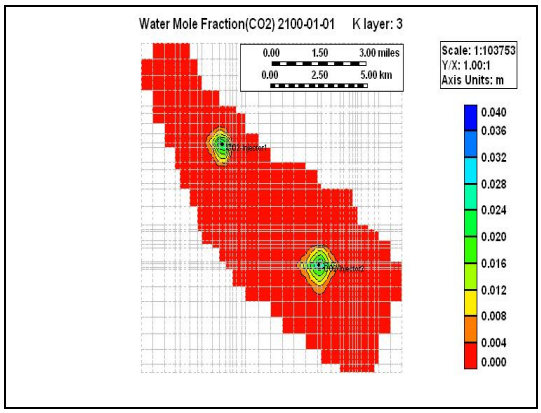

Figure B.50 Map of CO_2 Mole Fraction in Water at 2100 (100 years) for Run 1a: field case, layer 3

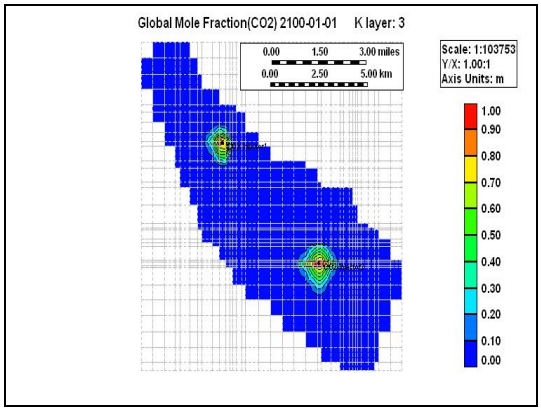

Figure B.51 Map of CO_2 Global Mole Fraction at 2100 (100 years) for Run 1a: field case, layer 3

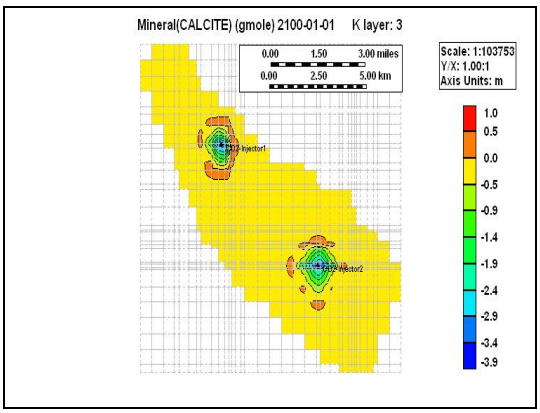

Figure B.52 Map of Calcite Dissolution / Precipitation at 2100 (100 years) for Run 1a: field case, layer 3

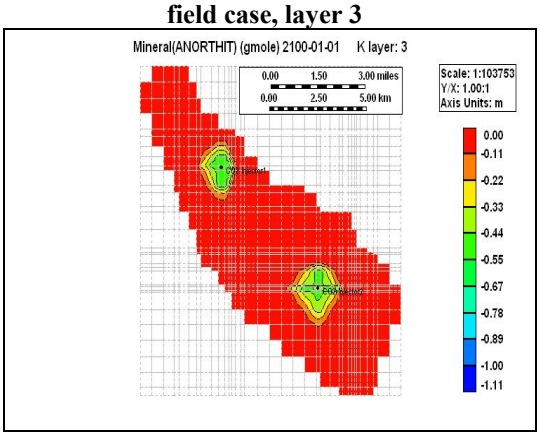

Figure B.53 Map of Anorthite Dissolution / Precipitation at 2100 (100 years) for Run 1a: field case, layer 3

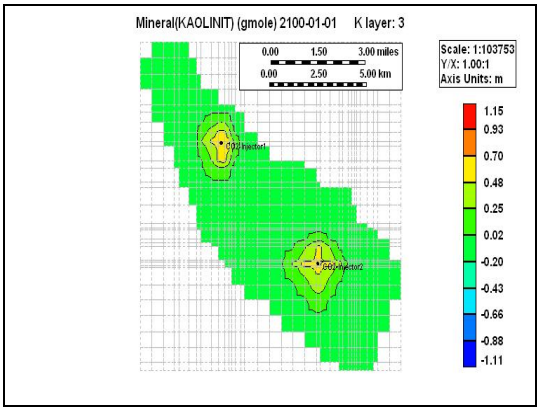

Figure B.54 Map of Kaolinite Dissolution / Precipitation at 2100 (100 years) for Run 1a: field case, layer 3

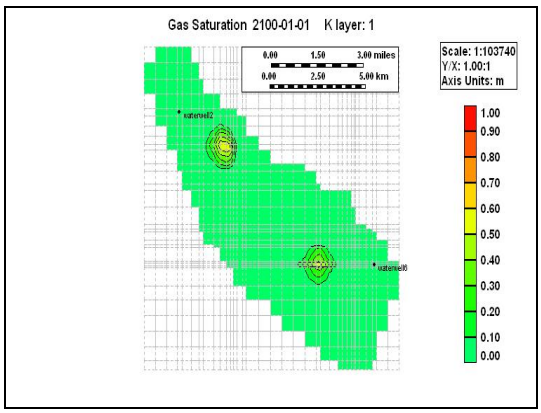

Figure B.55 Map of CO_2 Saturation at 2100 (100 years) for Run 2a: field case, layer 1

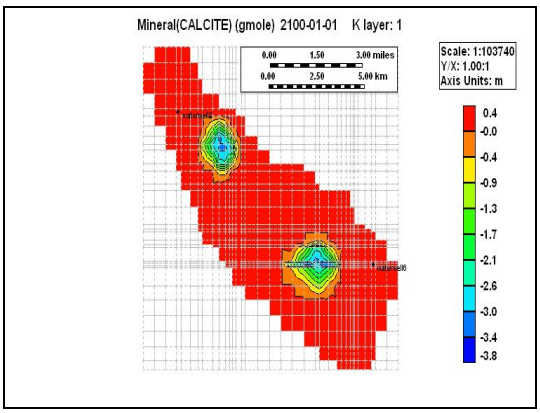

Figure B.58 Map of Calcite Dissolution / Precipitation at 2100 (100 years) for Run 2a: field case, layer 1

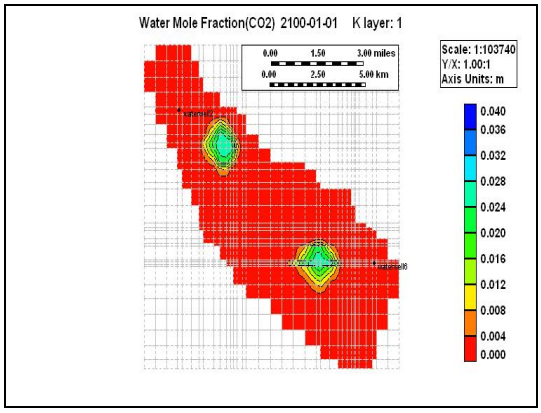

Figure B.56 Map of CO_2 Mole Fraction in Water at 2100 (100 years) for Run 2a: field case, layer 1

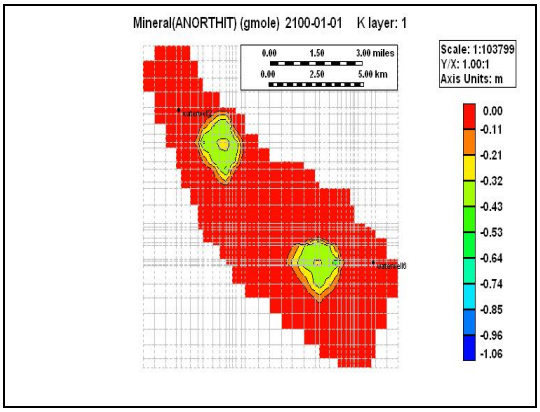

Figure B.59 Map of Anorthite Dissolution / Precipitation at 2100 (100 years) for Run 2a: field case, layer 1

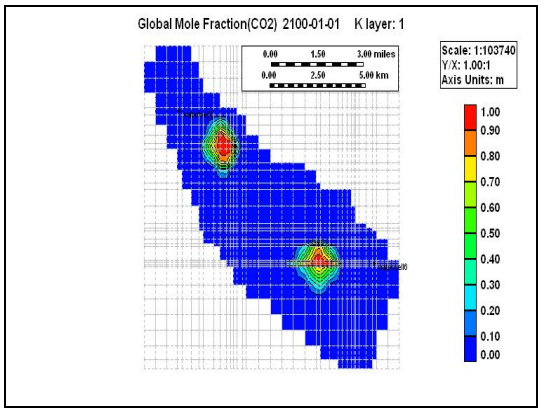

Figure B.57 Map of CO_2 Global Mole Fraction at 2100 (100 years) for Run 2a: field case, layer 1

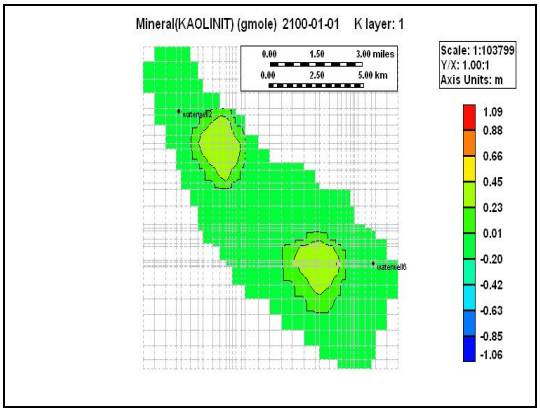

Figure B.60 Map of Kaolinite Dissolution / Precipitation at 2100 (100 years) for Run 2a: field case, layer 1

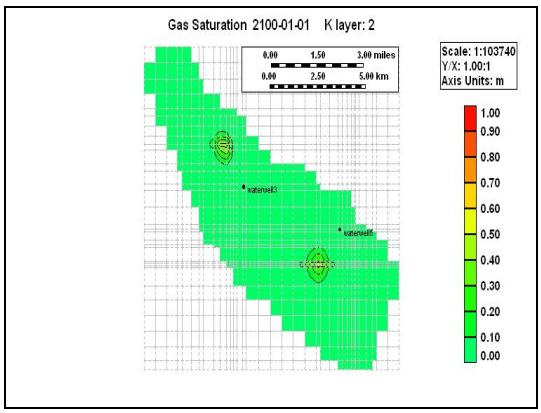

Figure B.61 Map of CO_2 Saturation at 2100 (100 years) for Run 2a: field case, layer 2

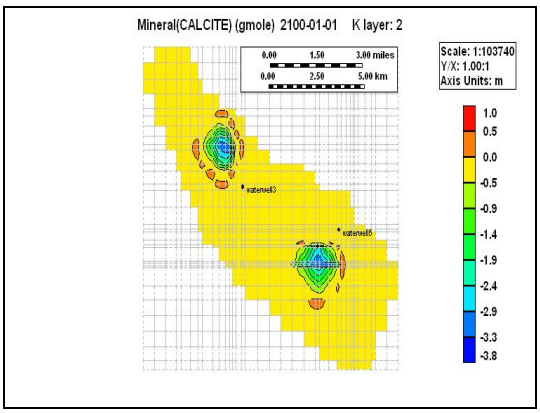

Figure B.64 Map of Calcite Dissolution / Precipitation at 2100 (100 years) for Run 2a: field case, layer 2

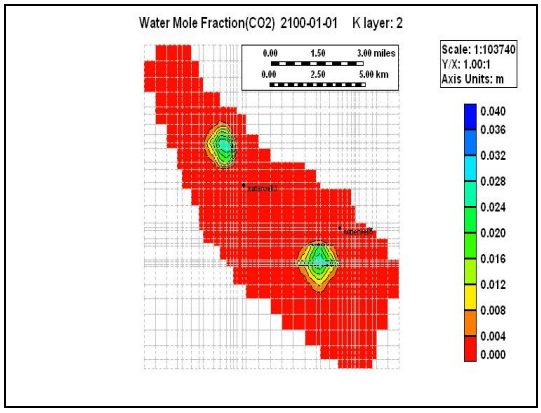

Figure B.62 Map of CO_2 Mole Fraction in Water at 2100 (100 years) for Run 2a: field case, layer 2

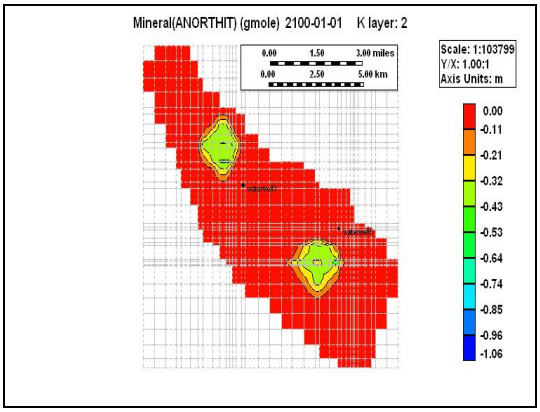

Figure B.65 Map of Anorthite Dissolution / Precipitation at 2100 (100 years) for Run 2a: field case, layer 2

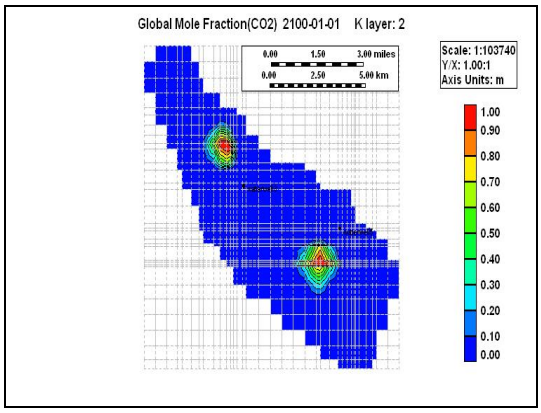

Figure B.63 Map of CO_2 Global Mole Fraction at 2100 (100 years) for Run 2a: field case, layer 2

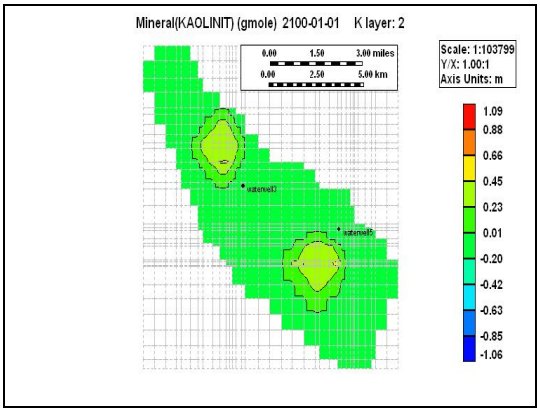

Figure B.66 Map of Kaolinite Dissolution / Precipitation at 2100 (100 years) for Run 2a: field case, layer 2

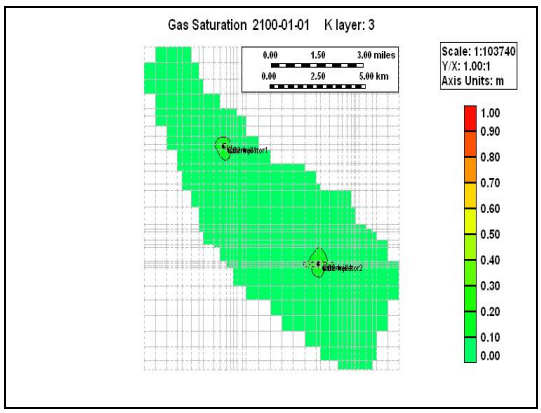

Figure B.67 Map of CO_2 Saturation at 2100 (100 years) for Run 2a: field case, layer 3

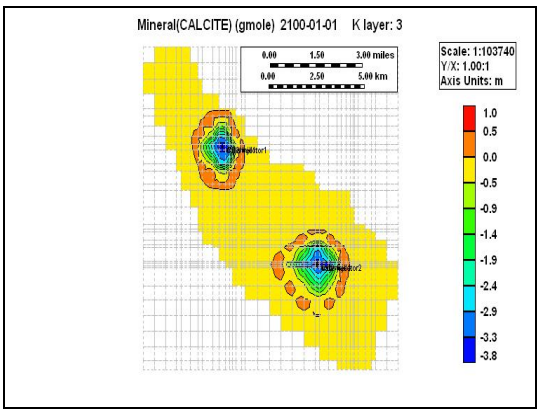

Figure B.70 Map of Calcite Dissolution / Precipitation at 2100 (100 years) for Run 2a: field case, layer 3

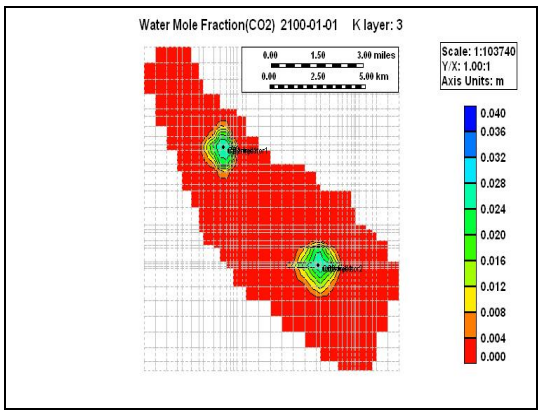

Figure B.68 Map of CO_2 Mole Fraction in Water at 2100 (100 years) for Run 2a: field case, layer 3

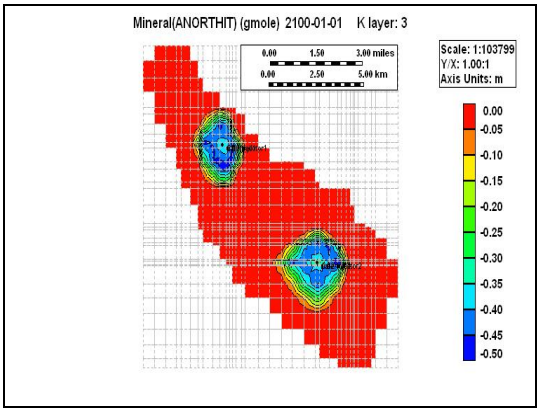

Figure B.71 Map of Anorthite Dissolution / Precipitation at 2100 (100 years) for Run 2a: field case, layer 3

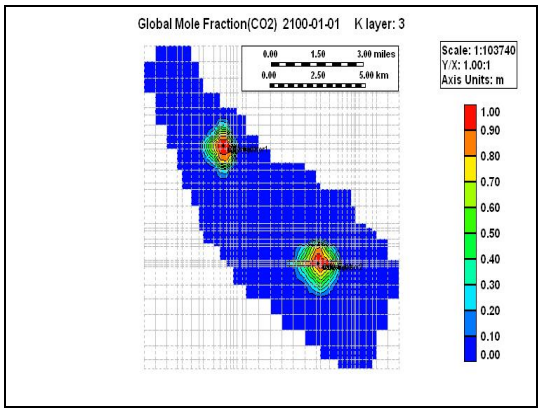

Figure B.69 Map of CO_2 Global Mole Fraction at 2100 (100 years) for Run 2a: field case, layer 3

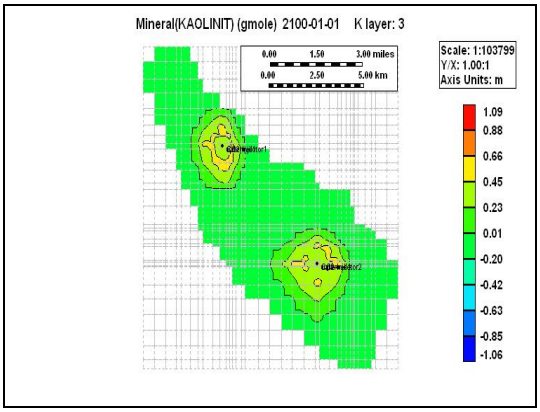

Figure B.72 Map of Kaolinite Dissolution / Precipitation at 2100 (100 years) for Run 2a: field case, layer 3

APPENDIX C

CO_2 Injection Histories, CO_2 Saturation, CO_2 Mole Fraction in Water, Calcite Dissolution / Precipitation, Anorthite Dissolution / Precipitation, Kaolinite Dissolution / Precipitation Plots for Runs 4b through 12b for Single-Well Aquifer Model

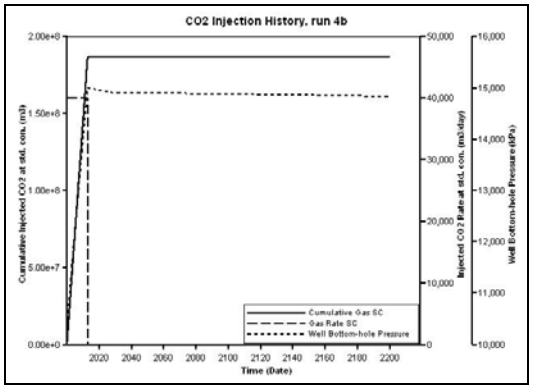

Figure C.73 CO_2 Injection History for Run 4b: single-well case, (CO_2 injection rate = 40000 sm^3/d)

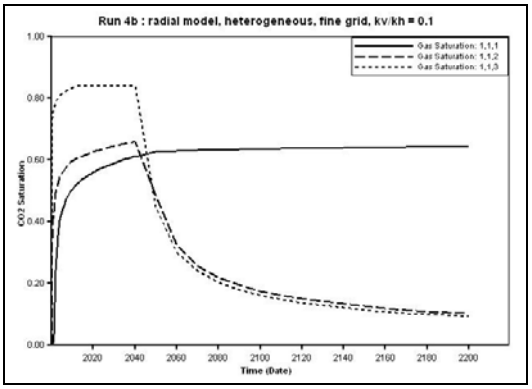

Figure C.74 CO_2 Saturation for Run 4b: single-well case

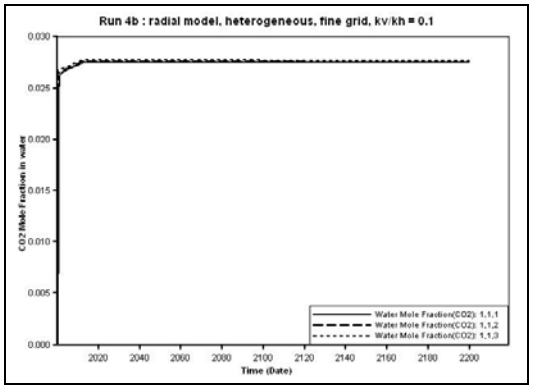

Figure C.75 CO_2 Mole Fraction in Water for Run 4b: single-well case

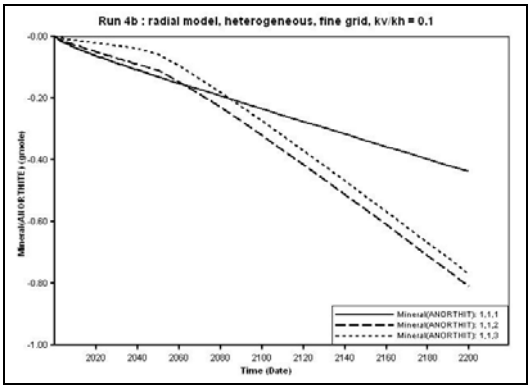

Figure C.77 AnorthiteDissolution / Precipitation for Run 4b: single-well case

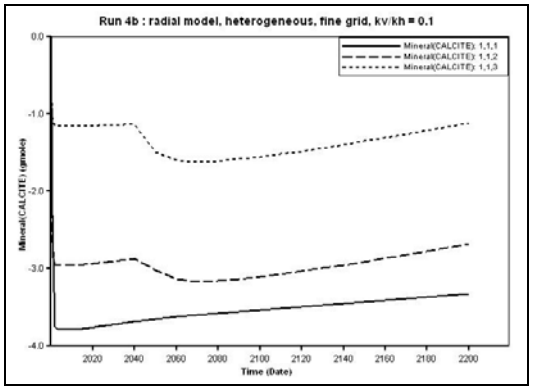

Figure C.76 Calcite Dissolution / Precipitation for Run 4b: single-well case

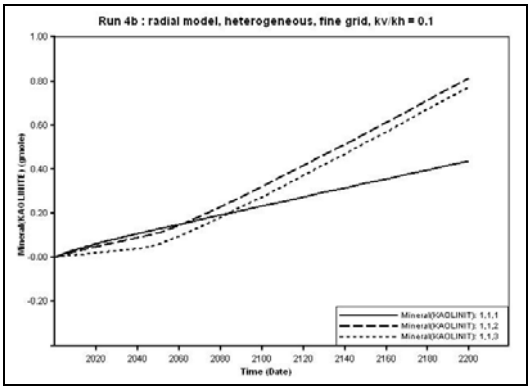

Figure C.78 Kaolinite Dissolution / Precipitation for Run 4b: single-well case

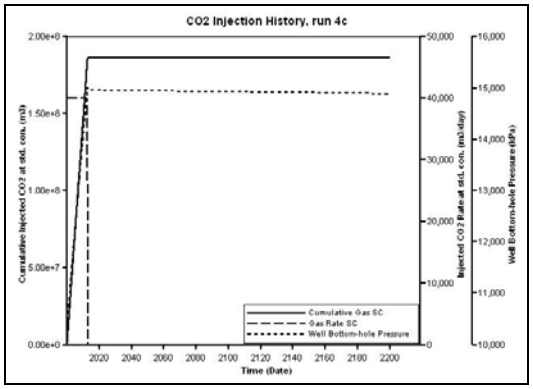

Figure C.79 CO_2 Injection History for Run 4c: single-well case, (CO_2 injection rate = 40000 sm^3/d)

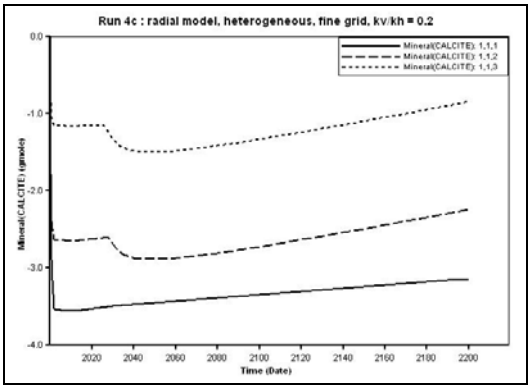

Figure C.82 Calcite Dissolution / Precipitation for Run 4c: single-well case

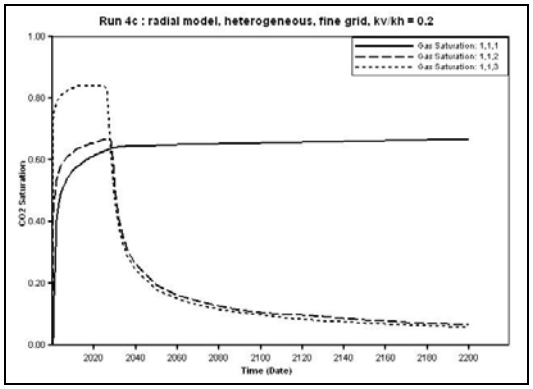

Figure C.80 CO_2 Saturation for Run 4c: single-well case

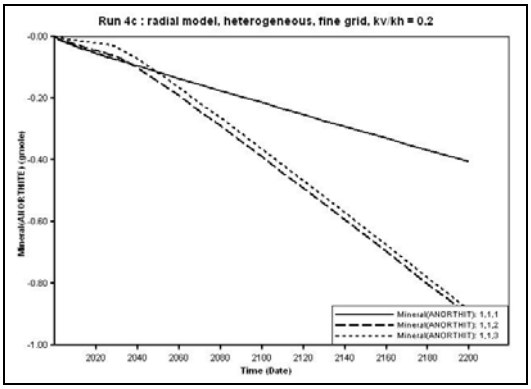

Figure C.83 AnorthiteDissolution / Precipitation for Run 4c: single-well case

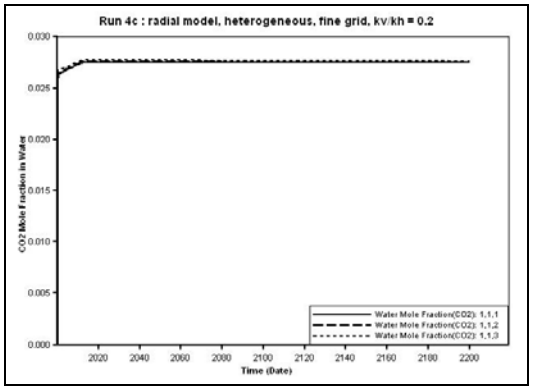

Figure C.81 CO_2 Mole Fraction in Water for Run 4c: single-well case

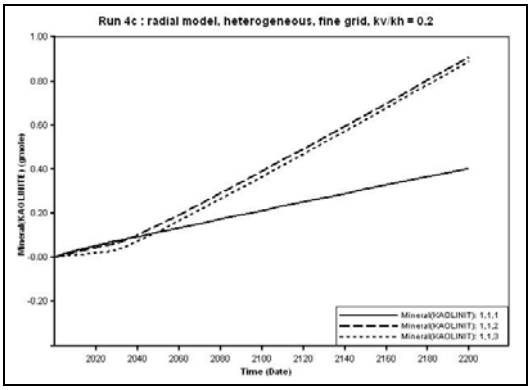

Figure C.84 Kaolinite Dissolution / Precipitation for Run 4c: single-well case

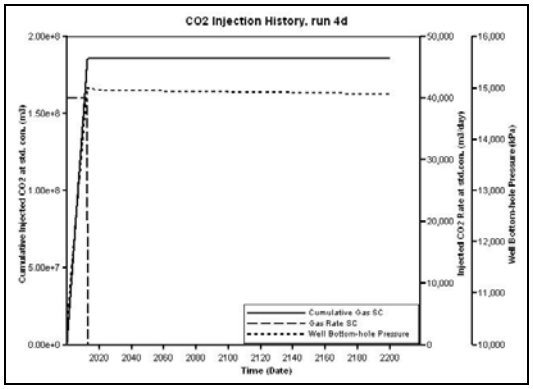

Figure C.85 CO_2 Injection History for Run 4d: single-well case, (CO_2 injection rate = 40000 sm^3/d)

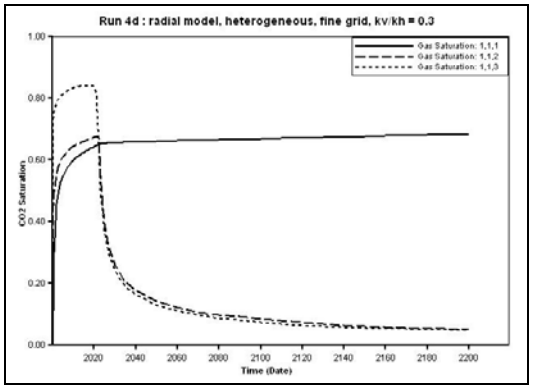

Figure C.86 CO_2 Saturation for Run 4d: single-well case

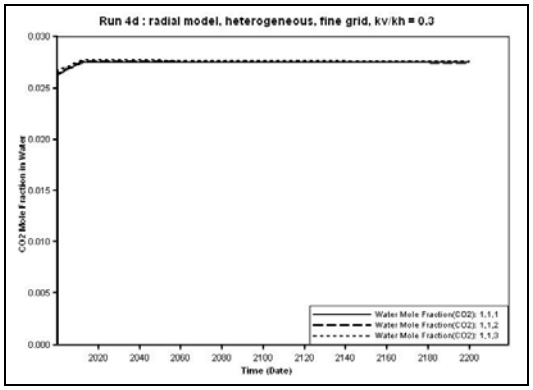

Figure C.87 CO_2 Mole Fraction in Water for Run 4d: single-well case

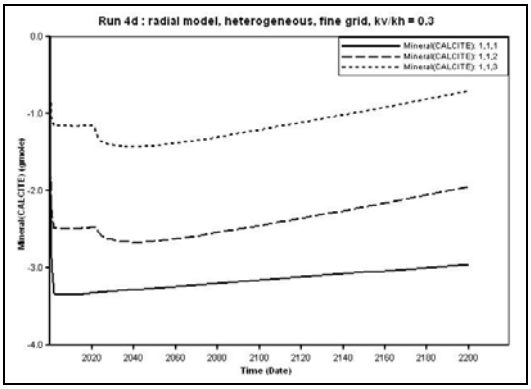

Figure C.88 Calcite Dissolution / Precipitation for Run 4d: single-well case

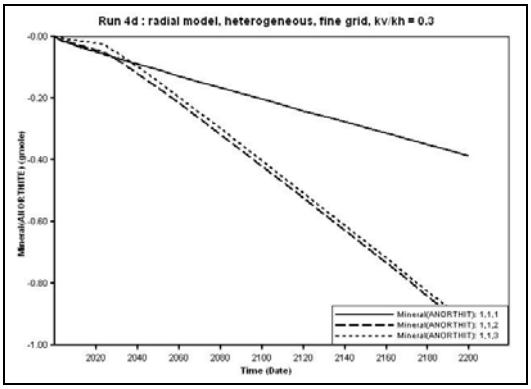

Figure C.89 AnorthiteDissolution / Precipitation for Run 4d: single-well case

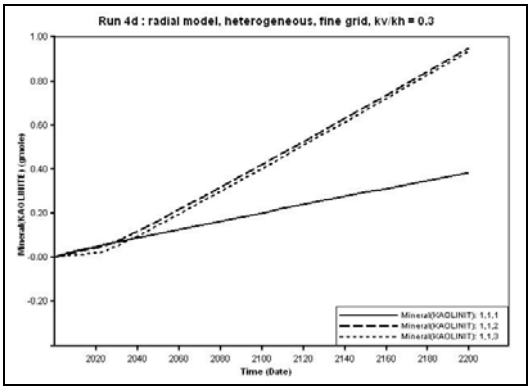

Figure C.90 Kaolinite Dissolution / Precipitation for Run 4d: single-well case

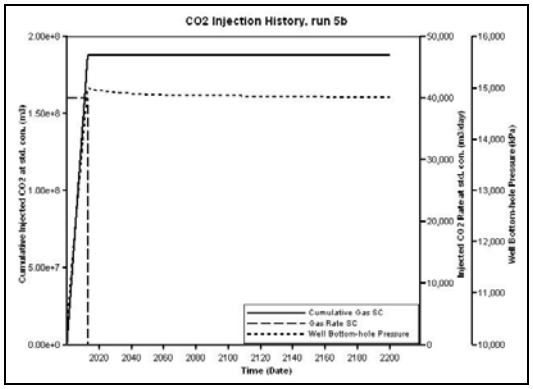

Figure C.91 CO_2 Injection History for Run 5b: single-well case, (CO_2 injection rate = 40000 sm^3/d)

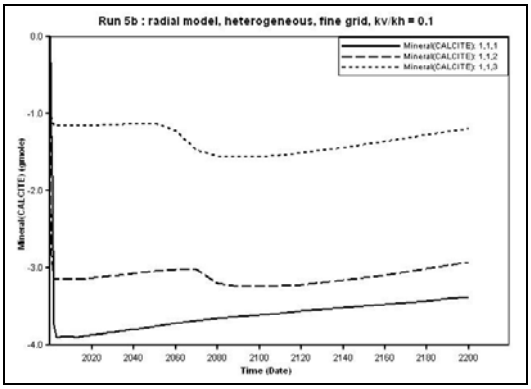

Figure C.94 Calcite Dissolution / Precipitation for Run 5b: single-well case

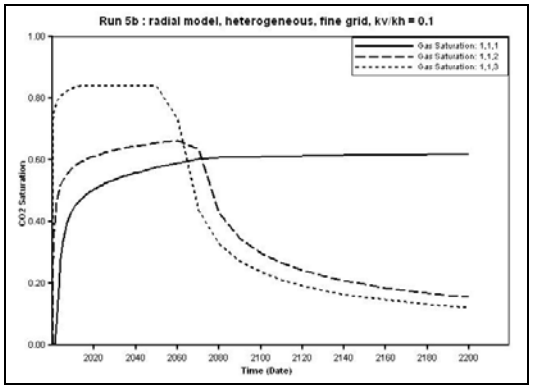

Figure C.92 CO_2 Saturation for Run 5b: single-well case

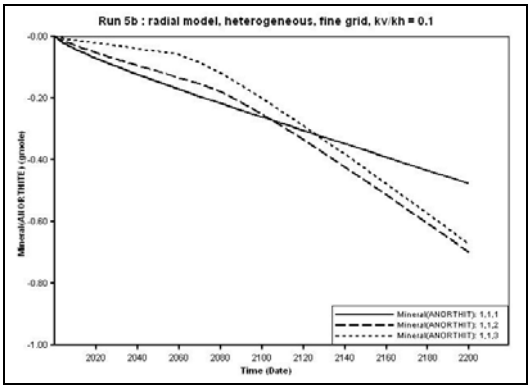

Figure C.95 AnorthiteDissolution / Precipitation for Run 5b: single-well case

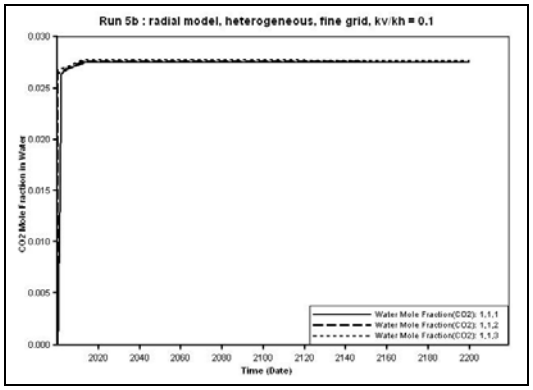

Figure C.93 CO_2 Mole Fraction in Water for Run 5b: single-well case

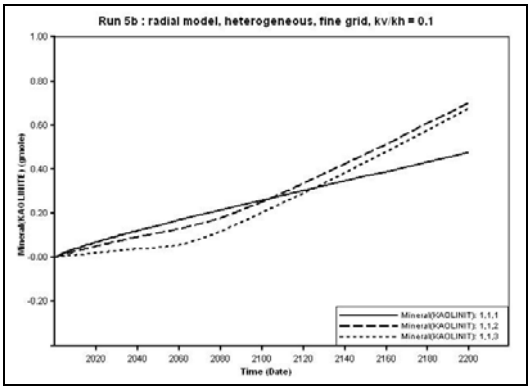

Figure C.96 Kaolinite Dissolution / Precipitation for Run 5b: single-well case

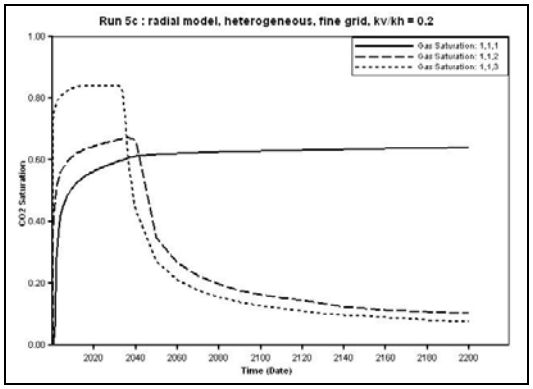

Figure C.97 CO_2 Injection History for Run 5c: single-well case, (CO_2 injection rate = 40000 sm^3/d)

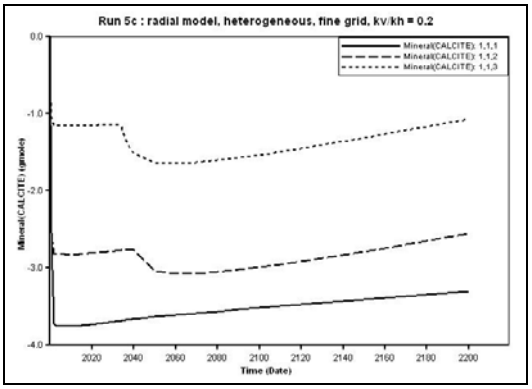

Figure C.100 Calcite Dissolution / Precipitation for Run 5c: single-well case

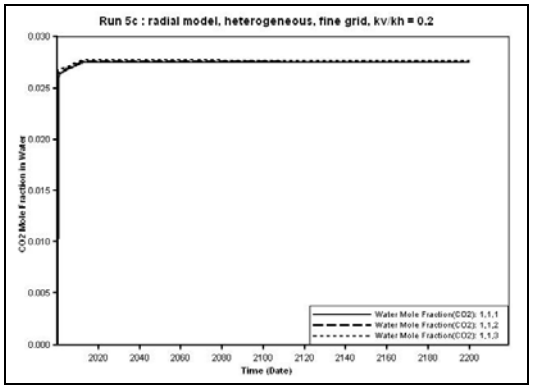

Figure C.98 CO_2 Saturation for Run 5c: single-well case

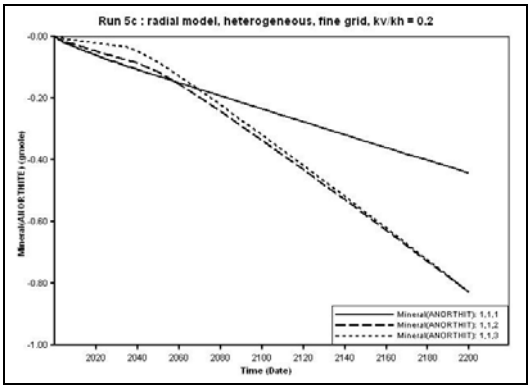

Figure C.101 AnorthiteDissolution / Precipitation for Run 5c: single-well case

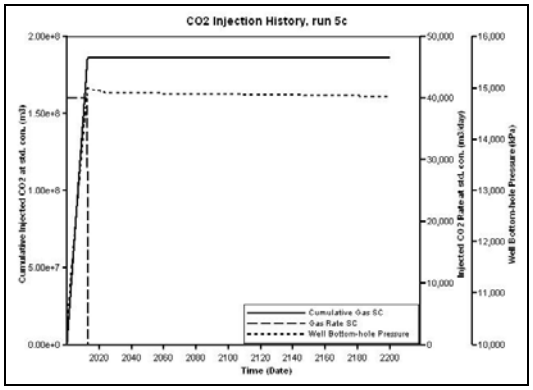

Figure C.99 CO_2 Mole Fraction in Water for Run 5c: single-well case

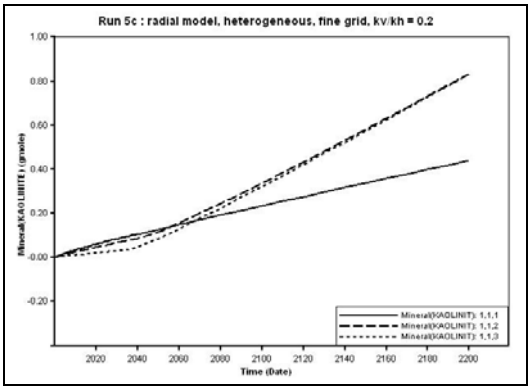

Figure C.102 Kaolinite Dissolution / Precipitation for Run 5c: single-well case

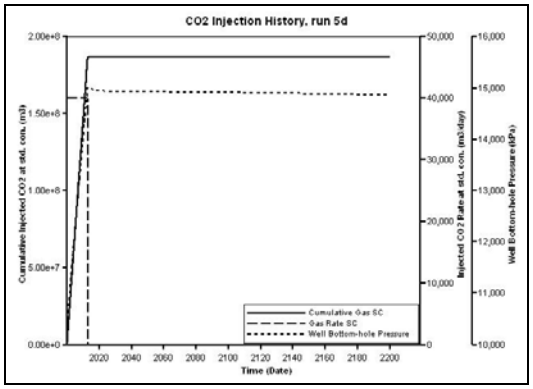

Figure C.103 CO_2 Injection History for Run 5d: single-well case, (CO_2 injection rate = 40000 sm^3/d)

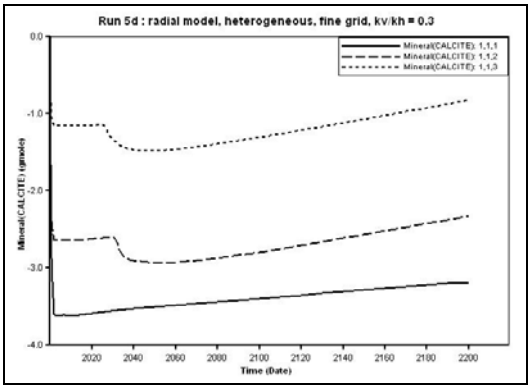

Figure C.106 Calcite Dissolution / Precipitation for Run 5d: single-well case

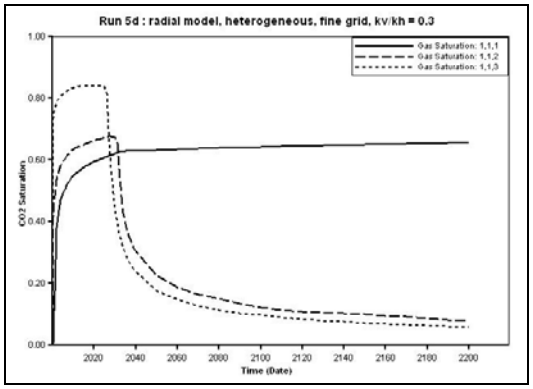

Figure C.104 CO_2 Saturation for Run 5d: single-well case

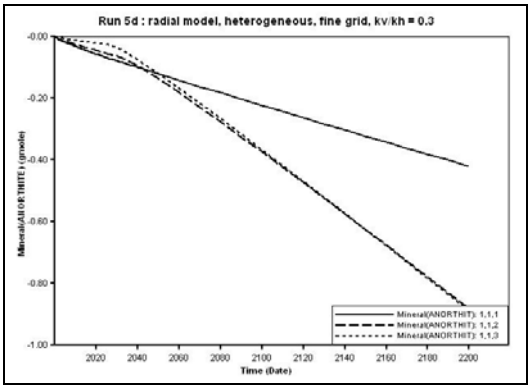

Figure C.107 AnorthiteDissolution / Precipitation for Run 5d: single-well case

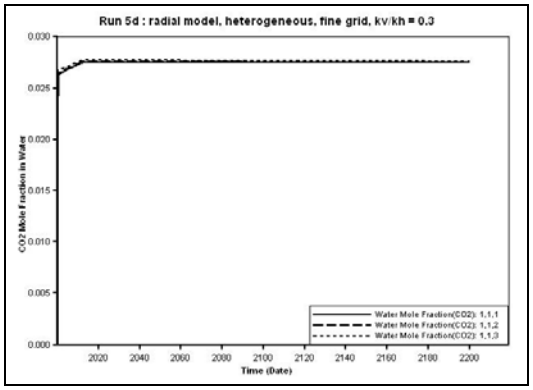

Figure C.105 CO_2 Mole Fraction in Water for Run 5d: single-well case

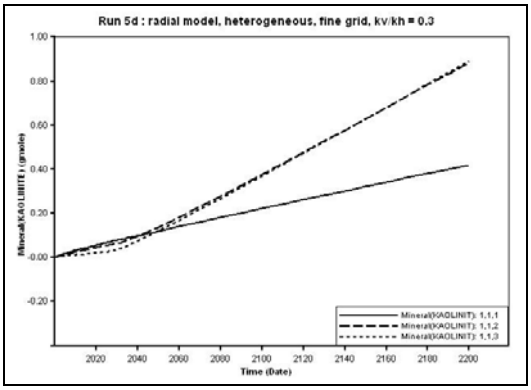

Figure C.108 Kaolinite Dissolution / Precipitation for Run 5d: single-well case

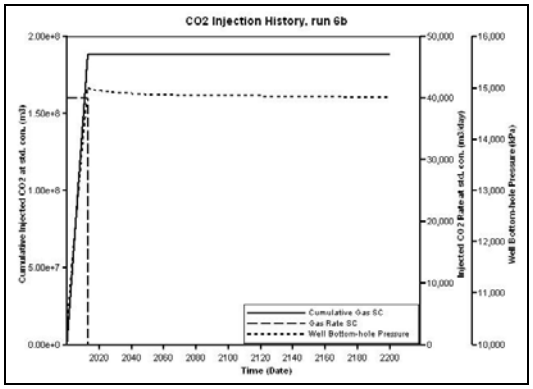

Figure C.109 CO_2 Injection History for Run 6b: single-well case, (CO_2 injection rate = 40000 sm^3/d)

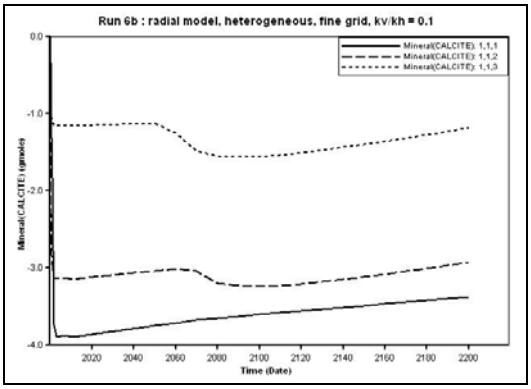

Figure C.112 Calcite Dissolution / Precipitation for Run 6b: single-well case

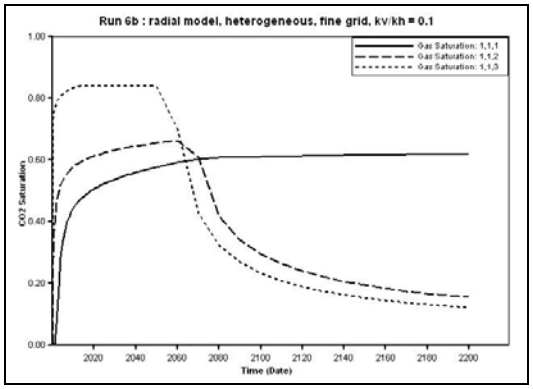

Figure C.110 CO_2 Saturation for Run 6b: single-well case

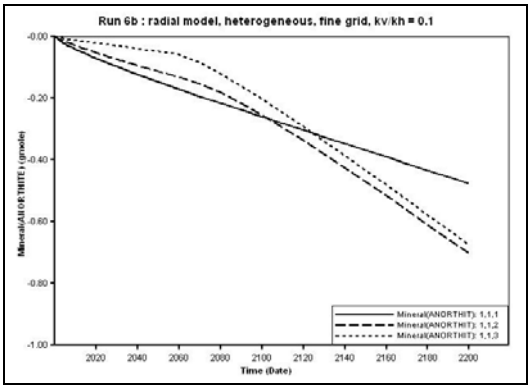

Figure C.113 AnorthiteDissolution / Precipitation for Run 6b: single-well case

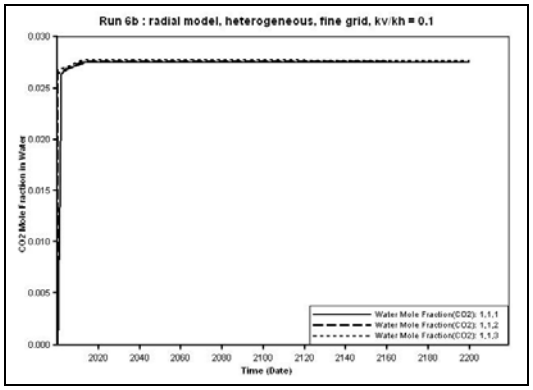

Figure C.111 CO_2 Mole Fraction in Water for Run 6b: single-well case

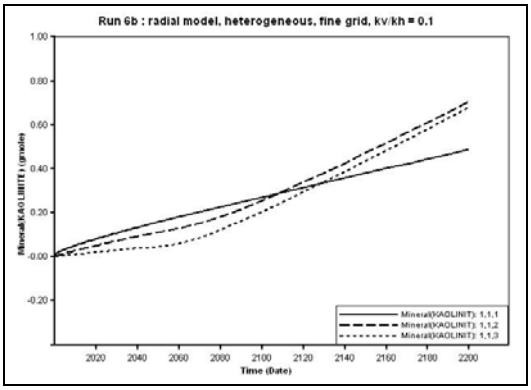

Figure C.114 Kaolinite Dissolution / Precipitation for Run 6b: single-well case

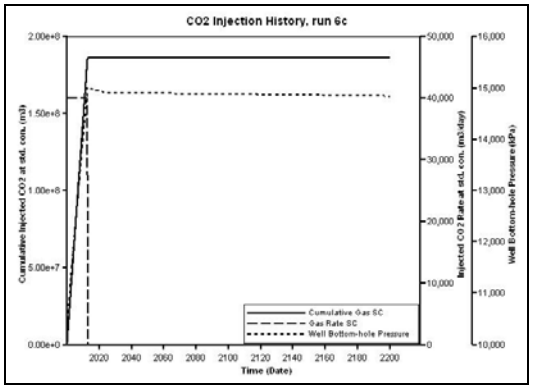

Figure C.115 CO_2 Injection History for Run 6c: single-well case, (CO_2 injection rate = 40000 sm^3/d)

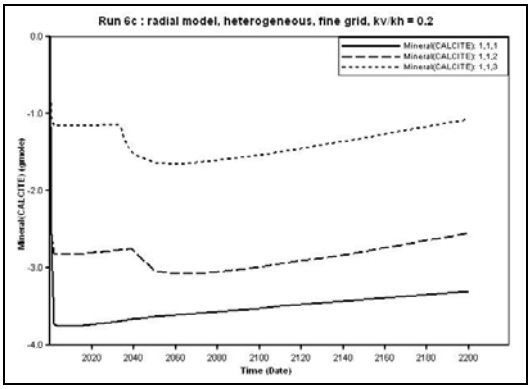

Figure C.118 Calcite Dissolution / Precipitation for Run 6c: single-well case

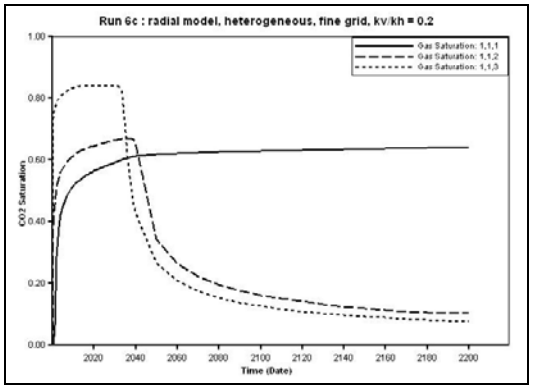

Figure C.116 CO_2 Saturation for Run 6c: single-well case

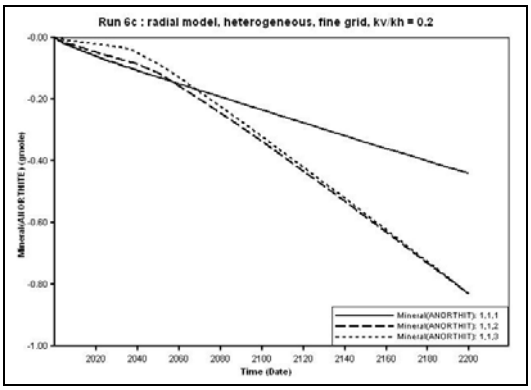

Figure C.119 AnorthiteDissolution / Precipitation for Run 6c: single-well case

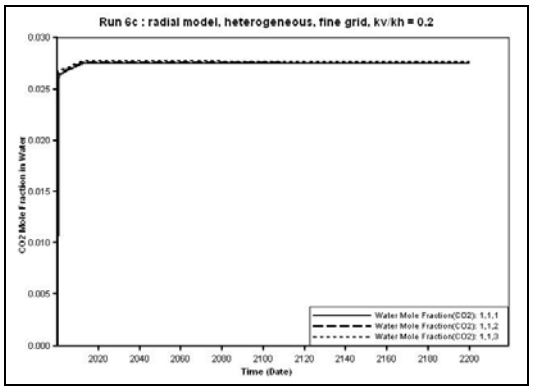

Figure C.117 CO_2 Mole Fraction in Water for Run 6c: single-well case

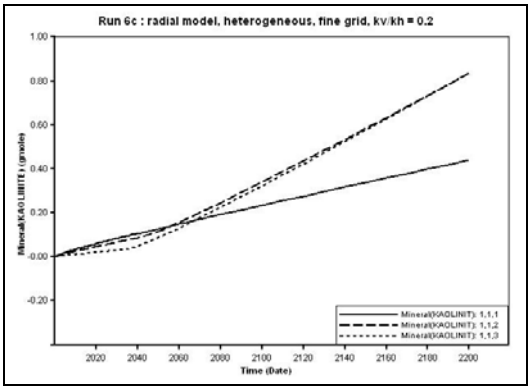

Figure C.120 Kaolinite Dissolution / Precipitation for Run 6c: single-well case

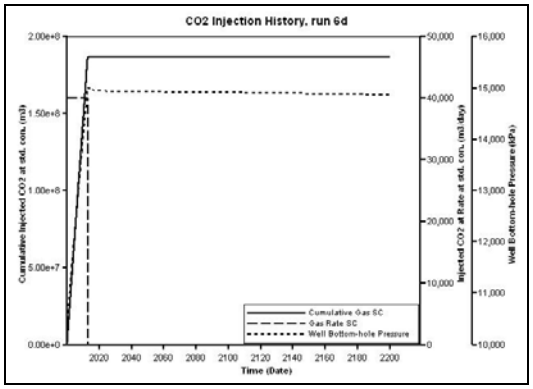

Figure C.121 CO_2 Injection History for Run 6d: single-well case, (CO_2 injection rate = 40000 sm^3/d)

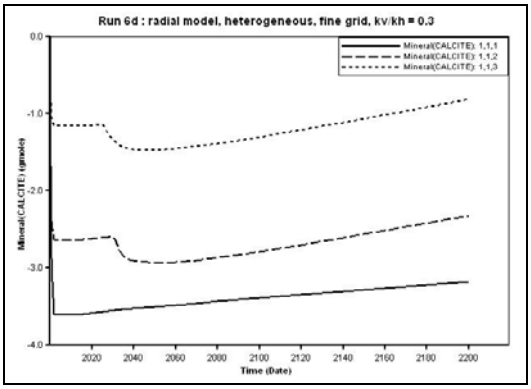

Figure C.124 Calcite Dissolution / Precipitation for Run 6d: single-well case

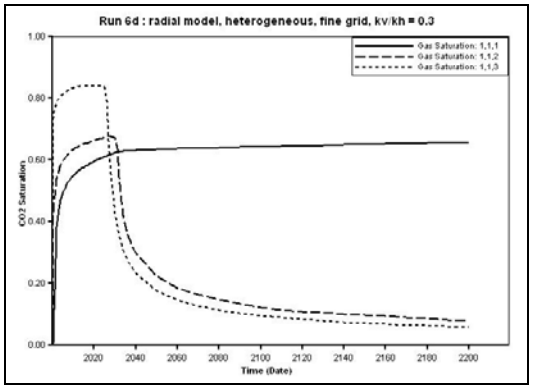

Figure C.122 CO_2 Saturation for Run 6d: single-well case

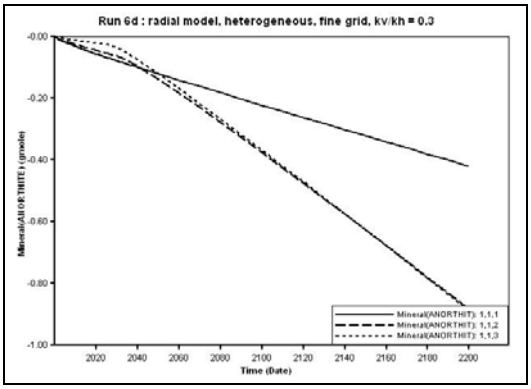

Figure C.125 AnorthiteDissolution / Precipitation for Run 6d: single-well case

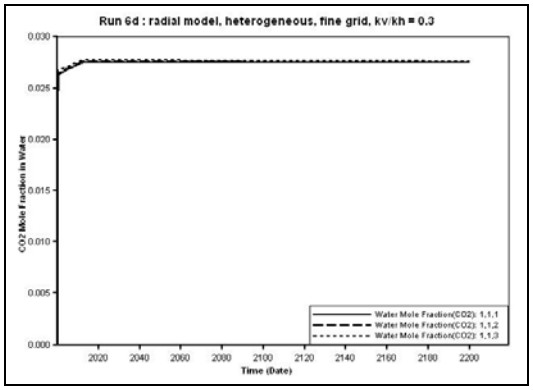

Figure C.123 CO_2 Mole Fraction in Water for Run 6d: single-well case

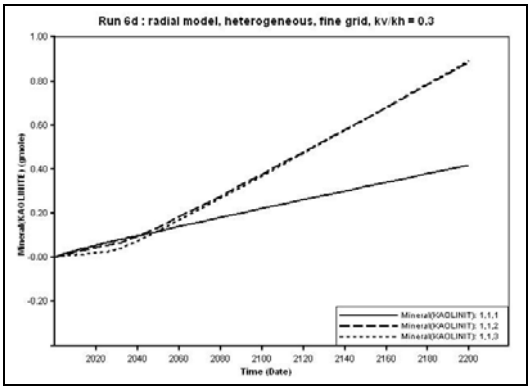

Figure C.126 Kaolinite Dissolution / Precipitation for Run 6d: single-well case

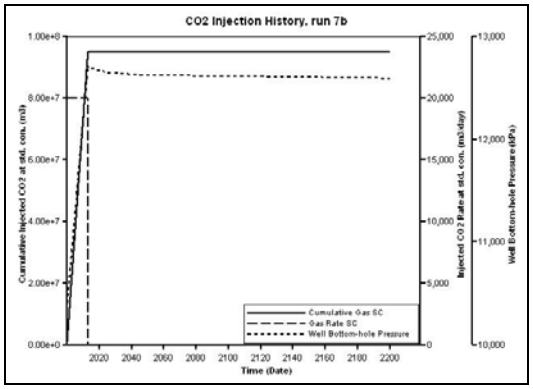

Figure C.127 CO_2 Injection History for Run 7b: single-well case, (CO_2 injection rate = 20000 sm^3/d)

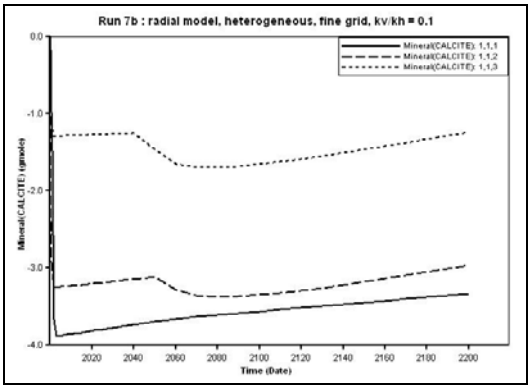

Figure C.130 Calcite Dissolution / Precipitation for Run 7b: single-well case

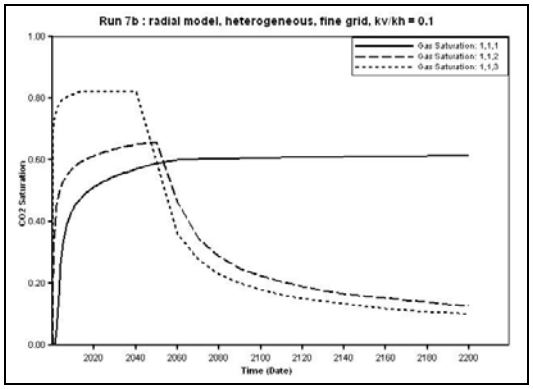

Figure C.128 CO_2 Saturation for Run 7b: single-well case

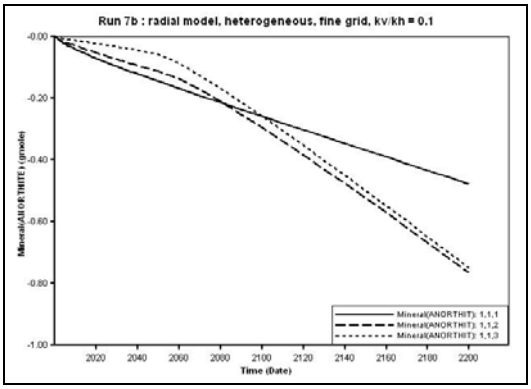

Figure C.131 AnorthiteDissolution / Precipitation for Run 7b: single-well case

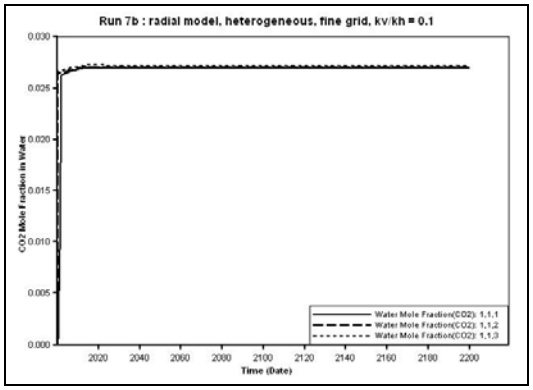

Figure C.129 CO_2 Mole Fraction in Water for Run 7b: single-well case

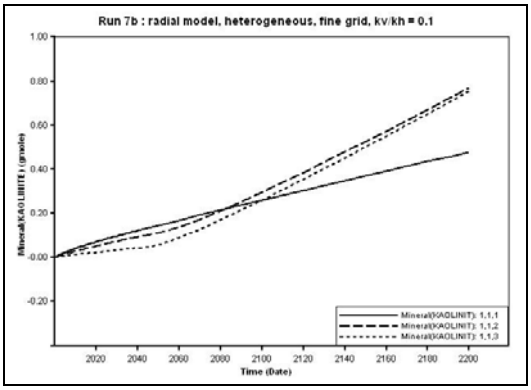

Figure C.132 Kaolinite Dissolution / Precipitation for Run 7b: single-well case

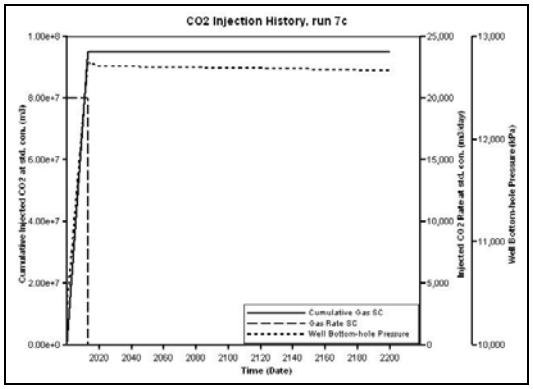

Figure C.133 CO_2 Injection History for Run 7c: single-well case, (CO_2 injection rate = 20000 sm^3/d)

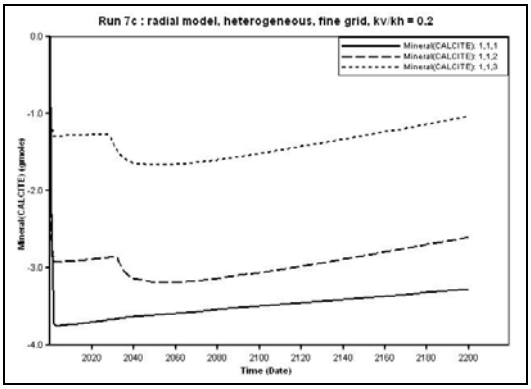

Figure C.136 Calcite Dissolution / Precipitation for Run 7c: single-well case

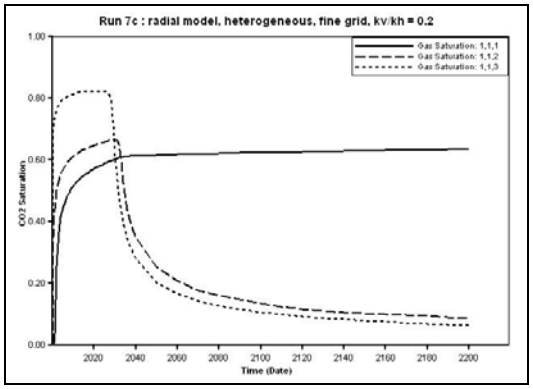

Figure C.134 CO_2 Saturation for Run 7c: single-well case

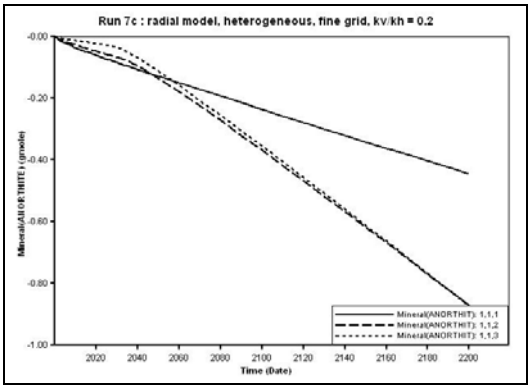

Figure C.137 AnorthiteDissolution / Precipitation for Run 7c: single-well case

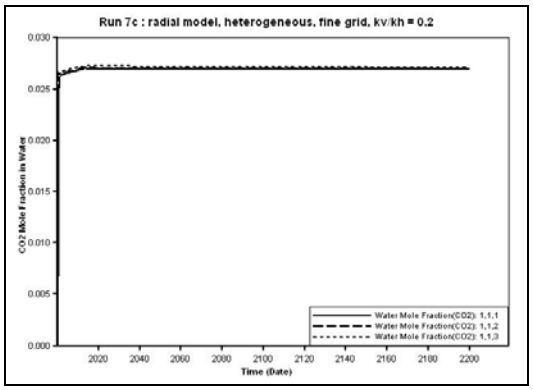

Figure C.135 CO_2 Mole Fraction in Water for Run 7c: single-well case

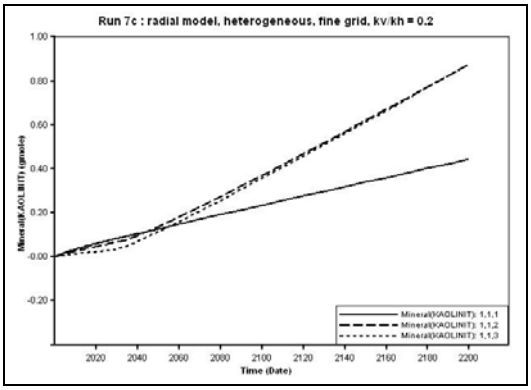

Figure C.138 Kaolinite Dissolution / Precipitation for Run 7c: single-well case

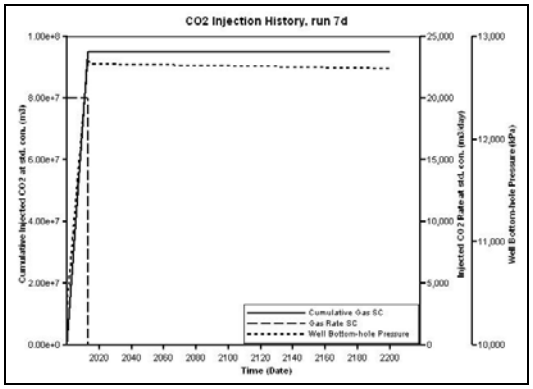

Figure C.139 CO_2 Injection History for Run 7d: single-well case, (CO_2 injection rate = 20000 sm^3/d)

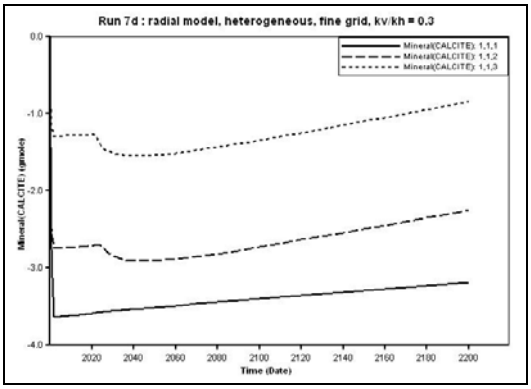

Figure C.142 Calcite Dissolution / Precipitation for Run 7d: single-well case

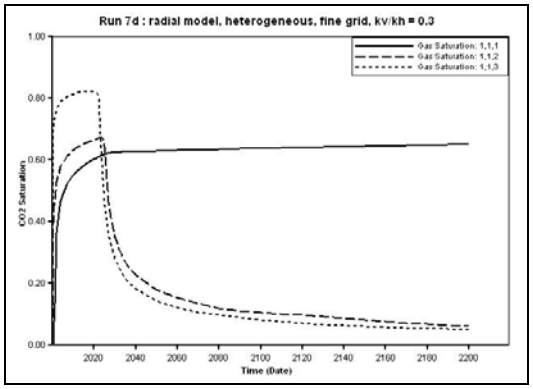

Figure C.140 CO_2 Saturation for Run 7d: single-well case

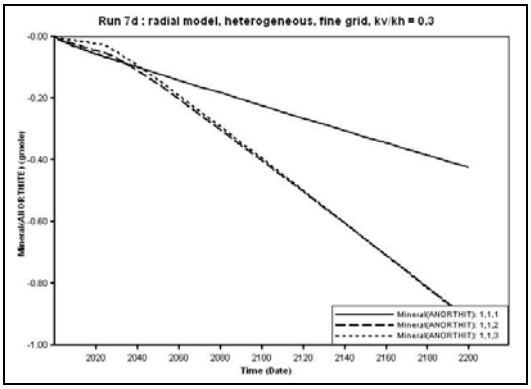

Figure C.143 AnorthiteDissolution / Precipitation for Run 7d: single-well case

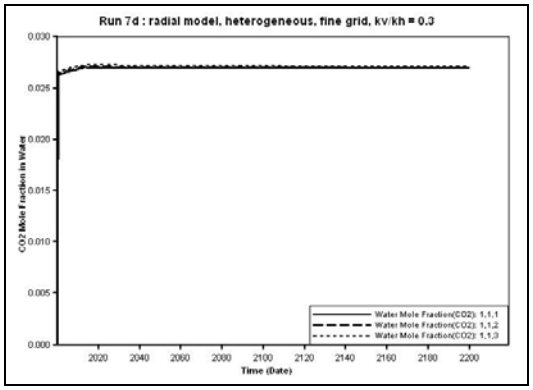

Figure C.141 CO_2 Mole Fraction in Water for Run 7d: single-well case

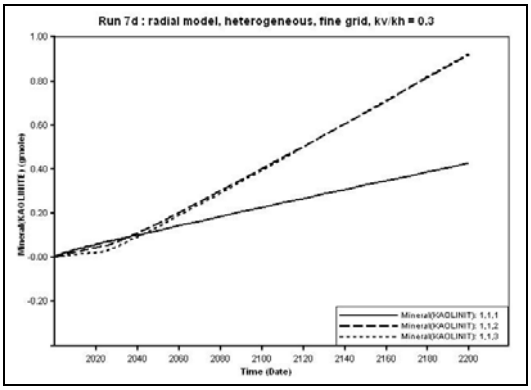

Figure C.144 Kaolinite Dissolution / Precipitation for Run 7d: single-well case

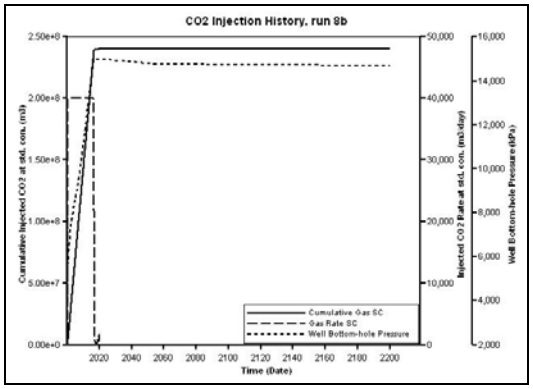

Figure C.145 CO_2 Injection History for Run 8b: single-well case, (CO_2 injection rate = 40000 sm^3/d)

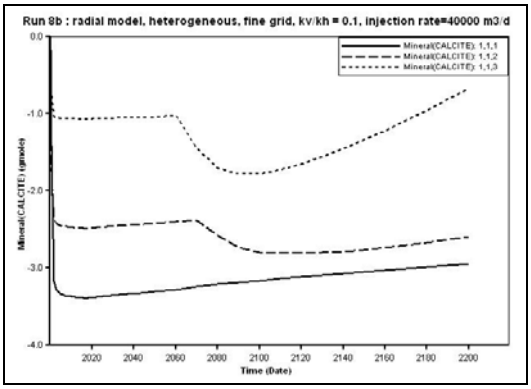

Figure C.148 Calcite Dissolution / Precipitation for Run 8b: single-well case

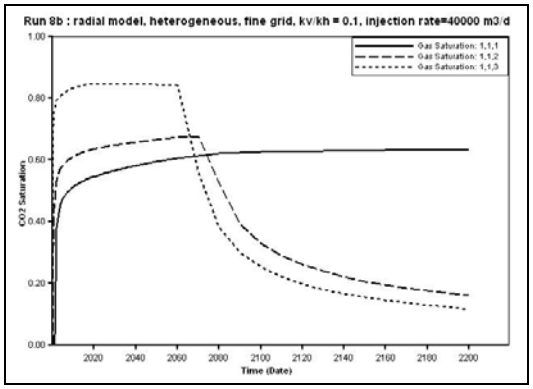

Figure C.146 CO_2 Saturation for Run 8b: single-well case

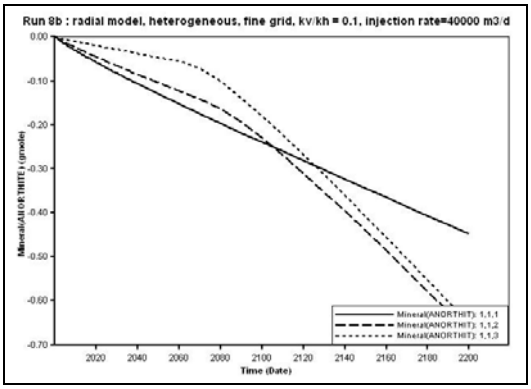

Figure C.149 AnorthiteDissolution / Precipitation for Run 8b: single-well case

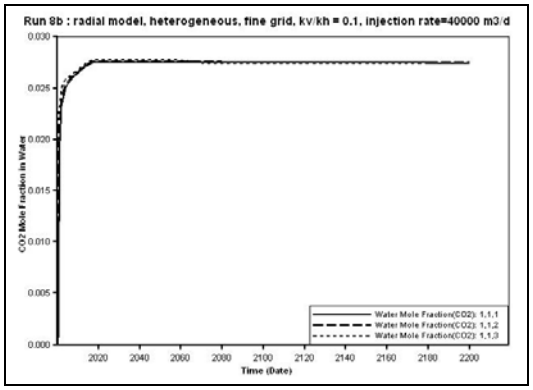

Figure C.147 CO_2 Mole Fraction in Water for Run 8b: single-well case

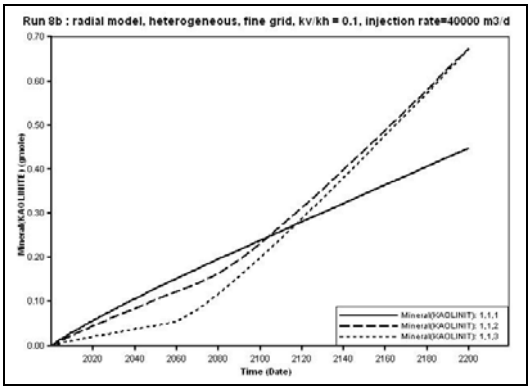

Figure C.150 Kaolinite Dissolution / Precipitation for Run 8b: single-well case

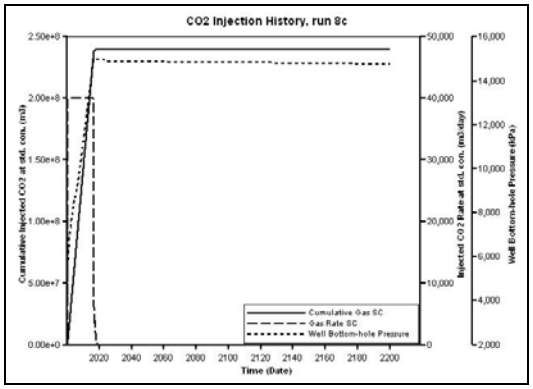

Figure C.151 CO_2 Injection History for Run 8c: single-well case, (CO_2 injection rate = 40000 sm^3/d)

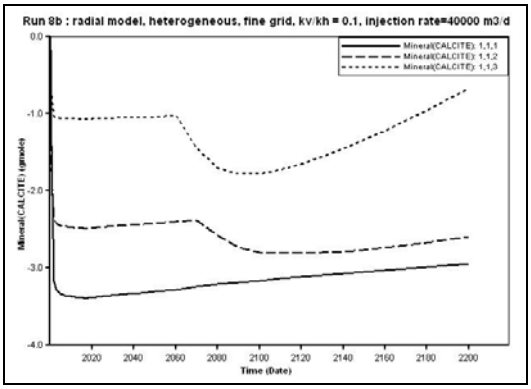

Figure C.154 Calcite Dissolution / Precipitation for Run 8c: single-well case

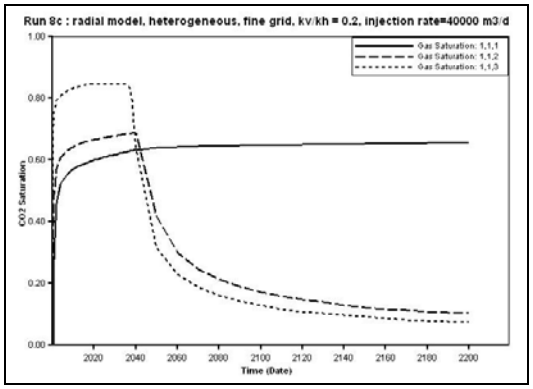

Figure C.152 CO_2 Saturation for Run 8c: single-well case

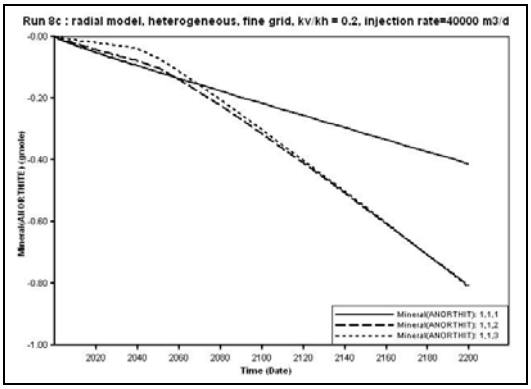

Figure C.155 AnorthiteDissolution / Precipitation for Run 8c: single-well case

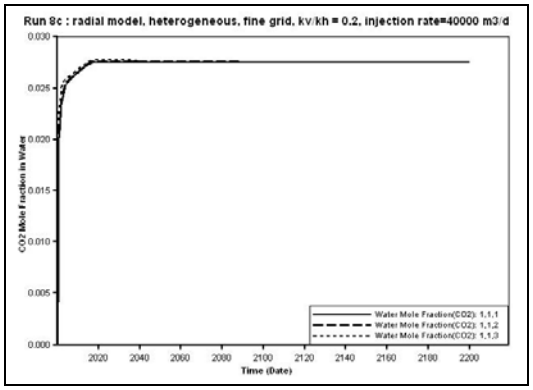

Figure C.153 CO_2 Mole Fraction in Water for Run 8c: single-well case

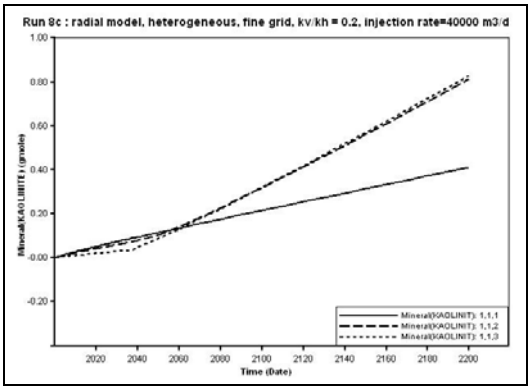

Figure C.156 Kaolinite Dissolution / Precipitation for Run 8c: single-well case

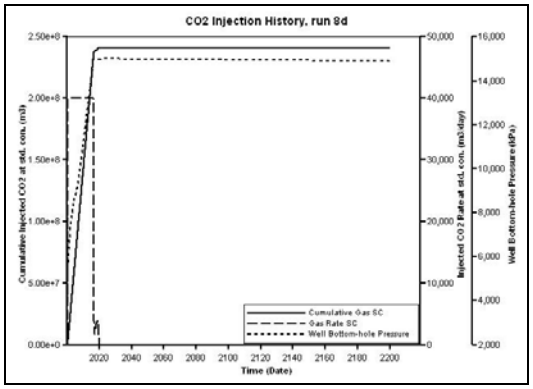

Figure C.157 CO_2 Injection History for Run 8d: single-well case, (CO_2 injection rate = 40000 sm^3/d)

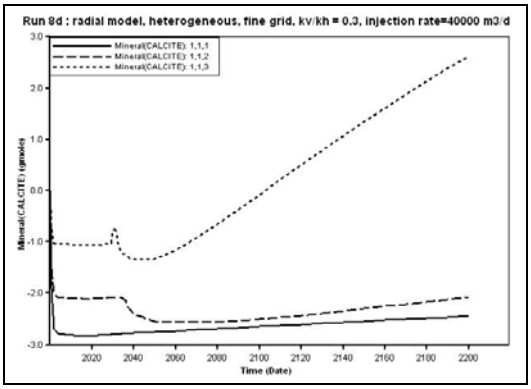

Figure C.160 Calcite Dissolution / Precipitation for Run 8d: single-well case

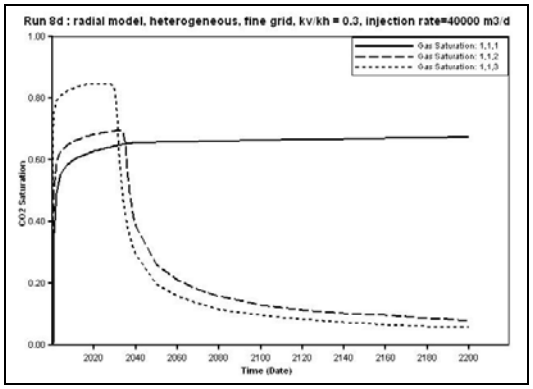

Figure C.158 CO_2 Saturation for Run 8d: single-well case

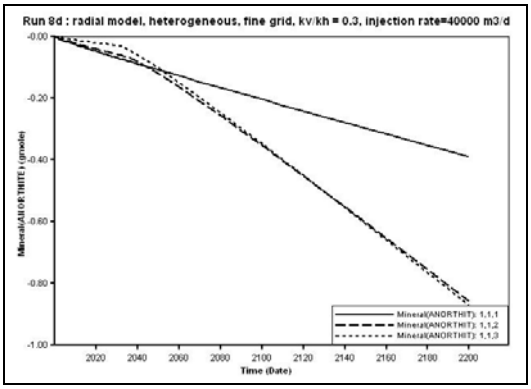

Figure C.161 AnorthiteDissolution / Precipitation for Run 8d: single-well case

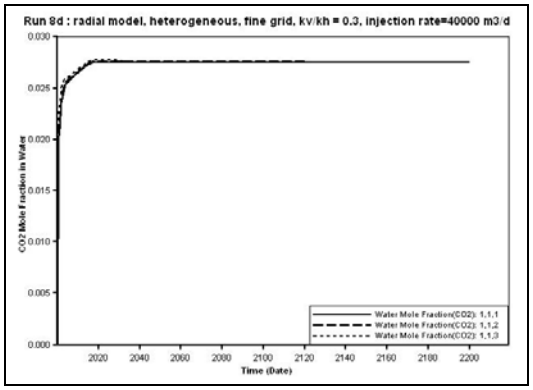

Figure C.159 CO_2 Mole Fraction in Water for Run 8d: single-well case

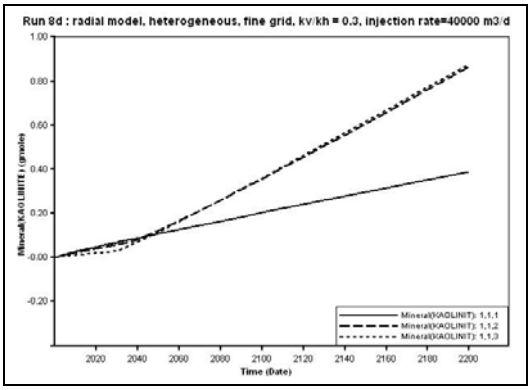

Figure C.162 Kaolinite Dissolution / Precipitation for Run 8d: single-well case

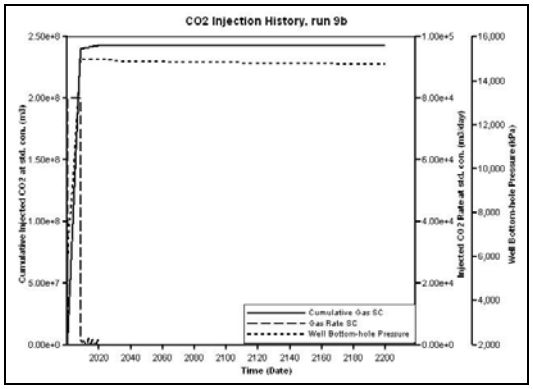

Figure C.163 CO_2 Injection History for Run 9b: single-well case, (CO_2 injection rate = 80000 sm^3/d)

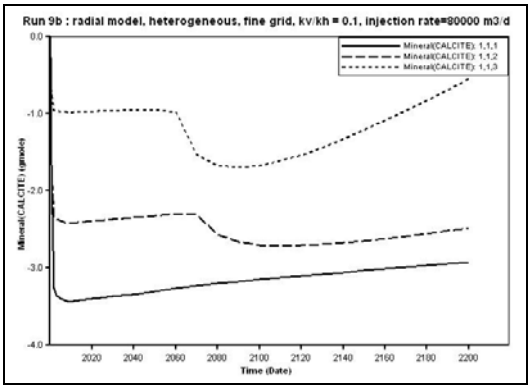

Figure C.166 Calcite Dissolution / Precipitation for Run 9b: single-well case

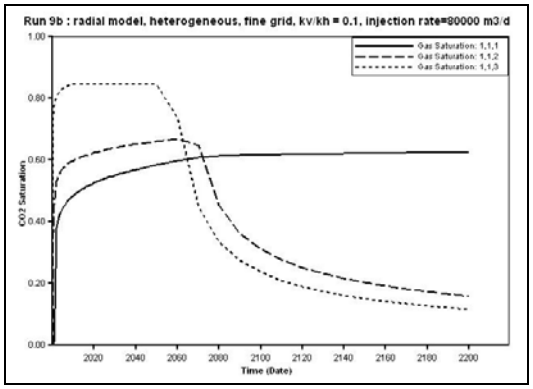

Figure C.164 CO_2 Saturation for Run 9b: single-well case

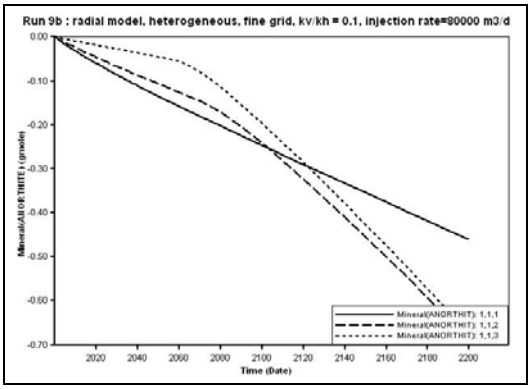

Figure C.167 AnorthiteDissolution / Precipitation for Run 9b: single-well case

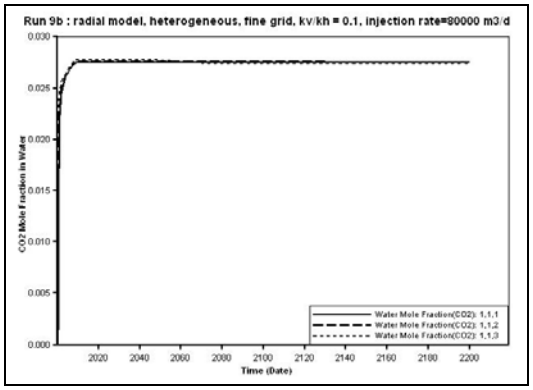

Figure C.165 CO_2 Mole Fraction in Water for Run 9b: single-well case

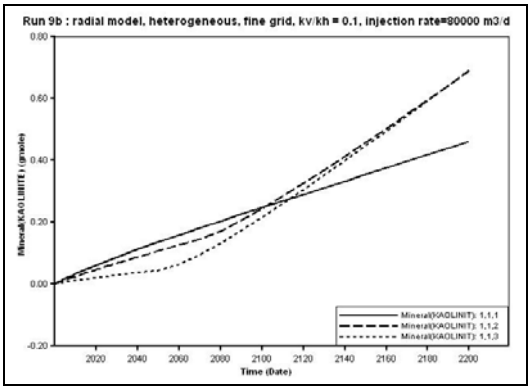

Figure C.168 Kaolinite Dissolution / Precipitation for Run 9b: single-well case

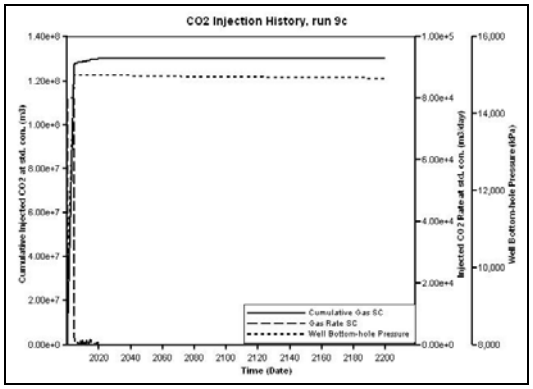

Figure C.169 CO_2 Injection History for Run 9c: single-well case, (CO_2 injection rate = 80000 sm^3/d)

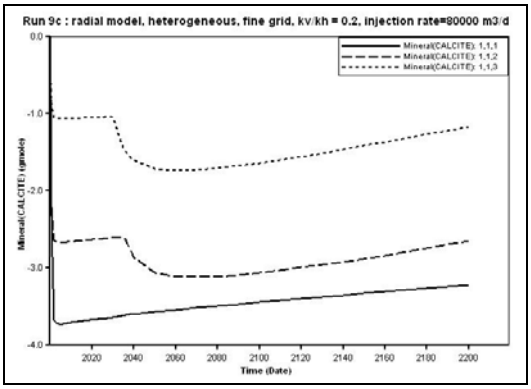

Figure C.172 Calcite Dissolution / Precipitation for Run 9c: single-well case

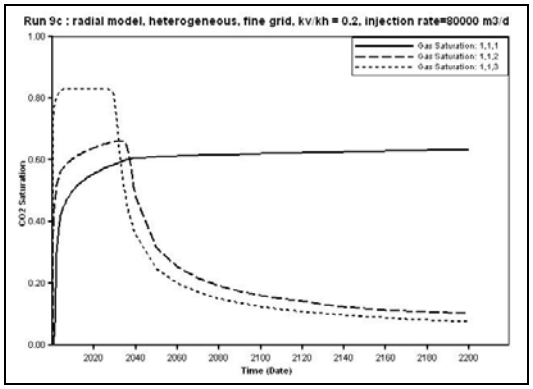

Figure C.170 CO_2 Saturation for Run 9c: single-well case

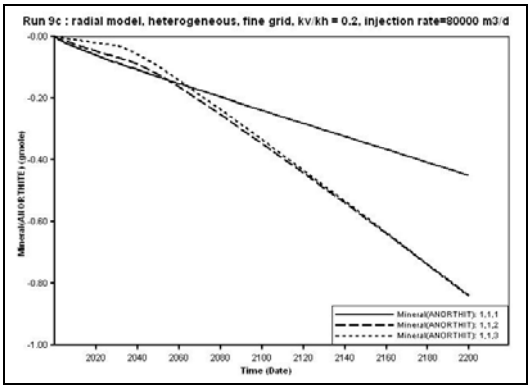

Figure C.173 AnorthiteDissolution / Precipitation for Run 9c: single-well case

Figure C.171 CO_2 Mole Fraction in Water for Run 9c: single-well case

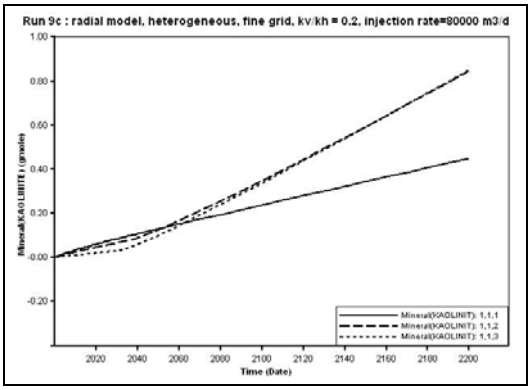

Figure C.174 Kaolinite Dissolution / Precipitation for Run 9c: single-well case

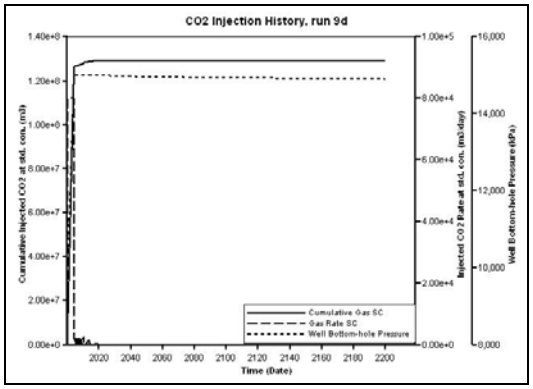

Figure C.175 CO_2 Injection History for Run 9d: single-well case, (CO_2 injection rate = 80000 sm^3/d)

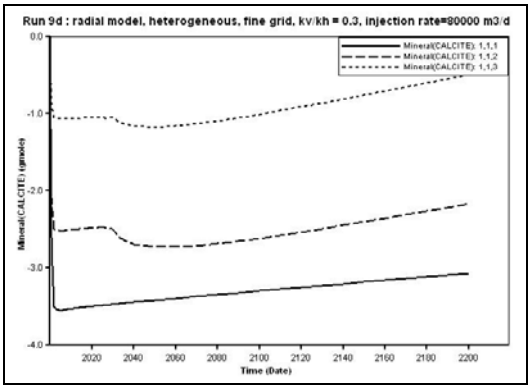

Figure C.178 Calcite Dissolution / Precipitation for Run 9d: single-well case

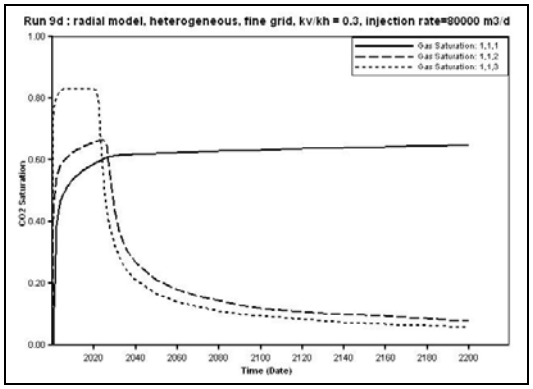

Figure C.176 CO_2 Saturation for Run 9d: single-well case

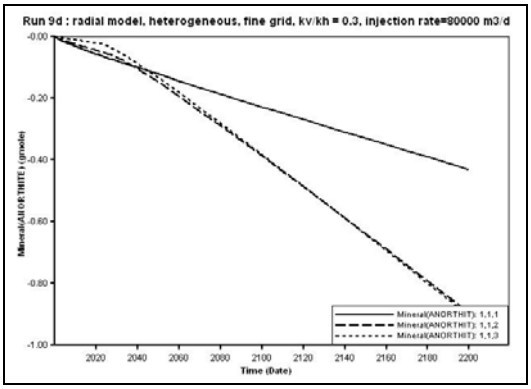

Figure C.179 AnorthiteDissolution / Precipitation for Run 9d: single-well case

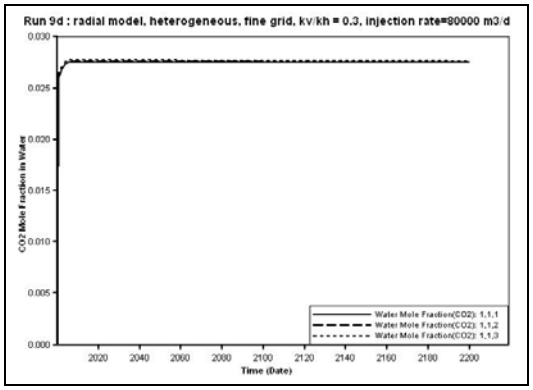

Figure C.177 CO_2 Mole Fraction in Water for Run 9d: single-well case

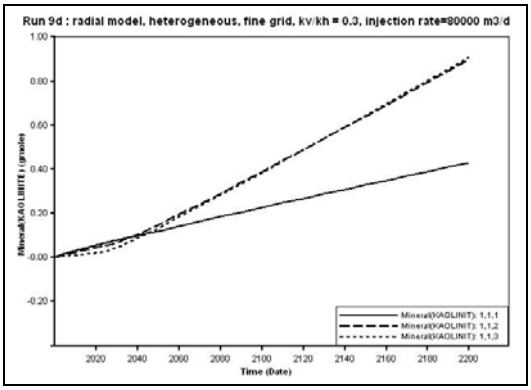

Figure C.180 Kaolinite Dissolution / Precipitation for Run 9d: single-well case

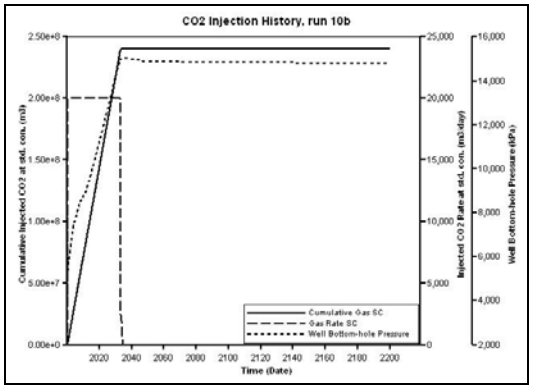

Figure C.181 CO_2 Injection History for Run 10b: single-well case, (CO_2 injection rate = 20000 sm^3/d)

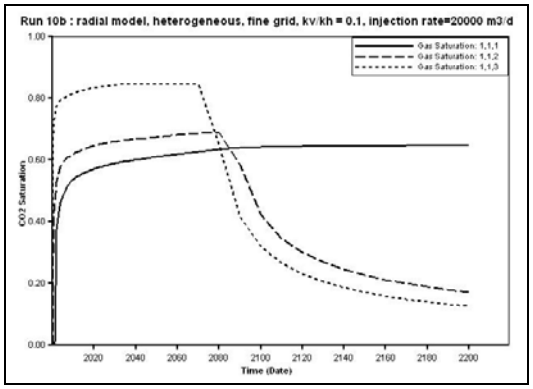

Figure C.182 CO_2 Saturation for Run 10b: single-well case

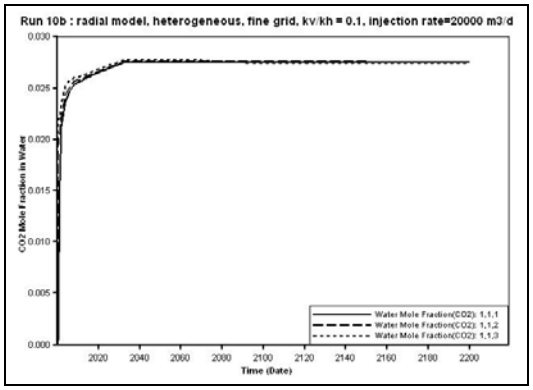

Figure C.183 CO_2 Mole Fraction in Water for Run 10b: single-well case

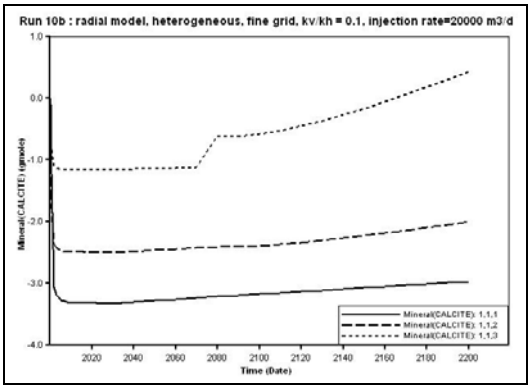

Figure C.184 Calcite Dissolution / Precipitation for Run 10b: single-well case

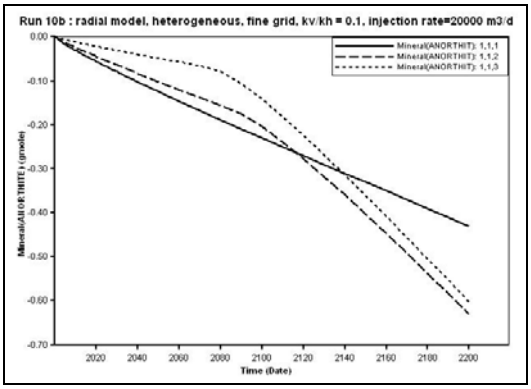

Figure C.185 AnorthiteDissolution / Precipitation for Run 10b: single-well case

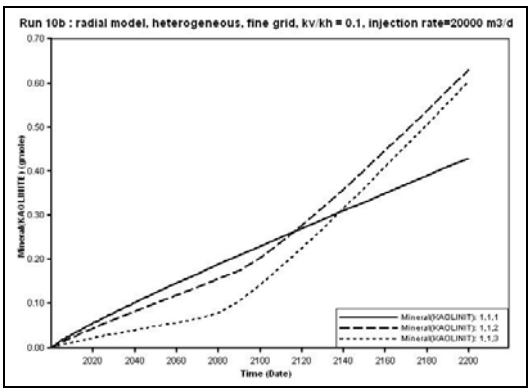

Figure C.186 Kaolinite Dissolution / Precipitation for Run 10b: single-well case

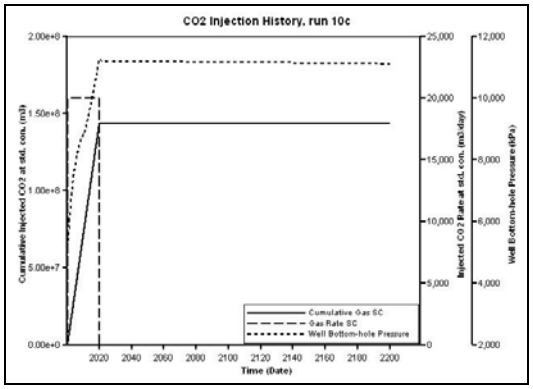

Figure C.187 CO_2 Injection History for Run 10c: single-well case, (CO_2 injection rate = 20000 sm^3/d)

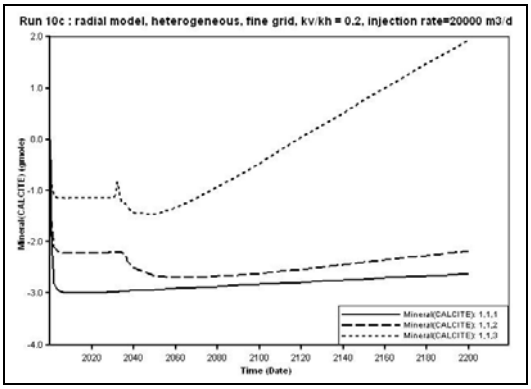

Figure C.190 Calcite Dissolution / Precipitation for Run 10c: single-well case

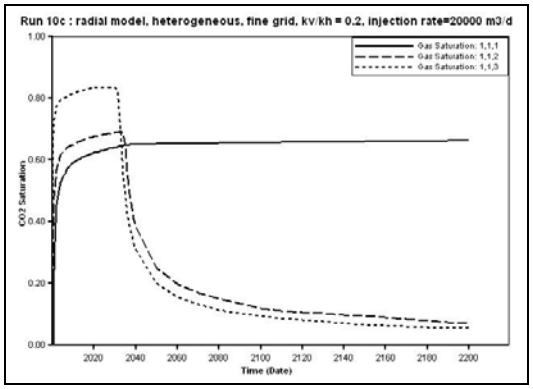

Figure C.188 CO_2 Saturation for Run 10c: single-well case

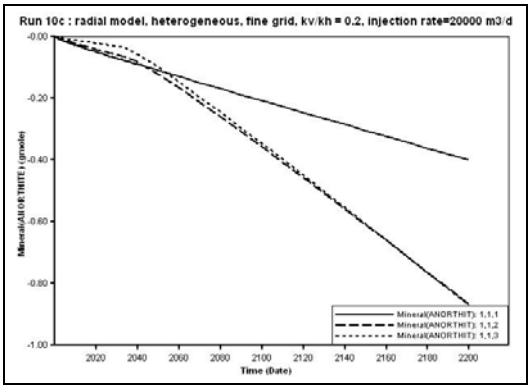

Figure C.191 AnorthiteDissolution / Precipitation for Run 10c: single-well case

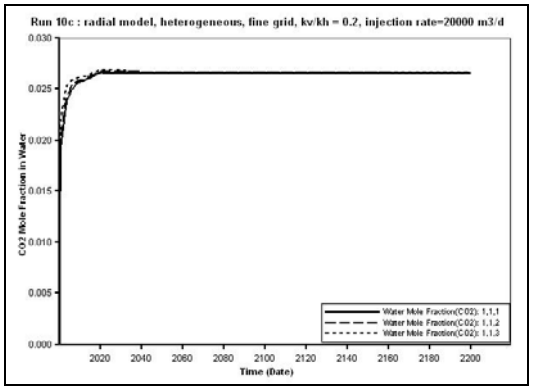

Figure C.189 CO_2 Mole Fraction in Water for Run 10c: single-well case

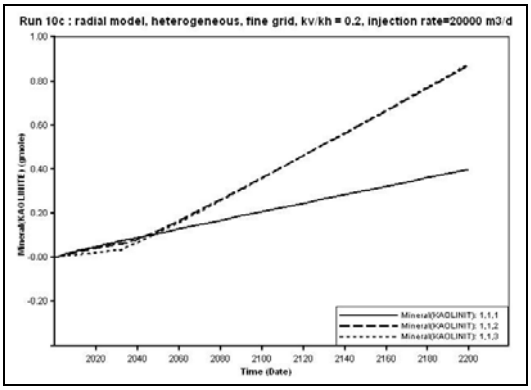

Figure C.192 Kaolinite Dissolution / Precipitation for Run 10c: single-well case

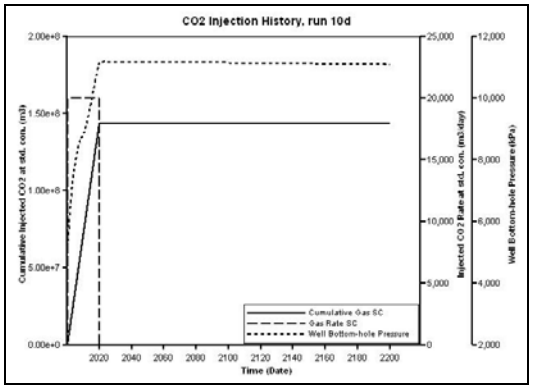

Figure C.193 CO_2 Injection History for Run 10d: single-well case, (CO_2 injection rate = 20000 sm^3/d)

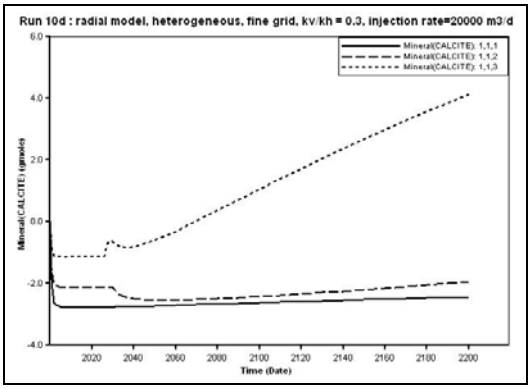

Figure C.196 Calcite Dissolution / Precipitation for Run 10d: single-well case

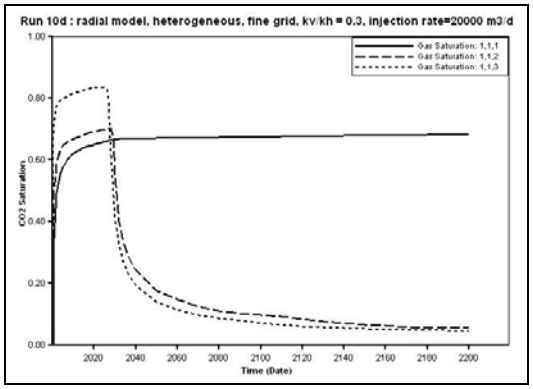

Figure C.194 CO_2 Saturation for Run 10d: single-well case

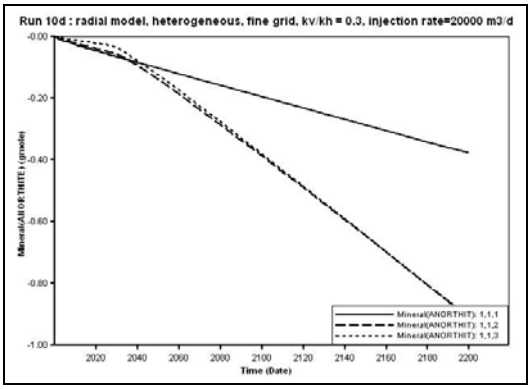

Figure C.197 AnorthiteDissolution / Precipitation for Run 10d: single-well case

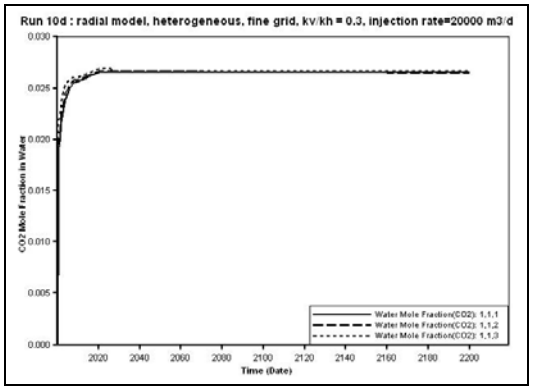

Figure C.195 CO_2 Mole Fraction in Water for Run 10d: single-well case

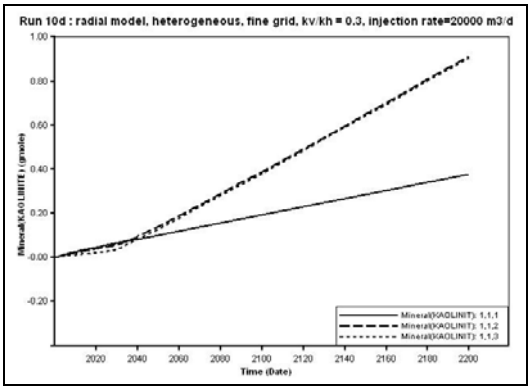

Figure C.198 Kaolinite Dissolution / Precipitation for Run 10d: single-well case

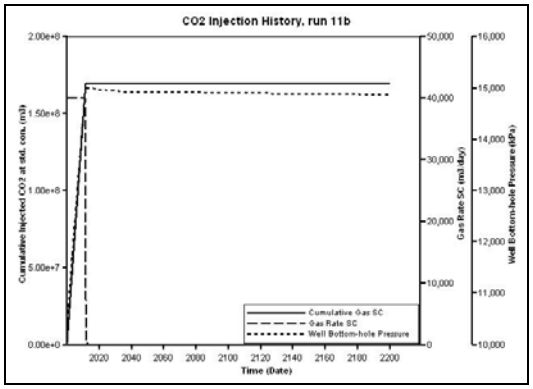

Figure C.199 CO_2 Injection History for Run 11b: single-well case, (CO_2 injection rate = 40000 sm^3/d)

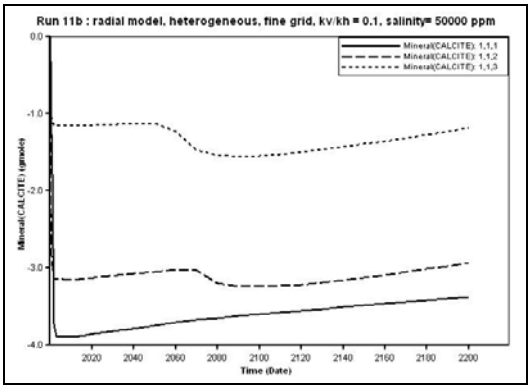

Figure C.202 Calcite Dissolution / Precipitation for Run 11b: single-well case

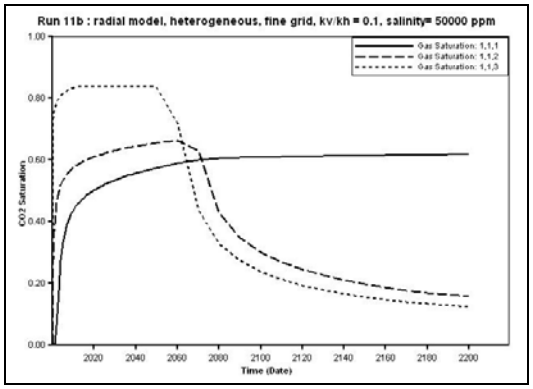

Figure C.200 CO_2 Saturation for Run 11b: single-well case

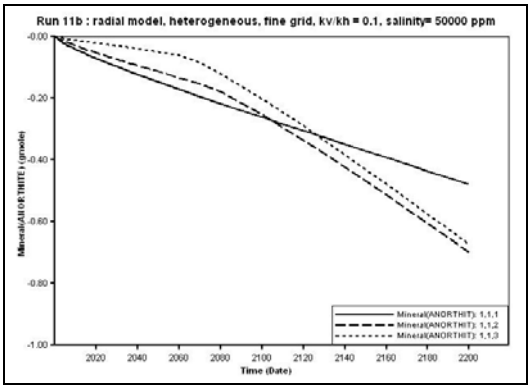

Figure C.203 AnorthiteDissolution / Precipitation for Run 11b: single-well case

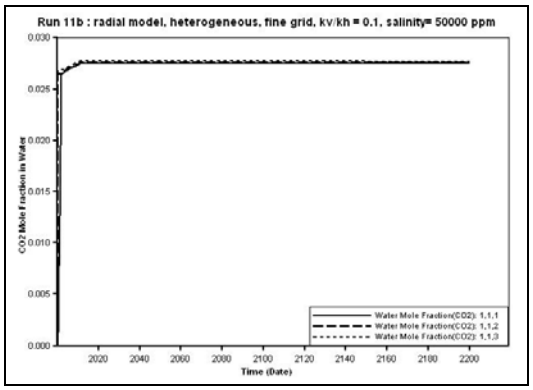

Figure C.201 CO_2 Mole Fraction in Water for Run 11b: single-well case

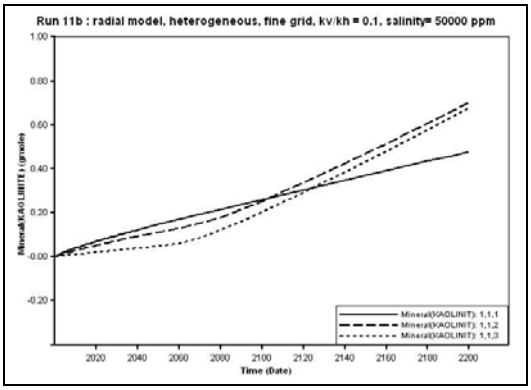

Figure C.204 Kaolinite Dissolution / Precipitation for Run 11b: single-well case

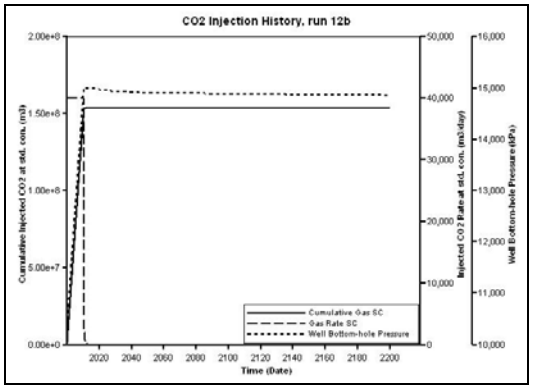

Figure C.205 CO_2 Injection History for Run 12b: single-well case, (CO_2 injection rate = 40000 sm^3/d)

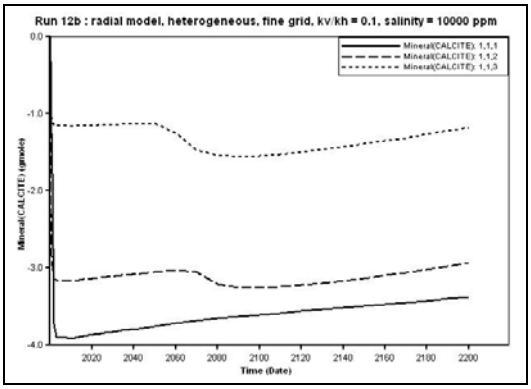

Figure C.208 Calcite Dissolution / Precipitation for Run 12b: single-well case

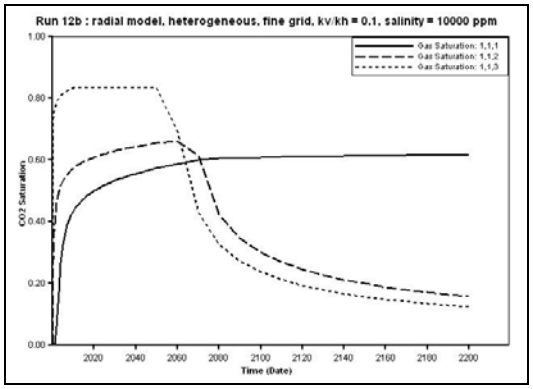

Figure C.206 CO_2 Saturation for Run 12b: single-well case

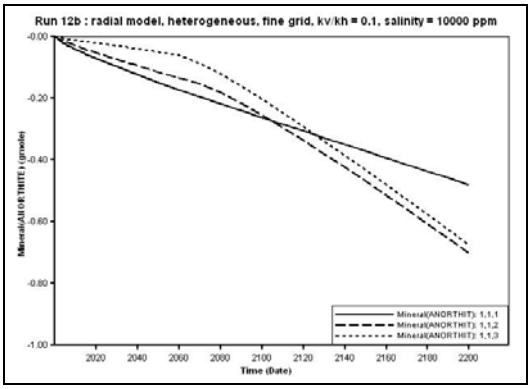

Figure C.209 AnorthiteDissolution / Precipitation for Run 12b: single-well case

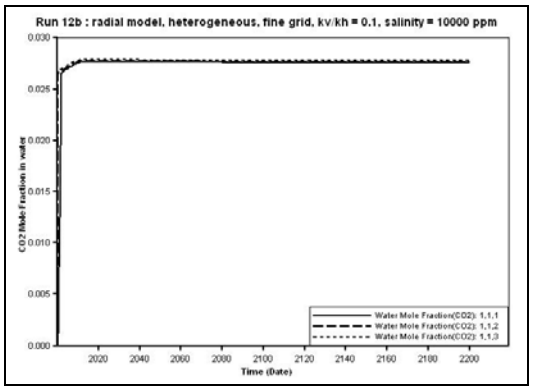

Figure C.207 CO_2 Mole Fraction in Water for Run 12b: single-well case

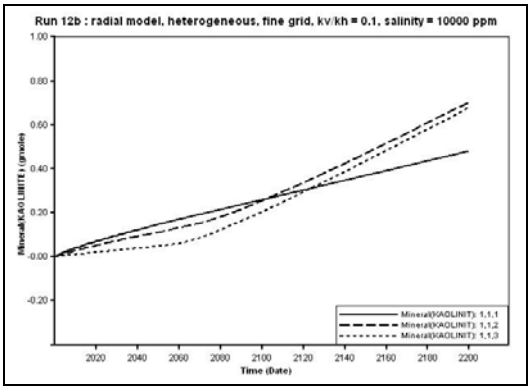

Figure C.210 Kaolinite Dissolution / Precipitation for Run 12b: single-well case

APPENDIX D

CO_2 Propagations in Layer 1 (top layer) for a Single-well Aquifer Model

Table D.1 CO_2 Propagation in layer 1 for Run 4b, single-well model

Date	2001	2005	2006	2014	2017	2020	2040	2200
Distance (m)	1 (years)	5	6	14	17	20	40	200
0.0	1	1	1	1	1	1	1	1
0.50	0.9914	0.9994	0.9994	0.9996	0.9996	0.9996	0.9996	0.9996
14.00	0.0114	0.9993	0.9994	0.9995	0.9995	0.9996	0.9996	0.9996
52.50	0.0010	0.0300	0.4084	0.9995	0.9995	0.9995	0.9995	0.9996
102.50	0.0010	0.0009	0.0009	0.2088	0.9984	0.9993	0.9994	0.9995
117.50	0.0010	0.0009	0.0009	0.0202	0.1856	0.9950	0.9993	0.9995
135.00	0.0010	0.0009	0.0009	0.0019	0.0150	0.0779	0.9972	0.9978
156.25	0.0010	0.0009	0.0009	0.0009	0.0015	0.0052	0.0727	0.0752
180.00	0.0010	0.0009	0.0009	0.0008	0.0009	0.0010	0.0041	0.0051

Table D.2 CO_2 Propagation in layer 1 for Run 4c, single-well model

Date	2001	2002	2004	2005	2009	2011	2014	2018	2025	2050	2200
Distance (m)	1 (years)	2	4	5	9	11	14	18	25	50	200
0	1.000	1.000	1.000	1.000	1.000	1.000	1.000	1.000	1.000	1.000	1.000
0.50	0.999	0.999	0.999	0.999	1.000	1.000	1.000	1.000	1.000	1.000	1.000
14.00	0.472	0.999	0.999	0.999	1.000	1.000	1.000	1.000	1.000	1.000	1.000
52.50	0.001	0.001	0.062	0.999	0.999	1.000	1.000	1.000	1.000	1.000	1.000
102.50	0.001	0.001	0.001	0.001	0.154	0.998	0.999	0.999	0.999	0.999	1.000
117.50	0.001	0.001	0.001	0.001	0.014	0.161	0.999	0.999	0.999	0.999	0.999
135.00	0.001	0.001	0.001	0.001	0.001	0.012	0.207	0.998	0.999	0.999	0.999
156.25	0.001	0.001	0.001	0.001	0.001	0.001	0.014	0.120	0.336	0.323	0.137
180.00	0.001	0.001	0.001	0.001	0.001	0.001	0.001	0.007	0.014	0.015	0.013
205.00	0.001	0.001	0.001	0.001	0.001	0.001	0.001	0.001	0.001	0.001	0.002

Table D.3 CO_2 Propagation in layer 1 for Run 4d, single-well model

Date	2001	2003	2004	2007	2009	2011	2015	2020	2040	2200
Distance (m)	1 (years)	3	4	7	9	11	15	20	40	200
0	1.0000	1.0000	1.0000	1.0000	1.0000	1.0000	1.0000	1.0000	1.0000	1.0000
0.50	0.9992	0.9995	0.9995	0.9996	0.9996	0.9996	0.9996	0.9996	0.9996	0.9996
14.00	0.9938	0.9994	0.9995	0.9995	0.9996	0.9996	0.9996	0.9996	0.9996	0.9996
52.50	0.0010	0.0177	0.9989	0.9995	0.9995	0.9995	0.9996	0.9996	0.9996	0.9996
102.50	0.0010	0.0010	0.0009	0.0925	0.9981	0.9993	0.9995	0.9995	0.9995	0.9996
117.50	0.0010	0.0010	0.0009	0.0066	0.1522	0.9980	0.9994	0.9994	0.9995	0.9995
135.00	0.0010	0.0010	0.0009	0.0011	0.0109	0.1134	0.9989	0.9993	0.9993	0.9989
156.25	0.0010	0.0010	0.0009	0.0009	0.0013	0.0076	0.1940	0.9016	0.7457	0.1196
180.00	0.0010	0.0010	0.0009	0.0009	0.0009	0.0011	0.0109	0.0235	0.0237	0.0158
205.00	0.0010	0.0010	0.0009	0.0009	0.0009	0.0009	0.0012	0.0016	0.0017	0.0022

Table D.4 CO_2 Propagation in layer 1 for Run 5b, single-well model

Date	2001	2002	2003	2007	2010	2020	2025	2035	2200
Distance (m)	1 (years)	2	3	7	10	20	25	35	200
0	1.0000	1.0000	1.0000	1.0000	1.0000	1.0000	1.0000	1.0000	1.0000
0.50	0.4127	0.9957	0.9985	0.9994	0.9994	0.9995	0.9995	0.9996	0.9996
14.00	0.0040	0.1966	0.9754	0.9992	0.9994	0.9995	0.9995	0.9995	0.9996
52.50	0.0010	0.0010	0.0010	0.2752	0.9967	0.9994	0.9995	0.9995	0.9996
102.50	0.0010	0.0010	0.0010	0.0009	0.0009	0.1704	0.9974	0.9993	0.9995
117.50	0.0010	0.0010	0.0010	0.0009	0.0009	0.0189	0.1423	0.9978	0.9994
135.00	0.0010	0.0010	0.0010	0.0009	0.0009	0.0020	0.0119	0.1196	0.9951
156.25	0.0010	0.0010	0.0010	0.0009	0.0009	0.0009	0.0014	0.0092	0.0597
180.00	0.0010	0.0010	0.0010	0.0009	0.0009	0.0008	0.0009	0.0012	0.0030

Table D.5 CO_2 Propagation in layer 1 for Run 5c, single-well model

Date	2001	2002	2006	2007	2012	2013	2014	2015	2016	2017	2020	2022	2025	2040	2200
Distance (m)	1 (years)	2	6	7	12	13	14	15	16	17	20	22	25	40	200
0	1.000	1.000	1.000	1.000	1.000	1.000	1.000	1.000	1.000	1.000	1.000	1.000	1.000	1.000	1.000
1.00	0.995	0.999	0.999	0.999	1.000	1.000	1.000	1.000	1.000	1.000	1.000	1.000	1.000	1.000	1.000
14.00	0.038	0.994	0.999	0.999	1.000	1.000	1.000	1.000	1.000	1.000	1.000	1.000	1.000	1.000	1.000
53.00	0.001	0.001	0.736	0.999	0.999	0.999	0.999	1.000	1.000	1.000	1.000	1.000	1.000	1.000	1.000
103.00	0.001	0.001	0.001	0.001	0.121	0.322	0.986	0.998	0.999	0.999	0.999	0.999	0.999	0.999	1.000
118.00	0.001	0.001	0.001	0.001	0.011	0.030	0.076	0.152	0.303	0.823	0.999	0.999	0.999	0.999	0.999
135.00	0.001	0.001	0.001	0.001	0.001	0.003	0.005	0.012	0.024	0.045	0.174	0.450	0.990	0.998	0.999
156.00	0.001	0.001	0.001	0.001	0.001	0.001	0.001	0.001	0.002	0.003	0.013	0.025	0.053	0.104	0.098
180.00	0.001	0.001	0.001	0.001	0.001	0.001	0.001	0.001	0.001	0.001	0.001	0.002	0.003	0.006	0.008

Table D.6 CO_2 Propagation in layer 1 for Run 5d, single-well model

Date	2001	2002	2005	2010	2012	2013	2015	2016	2017	2020	2040	2200
Distance (m)	1 (years)	2	5	10	12	13	15	16	17	20	40	200
0	1	1	1	1	1	1	1	1	1	1	1	1
0.50	0.998	0.999	0.999	1.000	1.000	1.000	1.000	1.000	1.000	1.000	1.000	1.000
14.00	0.298	0.999	0.999	1.000	1.000	1.000	1.000	1.000	1.000	1.000	1.000	1.000
52.50	0.001	0.001	0.985	0.999	1.000	1.000	1.000	1.000	1.000	1.000	1.000	1.000
102.50	0.001	0.001	0.001	0.232	0.998	0.999	0.999	0.999	0.999	0.999	0.999	1.000
117.50	0.001	0.001	0.001	0.022	0.190	0.683	0.999	0.999	0.999	0.999	0.999	0.999
135.00	0.001	0.001	0.001	0.002	0.016	0.040	0.172	0.395	0.916	0.998	0.999	0.999
156.25	0.001	0.001	0.001	0.001	0.002	0.003	0.013	0.023	0.039	0.104	0.249	0.147
180.00	0.001	0.001	0.001	0.001	0.001	0.001	0.001	0.002	0.003	0.006	0.013	0.014
205.00	0.001	0.001	0.001	0.001	0.001	0.001	0.001	0.001	0.001	0.001	0.001	0.002

Table D.7 CO_2 Propagation in layer 1 for Run 6b, single-well model

Date	2001	2002	2003	2007	2008	2020	2022	2023	2028	2030	2035	2050	2060	2200
Distance (m)	1 (year)	2	3	7	8	20	22	23	28	30	35	50	60	200
0	1	1	1	1	1	1	1	1	1	1	1	1	1	1
0.50	0.430	0.996	0.999	0.999	0.999	1.000	1.000	1.000	1.000	1.000	1.000	1.000	1.000	1.000
14.00	0.004	0.212	0.980	0.999	0.999	1.000	1.000	1.000	1.000	1.000	1.000	1.000	1.000	1.000
52.50	0.001	0.001	0.001	0.294	0.921	0.999	0.999	0.999	0.999	1.000	1.000	1.000	1.000	1.000
102.50	0.001	0.001	0.001	0.001	0.001	0.181	0.607	0.983	0.999	0.999	0.999	0.999	0.999	0.999
117.50	0.001	0.001	0.001	0.001	0.001	0.020	0.049	0.077	0.410	0.936	0.998	0.999	0.999	0.999
135.00	0.001	0.001	0.001	0.001	0.001	0.002	0.004	0.006	0.031	0.052	0.128	0.692	0.962	0.997
156.25	0.001	0.001	0.001	0.001	0.001	0.001	0.001	0.001	0.003	0.004	0.010	0.032	0.037	0.063
180.00	0.001	0.001	0.001	0.001	0.001	0.001	0.001	0.001	0.001	0.001	0.001	0.002	0.002	0.003

Table D.8 CO_2 Propagation in layer 1 for Run 6c, single-well model

Date	2001	2002	2006	2013	2015	2020	2023	2030	2050	2200
Distance (m)	1 (year)	2	6	13	15	20	23	30	50	200
0	1	1	1	1	1	1	1	1	1	1
0.50	0.995	0.999	0.999	1.000	1.000	1.000	1.000	1.000	1.000	1.000
14.00	0.040	0.994	0.999	1.000	1.000	1.000	1.000	1.000	1.000	1.000
52.50	0.001	0.001	0.768	0.999	1.000	1.000	1.000	1.000	1.000	1.000
102.50	0.001	0.001	0.001	0.363	0.998	0.999	0.999	0.999	0.999	1.000
117.50	0.001	0.001	0.001	0.033	0.162	0.999	0.999	0.999	0.999	0.999
135.00	0.001	0.001	0.001	0.003	0.013	0.195	0.862	0.998	0.999	0.999
156.25	0.001	0.001	0.001	0.001	0.001	0.014	0.037	0.094	0.118	0.109
180.00	0.001	0.001	0.001	0.001	0.001	0.001	0.002	0.005	0.007	0.009

Table D.9 CO_2 Propagation in layer 1 for Run 6d, single-well model

Date	2001	2002	2005	2010	2011	2012	2013	2016	2020	2025	2050	2200
Distance (m)	1 (years)	2	5	10	11	12	13	16	20	25	50	200
0	1	1	1	1	1	1	1	1	1	1	1	1
0.50	0.998	0.999	0.999	1.000	1.000	1.000	1.000	1.000	1.000	1.000	1.000	1.000
14.00	0.332	0.999	0.999	1.000	1.000	1.000	1.000	1.000	1.000	1.000	1.000	1.000
52.50	0.001	0.001	0.992	0.999	1.000	1.000	1.000	1.000	1.000	1.000	1.000	1.000
102.50	0.001	0.001	0.001	0.257	0.991	0.999	0.999	0.999	0.999	0.999	0.999	1.000
117.50	0.001	0.001	0.001	0.024	0.084	0.207	0.822	0.999	0.999	0.999	0.999	0.999
135.00	0.001	0.001	0.001	0.002	0.006	0.017	0.045	0.483	0.998	0.999	0.999	0.999
156.25	0.001	0.001	0.001	0.001	0.001	0.002	0.003	0.025	0.115	0.236	0.314	0.180
180.00	0.001	0.001	0.001	0.001	0.001	0.001	0.001	0.002	0.007	0.012	0.014	0.017
205.00	0.001	0.001	0.001	0.001	0.001	0.001	0.001	0.001	0.001	0.001	0.001	0.002

Table D.10 CO_2 Propagation in layer 1 for Run 7b, single-well model

Date	2001	2002	2003	2004	2010	2011	2012	2030	2035	2050	2200
Distance (m)	1 (years)	2	3	4	10	11	12	30	35	50	200
0	1	1	1	1	1	1	1	1	1	1	1
0.50	0.288	0.994	0.998	0.999	0.999	0.999	0.999	1.000	1.000	1.000	1.000
14.00	0.002	0.032	0.579	0.993	0.999	0.999	0.999	1.000	1.000	1.000	1.000
52.50	0.001	0.001	0.001	0.001	0.113	0.359	0.914	0.999	0.999	0.999	0.999
102.50	0.001	0.001	0.001	0.001	0.001	0.001	0.001	0.216	0.475	0.975	0.995
117.50	0.001	0.001	0.001	0.001	0.001	0.001	0.001	0.020	0.037	0.063	0.117
135.00	0.001	0.001	0.001	0.001	0.001	0.001	0.001	0.002	0.003	0.004	0.009

Table D.11 CO_2 Propagation in layer 1 for Run 7c, single-well model

Date	2001	2002	2008	2009	2018	2019	2020	2030	2050	2200
Distance (m)	1 (years)	2	8	9	18	19	20	30	50	200
0	1	1	1	1	1	1	1	1	1	1
0.50	0.992	0.999	0.999	0.999	1.000	1.000	1.000	1.000	1.000	1.000
14.00	0.004	0.849	0.999	0.999	1.000	1.000	1.000	1.000	1.000	1.000
52.50	0.001	0.001	0.324	0.999	0.999	0.999	0.999	0.999	0.999	1.000
102.50	0.001	0.001	0.001	0.001	0.395	0.719	0.981	0.998	0.999	0.999
117.50	0.001	0.001	0.001	0.001	0.031	0.047	0.067	0.164	0.181	0.159
135.00	0.001	0.001	0.001	0.001	0.002	0.003	0.004	0.011	0.013	0.019

Table D.12 CO_2 Propagation in layer 1 for Run 7d, single-well model

Date	2001	2002	2006	2007	2013	2014	2015	2020	2030	2040	2200
Distance (m)	1 (years)	2	6	7	13	14	15	20	30	40	200
0	1	1	1	1	1	1	1	1	1	1	1
0.50	0.998	0.999	0.999	0.999	1.000	1.000	1.000	1.000	1.000	1.000	1.000
14.00	0.009	0.997	0.999	0.999	1.000	1.000	1.000	1.000	1.000	1.000	1.000
52.50	0.001	0.001	0.120	0.998	0.999	0.999	0.999	0.999	1.000	1.000	1.000
102.50	0.001	0.001	0.001	0.001	0.134	0.331	0.931	0.999	0.999	0.999	0.999
117.50	0.001	0.001	0.001	0.001	0.012	0.027	0.057	0.269	0.376	0.373	0.186
135.00	0.001	0.001	0.001	0.001	0.001	0.002	0.004	0.018	0.021	0.023	0.027
156.25	0.001	0.001	0.001	0.001	0.001	0.001	0.001	0.002	0.002	0.002	0.003

Table D.13 CO_2 Propagation in layer 1 for Run 8b, single-well model

Date	2001	2002	2004	2013	2014	2016	2017	2019	2020	2021	2023	2024	2028	2029	2030	2040	2050	2060	2200
Distance (m)	1 (years)	2	4	13	14	16	17	19	20	21	23	24	28	29	30	40	50	60	200
0	1	1	1	1	1	1	1	1	1	1	1	1	1	1	1	1	1	1	1
0.50	0.952	0.997	0.998	1.000	1.000	1.000	1.000	1.000	1.000	1.000	1.000	1.000	1.000	1.000	1.000	1.000	1.000	1.000	1.000
14.00	0.046	0.995	0.998	0.999	0.999	1.000	1.000	1.000	1.000	1.000	1.000	1.000	1.000	1.000	1.000	1.000	1.000	1.000	1.000
52.50	0.002	0.001	0.989	0.999	0.999	0.999	0.999	0.999	0.999	0.999	0.999	0.999	1.000	1.000	1.000	1.000	1.000	1.000	1.000
102.50	0.002	0.001	0.001	0.248	0.973	0.999	0.999	0.999	0.999	0.999	0.999	0.999	0.999	0.999	0.999	0.999	0.999	1.000	1.000
117.50	0.002	0.001	0.001	0.028	0.072	0.310	0.900	0.999	0.999	0.999	0.999	0.999	0.999	0.999	0.999	0.999	0.999	0.999	1.000
135.00	0.002	0.001	0.001	0.004	0.008	0.038	0.078	0.286	0.760	0.996	0.999	0.999	0.999	0.999	0.999	0.999	0.999	0.999	0.999
156.25	0.002	0.001	0.001	0.001	0.002	0.005	0.010	0.041	0.078	0.147	0.457	0.978	0.999	0.999	0.999	0.999	0.999	0.999	0.999
180.00	0.002	0.001	0.001	0.001	0.001	0.001	0.001	0.003	0.006	0.011	0.032	0.054	0.359	0.646	0.968	0.999	0.999	0.999	0.999
205.00	0.002	0.001	0.001	0.001	0.001	0.001	0.001	0.001	0.001	0.001	0.002	0.003	0.015	0.022	0.031	0.227	0.709	0.957	0.992
230.00	0.002	0.001	0.001	0.001	0.001	0.001	0.001	0.001	0.001	0.001	0.001	0.001	0.001	0.002	0.002	0.011	0.024	0.028	0.040
255.00	0.002	0.001	0.001	0.001	0.001	0.001	0.001	0.001	0.001	0.001	0.001	0.001	0.001	0.001	0.001	0.001	0.001	0.001	0.002

Table D.14 CO_2 Propagation in layer 1 for Run 8c, single-well model

Date	2001	2002	2003	2005	2007	2010	2011	2012	2020	2023	2026	2040	2200
Distance (m)	1 (years)	2	3	5	7	10	11	12	20	23	26	40	200
0	1	1	1	1	1	1	1	1	1	1	1	1	1
0.50	0.996	0.998	0.998	0.999	0.999	1.000	1.000	1.000	1.000	1.000	1.000	1.000	1.000
14.00	0.554	0.997	0.998	0.999	0.999	0.999	1.000	1.000	1.000	1.000	1.000	1.000	1.000
52.50	0.002	0.006	0.998	0.999	0.999	0.999	0.999	0.999	1.000	1.000	1.000	1.000	1.000
102.50	0.002	0.001	0.003	0.523	0.969	0.999	0.999	0.999	0.999	0.999	0.999	1.000	1.000
135.00	0.002	0.001	0.001	0.003	0.010	0.204	0.536	0.996	0.999	0.999	0.999	0.999	1.000
205.00	0.002	0.001	0.001	0.001	0.001	0.001	0.001	0.001	0.095	0.372	0.972	0.998	0.998
230.00	0.002	0.001	0.001	0.001	0.001	0.001	0.001	0.001	0.005	0.016	0.036	0.074	0.065
255.00	0.002	0.001	0.001	0.001	0.001	0.001	0.001	0.001	0.001	0.001	0.002	0.003	0.002

Table D.15 CO_2 Propagation in layer 1 for Run 8d, single-well model

Date	2001	2002	2003	2004	2007	2008	2009	2018	2019	2025	2040	2200
Distance (m)	1 (years)	2	3	4	7	8	9	18	19	25	40	200
0	1	1	1	1	1	1	1	1	1	1	1	1
0.50	0.996	0.998	0.998	0.999	0.999	0.999	1.000	1.000	1.000	1.000	1.000	1.000
14.00	0.995	0.998	0.998	0.999	0.999	0.999	0.999	1.000	1.000	1.000	1.000	1.000
52.50	0.002	0.986	0.998	0.998	0.999	0.999	0.999	1.000	1.000	1.000	1.000	1.000
102.50	0.002	0.001	0.338	0.997	0.999	0.999	0.999	0.999	0.999	1.000	1.000	1.000
135.00	0.002	0.001	0.002	0.032	0.158	0.389	0.994	0.999	0.999	0.999	0.999	1.000
205.00	0.002	0.001	0.001	0.001	0.001	0.001	0.001	0.366	0.714	0.998	0.999	0.998
230.00	0.002	0.001	0.001	0.001	0.001	0.001	0.001	0.016	0.025	0.096	0.116	0.081
255.00	0.002	0.001	0.001	0.001	0.001	0.001	0.001	0.001	0.001	0.004	0.004	0.003

Table D.16 CO_2 Propagation in layer 1 for Run 9b, single-well model

Date	2001	2002	2005	2006	2007	2012	2013	2014	2018	2020	2023	2025	2050	2080	2200
Distance (m)	1 (years)	2	5	6	7	12	13	14	18	20	23	25	50	80	200
0	1	1	1	1	1	1	1	1	1	1	1	1	1	1	1
0.50	0.990	0.998	0.999	0.999	0.999	1.000	1.000	1.000	1.000	1.000	1.000	1.000	1.000	1.000	1.000
14.00	0.169	0.997	0.999	0.999	0.999	0.999	0.999	0.999	1.000	1.000	1.000	1.000	1.000	1.000	1.000
52.50	0.001	0.002	0.185	0.695	0.988	0.999	0.999	0.999	0.999	0.999	0.999	0.999	1.000	1.000	1.000
102.50	0.001	0.001	0.001	0.001	0.001	0.175	0.330	0.992	0.999	0.999	0.999	0.999	0.999	0.999	1.000
135.00	0.001	0.001	0.001	0.001	0.001	0.004	0.008	0.016	0.225	0.986	0.999	0.999	0.999	0.999	0.999
156.25	0.001	0.001	0.001	0.001	0.001	0.001	0.002	0.003	0.034	0.109	0.501	0.996	0.999	0.999	0.999
205.00	0.001	0.001	0.001	0.001	0.001	0.001	0.001	0.001	0.001	0.001	0.002	0.004	0.154	0.287	0.424
230.00	0.001	0.001	0.001	0.001	0.001	0.001	0.001	0.001	0.001	0.001	0.001	0.001	0.008	0.010	0.016
255.00	0.001	0.001	0.001	0.001	0.001	0.001	0.001	0.001	0.001	0.001	0.001	0.001	0.001	0.001	0.001

Table D.17 CO_2 Propagation in layer 1 for Run 9c, single-well model

Date	2001	2002	2006	2007	2008	2013	2014	2015	2018	2020	2023	2030	2050	2080	2200
Distance (m)	1 (years)	2	6	7	8	13	14	15	18	20	23	30	50	80	200
0	1	1	1	1	1	1	1	1	1	1	1	1	1	1	1
0.50	0.996	0.999	0.999	0.999	1.000	1.000	1.000	1.000	1.000	1.000	1.000	1.000	1.000	1.000	1.000
14.00	0.012	0.985	0.999	0.999	0.999	1.000	1.000	1.000	1.000	1.000	1.000	1.000	1.000	1.000	1.000
52.50	0.001	0.001	0.218	0.702	0.997	0.999	0.999	0.999	0.999	0.999	0.999	0.999	1.000	1.000	1.000
102.50	0.001	0.001	0.001	0.001	0.001	0.106	0.274	0.956	0.999	0.999	0.999	0.999	0.999	0.999	0.999
117.50	0.001	0.001	0.001	0.001	0.001	0.012	0.025	0.057	0.271	0.772	0.996	0.998	0.999	0.999	0.999
135.00	0.001	0.001	0.001	0.001	0.001	0.002	0.003	0.005	0.028	0.057	0.115	0.201	0.420	0.654	0.357
156.25	0.001	0.001	0.001	0.001	0.001	0.001	0.001	0.001	0.003	0.006	0.012	0.024	0.039	0.060	0.084
180.00	0.001	0.001	0.001	0.001	0.001	0.001	0.001	0.001	0.001	0.001	0.001	0.002	0.002	0.003	0.007

Table D.18 CO_2 Propagation in layer 1 for Run 9d, single-well model

Date	2001	2002	2005	2006	2010	2011	2013	2014	2020	2025	2035	2060	2200
Distance (m)	1 (years)	2	5	6	10	11	13	14	20	25	35	60	200
0	1	1	1	1	1	1	1	1	1	1	1	1	1
0.50	0.999	0.999	1.000	1.000	1.000	1.000	1.000	1.000	1.000	1.000	1.000	1.000	1.000
14.00	0.066	0.998	0.999	0.999	1.000	1.000	1.000	1.000	1.000	1.000	1.000	1.000	1.000
52.50	0.001	0.001	0.156	0.998	0.999	0.999	0.999	0.999	1.000	1.000	1.000	1.000	1.000
102.50	0.001	0.001	0.001	0.001	0.300	0.995	0.999	0.999	0.999	0.999	0.999	0.999	1.000
117.50	0.001	0.001	0.001	0.001	0.023	0.085	0.428	0.955	0.999	0.999	0.999	0.999	0.999
135.00	0.001	0.001	0.001	0.001	0.003	0.007	0.037	0.066	0.271	0.451	0.822	0.980	0.301
156.25	0.001	0.001	0.001	0.001	0.001	0.001	0.004	0.006	0.029	0.039	0.049	0.072	0.070
180.00	0.001	0.001	0.001	0.001	0.001	0.001	0.001	0.001	0.002	0.002	0.003	0.003	0.007

Table D.19 CO_2 Propagation in layer 1 for Run 10b, single-well model

Date	2001	2002	2005	2007	2008	2010	2015	2017	2018	2021	2022	2025	2026	2027	2032	2033	2034	2040	2050	2200
Distance (m)	1 (years)	2	5	7	8	10	15	17	18	21	22	25	26	27	32	33	34	40	50	200
0	1	1	1	1	1	1	1	1	1	1	1	1	1	1	1	1	1	1	1	1
0.50	0.809	0.996	0.998	0.999	0.999	0.999	0.999	0.999	0.999	1.000	1.000	1.000	1.000	1.000	1.000	1.000	1.000	1.000	1.000	1.000
14.00	0.004	0.955	0.998	0.998	0.999	0.999	0.999	0.999	0.999	0.999	1.000	1.000	1.000	1.000	1.000	1.000	1.000	1.000	1.000	1.000
52.50	0.002	0.001	0.997	0.998	0.998	0.999	0.999	0.999	0.999	0.999	0.999	0.999	0.999	0.999	1.000	1.000	1.000	1.000	1.000	1.000
102.50	0.002	0.001	0.001	0.137	0.570	0.816	0.997	0.999	0.999	0.999	0.999	0.999	0.999	0.999	0.999	0.999	0.999	0.999	0.999	1.000
117.50	0.002	0.001	0.001	0.012	0.037	0.056	0.234	0.640	0.987	0.999	0.999	0.999	0.999	0.999	0.999	0.999	0.999	0.999	0.999	1.000
135.00	0.002	0.001	0.001	0.002	0.004	0.005	0.033	0.082	0.133	0.482	0.931	0.999	0.999	0.999	0.999	0.999	0.999	0.999	0.999	0.999
156.25	0.002	0.001	0.001	0.001	0.001	0.001	0.004	0.011	0.018	0.069	0.107	0.322	0.550	0.968	0.999	0.999	0.999	0.999	0.999	0.999
180.00	0.002	0.001	0.001	0.001	0.001	0.001	0.001	0.002	0.002	0.006	0.008	0.028	0.040	0.058	0.349	0.573	0.940	0.999	0.999	0.999
205.00	0.002	0.001	0.001	0.001	0.001	0.001	0.001	0.001	0.001	0.001	0.001	0.002	0.003	0.004	0.016	0.022	0.032	0.153	0.990	0.998
230.00	0.002	0.001	0.001	0.001	0.001	0.001	0.001	0.001	0.001	0.001	0.001	0.001	0.001	0.001	0.001	0.002	0.002	0.009	0.049	0.093
255.00	0.002	0.001	0.001	0.001	0.001	0.001	0.001	0.001	0.001	0.001	0.001	0.001	0.001	0.001	0.001	0.001	0.001	0.001	0.002	0.003

Table D.20 CO_2 Propagation in layer 1 for Run 10c, single-well model

Date	2001	2002	2003	2004	2005	2006	2007	2012	2015	2017	2020	2021	2025	2035	2200
Distance (m)	1 (years)	2	3	4	5	6	7	12	15	17	20	21	25	35	200
0	1	1	1	1	1	1	1	1	1	1	1	1	1	1	1
0.50	0.995	0.997	0.998	0.998	0.998	0.999	0.999	0.999	1.000	1.000	1.000	1.000	1.000	1.000	1.000
14.00	0.158	0.997	0.997	0.998	0.998	0.999	0.999	0.999	0.999	1.000	1.000	1.000	1.000	1.000	1.000
52.50	0.002	0.001	0.760	0.997	0.998	0.998	0.998	0.999	0.999	0.999	0.999	0.999	0.999	0.999	0.999
102.50	0.002	0.001	0.001	0.013	0.967	0.997	0.998	0.999	0.999	0.999	0.999	0.999	0.999	0.999	0.999
117.50	0.002	0.001	0.001	0.002	0.076	0.591	0.990	0.998	0.999	0.999	0.999	0.999	0.999	0.999	0.999
135.00	0.002	0.001	0.001	0.001	0.006	0.051	0.141	0.311	0.997	0.999	0.999	0.999	0.999	0.999	0.999
156.25	0.002	0.001	0.001	0.001	0.001	0.005	0.014	0.041	0.198	0.646	0.999	0.999	0.999	0.999	0.999
180.00	0.002	0.001	0.001	0.001	0.001	0.001	0.002	0.003	0.015	0.042	0.175	0.394	0.997	0.998	0.998
205.00	0.002	0.001	0.001	0.001	0.001	0.001	0.001	0.001	0.001	0.003	0.009	0.016	0.070	0.106	0.099
230.00	0.002	0.001	0.001	0.001	0.001	0.001	0.001	0.001	0.001	0.001	0.001	0.001	0.004	0.005	0.006

Table D.21 CO_2 Propagation in layer 1 for Run 10d, single-well model

Date	2001	2002	2003	2004	2005	2006	2007	2008	2009	2013	2014	2015	2018	2019	2020	2035	2200
Distance (m)	1 (years)	2	3	4	5	6	7	8	9	13	14	15	18	19	20	35	200
0	1	1	1	1	1	1	1	1	1	1	1	1	1	1	1	1	1
0.50	0.996	0.997	0.998	0.998	0.999	0.999	0.999	0.999	0.999	0.999	1.000	1.000	1.000	1.000	1.000	1.000	1.000
14.00	0.566	0.997	0.998	0.998	0.998	0.999	0.999	0.999	0.999	0.999	0.999	0.999	1.000	1.000	1.000	1.000	1.000
52.50	0.002	0.003	0.997	0.998	0.998	0.998	0.998	0.999	0.999	0.999	0.999	0.999	0.999	0.999	0.999	0.999	1.000
102.50	0.002	0.001	0.002	0.636	0.997	0.998	0.998	0.998	0.999	0.999	0.999	0.999	0.999	0.999	0.999	0.999	0.999
117.50	0.002	0.001	0.001	0.036	0.774	0.995	0.997	0.998	0.998	0.999	0.999	0.999	0.999	0.999	0.999	0.999	0.999
135.00	0.002	0.001	0.001	0.003	0.063	0.241	0.585	0.867	0.926	0.998	0.999	0.999	0.999	0.999	0.999	0.999	0.999
156.25	0.002	0.001	0.001	0.001	0.006	0.027	0.057	0.081	0.089	0.282	0.584	0.990	0.999	0.999	0.999	0.999	0.999
180.00	0.002	0.001	0.001	0.001	0.001	0.002	0.004	0.005	0.005	0.019	0.035	0.065	0.383	0.765	0.990	0.999	0.998
205.00	0.002	0.001	0.001	0.001	0.001	0.001	0.001	0.001	0.001	0.002	0.002	0.003	0.015	0.025	0.041	0.159	0.117
230.00	0.002	0.001	0.001	0.001	0.001	0.001	0.001	0.001	0.001	0.001	0.001	0.001	0.001	0.002	0.002	0.007	0.008

Table D.22 CO_2 Propagation in layer 1 for Run 11b, single-well model

Date	2001	2002	2003	2007	2008	2009	2015	2020	2023	2024	2025	2030	2032	2035	2050	2100	2200
Distance (m)	1 (years)	2	3	7	8	9	15	20	23	24	25	30	32	35	50	100	200
0	1	1	1	1	1	1	1	1	1	1	1	1	1	1	1	1	1
0.50	0.405	0.996	0.998	0.999	0.999	0.999	0.999	1.000	1.000	1.000	1.000	1.000	1.000	1.000	1.000	1.000	1.000
4.50	0.090	0.974	0.997	0.999	0.999	0.999	0.999	1.000	1.000	1.000	1.000	1.000	1.000	1.000	1.000	1.000	1.000
14.00	0.004	0.188	0.971	0.999	0.999	0.999	0.999	0.999	1.000	1.000	1.000	1.000	1.000	1.000	1.000	1.000	1.000
52.50	0.001	0.001	0.001	0.214	0.799	0.989	0.999	0.999	0.999	0.999	0.999	0.999	0.999	1.000	1.000	1.000	1.000
102.50	0.001	0.001	0.001	0.001	0.001	0.001	0.008	0.101	0.338	0.592	0.961	0.999	0.999	0.999	0.999	0.999	0.999
117.50	0.001	0.001	0.001	0.001	0.001	0.001	0.001	0.010	0.033	0.048	0.069	0.237	0.403	0.918	0.998	0.999	0.999
135.00	0.001	0.001	0.001	0.001	0.001	0.001	0.001	0.001	0.003	0.004	0.005	0.021	0.030	0.051	0.149	0.312	0.353
156.25	0.001	0.001	0.001	0.001	0.001	0.001	0.001	0.001	0.001	0.001	0.001	0.002	0.003	0.004	0.011	0.017	0.026
180.00	0.001	0.001	0.001	0.001	0.001	0.001	0.001	0.001	0.001	0.001	0.001	0.001	0.001	0.001	0.001	0.002	0.002

Table D.23 CO_2 Propagation in layer 1 for Run 12b, single-well model

Date	2001	2002	2003	2007	2008	2009	2015	2020	2023	2025	2026	2027	2028	2030	2035	2038	2050	2200
Distance (m)	1 (years)	2	3	7	8	9	15	20	23	25	26	27	28	30	35	38	50	200
0	1	1	1	1	1	1	1	1	1	1	1	1	1	1	1	1	1	1
0.50	0.396	0.995	0.998	0.999	0.999	0.999	0.999	1.000	1.000	1.000	1.000	1.000	1.000	1.000	1.000	1.000	1.000	1.000
14.00	0.004	0.174	0.961	0.999	0.999	0.999	0.999	0.999	1.000	1.000	1.000	1.000	1.000	1.000	1.000	1.000	1.000	1.000
52.50	0.001	0.001	0.001	0.163	0.674	0.985	0.999	0.999	0.999	0.999	0.999	0.999	0.999	0.999	0.999	1.000	1.000	1.000
102.50	0.001	0.001	0.001	0.001	0.001	0.001	0.005	0.048	0.150	0.293	0.449	0.708	0.966	0.996	0.999	0.999	0.999	0.999
117.50	0.001	0.001	0.001	0.001	0.001	0.001	0.001	0.005	0.016	0.030	0.040	0.053	0.070	0.110	0.225	0.353	0.984	0.998
135.00	0.001	0.001	0.001	0.001	0.001	0.001	0.001	0.001	0.002	0.003	0.003	0.004	0.005	0.008	0.019	0.027	0.056	0.102
156.25	0.001	0.001	0.001	0.001	0.001	0.001	0.001	0.001	0.001	0.001	0.001	0.001	0.001	0.001	0.002	0.002	0.004	0.007

Table D.24 Comparison of CO_2 Propagations for each run at 2001 and 2007

Time (year)	2001												2007										
Radius (m)	0	0.50	14.00	52.50	102.50	117.50	135.00	156.25	180.00	205.00	230.00	255.00	0.50	14.00	52.50	102.50	117.50	135.00	156.25	180.00	205.00	230.00	255.00
Run 4b	1.0	0.991	0.011	0.001	0.001	0.001	0.001	0.001	0.001				0.999	0.999	0.995	0.001	0.001	0.001	0.001	0.001			
Run 4c	1.0	0.999	0.472	0.001	0.001	0.001	0.001	0.001	0.001	0.001			1.000	1.000	0.999	0.004	0.001	0.001	0.001	0.001	0.001		
Run 4d	1.0	0.999	0.994	0.001	0.001	0.001	0.001	0.001	0.001	0.001			1.000	1.000	0.999	0.092	0.007	0.001	0.001	0.001	0.001		
Run 5b	1.0	0.413	0.004	0.001	0.001	0.001	0.001	0.001	0.001				0.999	0.999	0.275	0.001	0.001	0.001	0.001	0.001			
Run 5c	1.0	0.995	0.038	0.001	0.001	0.001	0.001	0.001	0.001				0.999	0.999	0.999	0.001	0.001	0.001	0.001	0.001			
Run 5d	1.0	0.998	0.298	0.001	0.001	0.001	0.001	0.001	0.001	0.001			1.000	0.999	0.999	0.002	0.001	0.001	0.001	0.001	0.001		
Run 6b	1.0	0.430	0.004	0.001	0.001	0.001	0.001	0.001	0.001				0.999	0.999	0.294	0.001	0.001	0.001	0.001	0.001			
Run 6c	1.0	0.995	0.040	0.001	0.001	0.001	0.001	0.001	0.001				0.999	0.999	0.999	0.001	0.001	0.001	0.001	0.001			
Run 6d	1.0	0.998	0.332	0.001	0.001	0.001	0.001	0.001	0.001	0.001			1.000	0.999	0.999	0.002	0.001	0.001	0.001	0.001	0.001		
Run 7b	1.0	0.288	0.002	0.001	0.001	0.001	0.001						0.999	0.999	0.001	0.001	0.001	0.001					
Run 7c	1.0	0.992	0.004	0.001	0.001	0.001	0.001						0.999	0.999	0.040	0.001	0.001	0.001					
Run 7d	1.0	0.998	0.009	0.001	0.001	0.001	0.001	0.001					0.999	0.999	0.998	0.001	0.001	0.001	0.001				
Run 8b	1.0	0.952	0.046	0.002	0.002	0.002	0.002	0.002	0.002	0.002	0.002	0.002	0.999	0.999	0.998	0.002	0.001	0.001	0.001	0.001	0.001	0.001	0.001
Run 8c	1.0	0.996	0.554	0.002	0.002	0.002	0.002	0.002	0.002				0.999	0.999	0.999	0.969	0.010	0.001	0.001	0.001			
Run 8d	1.0	0.996	0.995	0.002	0.002	0.002	0.002	0.002	0.002				0.999	0.999	0.999	0.999	0.465	0.158	0.001	0.001			
Run 9b	1.0	0.990	0.169	0.001	0.001	0.001	0.001	0.001	0.001	0.001			0.999	0.999	0.988	0.001	0.001	0.001	0.001	0.001	0.001		
Run 9c	1.0	0.996	0.012	0.001	0.001	0.001	0.001	0.001	0.001				0.999	0.999	0.702	0.001	0.001	0.001	0.001	0.001			
Run 9d	1.0	0.999	0.066	0.001	0.001	0.001	0.001	0.001	0.001				1.000	0.999	0.999	0.002	0.001	0.001	0.001	0.001			
Run 10b	1.0	0.809	0.004	0.002	0.002	0.002	0.002	0.002	0.002	0.002	0.002	0.002	0.999	0.998	0.998	0.137	0.012	0.002	0.001	0.001	0.001	0.001	0.001
Run 10c	1.0	0.995	0.158	0.002	0.002	0.002	0.002	0.002	0.002	0.002	0.002		0.999	0.999	0.998	0.998	0.990	0.141	0.014	0.002	0.001	0.001	
Run 10d	1.0	0.996	0.566	0.002	0.002	0.002	0.002	0.002	0.002	0.002	0.002		0.999	0.999	0.998	0.998	0.997	0.585	0.057	0.004	0.001	0.001	
Run 11b	1.0	0.405	0.090	0.001	0.001	0.001	0.001	0.001	0.001	0.001			0.999	0.999	0.214	0.001	0.001	0.001	0.001	0.001	0.001		
Run 12b	1.0	0.396	0.004	0.001	0.001	0.001	0.001	0.001					0.999	0.999	0.163	0.001	0.001	0.001	0.001				

Table D.25 Comparison of CO_2 Propagations for each run at 2013 and 2025

Time (year)	2013											2025										
Radius (m)	**0.50**	**14.00**	**52.50**	**102.50**	**117.50**	**135.00**	**156.25**	**180.00**	**205.00**	**230.00**	**255.00**	**0.50**	**14.00**	**52.50**	**102.50**	**117.50**	**135.00**	**156.25**	**180.00**	**205.00**	**230.00**	**255.00**
Run 4b	1.000	1.000	0.999	0.094	0.008	0.001	0.001	0.001				1.000	1.000	1.000	0.999	0.999	0.457	0.025	0.002			
Run 4c	1.000	1.000	1.000	0.999	0.997	0.094	0.006	0.001	0.001			1.000	1.000	1.000	0.999	0.999	0.999	0.336	0.014	0.001		
Run 4d	1.000	1.000	1.000	0.999	0.999	0.993	0.057	0.003	0.001			1.000	1.000	1.000	0.999	0.999	0.999	0.920	0.024	0.002		
Run 5b	0.999	0.999	0.999	0.003	0.001	0.001	0.001	0.001				1.000	1.000	0.999	0.997	0.142	0.012	0.001	0.001			
Run 5c	1.000	1.000	0.999	0.322	0.030	0.003	0.001	0.001				1.000	1.000	1.000	0.999	0.999	0.990	0.053	0.003			
Run 5d	1.000	1.000	1.000	0.999	0.683	0.040	0.003	0.001	0.001			1.000	1.000	1.000	0.999	0.999	0.999	0.198	0.011	0.001		
Run 6b	0.999	0.999	0.999	0.003	0.001	0.001	0.001	0.001				1.000	1.000	0.999	0.998	0.151	0.013	0.001	0.001			
Run 6c	1.000	1.000	0.999	0.363	0.033	0.003	0.001	0.001				1.000	1.000	1.000	0.999	0.999	0.993	0.058	0.003			
Run 6d	1.000	1.000	1.000	0.999	0.822	0.045	0.003	0.001	0.001			1.000	1.000	1.000	0.999	0.999	0.999	0.236	0.012	0.001		
Run 7b	0.999	0.999	0.998	0.001	0.001	0.001						1.000	0.999	0.999	0.079	0.006	0.001					
Run 7c	1.000	1.000	0.999	0.008	0.001	0.001						1.000	1.000	0.999	0.998	0.140	0.010					
Run 7d	1.000	1.000	0.999	0.134	0.012	0.001	0.001					1.000	1.000	1.000	0.999	0.355	0.021	0.002				
Run 8b	1.000	0.999	0.999	0.248	0.028	0.004	0.001	0.001	0.001	0.001	0.001	1.000	1.000	1.000	0.999	0.999	0.999	0.997	0.085	0.005	0.001	0.001
Run 8c	1.000	1.000	0.999	0.999	0.999	0.999	0.002	0.001	0.001			1.000	1.000	1.000	0.999	0.999	0.999	0.828	0.028	0.001		
Run 8d	1.000	1.000	0.999	0.999	0.999	0.999	0.016	0.001	0.001			1.000	1.000	1.000	1.000	0.999	0.999	0.998	0.096	0.004		
Run 9b	1.000	0.999	0.999	0.330	0.042	0.008	0.002	0.001	0.001	0.001		1.000	1.000	0.999	0.999	0.999	0.999	0.996	0.004	0.001	0.001	
Run 9c	1.000	1.000	0.999	0.106	0.012	0.002	0.001	0.001				1.000	1.000	0.999	0.999	0.998	0.145	0.016	0.001			
Run 9d	1.000	1.000	0.999	0.999	0.428	0.037	0.004	0.001				1.000	1.000	1.000	0.999	0.999	0.451	0.039	0.002			
Run 10b	0.999	0.999	0.999	0.947	0.109	0.010	0.002	0.001	0.001	0.001	0.001	1.000	1.000	0.999	0.999	0.999	0.999	0.322	0.028	0.002	0.001	0.001
Run 10c	0.999	0.999	0.999	0.999	0.999	0.551	0.068	0.005	0.001	0.001		1.000	1.000	0.999	0.999	0.999	0.999	0.999	0.997	0.070	0.004	
Run 10d	0.999	0.999	0.999	0.999	0.999	0.998	0.282	0.019	0.002	0.001		1.000	1.000	0.999	0.999	0.999	0.999	0.999	0.999	0.149	0.007	
Run 11b	0.999	0.999	0.999	0.999	0.998	0.002	0.001	0.001	0.001			1.000	1.000	1.000	0.999	0.999	0.961	0.069	0.005	0.001	0.001	
Run 12b	0.999	0.999	0.999	0.002	0.001	0.001	0.001					1.000	1.000	0.999	0.293	0.030	0.003	0.001				

Table D.26 Comparison of CO_2 Propagations for each run at 2050 and 2200

Time (year)	2050											2200										
Radius (m)	**0.50**	**14.00**	**52.50**	**102.50**	**117.50**	**135.00**	**156.25**	**180.00**	**205.00**	**230.00**	**255.00**	**0.50**	**14.00**	**52.50**	**102.50**	**117.50**	**135.00**	**156.25**	**180.00**	**205.00**	**230.00**	**255.00**
Run 4b	1.000	1.000	1.000	0.999	0.999	0.998	0.074	0.004				1.000	1.000	1.000	1.000	0.999	0.998	0.075	0.005			
Run 4c	1.000	1.000	1.000	0.999	0.999	0.999	0.323	0.015	0.001			1.000	1.000	1.000	1.000	0.999	0.999	0.137	0.013	0.002		
Run 4d	1.000	1.000	1.000	1.000	0.999	0.999	0.620	0.024	0.002			1.000	1.000	1.000	1.000	0.999	0.999	0.120	0.016	0.002		
Run 5b	1.000	1.000	1.000	0.999	0.999	0.588	0.030	0.002				1.000	1.000	1.000	0.999	0.999	0.995	0.060	0.003			
Run 5c	1.000	1.000	1.000	0.999	0.999	0.998	0.106	0.006				1.000	1.000	1.000	1.000	0.999	0.999	0.098	0.008			
Run 5d	1.000	1.000	1.000	0.999	0.999	0.999	0.243	0.013	0.001			1.000	1.000	1.000	1.000	0.999	0.999	0.147	0.014	0.002		
Run 6b	1.000	1.000	1.000	0.999	0.999	0.692	0.032	0.002				1.000	1.000	1.000	0.999	0.999	0.997	0.063	0.003			
Run 6c	1.000	1.000	1.000	0.999	0.999	0.999	0.118	0.007				1.000	1.000	1.000	1.000	0.999	0.999	0.109	0.009			
Run 6d	1.000	1.000	1.000	0.999	0.999	0.999	0.314	0.014	0.001			1.000	1.000	1.000	1.000	0.999	0.999	0.180	0.017	0.002		
Run 7b	1.000	1.000	0.999	0.975	0.063	0.004						1.000	1.000	0.999	0.995	0.117	0.009					
Run 7c	1.000	1.000	0.999	0.999	0.181	0.013						1.000	1.000	1.000	0.999	0.159	0.019					
Run 7d	1.000	1.000	1.000	0.999	0.358	0.024	0.002					1.000	1.000	1.000	0.999	0.186	0.027	0.003				
Run 8b	1.000	1.000	1.000	0.999	0.999	0.999	0.999	0.999	0.709	0.024	0.001	1.000	1.000	1.000	1.000	1.000	0.999	0.999	0.999	0.992	0.040	0.002
Run 8c	1.000	1.000	1.000	1.000	0.999	0.999	0.998	0.074	0.003			1.000	1.000	1.000	1.000	1.000	1.000	0.998	0.065	0.002		
Run 8d	1.000	1.000	1.000	1.000	1.000	1.000	0.999	0.115	0.004			1.000	1.000	1.000	1.000	1.000	1.000	0.998	0.081	0.003		
Run 9b	1.000	1.000	1.000	0.999	0.999	0.999	0.999	0.154	0.008	0.001		1.000	1.000	1.000	1.000	0.999	0.999	0.999	0.424	0.016	0.001	
Run 9c	1.000	1.000	1.000	0.999	0.999	0.420	0.039	0.002				1.000	1.000	1.000	0.999	0.999	0.357	0.084	0.007			
Run 9d	1.000	1.000	1.000	0.999	0.999	0.977	0.064	0.003				1.000	1.000	1.000	1.000	0.999	0.301	0.070	0.007			
Run 10b	1.000	1.000	1.000	0.999	0.999	0.999	0.999	0.999	0.990	0.049	0.002	1.000	1.000	1.000	1.000	1.000	0.999	0.999	0.999	0.998	0.093	0.003
Run 10c	1.000	1.000	0.999	0.999	0.999	0.999	0.999	0.998	0.107	0.006		1.000	1.000	0.999	0.999	0.999	0.999	0.999	0.998	0.099	0.006	
Run 10d	1.000	1.000	0.999	0.999	0.999	0.999	0.999	0.999	0.156	0.008		1.000	1.000	1.000	0.999	0.999	0.999	0.999	0.998	0.117	0.008	
Run 11b	1.000	1.000	1.000	1.000	0.999	0.999	0.998	0.149	0.011	0.001		1.000	1.000	1.000	1.000	0.999	0.999	0.999	0.353	0.026	0.002	
Run 12b	1.000	1.000	1.000	0.999	0.984	0.056	0.004					1.000	1.000	1.000	0.999	0.998	0.102	0.007				

APPENDIX E

E.1 3-D Map of CO_2 saturation as a free gas, soluble CO_2 mole fraction in water and precipitated CO_2 as Calcite dissolution / precipitation, CO_2 Global Mole Fraction, Kaolinite dissolution / precipitation and Anorthite dissolution / precipitation at 2013, 2030 and 2200 years for Run 5b, single-well aquifer model

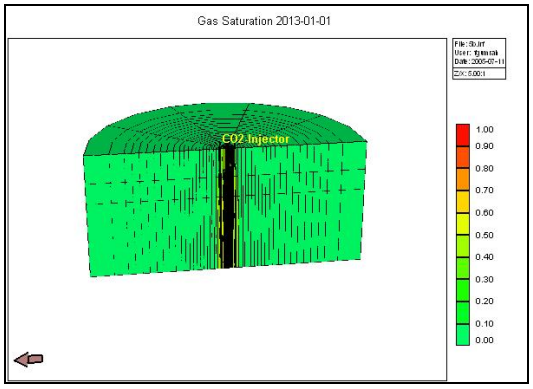

Figure E. 1 Map of CO_2 Saturation after CO_2 Injetion has been ceased at 2013 (13 years) for Run 5b: single-well aquifer model

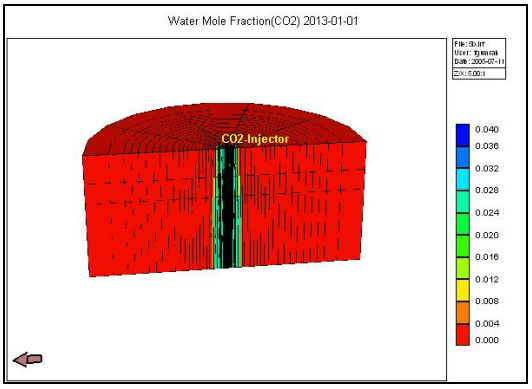

Figure E. 2 Map of CO_2 Mole Fraction in Water after CO_2 Injetion has been ceased at 2013 (13 years) for Run 5b: single-well aquifer model

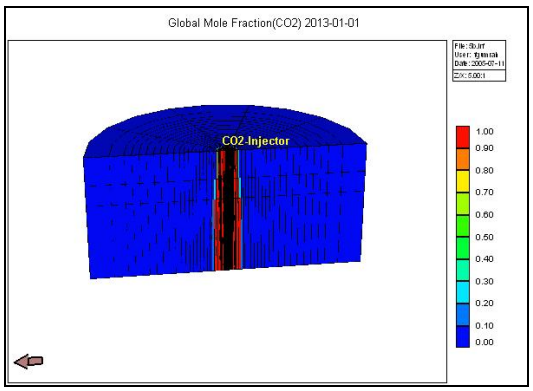

Figure E. 3 Map of CO_2 Global Mole Fraction after CO_2 Injetion has been ceased at 2013 (13 years) for Run 5b: single-well aquifer model

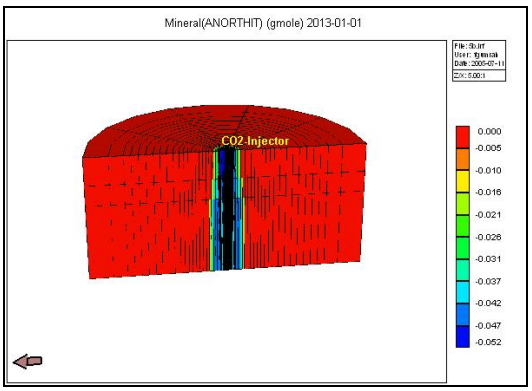

Figure E. 5 Map of Anorthite Dissolution / Precipitation after CO_2 Injetion has been ceased at 2013 (13 years) for Run 5b: single-well aquifer model

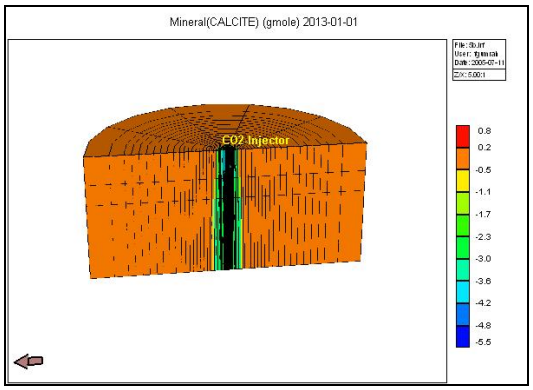

Figure E. 4 Map of Calcite Dissolution / Precipitation after CO_2 Injetion has been ceased at 2013 (13 years) for Run 5b: single-well aquifer model

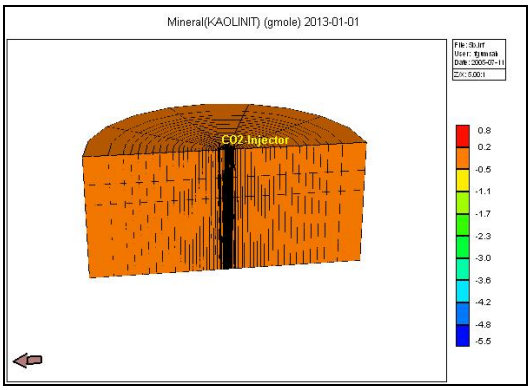

Figure E. 6 Map of Kaolinite Dissolution / Precipitation after CO_2 Injetion has been ceased at 2013 (13 years) for Run 5b: single-well aquifer model

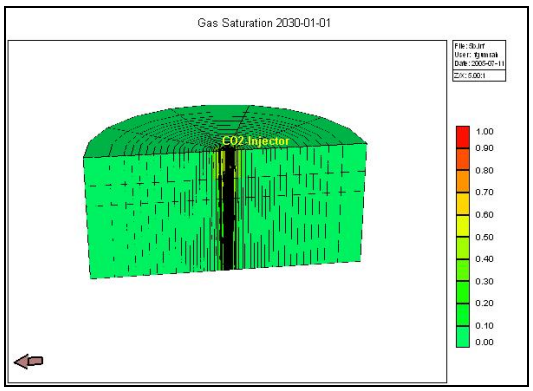

Figure E. 7 Map of CO_2 Saturation at 2030 (30 years) for Run 5b: single-well aquifer model

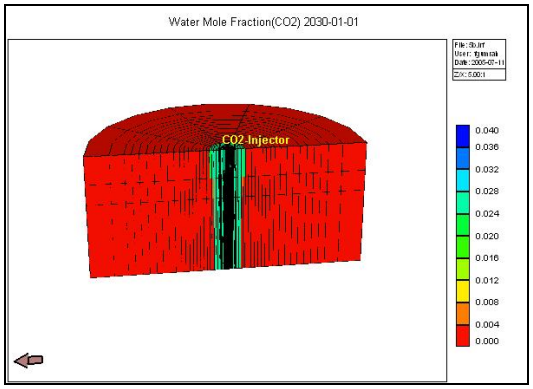

Figure E. 8 Map of CO_2 Mole Fraction in Water at 2030 (30 years) for Run 5b: single-well aquifer model

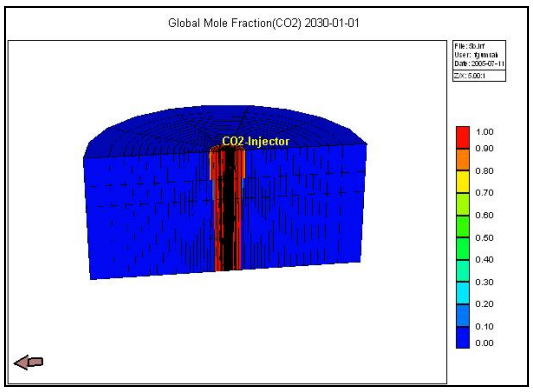

Figure E. 9 Map of CO_2 Global Mole Fraction at 2030 (30 years) for Run 5b: single-well aquifer model

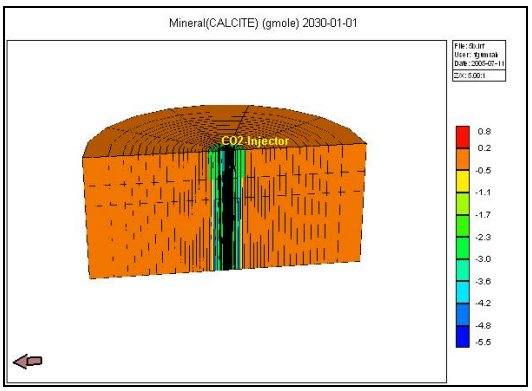

Figure E. 10 Map of Calcite Dissolution / Precipitation at 2030 (30 years) for Run 5b: single-well aquifer model

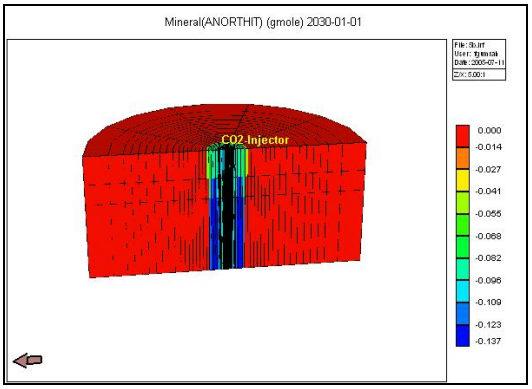

Figure E. 11 Map of Anorthite Dissolution / Precipitation at 2030 (30 years) for Run 5b: single-well aquifer model

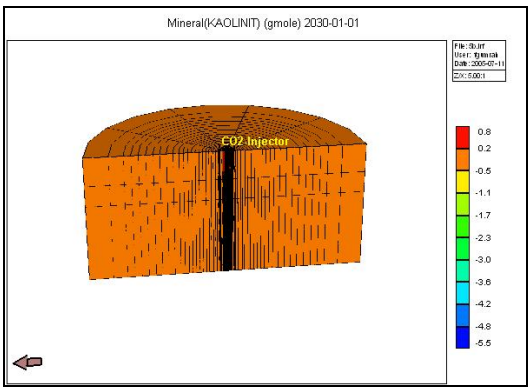

Figure E. 12 Map of Kaolinite Dissolution / Precipitation at 2030 (30 years) for Run 5b: single-well aquifer model

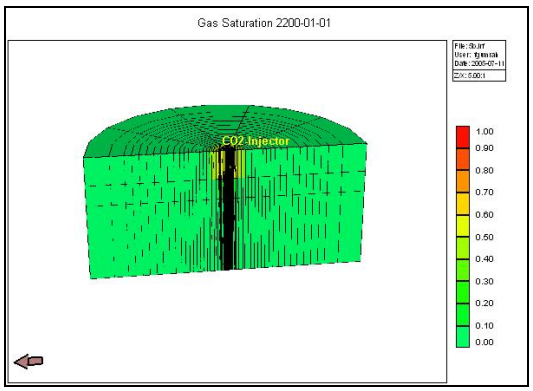

Figure E. 13 Map of CO_2 Saturation at 2200 (200 years) for Run 5b: single-well aquifer model

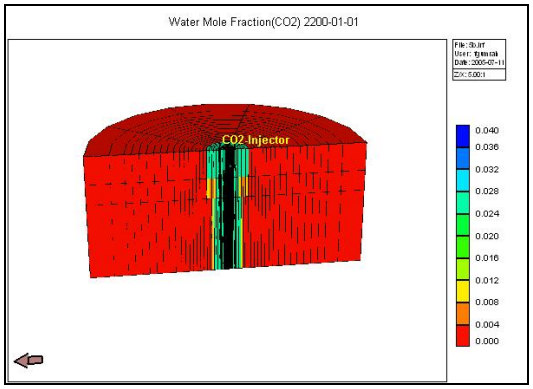

Figure E. 14 Map of CO_2 Mole Fraction in Water at 2200 (200 years) for Run 5b: single-well aquifer model

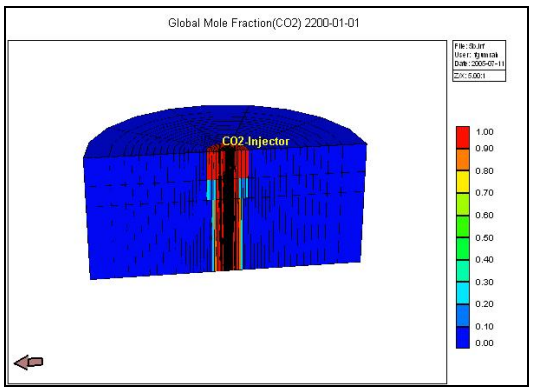

Figure E. 15 Map of CO_2 Global Mole Fraction at 2200 (200 years) for Run 5b: single-well aquifer model

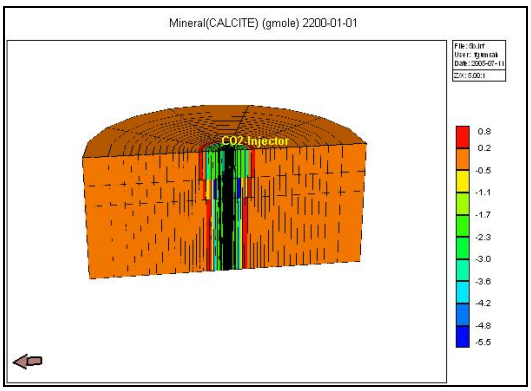

Figure E. 16 Map of Calcite Dissolution / Precipitation at 2200 (200 years) for Run 5b: single-well aquifer model

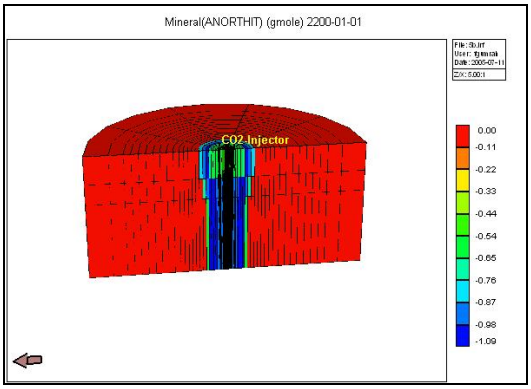

Figure E. 17 Map of Anorthite Dissolution / Precipitation at 2200 (200 years) for Run 5b: single-well aquifer model

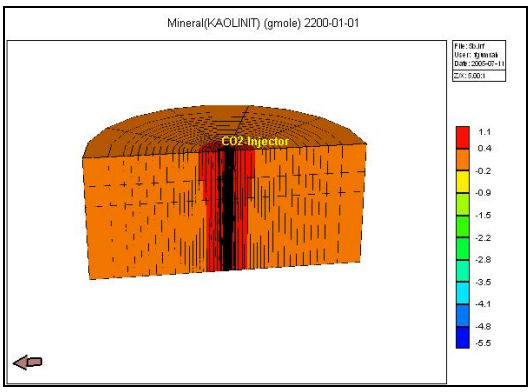

Figure E. 18 Map of Kaolinite Dissolution / Precipitation at 2200 (200 years) for Run 5b: single-well aquifer model

E.2 3-D Map of CO_2 saturation as a free gas, soluble CO_2 mole fraction in water and precipitated CO_2 as Calcite dissolution / precipitation, CO_2 Global Mole Fraction, Kaolinite dissolution / precipitation and Anorthite dissolution / precipitation at 2020, 2030 and 2200 years for Run 8b, single-well aquifer model

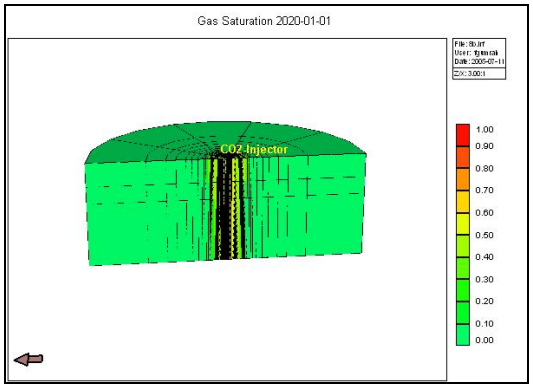

Figure E. 19 Map of CO_2 Saturation after CO_2 Injection has been ceased at 2020 (20 years) for Run 8b: single-well aquifer model

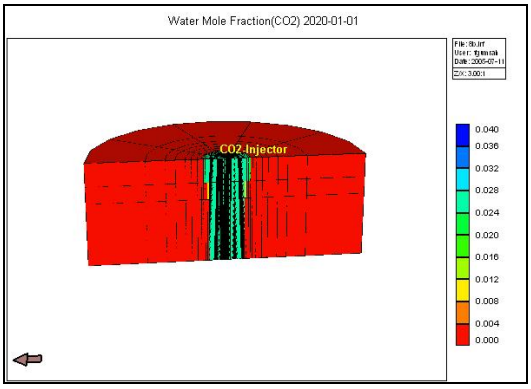

Figure E. 20 Map of CO_2 Mole Fraction in Water after CO_2 Injection has been ceased at 2020 (20 years) for Run 8b: single-well aquifer model

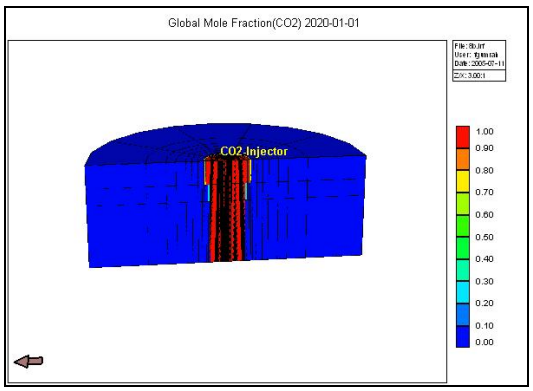

Figure E. 21 Map of CO_2 Global Mole Fraction after CO_2 Injection has been ceased at 2020 (20 years) for Run 8b: single-well aquifer model

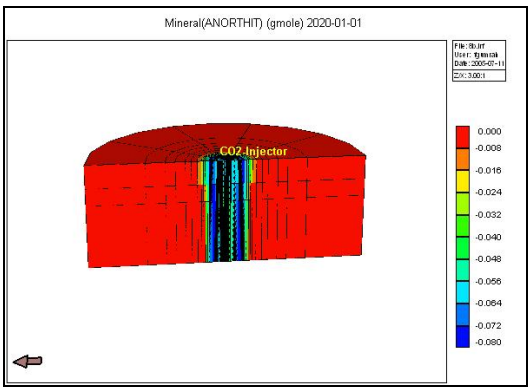

Figure E. 23 Map of Anorthite Dissolution / Precipitation after CO_2 Injection has been ceased at 2020 (20 years) for Run 8b: single-well aquifer model

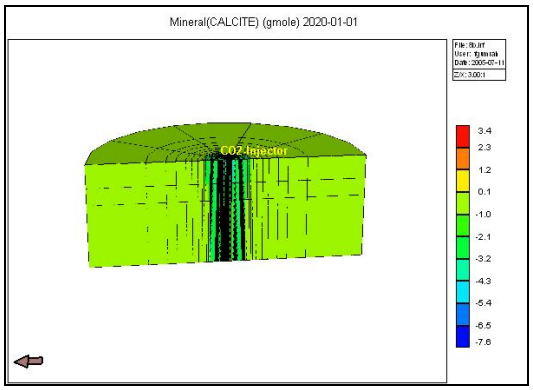

Figure E. 22 Map of Calcite Dissolution / Precipitation after CO_2 Injection has been ceased at 2020 (20 years) for Run 8b: single-well aquifer model

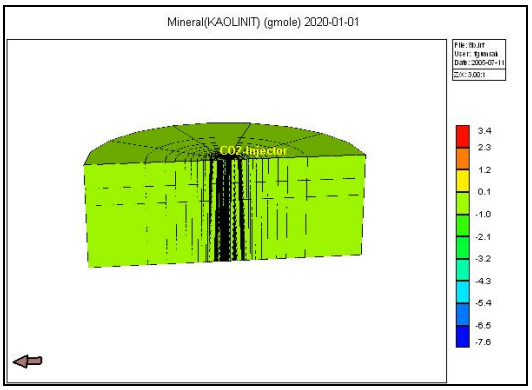

Figure E. 24 Map of Kaolinite Dissolution / Precipitation after CO_2 Injection has been ceased at 2020 (20 years) for Run 8b: single-well aquifer model

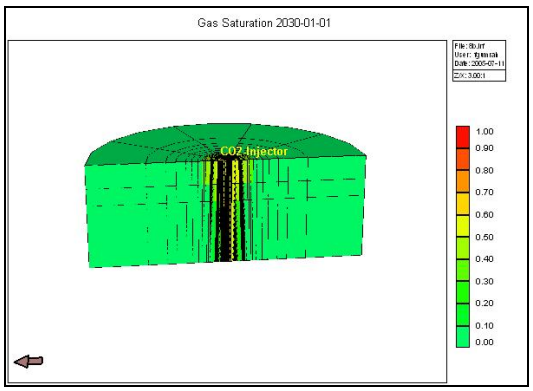

Figure E. 25 Map of CO_2 Saturation at 2030 (30 years) for Run 8b: single-well aquifer model

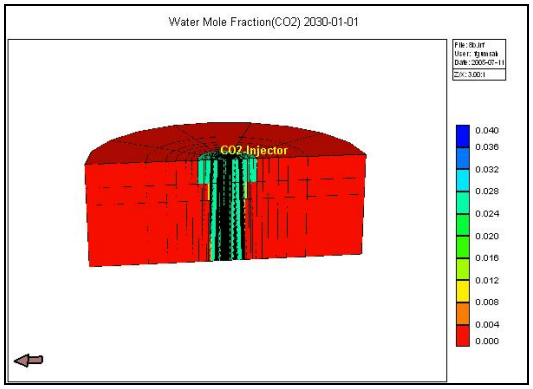

Figure E. 26 Map of CO_2 Mole Fraction in Water at 2030 (30 years) for Run 8b: single-well aquifer model

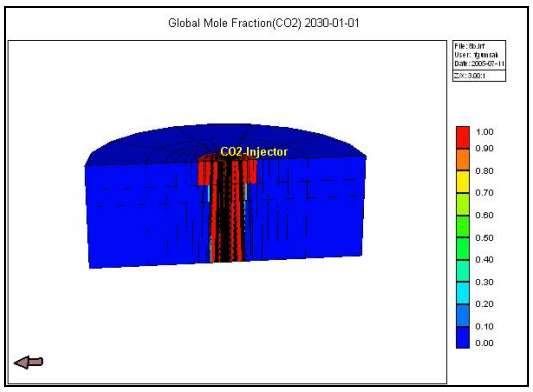

Figure E. 27 Map of CO_2 Global Mole Fraction at 2030 (30 years) for Run 8b: single-well aquifer model

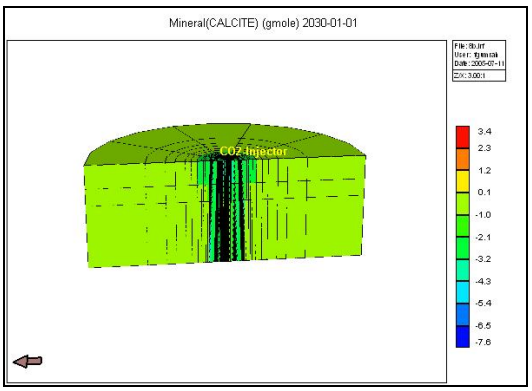

Figure E. 28 Map of Calcite Dissolution / Precipitation at 2030 (30 years) for Run 8b: single-well aquifer model

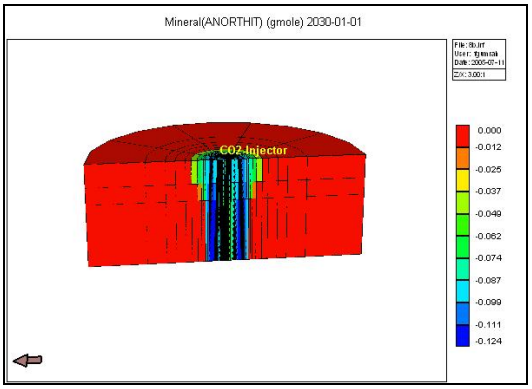

Figure E. 29 Map of Anorthite Dissolution / Precipitation at 2030 (30 years) for Run 8b: single-well aquifer model

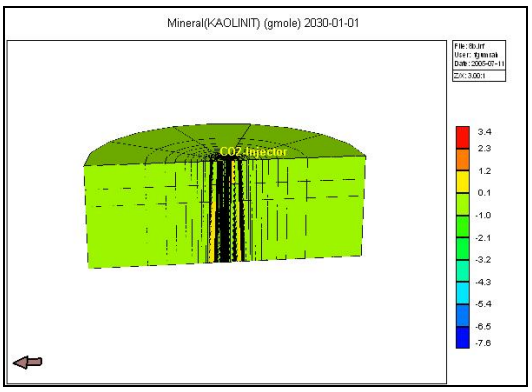

Figure E. 30 Map of Kaolinite Dissolution / Precipitation at 2030 (30 years) for Run 8b: single-well aquifer model

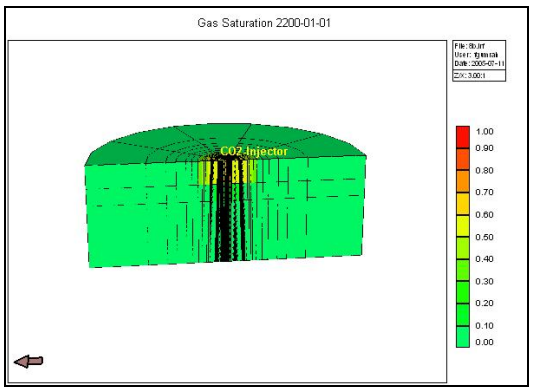

Figure E. 31 Map of CO_2 Saturation at 2200 (200 years) for Run 8b: single-well aquifer model

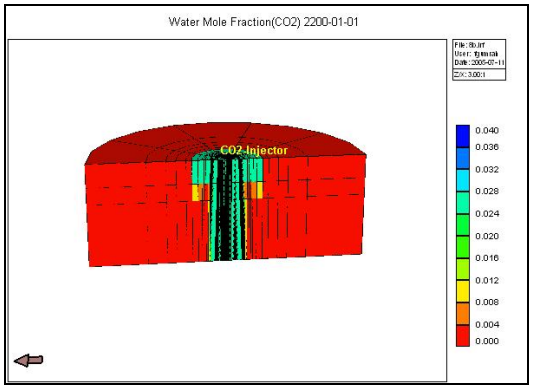

Figure E. 32 Map of CO_2 Mole Fraction in Water at 2200 (200 years) for Run 8b: single-well aquifer model

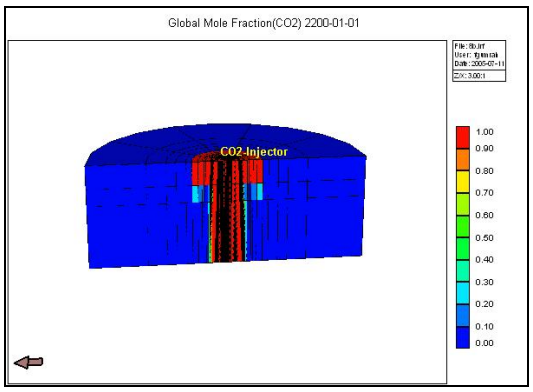

Figure E. 33 Map of CO_2 Global Mole Fraction at 2200 (200 years) for Run 8b: single-well aquifer model

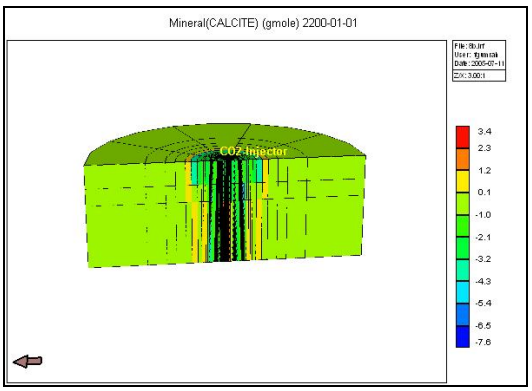

Figure E. 34 Map of Calcite Dissolution / Precipitation at 2200 (200 years) for Run 8b: single-well aquifer model

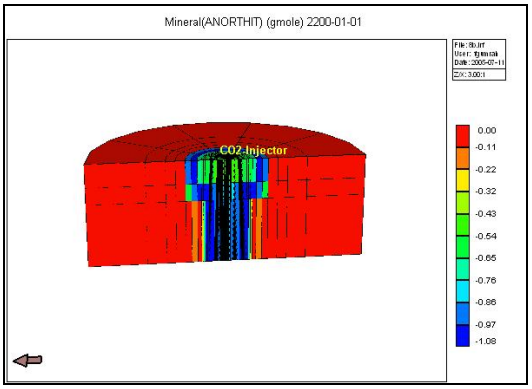

Figure E. 35 Map of Anorthite Dissolution / Precipitation at 2200 (200 years) for Run 8b: single-well aquifer model

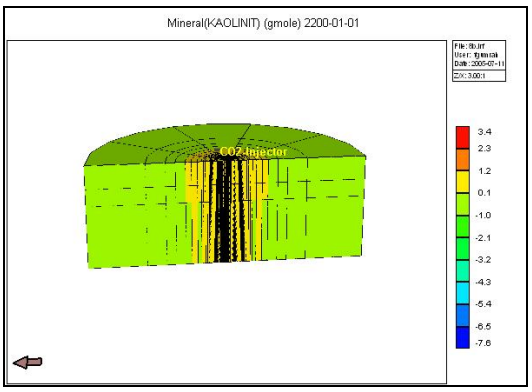

Figure E. 36 Map of Kaolinite Dissolution / Precipitation at 2200 (200 years) for Run 8b: single-well aquifer model

APPENDIX F

CO_2 Injection Histories, CO_2 Saturation, CO_2 Mole Fraction in Water, Calcite Dissolution / Precipitation, Anorthite Dissolution / Precipitation, Kaolinite Dissolution / Precipitation Plots for Runs 5e and 8e for Single-Well Aquifer Model

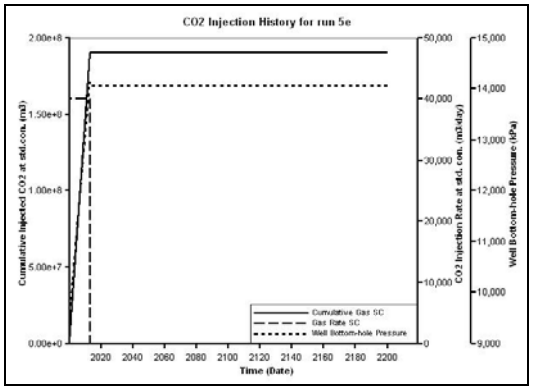

Figure F. 1 CO_2 Injection History for Run 5e: single-well case, (CO_2 injection rate = 40000 sm^3/d)

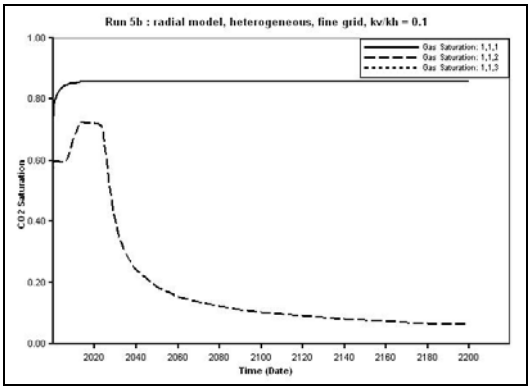

Figure F. 2 CO_2 Saturation for Run 5e: single-well case

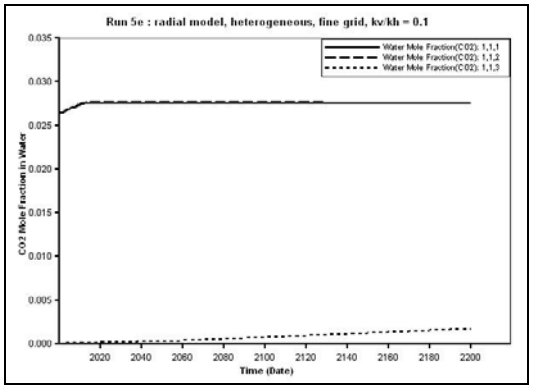

Figure F. 3 CO_2 Mole Fraction in Water for Run 5e: single-well case

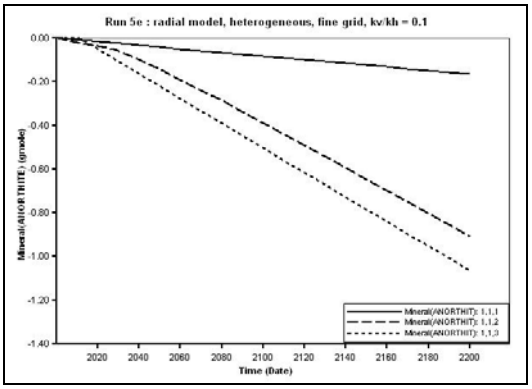

Figure F. 5 AnorthiteDissolution / Precipitation for Run 5e: single-well case

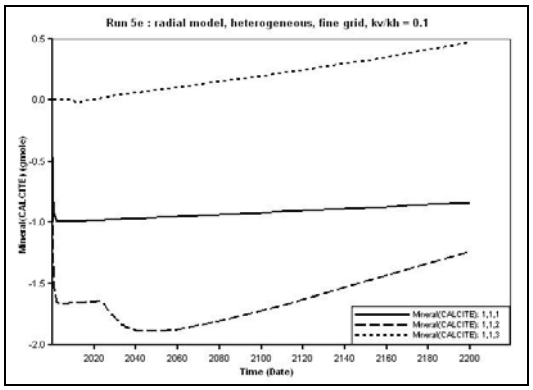

Figure F. 4 Calcite Dissolution / Precipitation for Run 5e: single-well case

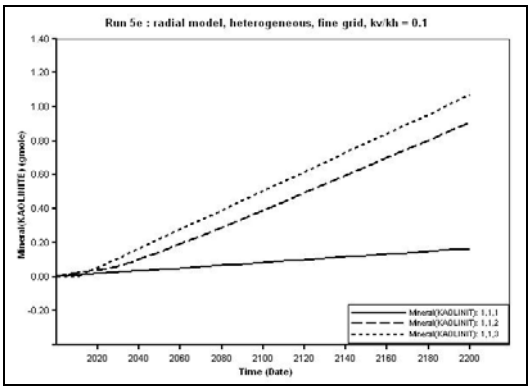

Figure F. 6 Kaolinite Dissolution / Precipitation for Run 5e: single-well case

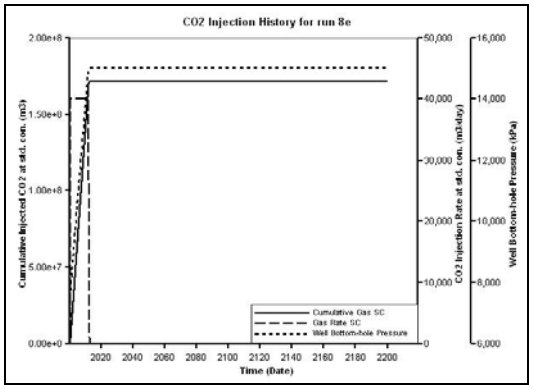

Figure F. 7 CO_2 Injection History for Run 8e: single-well case, (CO_2 injection rate = 40000 sm^3/d)

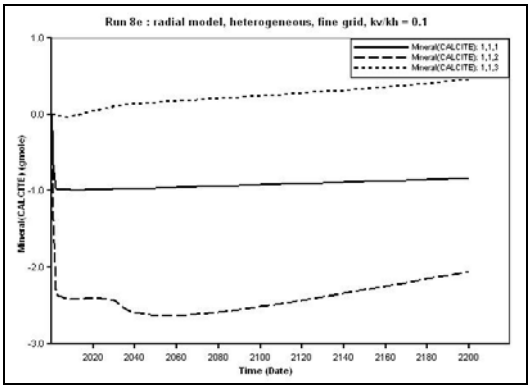

Figure F. 10 Calcite Dissolution / Precipitation for Run 8e: single-well case

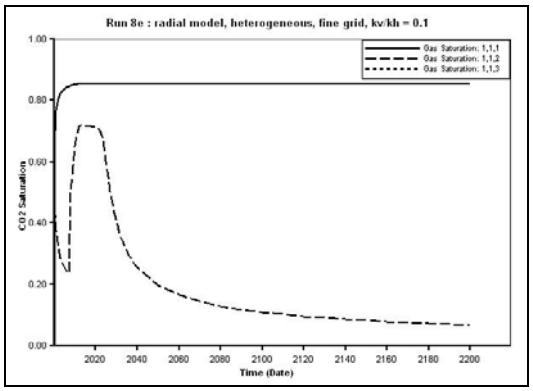

Figure F. 8 CO_2 Saturation for Run 8e: single-well case

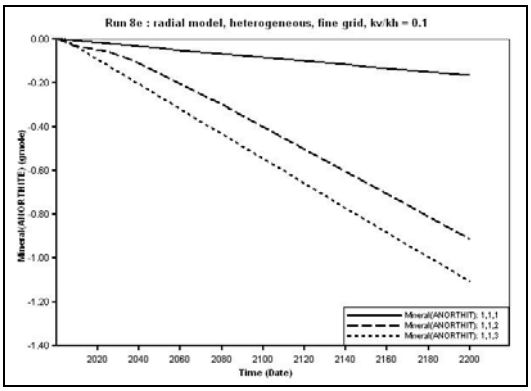

Figure F. 11 AnorthiteDissolution / Precipitation for Run 8e: single-well case

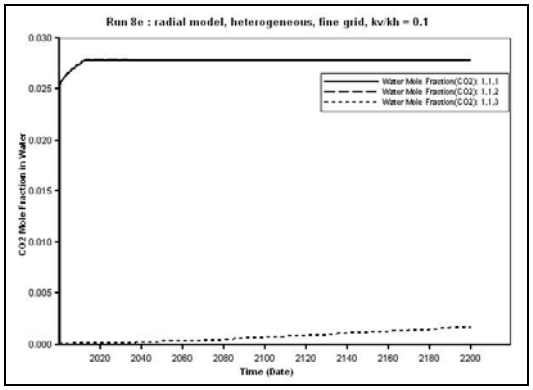

Figure F. 9 CO_2 Mole Fraction in Water for Run 8e: single-well case

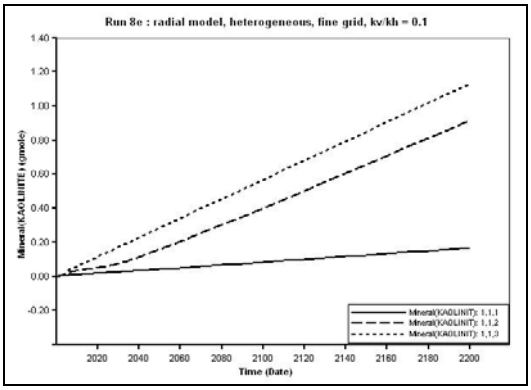

Figure F. 12 Kaolinite Dissolution / Precipitation for Run 8e: single-well case